Titre: Title:	Production of Chitosan Micro and Nanospheres for the Formulation of Antibacterial Food Packaging Materials
Auteur: Author:	Nury Haydée Ardila Gualdron
Date:	2017
Type:	Mémoire ou thèse / Dissertation or Thesis
Référence: Citation:	Ardila Gualdron, N. H. (2017). Production of Chitosan Micro and Nanospheres for the Formulation of Antibacterial Food Packaging Materials [Thèse de doctorat, École Polytechnique de Montréal]. PolyPublie. https://publications.polymtl.ca/2579/

URL de PolyPublie: PolyPublie URL:	https://publications.polymtl.ca/2579/
Directeurs de recherche: Advisors:	Marie-Claude Heuzey, & Abdellah Ajji
Programme: Program:	Génie chimique

UNIVERSITÉ DE MONTRÉAL

PRODUCTION OF CHITOSAN MICRO AND NANOSPHERES FOR THE FORMULATION OF ANTIBACTERIAL FOOD PACKAGING MATERIALS

NURY HAYDÉE ARDILA GUALDRÓN

DÉPARTEMENT DE GÉNIE CHIMIQUE

ÉCOLE POLYTECHNIQUE DE MONTRÉAL

THÈSE PRÉSENTÉE EN VUE DE L'OBTENTION

DU DIPLÔME DE PHILOSOPHIAE DOCTOR

(GÉNIE CHIMIQUE)

MAI 2017

UNIVERSITÉ DE MONTRÉAL

ÉCOLE POLYTECHNIQUE DE MONTRÉAL

Cette thèse intitulée:

PRODUCTION OF CHITOSAN MICRO AND NANOSPHERES FOR THE FORMULATION OF ANTIBACTERIAL FOOD PACKAGING MATERIALS

présentée par : ARDILA GUALDRÓN Nury Haydée

en vue de l'obtention du diplôme de : Philosophiae Doctor

a été dûment acceptée par le jury d'examen constitué de :

Mme DESCHÊNES Louise, Ph. D., présidente

Mme HEUZEY Marie-Claude, Ph. D., membre et directrice de recherche

M. AJJI Abdellah, Ph. D., membre et codirecteur de recherche

M. CARREAU Pierre, Ph. D., membre

M. ARUL Joseph, Ph. D., membre externe

DEDICATION

To God, my beloved husband and beautiful daughter, and my beloved parents, brother and sister

ACKNOWLEDGEMENTS

I would like to express my gratitude to all who have being part of my new life in Canada. Colleagues that became friends and friends that became like a family. All of you have made that even if family is far, life is easier and enjoyable.

I would like also to express my deep gratitude to my advisor, Professor Marie-Claude Heuzey, and co-advisor, Professor Abdellah Ajji, who gave me not only the knowledge, support and encouragement for the successful completion of this project, but also their patience and motivation in each activity I was participating. It was really pleasant and it was a very enriching experience to work with them.

Besides my supervisors, I would like to thank the rest of my thesis committee, namely Professor Louise Deschênes, Professor Pierre Carreau and Professor Joseph Arul for accepting to evaluate my thesis.

I am so thankful to Professor France Daigle at Université de Montréal for her training and continuous support in the antibacterial tests.

I acknowledge the help and hard work of Zineb Ajji and Nelson Medina in the realisation of electrospraying and electrospinning tests during their internship and Master project, respectively.

I also want to thank Professor Jason Tavares and Nick Virgilio for their advice, coaching sessions and encouraging me in different academic activities during my studies.

Also special thanks to Professor Basil Favis for letting me join to students CREPEC committee in 2014. It was a very enriching experience for my professional and personal life. In addition, I thank Diane, Alyson and the student committee of that year for all the experience we share.

Many thanks to Ahmad Zohrevand who introduced me to the SPE committee. Special thanks to Marie-France Sosa, Professor Nicole Demarquette and Doru Davidescu for letting me to be part of the activities and their committee since 2013.

A deep thank to Aziz Guellouz for the coaching sessions, advices and continuous support during the *Technopreneur* program. Also special thanks to the ChitoPack team Mounia Arkoun, Valéry Kovalenko and Riham Hammouda.

I would also like to extend my thanks to the technical and administrative staff of the Chemical Engineering Department at Polytechnique de Montréal for their help and kind cooperation during my PhD, especially to Claire Cerclé, Mélina Hamdine, Martine Lamarche and Gino Robin.

I want to thank my dear friend Mounia Arkoun for her kind help in translating the abstract of this thesis to French and for her continued support not only for the long and continuous discussions about the project but also in my personal life. I was lucky to work with her as a partner in the different academic activities during my studies.

A sincere appreciation to all people who have been part of the rheology and electrospinning group meetings for their continuous feedback. A special thanks to my dear friends and colleagues Hoda, Hajer, Hanan, Fatemeh, Gilles, Andrea, Marie, Changsheng, Xiaoyan, Davood, Mariam, Helia, Qinghua, Thibault, Amir, Sandra, Jaime, Shirley, Richard, Didac, Juan, Mar, Pau, Ricardo, Lina, Jesus and Manuel.

A big appreciation to the dedicated team of Les Petits génies, specially to Martine, Alcina, Marie-Danielle, Fatima, Amina, Farida, Lizbeth and Rosa.

Finally, all my accomplishments and deep gratitude go to my parents, my brother, my sister, especially to my husband and daughter Violette who give me the support in all my life.

RÉSUMÉ

L'emballage alimentaire actif est un sujet de recherche en cours. La fabrication de nouveaux matériaux d'emballage pour améliorer la sécurité alimentaire et la préservation des aliments est un sujet d'intérêt continu. Le chitosane est un polysaccharide d'origine marine, non toxique ayant un grand potentiel pour être utilisé comme biomatériau antimicrobien, compte tenu de son activité antibactérienne. En outre, le chitosane est utilisé comme un additif alimentaire et a d'ailleurs reçu le statut de «Generally Recognized As Safe» (GRAS) par la Food and Drug Administration (FDA) des États-Unis. Par conséquent, le chitosane peut être considéré comme un candidat idéal dans des applications liées à l'industrie alimentaire.

Le présent travail de recherche porte sur la production de nanosphères de chitosane pour la formulation de matériaux d'emballage alimentaire antibactériens. Le projet de recherche a été réalisé en trois étapes. La première étape traite de l'étude de l'influence de différents facteurs environnementaux, microbiens et caractéristiques du chitosane sur son activité antibactérienne, lorsqu'il est utilisé sous une forme solide discontinue, comme la poudre et les flocons. L'activité antimicrobienne a été évaluée contre une souche Gram-négatif (*Escherichia coli*) et deux souches Gram-positif (*Listeria innocua* et *Staphylococcus aureus*), qui sont généralement responsables de la détérioration des aliments. Les résultats ont montré que le chitosane nécessite une solubilisation partielle pour l'exercice de son activité antibactérienne. En outre, des conditions de température adéquates, la force ionique (salinité) et la présence d'un support physique solide peuvent favoriser l'effet antibactérien. La souche *E. coli* s'est révélée plus affectée par le chitosane, suivie de *L. innocua* et *S. aureus*. D'autre part, l'action antibactérienne a augmenté avec la concentration en chitosane jusqu'à un point critique au-dessus duquel cet effet a diminué. Cet effet pourrait être la conséquence des protéines restantes dans le chitosane et qui peuvent servir de nutriments pour les bactéries, limitant ainsi l'activité antibactérienne. Ces résultats sont prometteurs pour l'utilisation directe de la poudre et des flocons de chitosane en tant qu'agents antimicrobiens pour des applications dans l'emballage alimentaire.

La deuxième étape a consisté en la production de micro et nanosphères de chitosane par électropulvérisation. Les effets des paramètres de solution et de procédé sur la morphologie, la collecte des particules et la stabilité du procédé ont été étudiés. La cartographie de la stabilité du procédé a été établie selon les nombres adimensionnels suivants: Reynolds (*Re*), Peclet électrique

(*Pe*), Weber (*We*), Froude (*Fr*) et un paramètre de force électrostatique (Ω) qui relie les principales variables du procédé. La stabilité des solutions de chitosane par electropulvérisation nécessitait des valeurs relativement faibles pour les nombres *Re*, *Fr* et Ω, mais des valeurs relativement élevées pour les nombres *Pe* et *We*. Le procédé d'électropulvérisation constitue une nouvelle façon d'incorporer des nanosphères de chitosane dans les emballages alimentaires existants afin de leur fournir des propriétés antimicrobiennes et d'aider à prolonger la durée de conservation des produits alimentaires.

La troisième étape étudie l'effet de la forme physique du chitosane, à savoir les solutions, les poudres et les nanosphères, ainsi que la taille des particules sur l'activité antibactérienne contre deux souches pathogènes, *Staphylococcus aureus* et *Salmonella enterica* serovar Typhimurium, des bactéries généralement associées à des infections d'origine alimentaire. Les nanosphères de chitosane ont présenté des performances antibactériennes supérieures à celles de la poudre de chitosane. Ceci a été expliqué par la petite taille et la plus grande surface de contact des nanosphères avec les parois cellulaires bactériennes. Les nanosphères ont également affiché une activité antibactérienne plus élevée que celle du chitosane en solution, ce qui peut être le résultat d'une charge superficielle plus élevée et d'une petite taille solide. Il est considéré que si le chitosane en solution interagit avec la paroi cellulaire, il restera sous forme libre dans le milieu plutôt que d'adhérer aux cellules de façon permanente. D'autre part, les souches de *S. aureus* étaient plus sensibles à l'action des nanosphères et étaient moins sensibles aux variations des conditions de pH et de température du milieu. Cette étude est d'une grande importance en ce qui concerne les nombreuses applications possibles des nanosphères de chitosane dans divers domaines dont l'emballage alimentaire et le biomédical.

ABSTRACT

Active food packaging is an ongoing research topic. The fabrication of packaging materials to improve food safety and food preservation is a subject of continuous interest. Chitosan is a nontoxic polysaccharide that has great potential to be used as an antimicrobial biomaterial, given its antibacterial activity. Besides, chitosan is considered as "Generally recognized as safe" (GRAS) food additive by the US Food and Drug Administration (FDA), wherewith can be considered as candidate for food related applications.

The current research work focuses on the production of chitosan nanospheres for the formulation of antibacterial food packaging materials. The research project was conducted in three phases. The first phase deals with the evaluation of different environmental, microbial and characteristics of chitosan on its antibacterial activity, when used in a discontinuous solid form, such as neat chitosan powder and flakes. The microbial activity was evaluated against one Gram-negative (*Escherichia coli*) and two Gram-positive strains (*Listeria innocua* and *Staphylococcus aureus*), which are commonly found in food spoilage. Results showed that chitosan requires a partial solubilisation for the exertion of the antibacterial activity. In addition, adequate temperature conditions, low ionic strength and the presence of a solid physical support may promote the antibacterial effect. *E. coli* strains were found to be more sensitive to chitosan, followed by *L. innocua* and *S. aureus*. On the other hand, antibacterial action increased with concentration up to a critical point above which this effect decreased. This effect may be due to remaining proteins in chitosan, which may serve as nutrients for the bacteria, limiting the antibacterial activity. These results are promising for the direct use of chitosan powder and flakes as antimicrobial agents for food packaging applications.

The second phase consisted in the production of chitosan micro and nanospheres via electrospraying. Solution and processing parameters effects on the morphology, particle collection and processing stability were investigated. Mapping of the processing stability was established according to the following dimensionless numbers: Reynolds (*Re*), electric Peclet (*Pe*), Weber (*We*), Froude (*Fr*) and an electrostatic force parameter (Ω) which related the main variables of the process. The stability in the electrospraying of chitosan solutions required relatively low values for *Re*, *Fr* and Ω but relatively high values for *Pe* and *We* numbers. The electrospraying process may provide a novel way for incorporating chitosan nanospheres into existing food packaging to provide antimicrobial properties, and helping to extend the shelf-life of food products.

The third phase investigated the effect of chitosan physical form and particle size, namely solution, powder and nanospheres on the antibacterial activity, against two pathogen strains, *Staphylococcus aureus* and *Salmonella enterica* serovar Typhimurium, commonly associated with foodborne infection. Chitosan nanospheres displayed superior antibacterial performance than chitosan powder, explained by their small size and the larger surface area of contact of nanospheres with bacteria cell wall. Nanospheres also displayed higher antibacterial activity than chitosan in solution, which may be the result of the higher surface charge and solid and small size. It is believed that even though chitosan in solution interacts with the cell wall, it will remain as a free form in the medium rather than adhering into cells permanently. On the other hand, *S. aureus* strains were more sensitive to the action of nanospheres and were less influenced by the pH and temperature conditions of the medium. Given the remarkable antibacterial activity observed for chitosan nanospheres, this study is of great importance with respect to the many possible applications, such as in food packaging and in the biomedical field.

TABLE OF CONTENTS

LIST OF TABLES

LIST OF FIGURES

LIST OF ABBREVIATIONS

AB	Antibacterial
AcOH	Acetic acid
ANOVA	Analysis of variance
ATR	Attenuated Total Reflectance Spectroscopy
BHI	Brain Heart Infusion broth
C^*	Critical chain overlap concentration
C_c	Critical concentration
C_e	Critical entanglement concentration
CFU/mL	Colony forming units per milliliter
CS	Chitosan
CA	Citric acid
DCM	Dichloromethane
DDA	Degree of deacetylation
DMF	*N*,*N*-dimethyl formamide
DLS	Dynamic light scattering
EDS	Energy Dispersive X-ray spectroscopy
EDTA	Ethylenediaminetetraacetic acid
EVA	Ethylene vinyl acetate
F	Flakes

Fr	Froude number
FTIR	Fourier transform infrared spectroscopy
GPC	Gel Permeation Chromatography
GuHCl	Guanidinium chloride
HCl	Hydrochloric acid
κ^{-1}	Debye-length
KBr	Potassium bromide
KCl	Potassium chloride
KOH	Potassium hydroxide
LA	Lactic acid
LB	Luria Bertani
$MgCl_2$	Magnesium chloride
MW	Molecular weight
NaCl	Sodium chloride
NaOH	Sodium hydroxide
NIR	Near-infrared spectroscopy
P	Powder
PAGE	Polyacrylamide gel electrophoresis
PDI	Polydispersity index

PBS	Phosphate buffer saline
PCL	Poly (caprolactone)
Pe	Electric Peclet number
PLGA	Poly (lactic-co-glycolic acid)
Re	Reynolds number
RH	Relative humidity
Ω	Electrostatic force parameter
SDS	Sodium lauryl sulfate
SEC	Size-exclusion chromatography
SEM	Scanning electron microscope
SSA	Specific surface area
TEM	Transmission electron microscopy
TFA	Trifluoroacetic acid
TGA	Thermogravimetric analysis
We	Weber number

LIST OF APPENDICES

CHAPTER 1: INTRODUCTION

For years, foodborne diseases have been of great concern to public health. Two factors have contributed to the appearance of new diseases as well as the re-emergence of old ones, representing a significant risk for food safety. The first one is the industrialization that has led to rapid-growing mass production and hence to an inadequate harvesting, storage, handling and transportation of food; and the second one is the globalization that has allowed international trade, facilitating the entry of pathogens that previously were not a threat for health [1, 2].

Canada is one of the countries whose population has been affected by the outbreak of pathogens resulting from contaminated food. Bacteria including *Escherichia coli*, *Salmonella*, *Listeria*, and *Staphylococcus* have been reported in spoiled products such as raw meat and pork, tainted cold cuts, oysters, cantaloupes, spinach and cheese, causing several pathogenic diseases [3, 4]. Foodborne infections are known to affect not only industrialized, but also non-industrialized countries [1]. The latter ones are particularly affected due to a wide range of diseases and the lack of governmental regulations regarding food inspection and handling.

On the other hand, there is an increasing public, industrial and governmental concern about food waste. About 30 to 40% of the world's food production is wasted before consumption either because of inappropriate handling and transportation which could cause contamination with bacteria, or because the food has reached its expiry date. North American and European countries are the most affected. Just in Canada, the losses in wasted food reach $ 31 billion each year [5].

Different methods including the use of volatile gas indicators, oxygen absorbers, carbon dioxide scavengers, preservatives, moisture absorbers, among others, have been employed to extend the shelf life, maintain or improve the conditions of the packaged food and therefore to decrease food waste. Some of them, although appropriate for keeping freshness, are insufficient for keeping the food free of microorganisms. Therefore, technological solutions are being targeted to provide better public protection, decrease the economic losses for industry and reduce food spoilage. The fabrication of novel food packaging materials having antibacterial properties can be part of the solution to inhibit/eradicate pathogen growth, improving food safety and extending shelf life of food products. In this regard, chitosan is a highly promising candidate to be employed as biomaterial in food related applications, mainly due to its availability, nontoxicity and antimicrobial properties.

The present research aims towards the production of chitosan nanospheres for the formulation of antibacterial food packaging materials. To date, different studies have focused in evaluating the antimicrobial activity of chitosan solutions, gels, fibers and films [6-18]. However, micro and nanosize morphologies that allow increasing chitosan/cell interactions are on the target in recent research [19-21]. The first part of the current study focuses on the evaluation of the antibacterial activity of chitosan in a discontinuous solid form such as neat chitosan powder and flakes. Different environmental, microbial and characteristics of chitosan including pH, temperature, ionic strength, the presence of a solid physical support, bacterial species, as well as the effect of chitosan concentration and purity are investigated. The second part comprises the study of producing chitosan micro and nanospheres via electrospraying. Both processing and solution parameters are subjected to consideration. The third part compares the effect of chitosan physical form and particle size, namely solution, powders and nanospheres on the antibacterial activity, against two pathogen strains (*S. aureus* and *S.* Typhimurium) commonly found associated with foodborne infection. In our first study, chitosan in powder and flake forms reduced totally *E. coli* contamination, but displayed a limited antibacterial activity against the pathogen strain *S. aureus*. Therefore, pathogen strains, which are considered more resistant to antibacterial agents were considered relevant for testing the antibacterial activity of chitosan nanospheres. Environmental conditions such as pH and temperature are also considered. Given the remarkable antibacterial activity observed for chitosan nanospheres, the electrospraying process may provide a novel way for making chitosan-based food packaging materials. The incorporation of chitosan nanospheres into existing food packaging may be an alternative to further increase chitosan antimicrobial properties and lead to the formulation of new packaging materials. This novel packaging can impact the food industry and consumers by providing a way to inhibit bacterial growth and increase the shelf life of food products, such as chicken, beef and pork.

In addition, the results of a research project aimed at the development of new chitosan-based materials for wound healing, is presented in Appendix A. This subject was part of an NSERC-Engage project that was conducted during the accomplishment of this PhD. The antibacterial properties of chitosan can be combined with the regenerative properties of bacterial nanocellulose for potential biomedical applications. However, given that the two biopolymers cannot be solubilized in the same solvent, their processing become challenging and coaxial electrospinning was considered, as a new approach.

The main contributions of this research work are found in three scientific articles; the first one has been published in the journal *Molecules*, the second one has been submitted to the *Journal of Aerosol Science*, and the third one has been published in the *Journal of Food Science*. In addition, a fourth article is included as an appendix (Appendix A) in the thesis and reports the findings of a work performed in an NSERC-Engage project and comprises the results regarding the coaxial electrospinning of chitosan and bacterial nanocellulose for potential biomedical applications. This article has been published in the journal *Cellulose*.

Organization of the thesis

This thesis consists of the following chapters:

- Chapter 1: Introduction
- Chapter 2: Literature review
- Chapter 3: Objectives
- Chapter 4: Organization of the articles
- Chapters 5 to 7: The three articles reporting the main results of this research project
- Chapter 8: General discussion
- Chapter 9: Conclusions and recommendations for future work
- Appendix A: The fourth article reporting the main results of the NSERC-Engage Project
- Appendix B: Governing equations in the electrospraying process

CHAPTER 2: LITERATURE REVIEW

2.1 Chitosan

Chitosan is a natural cationic polysaccharide derived from chitin, the second polysaccharide most abundant in nature after cellulose [22]. Chitin is a biopolymer extracted from the exoskeleton of marine crustaceans such as crab, shrimp and lobsters; cuticle of insects and cell walls of fungi, mainly [23, 24]. The shells of marine crustaceans are the more convenient sources given the availability from the wastes of the fishing industry [25]. Generally, shells contain between 15 to 40 % of chitin, 20 to 40 % of proteins and 20 to 50 % of calcium carbonate, besides pigments and metal salts as minor components [24]. Due to its low solubility in organic solvents and low chemical reactivity, chitin is usually transformed into chitosan [22, 26].

Industrially, chitosan is obtained after several processing steps as shown in Figure 2.1. First, crustacean shells are subjected to a demineralization step under acid treatment with HCl to dissolve calcium carbonate, calcium phosphate and other mineral salts. Second, an alkaline treatment with NaOH or KOH follows, to solubilize the proteins. Third, a discolouration step with NaOH and ethanol is often done to remove pigments. Fourth, after a washing and drying step, chitin is obtained. Finally, a deacetylation step under concentrated alkaline conditions (concentrated NaOH) produces chitosan, which is the most important chitin derivative in terms of applications [23, 24].

The quality and properties of chitosan products such as purity, molecular weight (MW) and degree of deacetylation (DDA) depend on the conditions and treatment used for its preparation, including the concentration of the chemicals used and the sequence and time of the treatments for deproteination, decalcification and deacetylation [26, 27]. Most commercial chitosan grades are mainly produced by alkaline deacetylation of chitin. Recently, enzymatic hydrolysis in the presence of chitin deacetylase have been used to produce chitosan [26]. However it is not yet available for industrial scale [27, 28]. When the degree of deacetylation (DDA) is higher than 50 % chitin is named chitosan [23, 29]. The DDA usually ranges from 66 to 96 %, depending on the method used for its production, whilst the molecular weight ranges from 4 kDa to 2000 kDa that is much lower than chitin, which is usually larger than 1000 kDa [26, 30-32].

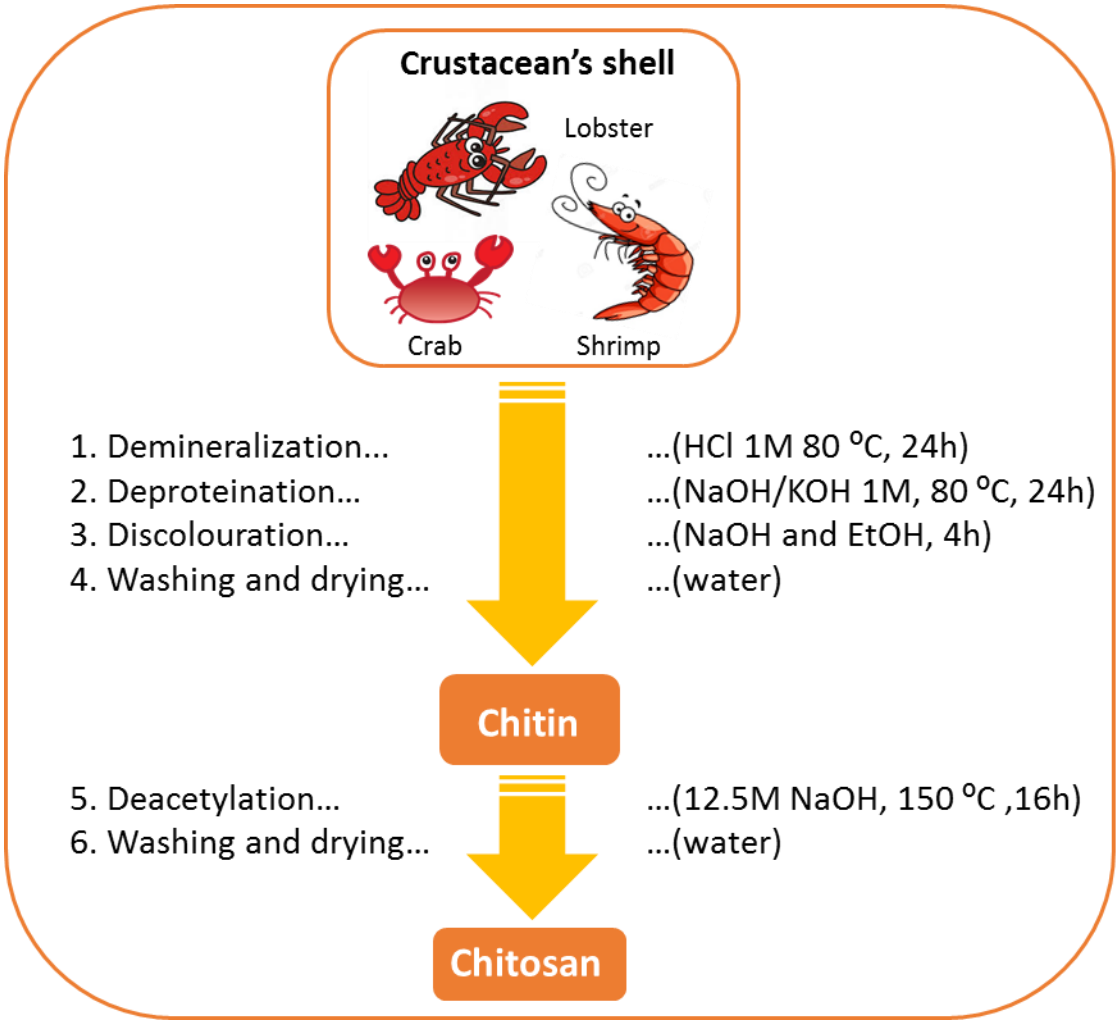

Figure 2.1: Industrial extraction of chitin and chitosan.

2.1.1 Elemental analysis

Depending on the extent of deacetylation, the nitrogen content of chitin and chitosan varies from 5 to 8% [25, 33]. Table 2.1 and Table 2.2 present the elemental analysis and trace metal content, respectively, in a chitosan sample [22, 34]. In addition to carbon, nitrogen and hydrogen, elements such as aluminum, calcium, silicon and iron are present in the material itself whilst chromium and copper come from the stainless steel reactor and distilled water respectively during processing [22].

Table 2.1: Elemental analysis (%) of chitosan and chitin; *N*-acetyl-glucosamine reference [34]. Adapted from [22].

Polymer	C	H	N
Chitosan	39.99	6.80	7.40
Chitin	43.53	6.12	6.26
N-acetyl glucosamine	43.53	7.15	6.26

Table 2.2: Trace metal content of chitosan (ppm) [35]. Adapted from [22].

Aluminum	5-50
Calcium	10-150
Copper	2
Iron	10-100
Lead	<10
Manganese	<1
Silicon	10-100
Titanium	<1
Silver	<1
Chromium	2.2
Cobalt	0.2
Zinc	0.3

2.1.2 Chemical structure

Structurally, chitin consists of 2-acetamido-2-deoxy-β-D-glucose through a β (1→4) linkage. Chitosan is the *N*-deacetylated derivative of chitin, however, this *N*-deacetylation is almost never complete [33]. Both the sequence and the content of the *N*-acetyl-D-glucosamine (acetylated unit) and D-glucosamine (deacetylated unit) in chitosan determine its properties and reactivity [32]. The structures of chitin and chitosan are presented in Figure 2.2.

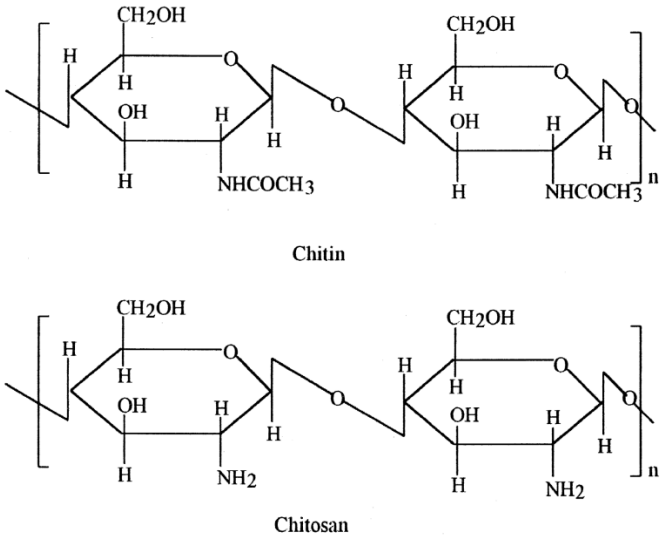

Figure 2.2: Structure of chitin and chitosan [25].

2.1.3 Solution properties

Due to the extensive intra- and intermolecular hydrogen bonding, and hydrophobic inter-chain interactions, chitosan degrades before melting, which makes it necessary to be dissolved in appropriate solvents [23, 25]. Chitosan is insoluble in water at neutral or basic pH values [22]. However, when the pH of the medium is lower than chitosan's pKa (6.2-6.5) [36, 37], amino groups undergo protonation making the polymer soluble in water [23, 26]. Chitosan is soluble in organic acids including formic, acetic, citric, pyruvic and lactic acid; and in inorganic acids such as nitric, hydrochloric, sulphuric and perchloric acids [22, 24, 38].

Chitosan solubility is mainly controlled by its DDA and MW. In general, the solubility increases at high DDA and low MW values. However, other parameters such as ionization degree, ionic strength, pH, type of solvent, concentration, chain flexibility, crystallinity, distribution of acetyl glucosamine units and time and temperature of the chemical deacetylation reaction may influence chitosan solution properties [23, 38-40]. In HCl and acetic acid, chitosan is soluble for a degree of protonation around 0.5 [39]. Chitosan solubility is reported for DDA>50% [41].

The viscosity of chitosan aqueous solutions is influenced by factors such as DDA (deacetylation time), MW, concentration, degree of protonation, ionic strength, pH and temperature [26]. In general, chitosan solution viscosity decreases with temperature and ionic strength; and it increases with chitosan concentration and MW [22, 38, 42-44]. However, a pH change in the polymer

solution may give different results depending on the types of acids employed [26]. With acetic acid, the viscosity of chitosan tends to increase with decreasing pH, whereas with HCl the viscosity decreases when pH is lowered. This relates to the degree of protonation of chitosan [26, 38, 45, 46]. In the first case, at low pH, intra and electrostatic repulsions due to protonation increase, hence promoting higher solubility, chain expansion and larger hydrodynamic volumes, which increase the viscosity. In the second case, also at low pH, the presence of large amounts of ions from a strong acid cause electrostatic charge screening (of the NH_3^+ groups), enhancing chain flexibility and hence decreasing viscosity [38, 46].

2.1.4 Antimicrobial properties

Chitosan exhibits suitable functional and biological properties, including antimicrobial activity [47]. Several authors have reported antimicrobial properties for chitosan under different physical forms including chitosan in solutions [6-10, 15, 16], gels [48], films [11-14, 17, 18], fibers [49-52] and micro and nanoparticles [19-21, 53-56], on different microorganism species [12, 18, 57, 58].

Literature reports chitosan antimicrobial effectiveness not only on inhibiting the growth of Gram-positive and Gram-negative [6, 59] bacteria but also yeast and molds [60]. The main difference between Gram-positive and Gram-negative strains is their membrane structure. Gram-positive strains are composed of one phospholipid bilayer and a thick peptidoglycan, whilst Gram-negative consist of two phospholipid bilayers and a thin peptidoglycan between them [51]. The antimicrobial properties of chitosan are affected by different factors: 1) microbial species and cell age [6, 61-63]; 2) environmental conditions such as pH, ionic strength, temperature and time [61, 63, 64]; 3) chitosan characteristics including source, MW, DDA, concentration and physical form [6, 16, 61, 62, 64-69]; among others.

The antimicrobial properties of chitosan have been used for food preservation. Ouattara *et al.* [14] demonstrated delayed growth or the complete inhibition of different kind of bacteria (including Enterobacteriaceae and *Serratia liquefaciens*) in processed meats covered with chitosan films and stored at 4°C up to 21 days. Bhale *et al.* [65] showed that albumin quality and eggs conservation increased by three weeks at 25 ºC in the case of eggs covered by chitosan coating solutions (pH 5.6). Coated eggs were overall acceptable to the consumer and did not differ from the control and commercial eggs regarding the organoleptic properties. Yingyuad *et al.* [60] dipped grilled pork samples in chitosan solutions with different chitosan concentrations and vacuum packaged. Their

results showed that the shelf life increased by at least two weeks compared to the samples that were not dipped. Throughout the storage period samples were found to be organoleptically acceptable and without significant changes in odour and colour.

Different pathogenic organisms including *Escherichia coli*, *Listeria* and *Salmonella* have been reported as being inhibited by chitosan, in contaminated beef, ham, turkey, sausages, pork and fish products [16, 60-62, 70, 71]. Chitosan also protected mice against infection by *Listeria monocytogenes*, suggesting that the antimicrobial action may also occurs in humans [72].

Muzzarelli *et al.* [59] reported the antibacterial effect of carboxybutyl chitosan on 298 pathogen strains including Gram-positive and Gram-negative bacteria and observed morphological damage of the cell wall and the internal cell structures. The bactericidal activity between the tested strains was different which suggested that different mechanisms of action of chitosan might be operating. However, the experiments were carried out with only a chitosan derivative, and results might differ in case of using unmodified chitosan.

Chitosan is also reported to be effective against yeast and molds. Roller and Covill [73] studied the antifungal properties of chitosan against 15 microorganisms (8 yeast and 7 filamentous fungi) associated with food spoilage, at different chitosan concentrations, pH and temperature conditions. Concentrations of 0.1, 1 and 5 g/l of chitosan were necessary to reduce the growth of *Zygosaccharomyces bailii*, *Mucor racemosus* and *Byssochlamys*, respectively. El Ghaouth *et al*. [74] reported the antifungal activity of chitosan coating on strawberry fruits inoculated with *Botrytis cinerea* and *Rhizopus stolonifer*. Although a complete inhibition of fungal growth was not achieved, chitosan coating reduced significantly spore germination and radial growth, and indicated that chitosan was fungistatic rather than fungicidal. These results assess the potential use of chitosan as natural food preservative.

Although the exact mechanism of the antimicrobial action of chitosan and its derivatives is still unknown, different mechanisms of growth inhibition have been proposed in literature [64, 75]:

1) Electrostatic interactions: at pH<pKa, chitosan amino groups are protonated, creating electrostatic interactions with the anionic cell wall components (lipopolysaccharides and proteins) of the microorganism.

2) The hydrophobic and chelating effects occurring at pH>pKa. *N*-acetylated chitosan and the presence of a long aliphatic chain in chitosan can favor the absorption onto cell walls via

hydrophobic interactions with cell wall proteins. As chelating agent, chitosan can selectively bind metals ions of the cell wall or from the medium, affecting bacteria stability and growth, respectively.

3) Inhibition of the synthesis of mRNA and DNA transcription, produced when small particle sizes and low molecular weight chitosan penetrate the cell wall of bacteria and combines with DNA.

4) Alteration of permeability, when high molecular weight chitosan or large size particles interact with cell surface blocking the entrance of essential nutrients to the cell or by forming an impermeable layer.

These mechanisms will eventually result in biological changes and the leakage of intracellular components, leading to cell death [32, 64].

As mentioned in 3) and 4), chitosan molecular weight can determine the mechanism of antimicrobial action, but also, the mechanism depends on bacterial type. Chitosan with molecular weight greater than 10 kDa have been found to inhibit bacterial growth regardless of its type [13, 66, 76]. Different studies [6, 10, 13, 67, 77] have demonstrated that, in general, chitosan antimicrobial activity increases with molecular weight when tested against Gram-positive bacteria, while for Gram-negative this activity is more efficient at low molecular weights.

With respect to molecular weight, two different mechanisms for the antimicrobial activity have been suggested: in Gram-positive bacteria, chitosan on the surface of the cell can form a polymer membrane, which inhibits nutrients from entering the cell. In Gram-negative ones, chitosan of low molecular weight might enter the cell through penetration, disturbing the physicochemical activities of bacteria cells until cell death [10, 78].

In addition, some authors reported higher effectiveness of chitosan against Gram-positive than Gram-negative bacteria, presumably due to the presence of lipid outer membrane in the latter that can be a barrier to chitosan. Others consider that Gram-negative bacteria are more sensitive to chitosan bioactivity because the negative charge on the cell surface of this bacteria is stronger than in Gram-positive, leading to more chitosan adsorbed and hence to a higher inhibitory activity [6, 7, 61, 63, 67, 75, 79].

Recently, Arkoun *et al.* [51] investigated the antibacterial mechanism of action for chitosan nanofibers. The results showed that chitosan nanofibers were both bacterial membrane

permeability disrupter and perforator. A series of four steps were proposed as the main mode of action for chitosan nanofibers. First, the adsorption of chitosan nanofibers onto bacterial surface; second, the perforation of the membrane; third, the leakage of cytosolic compounds including enzymes, proteins and DNA; and fourth, cell lysis and disintegration.

2.1.5 Processing

Chitosan is generally purchased in the form of fine powder, flakes or in solution, and can be processed into different physical forms through solubilisation in acidic media or by using an adequate solvent. Forms such as films [71, 80-83], fibers [84-89], micro and nanobeads [20, 31, 90-101], hydrogels [102-104], membranes [105] and sponge (foams) [106] of chitosan alone or in blends [105, 107-109] are produced by several technological processes for applications in different fields [110]. For instance, chitosan film is the most studied physical form with potential use as packaging material, given its promising results regarding the antibacterial activity [13, 18]. However, chitosan films have low mechanical and barrier properties, and therefore need to be blended with another polymer for the improvement of these properties [111, 112]. Chitosan films are generally produced by the solution casting/solvent evaporation method [60, 113], or by blending with a thermoplastic polymer via twin-screw extrusion [114-116].

Chitosan beads in the form of micro and nanospheres are of great interest in the biomedical field and are increasingly studied for drug delivery applications because of their small size and the large surface to volume ratio. Although the size of a nanoparticle is not clearly defined in literature, ASTM E2456-06 defines a nanoparticle as an ultrafine particle with at least one dimension in the range between 1 and 100 nm [117].

Several methods have been employed to produce micro and nanospheres of chitosan. The most used ones are emulsion cross-linking, coacervation/ precipitation, spray-drying, emulsion droplet coalescence, ionic gelation and electrospraying [30]. Others like reverse micellar [118] and sieving methods are less used [31]. The selection of any method depends upon factors such as particle size requirement, chemical and thermal stability and residual toxicity associated with the final product [31].

2.1.6 Applications

The unique properties of chitosan, including its nontoxicity [1] [26, 119], natural origin, biodegradability [26, 57], availability as well as the wide range of physical forms in which it could be transformed, are the main reason for its multiple applications. In particular, its antimicrobial properties [10, 16, 18, 63, 64, 120-122] and biocompatibility [6] make it of great interest in food packaging and biomedical applications, respectively. Chitosan has been approved as a food ingredient in Japan, Korea, Finland and Italy. In North America and Europe, it has received the "Generally recognized as safe" (GRAS) status by the US Food and Drug Administration (FDA), and has been used as food additive, nutritional supplement, natural health product and in drugs [32, 123, 124] . Other main applications of chitosan-based materials are cited in Table 2.3.

Table 2.3: Main applications for chitosan

Field	Application	References
Food sector	Food additive and preservative, antioxidant, emulsifying, thickener, cholesterol reductor, antibacterial coating, food packaging, dietary supplements.	[23, 26, 51, 61, 68, 71, 125, 126]
Biomedical	Anticoagulant, hemostatic, wound healing, wound dressing, encapsulation, antitumor, bone and cell culture, gene therapy, controlled drug delivery, engineering scaffolds.	[6, 23, 89, 106, 127-130]
Agriculture	Pesticide, fungicide, soil enrichment, seed coating.	[23, 71, 122, 131, 132]
Water and waste treatment	Membranes for water filtration (removal of metal ions such as Hg, Cd, Ni, Zn).	[23, 133, 134]

[1] On accounting of the low lethal dose (LD_{50}) value, which is in the same order of magnitude as the LD_{50} for sugar (16 and 30 g/kg body weight, for chitosan and sugar, respectively) [117].

2.2 Electrospraying process

Electrospraying is a method of electrodynamic atomization. Its principle is based on the theory of deformation of charged droplets developed by Lord Rayleigh in 1882, Zeleny in 1917 and Sir Taylor in 1964 [135, 136]. The schematic of a typical electrospraying setup is illustrated in Figure 2.3. The device consists of three main parts: a syringe pump that control the flow rate of the polymeric solution, a voltage generator (0 to 50 kV) and a metallic collector plate.

In electrospraying, a high voltage electric field is applied to a polymeric solution that is pumped through a syringe. The electric charge generated on the exiting liquid makes the droplet deforms into the shape of a Taylor cone from which a jet is ejected and elongated [92, 137, 138]. When the electrostatic forces in the fluid overcome the surface tension, the jet breaks into nano and micro droplets that eventually travel to a collector plate [30, 92, 139-141]. Different spraying modes can occur during electrospraying, the single cone-jet mode is the most desired because of its stability and reproducibility. Once the droplets are separated, the solvent is evaporated. Due to Coulomb repulsion of the charges, the droplets are well dispersed during the process [138].

Electrospraying is a relatively novel technique for the production of micro and nanospheres and its understanding and optimization are still under development [138]. There are four advantages in the use of electrospraying with respect to other conventional methods for the production of micro and nanoparticles: 1) one step processing which usually does not require extra drying; 2) no need for external dispersion/emulsion phase containing undesirable materials (generally toxic) for biomedical and food applications; 3) no high temperatures as in spray drying; and 4) better control over particle size, particle size distribution and morphology than in other methods. In the case of chitosan, which has the advantage of being soluble in aqueous acidic solutions, it avoids the use of hazardous organic solvents for the fabrication of micro and nanoparticles [92, 137].

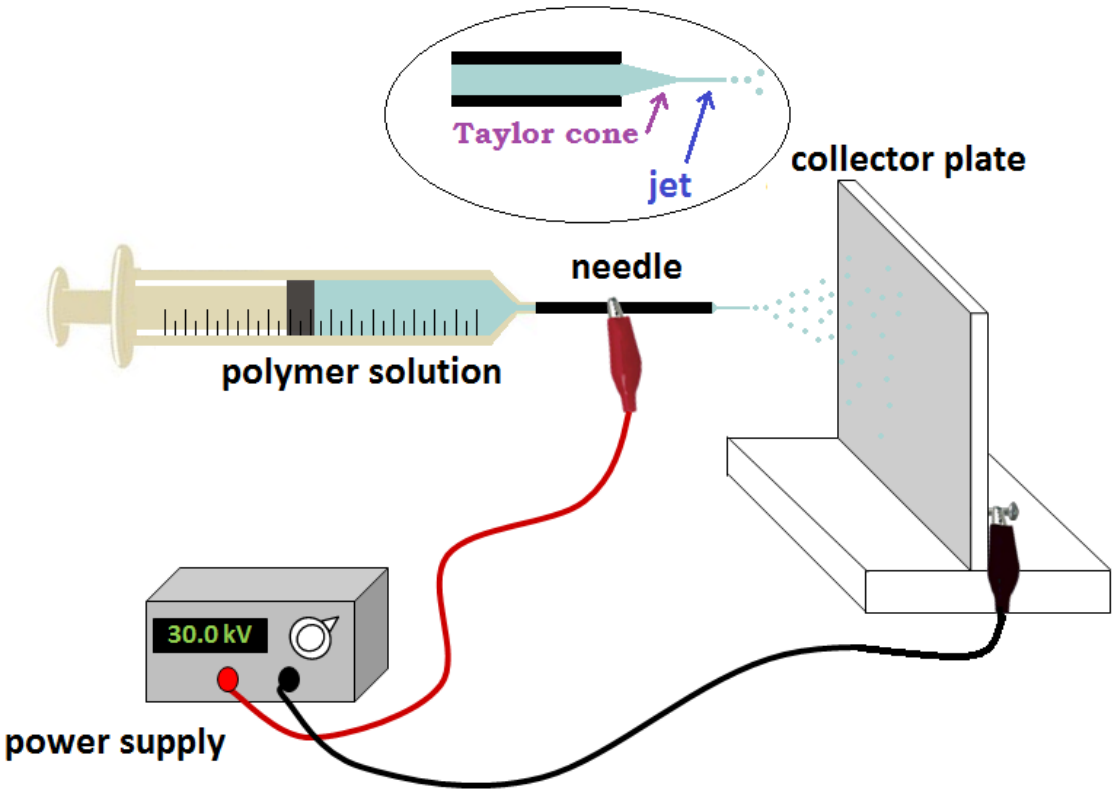

Figure 2.3: Electrospraying process

2.2.1 Parameters of the process

Table 2.4 shows the electrospraying processing parameters. Important parameters are not only polymer and solution properties such as molecular weight, concentration, viscosity, conductivity and surface tension, but also specific parameters of the electrospraying machine such as applied electric voltage, flow rate, tip-to-collector distance, temperature, needle gauge and the environmental conditions. All these parameters may affect the processing, size, morphology and reproducibility of the produced micro and nanospheres [86, 138, 142-144].

Table 2.4: Parameters for the processing via electrospraying

Processing conditions	Electric field	Voltage Distance tip to collector
	Flow rate Needle diameter Temperature	
Intrinsic properties of the solution	Conductivity Surface tension Viscosity	Concentration MW Solvent type
Ambient conditions	Humidity Temperature Pressure Air velocity	

2.2.1.1 Processing conditions

Electric field strength. The electric field strength (kV/cm) generally varies between 1 and 5 kV/cm. The currents that flow during the electrospraying process range from a few hundred nanoamperes to microamperes [145]. Voltages between 15 to 30 kV and distances between 5 to 25 cm are usually used. Short distances between needle and plate collector can generate a wet deposition of particles, causing coalescence of droplets. The shortest distance is determined as the distance that produces a shortcut. The optimum distance is the one that assures the complete evaporation of the solvent, the collection of the particles and a morphology with a narrow polydispersity [92, 137, 138].

Flow rate. This parameter along with solution parameters (polymer concentration and molecular weight, solvent type and conductivity) can control polymer entanglements and particle formation. A high flow rate can cause the formation of secondary and satellite droplets and produce particles with high polydispersity. An optimal value for the flow rate is essential in order to achieve higher

evaporation of the solvent and to avoid droplets clustering. [138]. Literature reports a wide range of values from 0.003 to 30 mL/h, for the electrospraying of different materials [146].

Needle gauge. Needle diameter is inversely proportional to its gauge. This is an important parameter in order to avoid coalescence of droplets and to have a reasonable collection and better particle formation. While lower needle gauge produces sputtering and broader size distributions, higher gauges allow narrowing the particle size range. Common needle gauges lie between 16 and 26 (1.194 and 0.260 mm, internal diameter, respectively) [137], although lower sizes in the order of 100 μm of internal diameter have also been reported [145].

Temperature. In general, the electrospraying process is conducted at ambient temperature. An increase in solution temperature can be favorable to the process because it decreases the surface tension and the viscosity of the solutions. An increase in temperature can also lead to a faster evaporation of the solvent, affecting particle size and morphology [147].

2.2.1.2 Intrinsic properties of the solutions

In general, variables such as polymer and solvent concentration, molecular weight, DDA (in the case of chitosan) affect the viscosity, surface tension, conductivity and chain entanglement, and influence the electrospraying process [143, 144].

Polymer concentration. As opposed to electrospinning where higher polymer concentrations are employed to form continuous fibers, the electrospraying process requires relatively low polymer concentrations to generate micro and nanoparticles [137]. Two concentrations, the one associated with critical chain overlap, C^*, and that for critical entanglement, C_e, determine the production of fibers or spheres [143] (see Figure 2.4). A dilute regime is obtained when polymer concentration is less than C^*, where there is no entanglement formation (Figure 2.4a). At higher polymer concentrations, the semi dilute unentangled regime is achieved and some entanglements are observed, but they are not sufficient to maintain the morphology of the droplets (Figure 2.4b). Well-defined droplets are obtained at the semi-dilute moderately entangled regime (Figure 2.4c), at polymer concentrations in the range $C_e<C<3C^*$; beyond this concentration, fiber emergence is attained [84, 92, 138, 143]. Stable fiber formation occurs at more than 2.5 entanglements per chain, or as $C>>C^*$ [143, 148] and increases with chitosan concentration [142].

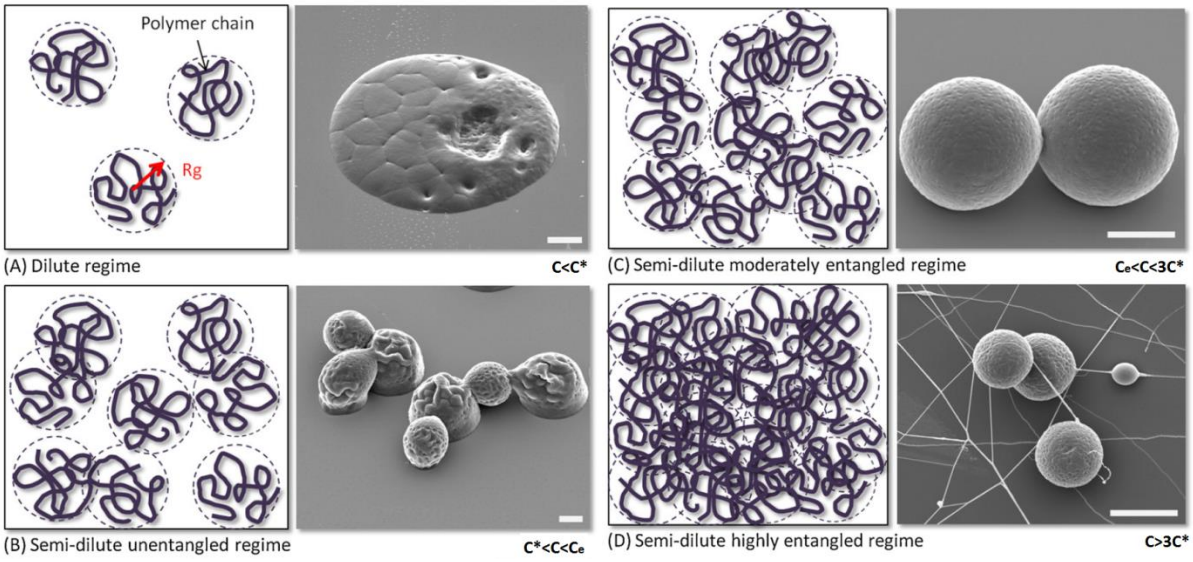

Figure 2.4: Physical representation at the molecular level of various entanglement regimes obtained for different polymer concentrations. C^*: critical chain overlap concentration, C_e: critical entanglement concentration. Adapted from [138]

Polymer molecular weight. In the same manner than concentration, molecular weight affects the value of the critical concentration at which beads and fibers are obtained from the process; however, this concentration should be below the one of process limiting viscosity [86]. Both molecular weight and concentration influence particle size and morphology owing to viscosity [149, 150]. Beads and fibers are generally formed at low and high molecular weights, respectively [86]. Molecular weight has also a significant effect on the rheological and electrical properties such as surface tension, viscosity and conductivity.

Solvent. Solvents with high vapor pressure (low boiling temperatures), which are highly volatile, are preferred in electrospraying. However, a fast evaporation of the solvent could hinder the diffusion of the polymer in the electrosprayed droplets and may lead to the formation of pores and hollow particles. The solvents more frequently used in electrospraying are acetone, acetic acid, acetonitrile, chloroform, 1,2-dichloroethane, dichloromethane (DCM), ethanol and *N*,*N*-dimethyl formamide (DMF), which can be used alone or combined [138]. Solvent concentration affects the morphology of electrosprayed droplets. Deposited particles with irregular shape can be obtained due to the solvent that is not evaporated before droplets reach the collector plate [138]. However, low concentrations of solvent may produce a phenomenon called sputtering, which affects process

stability and droplets deposition [137]. Remaining solvent content must be within the limits of safety standards. Solvent has also an important role in determining the conductivity of the electrosprayed solutions, a parameter that must be taken into account for the optimization of the process [138].

Viscosity. Viscosity along with conductivity are the dominant solution characteristics for the electrospraying process [142]. Spinning or spraying can be achieved depending on this value [144]. In general, low viscosity polymer solutions allows for droplets formation. However, relative low concentrations and hence low viscosities could limit the formation of the spherical shape and hinder the shrinkage of droplets during solvent evaporation [138, 151]. High viscosity solutions shift the cone-jet mode to higher voltages. Particle size can be controlled by the solution viscosity and operation parameters. A decrease in viscosity or an increase in conductivity decreases the particle size [138].

Surface tension. Surface tension is mainly affected by the solvent type and concentration, while being less influenced by polymer concentration [86]. A low surface tension of the solution along with a low conductivity is needed to obtain a stable process and the single cone-jet mode [138, 142]. Droplet and fiber formation can be determined by means of this parameter [86].

Electrical conductivity. Low electrical conductivity values are preferred in order to obtain the single cone-jet mode and a stable process [138, 142]; however, too low values can be unfavorable for the process [149] and a value of at least 0.01 μS/m is required for the current to flow [138]. When small particle sizes are required, an increase in the conductivity can lead to their formation due to enhanced Coulomb repulsion, but sufficient viscosity is needed to ensure that entanglement forces remains higher than the Coulomb ones to maintain the stability of the process [138, 142]. The solvent is the main parameter influencing the conductivity of the solutions [138].

2.2.1.3 Ambient conditions

Parameters such as field strength, conductivity and flow rate of the polymer solution affect the stability of the jet cone. Morphology and size of the droplets are mainly affected by concentration and molecular weight of the polymer, flow rate, vapor pressure of the solvent, electrospraying distance and environmental conditions of the chamber, including humidity, temperature, atmospheric pressure and air velocity [138].

High temperature conditions promote the rapid removal of the solvent affecting the particle size and shape. The rate of solvent evaporation and the solidification of the electrosprayed particles can also be influenced by atmospheric pressure, humidity and air velocity [152].

2.2.2 Governing equations of the process

The steady jet in electrospraying is governed by four steady state equations representing the conservation of mass and electric charges, the linear momentum balance and the Coulomb's law for the electric field [153, 154]. The complete development of the equations is shown in Appendix B.

- Mass conservation:

$$v\pi R^2 = Q$$

- Electric charge conservation:

$$\pi R^2 KE + 2\pi R v\sigma = I$$

- Momentum conservation:

$$\rho v v' = \frac{T'}{\pi R^2} + \frac{\sigma\sigma'}{\bar{\varepsilon}} + (\varepsilon - \bar{\varepsilon})EE' + \frac{\gamma}{R^2}R' + \rho g + 2\frac{\sigma E}{R}$$

- Coulomb's law for electric field:

$$E(z) = E_\infty - \ln\left(\frac{L}{R_0}\right)\left[\frac{4\pi}{\bar{\varepsilon}}\frac{d(\sigma R)}{dz} - \frac{1}{2}\left(\frac{\varepsilon}{\bar{\varepsilon}} - 1\right)\frac{d^2(ER^2)}{dz^2}\right]$$

where (in order of appearance) v is the axial velocity of the jet, R is the radius of the jet, Q is the flow rate, K is the conductivity of the solution, E is the axial component of the electric field inside the jet evaluated at the surface, σ is the surface charge density, I is the current carried by the jet, ρ is the solution density, T is the tensile force in the jet, $\bar{\varepsilon}$ is the dielectric constant of the air, ε is the dielectric constant of the jet, γ is the surface tension, g is the gravity, $E_\infty$is the external electric field, L is the length of the jet, R_0 is the initial radius of the jet (needle), z is the flow direction, and the variables containing the symbol " $'$ " refer to the derivative of the respective variables.

2.2.3 Electrospraying of chitosan

Many studies have successfully synthesized uniform particles of polymers such as poly (lactic-co-glycolic acid) (PLGA), poly (caprolactone) (PCL) and ethylene vinyl acetate (EVA) via the electrospraying process [92, 139-141]. However, relatively few studies have considered the electrospraying of chitosan solutions [137, 142, 155], despite the extensive investigations published regarding its electrospinnability and fiber formation [86, 89, 156-159].

The electrospraying of chitosan can be considered as a promising technique for the synthesis of defined size micro and nanoparticles. One of the main advantages is that chitosan is soluble in acetic acid, which is a nontoxic solvent with a low vapor pressure, which is desirable for the processing. Other advantages regarding the processing and final morphology obtained were exposed in Section 2.2. In addition of being a one-step process that does not require extra drying steps nor high temperature conditions, electrospraying allows to have better control over particle size, particle size distribution and morphology than with other conventional methods for micro and nanoparticle formation. However, the number of parameters for its optimization can be a complex task, and is a subject of ongoing research.

To date, studies relating the electrospraying ability of chitosan have been mainly focused on the determination of the processing parameters for particle formation [137, 142, 155]. The study of the intrinsic properties of chitosan solutions for the optimization and the complete understanding of this process started to be addressed recently. Kuo *et al.* [155], Arya *et al.* [137] and Zhang *et al.* [142] evaluated the effect of different processing or solution parameters to control particle size and particle size distribution. Their studies comprised the analysis of one chitosan grade characterized by a given MW and DDA. Chitosan particles with sizes in the range of 124 to 940 nm in diameter were reported. Recently, Gómez-Mascaraque *et al.* [160] described the effect of chitosan molecular weight on the electrospraying of chitosan microspheres, and its correlation with electrical conductivity, viscosity and surface tension of the solutions. No processing parameters were studied and chitosan with only one DDA was considered in their study. In addition, the viscosity of the solutions was studied at a particular shear rate of 200 s^{-1}, which is far from the one calculated, given the flow rate and needle size, in real electrospraying conditions (would be around 0.6 s^{-1} when considering their processing conditions).

Despite the few studies available on the electrospraying ability of chitosan, some information can be obtained from electrospinning, which has been a subject of numerous studies. For instance, Geng *et al*. [86] obtained chitosan beads when electrospinning chitosan/acetic solutions having different polymer and acetic acid concentration and with chitosan of different molecular weights. Beads were obtained for chitosan solutions prepared with a chitosan molecular weight of 106 kDa, at a concentration of 7 wt% and with acetic acid concentrations of less than 30 wt%. For a chitosan molecular weight of 30 kDa and 10 wt% of chitosan, 90 wt% of acetic acid content was needed.

2.3 Summary

The state of the art presented above shows that chitosan is a promising candidate for the formulation of new antibacterial food packaging materials because of its nontoxicity and antimicrobial properties. Up to now, the reported research has mainly pointed to the study of chitosan films, fibers and solutions, the latter being impractical for real industrial applications. Hence, there is still room for the study of the antibacterial activity of chitosan powder and flakes, which may be of industrial interest because no processing step is involved. In addition, few studies have been addressed on the evaluation of the antibacterial activity of chitosan micro and nanospheres. Moreover, the study of the physical form to optimize its antibacterial properties has not been conducted yet, nor the effect of pH, temperature and pathogen species. These latter parameters are of particular interest for practical and real applications in food industry.

On the other hand, the operating window and the influence of both processing and solution parameters for the electrospraying of chitosan solutions is still undetermined. It is needed to establish the proper relations between chitosan solutions and processing parameters to have an optimized process. This process has been recently studied with other polymers in drug delivery applications due to many of its advantages with respect to the conventional methods for micro and nanoparticle formation. The electrospraying process may provide a novel way for making chitosan-based food packaging materials. The direct electrospraying of chitosan solutions into conventional packaging materials (such as polyethylene, polypropylene, aluminium films, etc.) attached to a grounded collector, may allow the incorporation of chitosan nanoparticles and provide antimicrobial properties.

CHAPTER 3: OBJECTIVES

According to the literature review presented in Chapter 2, chitosan is a promising candidate for the formulation of new antibacterial food packaging materials. However, the antibacterial properties of chitosan in the solid state have not been addressed, nor the influence of its physical form. On the other hand, the operation window for the fabrication of chitosan micro and nanoparticles via electrospraying is still lacking. It is needed to establish proper relationships between chitosan solutions and processing parameters in order to have an optimized process. The main objective of this research is:

"To produce chitosan micro and nanospheres via the electrospraying process for the formulation of new antibacterial chitosan-based food packaging materials"

The specific objectives of the current research work are:

1) To identify the main factors affecting the antibacterial activity of chitosan in a discontinuous solid form, such as chitosan powder and flakes.

2) To study the influence of solution and process parameters on the electrospraying ability of chitosan and mapping the process stability and droplet formation.

3) To produce chitosan micro and nanospheres via electrospraying for study the effect of chitosan physical form (flake, solution, micro and nanospheres) on the antibacterial activity.

CHAPTER 4: ORGANIZATION OF THE ARTICLES

The following three chapters comprise the articles containing the main scientific findings of this study and represent the core of the thesis, which is presented in the form of three peer-reviewed journal papers.

Chapter 5 presents the results of the first paper "*Antibacterial Activity of Neat Chitosan Powder and Flakes"* that has been published in *Molecules* (VOL. 22, NO. 1, 100, 2017) (impact factor = 2.749). This journal was chosen because it is one of the leading journals that focuses on natural products and their properties. This paper was published in the special issue: "Antibacterial Materials and Coatings" on January 6th 2017. The manuscript investigates the influence of different environmental, microbial and intrinsic factors on the antibacterial activity of chitosan in a discontinuous solid form, such as powder and flakes. Factors including temperature, ionic strength, the presence of a solid physical support and chitosan purity are studied. A direct usage of chitosan in these forms may be of industrial interest because no processing step is involved. From the aforementioned factors, temperature, salt concentration and bacterial species are known to be the most critical in food spoilage and the most relevant in food preservation, and are considered altogether in this work. This systematic study was important to deepen our comprehensive understanding of chitosan antibacterial action and to broaden its activity and applicability.

Chapter 6 presents the results of the second paper "*Chitosan electrospraying: Mapping of process stability and droplet formation*" that has been submitted to *Journal of Aerosol Science* (impact factor = 2.627). This journal was selected because it is one of the most important journals in publishing works related to electrostatics and particulate matter. The manuscript investigates the influence of processing and solution parameters on the processability of chitosan solutions and particle collection and morphology of chitosan nanoparticles. In addition, the mapping of the stability of the processing was established by means of the dimensionless Reynolds, electric Peclet, Weber and Froude numbers and the electrostatic force parameter, which relate the main variables of the process.

Chapter 7 contains the results of the third article "*Effect of Chitosan Physical Form on Its Antibacterial Activity Against Pathogenic Bacteria*" that has been published in *Journal of Food Science* (VOL. 88, NO. 3, 679-686, 2017) (impact factor = 1.649). This journal was selected because it addresses research in the area of food microbiology and safety, nanoscale food science,

engineering and nanotechnology. This article was published on January 31st 2017. The manuscript investigates the antibacterial activity of chitosan nanospheres against two foodborne pathogens: *Staphylococcus aureus* and *Salmonella enterica* serovar Typhimurium at different pH and temperature conditions. In addition, the effect of chitosan physical form on its antibacterial activity is studied. Even though the antibacterial activity of chitosan has been widely studied, no report had compared the effect of particle size nor had analyzed the effect of pH and temperature on the antibacterial activity of chitosan nanospheres, to the best of our knowledge. This study was of great importance regarding the many possible applications, such as in food packaging and in the biomedical field.

Additionally, Appendix A presents the results of a fourth paper "*Chitosan-bacterial nanocellulose nanofibrous structures for potential wound dressing applications"* that has been published in *Cellulose* (VOL. 23, NO. 5, 3089-3104, 2016) (impact factor = 3.195). This journal was chosen because it is the leading journal devoted to the scientific research in the area of cellulose and related naturally occurring polymers such as chitosan. This paper was published on August 1st 2016. This manuscript investigates the processing via coaxial electrospinning for the development of nanostructures containing both chitosan and bacterial nanocellulose for potential wound dressing applications. The antibacterial properties of the obtained fibers mats were investigated against a non-pathogen strain of *E. coli*.

CHAPTER 5: ARTICLE 1: ANTIBACTERIAL ACTIVITY OF NEAT CHITOSAN POWDER AND FLAKES

Nury Ardila[1], France Daigle[2], Marie-Claude Heuzey[1] and Abdellah Ajji[1]

[1] Research Center for High Performance Polymer and Composite Systems (CREPEC), Department of Chemical Engineering, Polytechnique Montréal, P.O. Box 6079, Station Centre-Ville, Montréal, QC H3C 3A7, Canada

[2] Department of Microbiology, Infectiology and Immunology, Pavillon Roger-Gaudry, Université de Montréal, P.O. Box 6128, Station Centre-ville, Montréal, QC H3C 3J7, Canada

(This work was published online in *Molecules* on January 6th, 2017)

5.1 Abstract

This study investigates the antibacterial activity of chitosan powder and flakes against three different bacterial species, *Escherichia coli*, *Listeria innocua* and *Staphylococcus aureus*, which are frequent causes of food spoilage. The effect of chitosan concentration and purity, as well as the influence of temperature, ionic strength (salt) and impact of a solid physical support in the medium are examined. Results show that the antibacterial activity of neat chitosan: (i) requires partial solubilisation; (ii) can be promoted by environmental factors such as adequate temperature range, ionic strength and the presence of a solid physical support that may facilitate the attachment of bacteria; (iii) depends on bacterial species, with a sensitivity order of *E. coli* > *L. innocua* > *S. aureus*; and (iv) increases with chitosan concentration, up to a critical point above which this effect decreases. The latter may be due to remaining proteins in chitosan acting as nutrients for bacteria therefore limiting its antibacterial activity. These results on the direct use of chitosan powder and flakes as potential antimicrobial agents for food protection at pH values lower than the chitosan pKa (6.2–6.7) are promising.

5.2 Introduction

Chitin is a cellulose-like biopolymer consisting of linear chains of predominantly β-(1→4)-2-acetamido-2-deoxy-D-glucose (also named *N*-acetyl-D-glucosamine) residues. Due to its low solubility in organic solvents and low chemical reactivity, chitin is usually transformed into chitosan. Chitosan, the deacetylated form of chitin, is a polysaccharide composed mainly of repeating β-(1 → 4)-2-amino-2-deoxy-D-glucose (or D-glucosamine) units. Several properties of chitosan, including its natural origin, abundance, biodegradability, availability, biocompatibility, mucoadhesivity and reactivity make it attractive in different fields (biomedical, food industry, cosmetology, water purification, among others) [1–3]. In particular, its antimicrobial properties [4–6] along with its non-toxicity [7] make it of great interest in the food protection area [8–12].

Although inherent, the antimicrobial properties of chitosan are affected by different factors. Kong, Chen, Xing and Park [4] have classified most of them into four different types, namely: (1) microbial factors, including microorganism species and cell age; (2) environmental factors such as pH, ionic strength of the medium, temperature and reaction time; (3) intrinsic characteristic of chitosan, such as positive charge density (associated with degree of deacetylation, DDA), molecular weight (MW), chelating capacity, hydrophobic/hydrophilic characteristics and (4) physical state, specifically solution or solid state. Although different authors have evaluated the effects of some of the aforementioned factors on the antimicrobial activity of chitosan solutions [2,5,6,13–17], films [18–20], fibers [21–24], micro- and nanoparticles [25–28], to our knowledge no study has reported the inhibitory effect of chitosan in a neat discontinuous solid state, such as powder and flakes, nor on its mode of action. A direct usage of chitosan in these forms may be of industrial interest because no processing step is involved. Moreover, a systematic study of chitosan in this state is necessary for a deeper understanding of its antibacterial (AB) action and to broaden its activity and applicability. For example, processed discontinuous solid forms of chitosan such as micro- and nanobeads may be of significant interest in the development of new chitosan-based food packaging materials, but this is beyond the scope of the present work. On the other hand, the mode of antimicrobial action of chitosan powder and flakes may be considered different from the one for chitosan nanoparticles, given the special character of the latter such as their small size and high surface area, as well as the possibility to enter the cells through perfusion [26,29].

Furthermore, while factors such as pH, medium type, bacterial species, and chitosan concentration, MW and DDA have been widely studied for chitosan in solution [2,5,6,13,14,16,17], others such as temperature, ionic strength, the presence of a solid physical support and chitosan purity have received less attention. From the aforementioned factors, temperature, salt concentration (ionic strength) and bacterial species are known to be the most critical in food spoilage and the most relevant in food preservation, but have not been thoroughly considered altogether in chitosan-related studies and therefore are investigated in the present study. Apart from the above, humidity, which is known to be one of the major factors deteriorating the properties of food and accelerating the formation of undesirable organisms, will not be considered in the current research but in future investigations.

In this work, we examine the effect of different critical factors affecting food spoilage and preservation on the AB activity of chitosan in a neat discontinuous solid state (powder and flake-like forms), and under carefully controlled experimental conditions. More specifically, the influence of environmental and microbial factors such as temperature, ionic strength, the presence of a solid physical support, and bacterial species are investigated. Moreover, the effects of chitosan concentration and purity are analyzed. The results show that chitosan in powder and flake form exhibit a high antibacterial activity under conditions close to those of found in contaminated food products. Nonetheless, this activity can be affected positively or negatively by factors such as temperature, ionic strength, chitosan concentration, purity and bacterial species.

5.3 Results and Discussion

Table 5.1 presents the DDA, MW, polydispersity (PDI), moisture, ash and protein content as well as particle size values of the chitosan (CS) powder (P) and flakes (F) used. Chitosan flakes and powder have a DDA of 90% and 95%, respectively. In average, samples contain 9 wt/v % of moisture and low ash content (0.05%). In addition, chitosan flakes and powder include 8.8 and 176 mg of proteins per gram of chitosan, respectively. According to the suppliers both grades come from the same source (shrimp shells), hence differences in purity may be related to the conditions of the chemical treatment when transforming chitin into chitosan, including the sequence for deproteinization, decalcification and deacetylation, the concentration of the chemicals used and the soaking time [30,31].

Table 5.1: Chitosan grades.

CS Grade [a]	DDA (%)	MW (KDa)	PDI	Moisture (%)	Ash (%)	mg Protein/ g Chitosan	Mean particle size (μm)[d]
F-90-207 [b]	90	207	1.7	8.1 ± 0.2	0.05 ± 0.02	8.8 ± 0.2	670 ± 400
P-95-57 [c]	95	57	2.2	9.8 ± 0.1	0.05 ± 0.01	175.7 ± 0.3	55.1 ± 43.7

[a] First letter in the nomenclature indicates F-flakes, P-powder; the first number the DDA (%) and the second one the average molecular weight (Mw, KDa). [b] Biolog GmbH. [c] Primex. [d] Normal.

Regarding the MW and PDI, samples exhibit a weight average MW of 207 and 57 kDa and polydispersity indices of 1.7 and 2.2, respectively, which may also be related to different conditions during chemical treatment. Figure 5.1 presents the cumulative weight and number fraction as function of molar mass for chitosan. Chitosan flakes (F-90-207) have a narrower size distribution than chitosan powder (P-95-57). In addition, about 5% of chitosan flakes show a molecular weight between 30 to 50 kDa, whilst about 10% of the chitosan powder has a molecular weight near 10 kDa, which may indicate the presence of chitooligosaccharides.

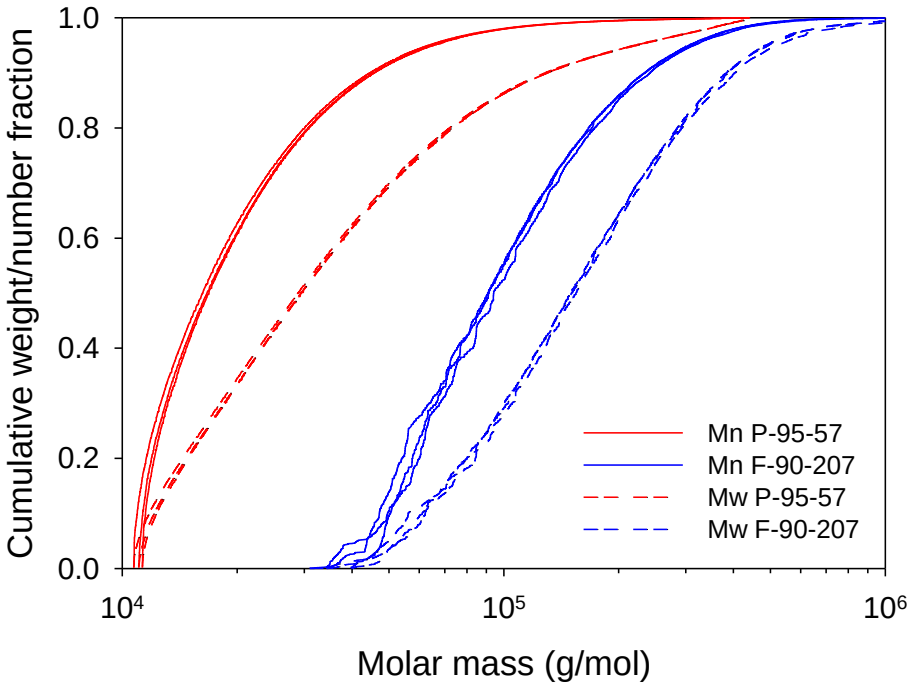

Figure 5.1: Cumulative weight (Mw)/number (Mn) fraction as a function of molar mass for chitosan powder and flakes.

5.3.1 SEM

5.3.1.1 Elemental Analysis

Table 5.2 presents the elemental analysis of chitosan. In addition to carbon, nitrogen and oxygen, chitosan samples (both powder and flakes) contain traces (in ppm) of sodium, calcium, chlorine, cobalt and magnesium, probably remaining from chitin and the different stages of the extraction and purification processes [32].

Table 5.2: Elemental analysis via EDS-SEM in chitosan grades.

Chitosan	Element										
	C	N	O	Na	Ca	Mg	S	Si	Co	Al	Cl
F-90-207	X	X	X	X	X	X		X	X	X	X
P-95-57	X	X	X	X	X	X	X		X	X	X

X indicates the elements present in the sample

5.3.1.2 Particle Size, Thickness, Shape and Particle Size Distribution

Figure 5.2 presents SEM micrographs of the chitosan samples. Their average particle size and particle size distribution are shown in Table 5.1 and Figure 5.2, respectively. According to the micrographs, chitosan flakes, which are of the order of millimeter size, present a thickness of 21.2 μm, an irregular shape, and higher particle size values and broader particle size distribution than the powder grade. In the case of powder, distribution is right-skewed and particles are of micrometer size (55 μm, in average). Considering both chitosan in flakes and powder as spheres having a bulk density of 0.3 g/cm^3 [33], the specific surface area varies from 0.03 (flakes) to 0.36 (powder) m^2/g (Figure 5.2). The specific surface area is considered an important factor for the antibacterial activity.

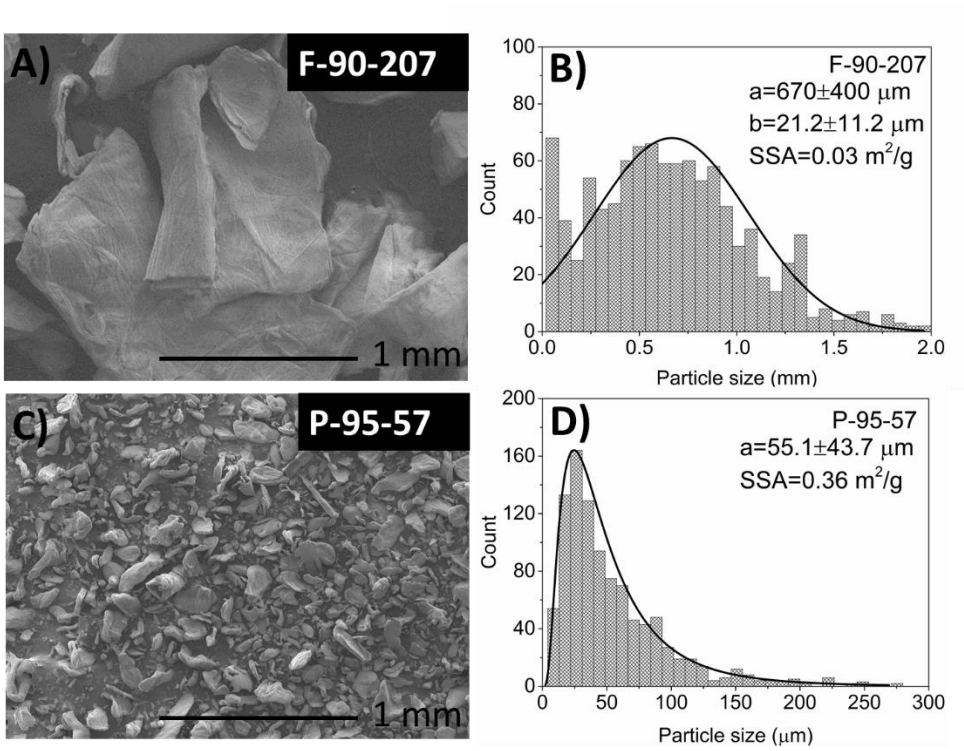

Figure 5.2: Chitosan in flakes and powder form (A, C) and their particle size distribution (B, normal distribution and D, log-normal distribution). The symbols a, b and SSA (in Figures B and D) represent the average particle size, thickness and the specific surface area, respectively. This figure has been modified with respect to the original article.

5.3.2 Antibacterial Assays

5.3.2.1 Effect of Chitosan Concentration

Figure 5.3 shows the effect of chitosan concentration for the two chitosan grades, when suspended in PBS. According to the results, the AB activity of chitosan increases with concentration up to a certain value, named the critical concentration, C_C, after which this activity decreases. The C_C was found to be between 0.4 and 1.2 wt/v % without any apparent pattern regarding DDA, MW, bacterial species or medium. The loss of antibacterial activity of chitosan powder and flakes at high chitosan concentrations is mainly related to impurities in the chitosan samples, as will be discussed below.

It is noteworthy that: (i) the pH of the medium varied between 5.8 and 7.0 after the incorporation of chitosan (0.01%–0.5% pH 5.8; 0.5%–1.0% pH 6.2; 1.0%–2.0% pH 6.5 and 2.0%–4.0% pH 7.0)

to the PBS medium (pH 5.8), which is mainly related to the increase of protonated chitosan amino groups (NH_3^+) and (ii) bacterial population in the control remained invariable in this pH range.

Protonation may also cause partial solubility of chitosan suspensions, given the pH of the medium. The potential solubility of chitosan powder and flakes during the AB tests was verified qualitatively by ATR spectroscopy, at a chitosan concentration of 0.4 wt/v %. Figure 5.4 compares the FTIR spectra of PBS with the filtrate of chitosan suspensions subjected to the same conditions as in the AB tests at 7 and 37 °C. Solubility of chitosan suspensions was confirmed given the identification of the main characteristic peaks of chitosan at 1345, 1420, 1560, 1655 and 3290 cm^{-1}, which correspond to a CO–NH deformation and to CH_2 group (amide III); C-H_2 stretching bending; amide II band and the N–H stretching of amine II; $CONH_2$ group and stretching of C=O (amide I); and –OH and –NH stretch, respectively. In particular, the amide I bands at 1655 cm^{-1} or the amide II band at 1560 cm^{-1} are identified as characteristic *N*-acetylation bands associated with amine and amide groups [34,35].

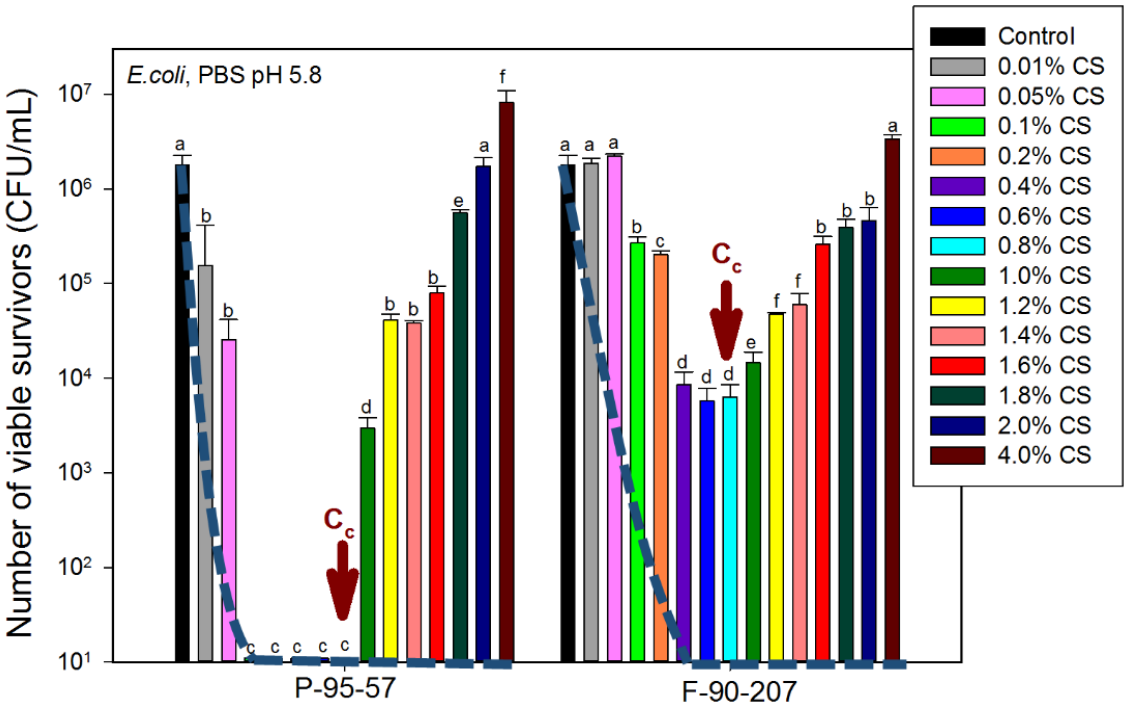

Figure 5.3: Effect of chitosan concentration in PBS on the number of viable survivors. C_c is the critical concentration above which the AB activity of chitosan decreases. Dashed lines represent the reduction in bacterial concentration after deproteinization. Samples are P-95-57 (powder) and F-90-207 (flakes). The number of viable organisms was the same after 18 and 48 h incubation on

the agar plates, suggesting that recovery from sub-lethal injury had not taken place. For each chitosan grade, means that do not share a letter are significantly different with a confidence level of 95% by Tukey Pairwise Comparisons.

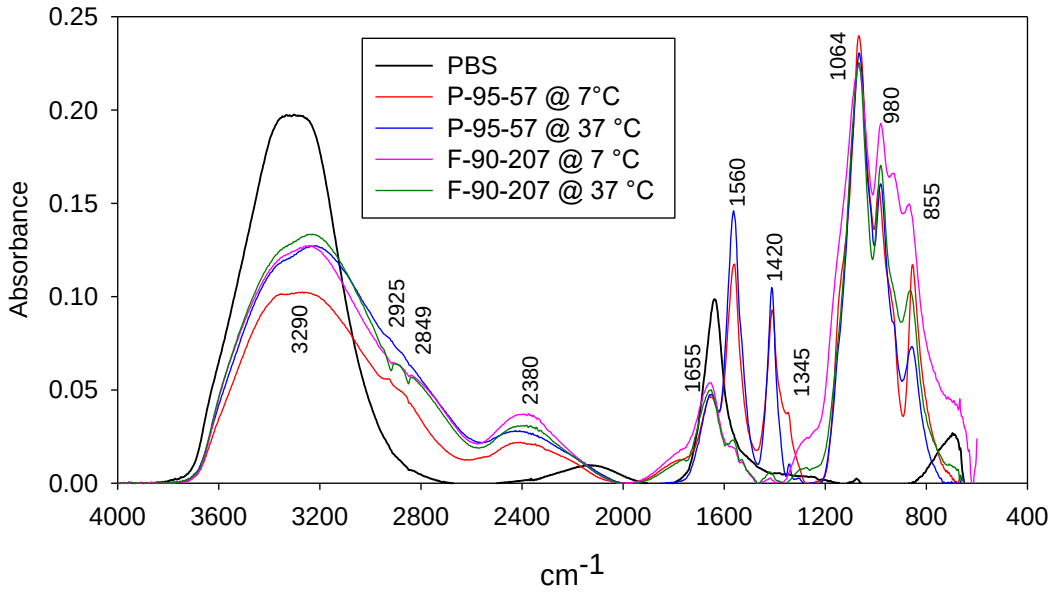

Figure 5.4: FTIR spectra: Peaks at 1345, 1420, 1560, 1655 and 3290 cm^{-1} confirm the solubility of chitosan powder and flakes in the suspensions during the AB tests.

Preliminary AB tests showed that chitosan powder and flakes were not active at pH values higher than the chitosan pK_a (6.2–6.5) [36,37], and indicated the need for a partially solubilized state to exert any AB effect. This point highlights the main difference with chitosan micro- and nanoparticles, in which the AB action of chitosan could be achieved at acidic and neutral pH values [25,26,28].

The contributions to the AB activity from the partially solubilized chitosan (filtrate subjected previously to the same conditions as in the AB tests) and from the solid-state particles were quantified. Figure 5.5 presents the decrease in bacterial density after exposure of *E. coli* to 0.4 wt/v % chitosan and to the filtrate from chitosan suspensions. AB results allowed quantifying a reduction of 4.0 and 2.5 log in bacterial density from the chitosan solubilized in the suspensions with powder and flakes, respectively. An additional contribution of 2.7 and 0.8 logs reduction to the AB activity was obtained by the presence of the chitosan powder and flakes, which may act as physical supports for the attachment of bacteria, as previously reported for the case of chitosan microspheres [27]. Hence, these results suggest that the presence of a solid form may favor chitosan

AB activity. In this regard, AB assays were performed in the presence of calcium carbonate particles ($CaCO_3$), a chemical compound lacking intrinsic AB activity.

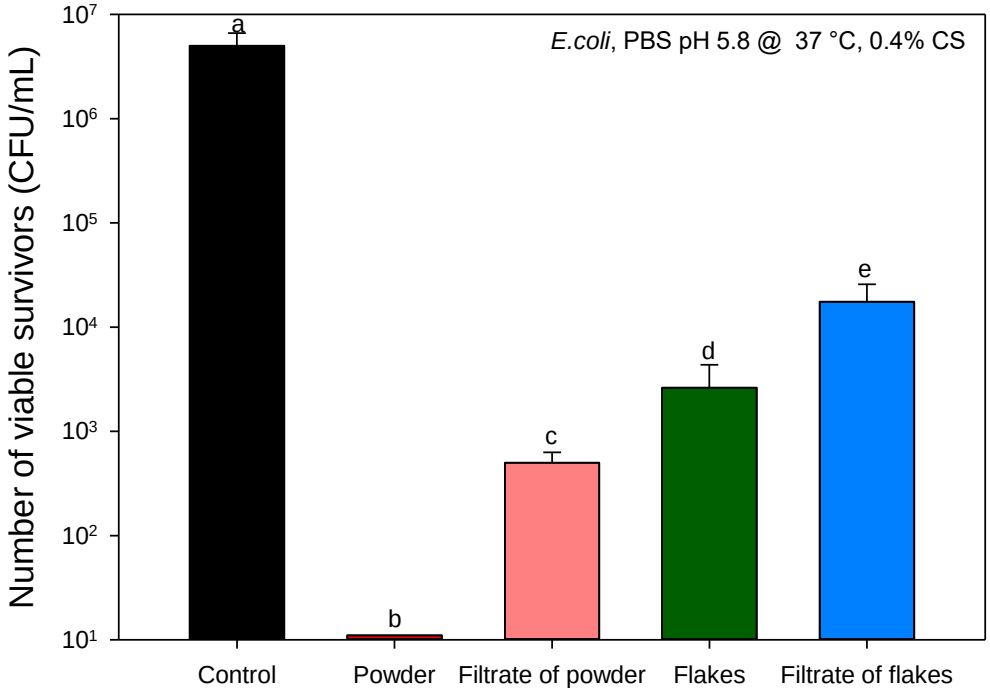

Figure 5.5: Recovery of viable bacteria after exposure of chitosan and filtrate from chitosan suspensions to *E. coli*. The number of viable organisms was the same after 18 and 48 h incubation on the agar plates, suggesting that recovery from sub-lethal injury had not taken place. Means that do not share a letter are significantly different with a confidence level of 95% by Tukey pairwise comparisons.

Figure 5.6 shows the surviving bacteria after exposure of *E. coli* to CS solution and $CaCO_3$. At a concentration of 0.01 wt/v %, CS solution reduces bacterial density by 1.4 log. However, *E. coli* reduction increases up to 4.8 logs when $CaCO_3$ is present in the medium. As $CaCO_3$ did not display AB activity in the absence of chitosan, these results indicate that the presence of a solid particles enhances the AB activity of the CS solution filtrate and may facilitate the attachment of bacteria. Similarly, chitosan powder and flakes may serve as physical solid supports to enhance the AB activity of the partially solubilized chitosan. Attachment of bacteria to chitosan is due to electrostatic interactions between the positively charged chitosan with the negatively charged cell surface. As $CaCO_3$ reacts in acid medium (given the HCl added to the medium when adjusting the

pH to 5.8) producing $CaCl_2$ and thereby Ca^{2+}, hence it is believed that bacteria may attach to calcium when seeking nutrients for microbial growth [38].

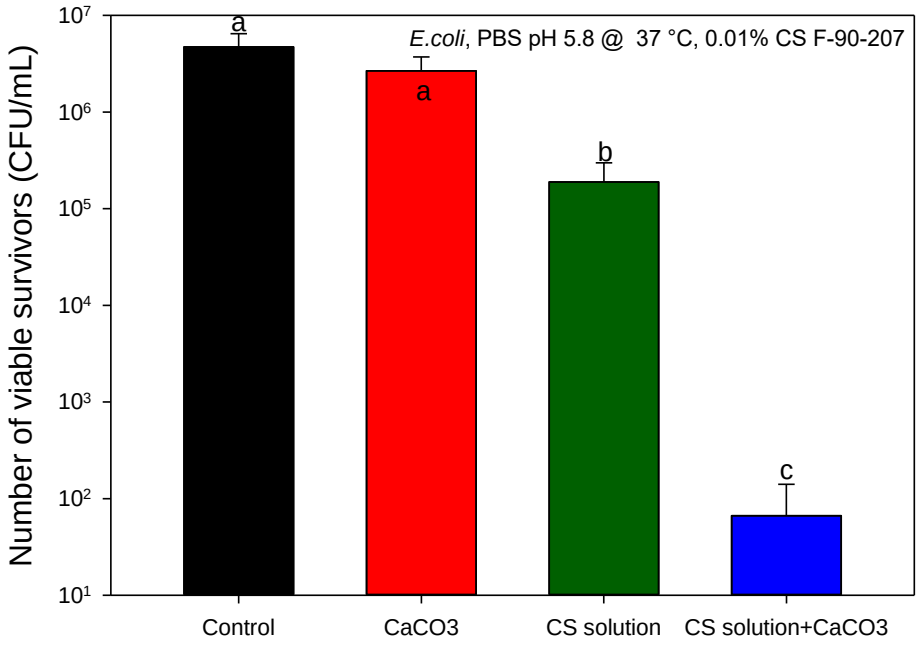

Figure 5.6: Recovery of viable bacteria after exposure of $CaCO_3$ and CS solution (F-90-207) to *E. coli*. The number of viable organisms was the same after 18 and 48 h incubation on the agar plates, suggesting that recovery from sub-lethal injury had not taken place. Means that do not share a letter are significantly different with a confidence level of 95% by Tukey pairwise comparisons.

Based on the previously discussed analyses, two hypotheses are considered to explain the existence of a critical chitosan concentration, as observed in Figure 5.3. The first one considers that a possible agglomeration of particles at the bottom of the assay tubes leaves less chitosan solubilized and fewer particles in contact with bacteria, thereby decreasing the AB activity of chitosan. However, AB tests conducted in Erlenmeyer flasks with higher surface area (approx. 16–25 times) than in assay tubes yielded the same trend than the ones presented in Figure 5.3, and consequently this hypothesis was rejected. The second hypothesis considerers that impurities, such as minerals and proteins remaining in chitosan [39] or chitosan itself may represent a nutrient source for bacteria and therefore be responsible for the decrease in the AB activity above the critical concentration. PBS buffer medium contains no nutrients for bacteria and at 4 wt/v % chitosan, bacterial density increases over the control and at a higher bacterial growth rate in chitosan powder than flakes, which is congruent with the higher protein content (Table 5.1). Besides, below the critical

concentration chitosan powder displayed higher activity, which is attributed to its higher DDA , lower MW and smaller particle size. This allows speculating that proteins act as nutrients for bacteria. Hence, a deproteinization step via enzymatic activity for these two chitosan grades was carried out, and the AB results are shown as dashed lines in Figure 5.3. Deproteinization was carried out under the action of *Protease K*, which is a specific enzyme that acts by breaking the peptide bonds of proteins, more specifically between the hydroxyl (COOH) and aminoacid (NH_2) lateral chains. The treatment with the enzyme was relatively short, to avoid any depolymerization of chitosan. After the removal of proteins, the AB activity of chitosan increases and lower concentrations are sufficient to eradicate bacteria. In addition, by increasing chitosan content, the AB activity increases up to a certain concentration and remains the same even if the concentration is further increased. Accordingly, impurities in solid state chitosan such as proteins can limit its AB efficacy. On the other hand, the low ash values reported in Table 5.1 discard a feeding effect from minerals. Chitosan itself (in the form of chito-oligosaccharides observed in Figure 5.1) as a nutrient source for bacteria was also discarded since at 4 wt/v % bacterial density was totally reduced only for deproteinized chitosan, while chito-oligosaccharides may be present before and after enzymatic treatment.

5.3.2.2 Identification of Proteins

Figure 5.7 shows a SDS-PAGE electrophoresis test result for the identification of the proteins remaining in the two chitosan samples, before and after deproteinization. High molecular weight proteins, in the range of 100–250 kDa, were detected in chitosan before the deproteinization step. Those are indicated as intense bands in Figure 5.7. Once proteins are removed, a decrease in the intensity of the bands is observed for both chitosan grades. This also confirms that proteins are mostly removed after the enzymatic treatment.

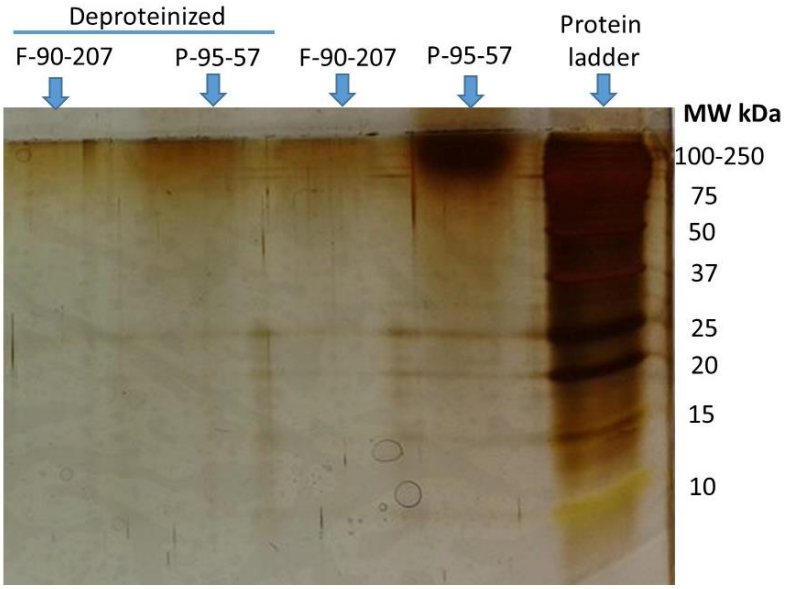

Figure 5.7: Identification of proteins before and after deproteinization of chitosan. Samples are P-95-57 (powder) and F-90-207 (flakes).

5.3.2.3 Effect of Temperature

Temperature is an important parameter to consider when seeking practical applications such as in the food packaging sector. Generally, in vitro AB tests of chitosan in solution form are carried out under optimal conditions for the growth and survival of bacteria, such as 37 °C in the case of *E. coli*. To our knowledge, the effect of temperature on the AB efficacy of chitosan in solution has barely been examined [40,41], not to mention in a discontinuous solid form.

Figure 5.8 shows the effectiveness of chitosan at 7 ± 1 °C and 37 ± 1 °C and pH of 5.8. These values correspond to temperatures close to those of refrigerated food products and optimal bacterial growth, respectively. As presented in Figure 5.8, the AB activity of chitosan highly depends on the incubation temperature, with a noticeably greater AB efficacy at 37 °C. At this temperature, a total inhibition of bacterial density for the powder chitosan grade, and a decrease in 3 log CFU/mL (approx. 99.9% of bacteria) for the flakes, are observed. By contrast, despite the fact that the AB activity strongly decreases at 7 °C, as shown in Figure 5.8, both chitosan grades reduce bacterial density by more than 1 log CFU/mL (approx. 90% of bacteria). Hence, notwithstanding the limiting effect of temperature and the fact that total inhibition of bacteria was not achieved, results are still promising regarding chitosan AB activity in refrigerated conditions. Similar results were reported

recently in which a higher susceptibility of bacteria to the action of chitosan nanoparticles in high temperature conditions was found [25].

Different factors may contribute to the stronger activity at 37 °C seen in both chitosan grades. First, as temperature controls the acid dissociation constant K_a ($pK_a = -\log K_a$) [42], an increase in the temperature favors the AB activity since K_a increases. In this work, the pK_a of chitosan powder and flakes was determined by titration [43] at 0 °C and 37 °C. The pK_a decreases from 6.7 to 6.6 for chitosan flakes, and from 6.6 to 6.2 for chitosan powder when the temperature increased from 0 to 37 °C, respectively. The smaller the value of pK_a, the larger the extent of dissociation and the number of protonated amino groups, which should favor the AB activity at higher temperature.

Second, a higher chitosan solubility and chain mobility may be achieved at 37 °C than at 7 °C. Figure 5.4 illustrated the potential solubility of chitosan powder and flakes at these temperatures. The higher AB activity of chitosan powder with respect to chitosan flakes at 37 °C may be accounted for by a lower particle size, lower MW and higher DDA content, which could favor its solubility, given the pH of the medium (5.8). In addition, chitosan powder has a higher content of low MW species (chito-oligosaccharides) as shown in Figure 5.1, which may have contributed to the higher AB effect [44].

Finally, Tsai and Su [40] have suggested that low temperature may induce changes in the bacterial cell structure by decreasing the number of binding sites on the surface (or electronegativity). Consequently, less protonated chitosan amino groups may interact with the available negatively charged sites in the bacteria surface, resulting in a decreased chitosan AB activity. In addition, *E. coli* is either a mesophile or a psychrotrophic and consequently a temperature of 7 ºC does not favor its biological activities, including its growth. According to our results, the AB activity for both chitosan grades is highly reduced when the temperature decreases but without significant difference regarding the efficacy between the two grades ($p > 0.05$), as observed at 37 °C ($p < 0.05$). Therefore, it is speculated that this mechanism (decrease of number of binding sites) may influence the most and strongly limits the AB efficacy, regardless of the chitosan grade.

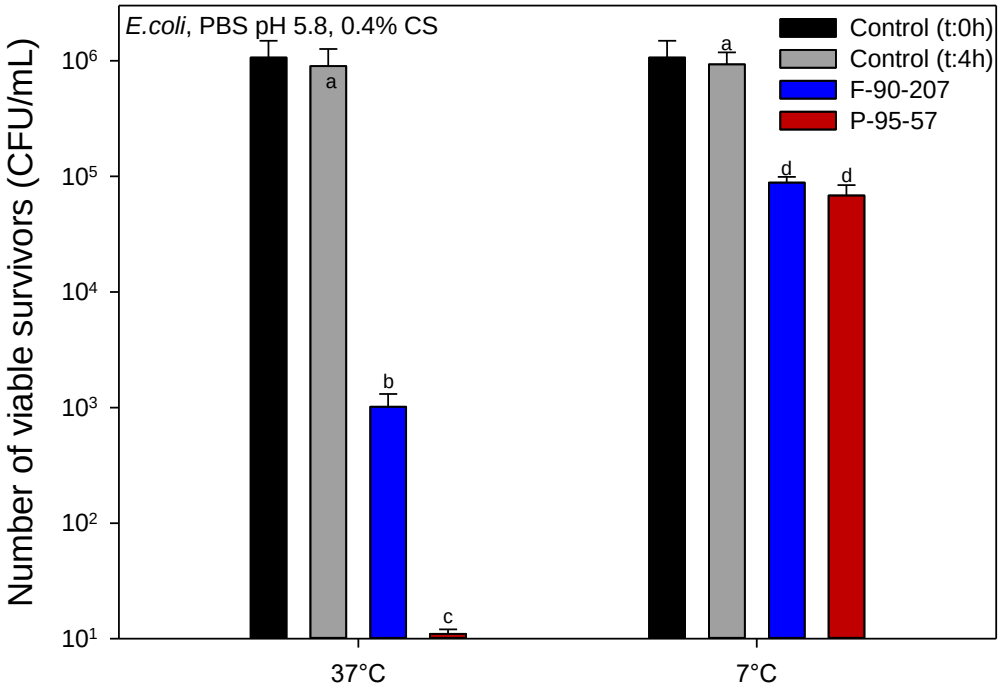

Figure 5.8: Effect of temperature on the antibacterial activity of chitosan (number of viable survivors). Bars with different letter are significantly different ($p < 0.05$). Samples are F-90-207 (flakes) and P-95-57 (powder). The number of viable organisms was the same after 18 and 48 h incubation on the agar plates, suggesting that recovery from sub-lethal injury had not taken place. Means that do not share a letter are significantly different with a confidence level of 95% by Tukey pairwise comparisons.

5.3.2.4 Effect of Salt Concentration and Ionic Strength

Salts are commonly incorporated into food as additives and preservatives. Their presence can favor the chelating capacity of chitosan for metal ions and consequently compromise its antibacterial properties. Figure 5.9 shows the effect of salt concentration and ionic strength (I) on the AB activity of chitosan flakes. As the concentration of NaCl and $MgCl_2$ increases from 0.1 M to 1.0 M, the AB activity of chitosan decreases. This effect can be explained through two mechanisms and the Debye-Hückel equation [4,45–47]. First, given the acidic conditions of the medium (pH 5.8), protonated chitosan amino groups may trigger electrostatic attraction of anionic compounds, including metal anions (chlorine, anionic ligands, etc.) [48]. Consequently, the interaction of chitosan with metal ions in the aqueous medium leaves less chitosan amino groups available for contact with bacteria. Secondly, the negatively charged components (lipopolysaccharides and

proteins) on the Gram-negative *E. coli* bacteria surface may interact with the existing cations in the medium instead of interacting with chitosan, consequently lowering the apparent AB activity. This interaction certainly occur given bacteria adsorb essential nutrients such as Ca^{2+} for microbial growth [38]. Otherwise, as electrolytes are dispersed in the medium, the electrostatic interactions of chitosan may be screened by the free charges, causing a net "double-layer" interaction decay with a characteristic length known as Debye-length κ^{-1} [49]. For an electrolyte:

$$\kappa^{-1} = [(\varepsilon_r \varepsilon_0 k_B T)/(2N_A e^2 I)]^{1/2} \quad (1)$$

where $\varepsilon_r, \varepsilon_0, k_B, T, N_A, e$ and I are the dielectric constant, permittivity of the free space, Boltzmann constant, absolute temperature, Avogadro number, elementary charge and ionic strength in the medium, respectively [47]. Since all previous parameters are the same in our study except for the ionic strength, κ^{-1} can be simplified as $\kappa^{-1} = KI^{-1/2}$ nm, where K is a constant. Accordingly, the Debye-length decreases with increasing ionic strength (or salt content in this case), explaining the decrease of the AB activity when NaCl or $MgCl_2$ are added. This is a consequence of a decrease of the electrostatic repulsions in chitosan (screening of the positively charged chitosan amino groups), limiting the interactions with the negatively charged bacterial surface.

In addition, our results show that the type of salt (ions) in the medium also influences the AB effectiveness of chitosan. This effect can be observed when analyzing the two types of salt at a concentration of 0.1 M. According to Figure 5.9, the AB efficacy of chitosan is weaker when Mg^{2+} ions are present in the medium in comparison with Na^+, i.e., the presence of Na^+ ions is less detrimental to the AB efficacy of chitosan. At 0.1 M, the ionic strength in the medium is three times higher for $MgCl_2$ than for NaCl, which implies a decrease of about 1.7 times κ^{-1}. Consequently, more charges are screened, limiting more significantly the AB activity. The same explanation is valid when comparing the AB efficacy of chitosan at 1.0 M NaCl ($I = 1.0\ M$, $\kappa^{-1} = 1\ K$ nm) with 0.1 M $MgCl_2$ ($I = 0.3\ M$, $\kappa^{-1} = 1.82\ K$ nm).

On the other hand, when a high concentration of salt is used (1.0 M), the inhibitory effect of chitosan fades more in comparison with 0.1 M, but by an equal amount for both salts ($p > 0.05$). Although the Debye-length theory is only valid at low concentrations and breaks down when the ionic strength is over 0.1 M [50,51], a rough approximation indicates that at 1.0 M, κ^{-1} is 1.0 K

nm and 0.6 *K* nm for NaCl and $MgCl_2$, respectively. In this case, despite the Debye-length is meaningfully different, no significant difference in the drop of the AB efficacy is observed, inferring that chitosan charges are totally screened. However, the concentration of salt is high enough to limit entirely the AB activity of chitosan as well as killing bacteria, as observed in the control samples containing no chitosan in Figure 5.9. Therefore, the small log reduction of *E. coli* by chitosan in the presence of 1.0 NaCl or $MgCl_2$ appears effectively due to salts. The death of *E. coli* cells is probably the result of their effort to reduce the concentration gradient of salt inside and outside the cell walls, causing morphological damage and loss of cellular integrity, given such a high salinity content [52].

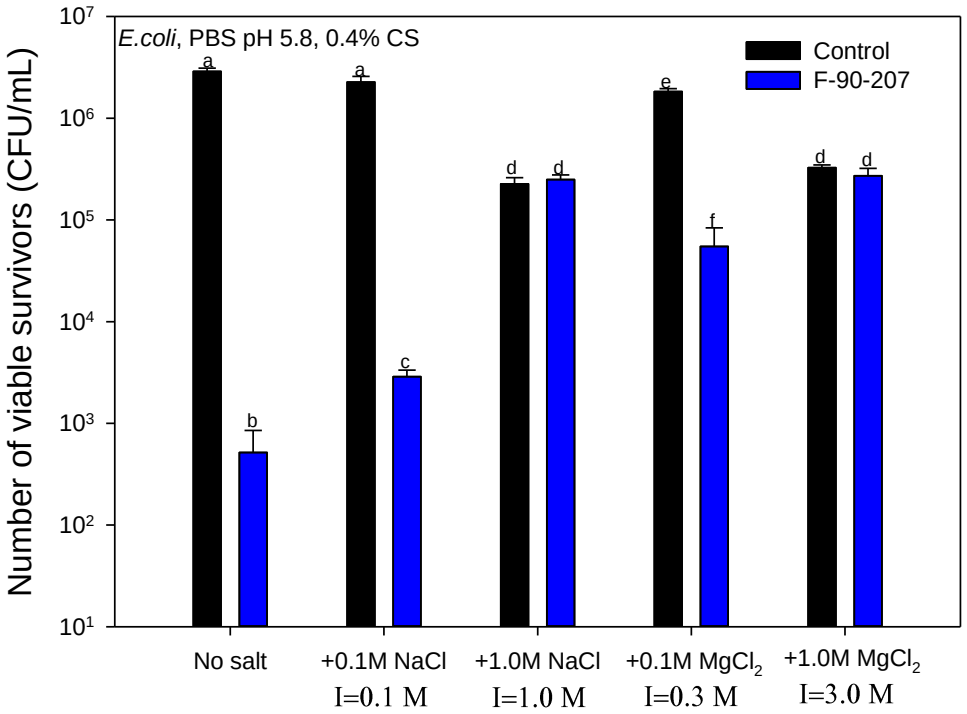

Figure 5.9: Effect of salt concentration and ionic strength (I) on the antibacterial activity of chitosan. Bars with different letters are significantly different ($p < 0.05$). Sample is F-90-207 (flakes). The number of viable organisms was the same after 18 and 48 h incubation on the agar plates, suggesting that recovery from sub-lethal injury had not taken place. Means that do not share a letter are significantly different with a confidence level of 95% by Tukey pairwise comparisons.

5.3.2.5 Influence of Bacterial Species

Table 5.3 presents the survival and reduction (%) of bacterial density when three different species of bacteria are in contact with chitosan. Chitosan presents a noticeable greater AB activity against *E. coli* in comparison with *L. innocua* and *S. aureus*. For instance, while *E. coli* density is reduced by more than 99.5% by either chitosan powder or flakes, *L. innocua* and *S. aureus* are more sensitive to the effect of chitosan in powder form.

Table 5.3: Recovery of viable bacteria on BHI agar after exposure to 0.4 wt/v % chitosan for 4 h at 37 °C.

Chitosan Type	Survival Bacteria (log CFU/mL)			Reduction * (%)		
	Gram$^-$	Gram$^+$		Gram$^-$	Gram$^+$	
	E. coli	*L. innocua*	*S. aureus*	*E. coli*	*L. innocua*	*S. aureus*
Control	6.5 ± 0.6 [a]	6.6 ± 0.5 [a]	7.5 ± 0.8 [a]	0.0	0.0	0.0
F-90-207	4.2 ± 0.4 [b]	5.4 ± 0.7 [b]	6.6 ± 0.9 [a]	99.5	93.1	88.2
P-95-57	0.0 [c]	0.0 [c]	6.1 ± 0.6 [a]	100	100	96.3

Results represent means of triplicate counts and were the same after 18 and 48 h of incubation on the agar plates, suggesting that the recovery from sub-lethal injury had not taken place. For each strain, means that do not share a letter are significantly different with a confidence level of 95% by Tukey Pairwise Comparisons. * The reduction in bacteria concentration is calculated according to Zheng & Zhu [6] $\frac{N_1-N_2}{N_1} \times 100\%$ where N_1 and N_2 are the number of colony on the plates before and after treatment, respectively.

Figure 5.10 shows the morphology of *E. coli*, *L. innocua* and *S. aureus* cells via TEM. *E. coli* and *L. innocua* cells shows typically rod-shaped forms of 3.41 ± 0.68 and 1.22 ± 0.20 μm in length, and 1.01 ± 0.2 and 0.53 ± 0.05 μm in height, respectively. However, *S. aureus* cells are spherical, with a diameter of 0.81 ± 0.16 μm. Those dimensions allow speculating that discontinuous solid state chitosan may interact more easily with *E. coli* rather than with *L. innocua* and *S. aureus* cells, which falls within the same sensitivity order seen in our findings. However, our recent study on chitosan nanoparticles demonstrated that the AB activity is independent of the size and form of the cells [25].

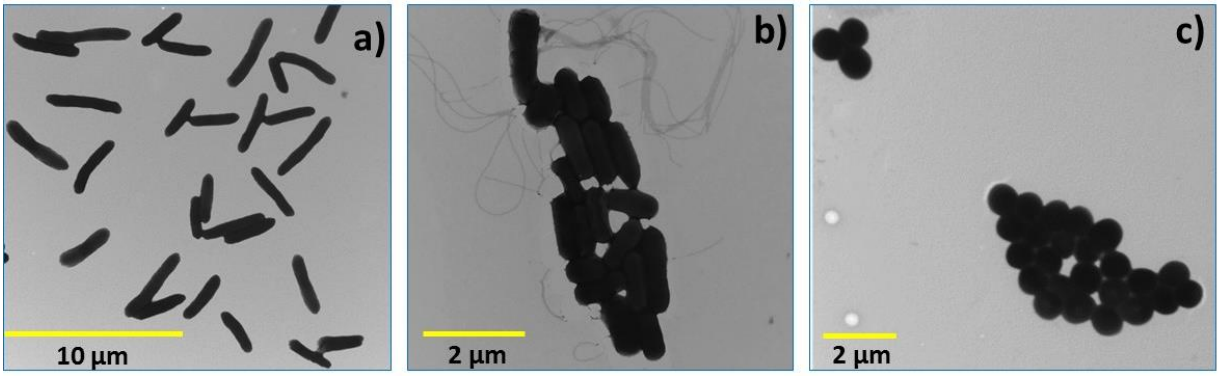

Figure 5.10: Morphology of intact: (**a**) *E. coli*; (**b**) *L. innocua*; (**c**) *S. aureus* cells. Images were kindly provided by Mounia Arkoun from the Chemical Engineering Department, Polytechnique Montréal.

Some studies on chitosan solutions have reported a higher sensitivity against Gram-negative species [2,5,53,54]. The higher sensitivity found in the case of *E. coli* (Gram-negative) in comparison with *L. innocua* and *S. aureus* (both Gram-positive) can be explained first in terms of the differences in the cell surface characteristics between the Gram types, such as hydrophilicity, negative charge density and adsorptive properties, besides an apparent adsorption of bacteria onto chitosan particles. A generally stronger net negative charge in the Gram-negative strains [55–57] may favor larger electrostatic interactions between the positively charged chitosan amino groups and the negatively charged bacteria surface. Notwithstanding that the cell surface of both Gram-positive and Gram-negative is negatively charged, the Gram-negative (*E. coli*) bacteria were more prone to adsorption, and hence were more susceptible to chitosan. Other factors such as higher hydrophilicity and adsorption of chitosan on cell wall in Gram-negative strains, with respect to Gram-positives ones, could increase the AB effect [56]. In addition to the above, the structural organization in the envelope/membrane constituents of Gram-positive and Gram-negative strains may play the most important role influencing the AB activity. Both strains have similar composition regarding phospholipids, glycoproteins, cholesterol and polysaccharides. However, the way they are placed and organized vary between the strains. For instance, Gram-positive consist of a single phospholipid layered membrane and a thick murein (peptidoglycan), while Gram-negative consist of a single phospholipid layered membrane a thinner peptidoglycan layer and covered by a phospholipidic bilayered membrane. The smaller thickness of the peptidoglycan layer

in Gram-negative strains (7 to 8 nm), in comparison to the Gram-positive strains (20 to 80 nm), may render it more sensitive to the action of chitosan [58].

However, despite the above, many reports have demonstrated higher AB activity of chitosan in solution form against *S. aureus* in comparison with *E. coli* [6,14,15,58], which is opposite to the findings of our current work. In those cases, authors explained the higher AB effect on the Gram-positive strains (such as *S. aureus*) as a consequence of the absence of the outer membrane barrier in comparison with the Gram-negative strains (such as *E. coli*) [14]. On the other hand, experimental data provided by Tsai et al. [59] allow to infer that the sensitivity of bacteria to chitosan is not dependent on the Gram-type (Gram-positive or Gram-negative) nor dependent on the bacterial species, but dependent on the strain. This would explain the controversial findings amongst different authors when comparing the effectiveness of chitosan.

Our results demonstrated that chitosan needs at least partial solubilisation for an AB effect. Thereby, the lower MW (which include the presence of low MW species or chito-oligosaccharides, even in small quantities) and the higher DDA favors the solubility of chitosan powder and its AB activity. Further research should be performed in order to quantify the solubility of each chitosan grade.

Owing to the size and shape of discontinuous solid state chitosan, it is considered that in addition to solubilisation, the AB action requires a direct contact between chitosan and the cell surface, with a probable microbial cell adsorption not only onto the surface of chitosan powder and flakes but also on the surface of $CaCO_3$ particles, which notably enhances the AB activity. However, having only chitosan particles will avoid the need of an additional solid support for optimum AB activity. Other studies have demonstrated the adsorption properties of chitosan powder and flakes to residues and for removal of metals [48,60]. The higher sensitivity of bacteria to powder chitosan might be due to the larger specific surface area and the closer similarity of its size order with the cells, when compared to chitosan flakes. It has been reported that lowering chitosan particle size improves the antibacterial activity [25]. Other properties such as higher lead sorption capacity [61] and higher cytotoxicity towards tumor cells [62] have also been reported as improving with decreasing particle size.

The mode of AB action may differ from that reported for chitosan nanoparticles [25], since the AB activity of powder and flakes require acidic pH and their sizes prevent them from penetrating into

cells as compared with nanoparticles. Hence, it is suggested that one part of the AB action is exerted by the direct contact of protonated chitosan powder's and flakes' surface with the negatively charged cell wall; and the other, by the solubilized chitosan which may deposit on bacteria surface affecting the cell permeability and leading to the leakage of proteinaceous and other intracellular constituents [27,63].

On the other hand, further research is required in order to evaluate the cytotoxicity of chitosan powder and flakes, which is critical for food packaging and other industrial applications. Different studies have evaluated the cytotoxicity of chitosan nanoparticles [62,64], which can be more critical than chitosan powder and flakes, because they could penetrate the cells through pervasion and alter the DNA and mRNA functions. For instance, Qi et al. [62] reported high cytotoxic activity of chitosan nanoparticles toward tumor cells while low toxicity against normal human liver cells.

5.4 Materials and Methods

5.4.1 Materials

Chitosan (CS) in powder (P) and flake form (F) were obtained from Primex (Siglufjordur, Iceland) and BioLog GmbH (Landsberg, Germany), respectively. They were characterized in terms of DDA, MW, polydispersity (PDI), moisture, ash, protein content and particle size, as presented in

Table 5.1. Protein bovine serum albumin (BSA)—98% purity—and enzyme proteinase K and Glacial acetic acid were obtained from Sigma Aldrich (Oakville, ON, Canada). Calcium carbonate ($CaCO_3$) with a particle size between 3 and 13 μm was obtained from Univar (Surrey, BC, Canada). All other chemicals and reagents were of analytical grade and used without further purification.

5.4.2 Bacteria Strains and Culture

Cultures of *Escherichia coli* (*E. coli* strain DH5α, non-pathogen), *Listeria innocua* (*L. innocua* strain ISPQ3284, non-pathogen), *Staphylococcus aureus* (*S. aureus* strain 54–73, pathogen) were obtained from the laboratory of microbiology, infectiology and immunology (Université de Montréal, Montréal, QC, Canada). They were selected as representative bacteria since they are some of the most frequent bacteria found in food spoilage.

5.4.3 Methods

5.4.3.1 Infrared Spectroscopy (FTIR)

The DDA values were verified and determined (when the company did not provide this information) via FTIR as described in Tsaih and Chen [65]. Samples were prepared in KBr disk form, where KBr disks were compounded from dry mixtures of about 1 mg of chitosan sample and 100 mg of KBr. FTIR spectra were recorded on a Spectrum 65 FT-IR spectrometer (Perkin-Elmer, Woodbridge, ON, Canada) with a resolution of 4 cm^{-1} and 32 accumulations in the wavenumber range of 600 to 4000 cm^{-1}.

5.4.3.2 Gel Permeation Chromatography (GPC)

The average MW and polydispersity index (PDI) for chitosan samples were determined by size-exclusion chromatography (SEC) as described in Lavertu et al. [66]. Measurements were performed on a Gel Permeation Chromatography (GPC) system consisting of an LC-20AD isocratic pump (Shimadzu, Kyoto, Japan), an autosampler SIL-20AC HT (Shimadzu), an oven CTO-20AC (Shimadzu) coupled with a Dawn HELEOS II multiangle laser light scattering detector (Wyatt Technology Co., Santa Barbara, CA, USA), an Optilab rEX interferometric refractometer (Wyatt Technology Co.), and two Shodex OHpak columns (SB-806M HQ and SB-805 HQ) connected in series. The mobile phase was an acidic aqueous buffer (AcOH 0.15 M, AcONa 0.1 M, NaN_3 0.4 mM, 0.1 M NaCl) and a chitosan *dn/dc* value of 0.205 was used (laser's wavelength of 658 nm).

5.4.3.3 Thermogravimetric Analysis (TGA)

5.4.3.3.1 Moisture Content

The moisture content in chitosan powder and flakes was determined according to the AOAC standard methods 930.15 [67] in a thermogravimetric analyzer TGA Q500 from TA Instruments (New Castle, DE, USA). Approximately 10 mg of chitosan were heated from room temperature to 150 °C, at a rate of 10 °C min^{-1} under a nitrogen atmosphere.

5.4.3.3.2 Ash Content

The ash content in chitosan powder and flakes was characterized according to the AOAC standard methods 942.05 [67] using the same thermogravimetric analyzer. Approximately 10 mg of chitosan were heated from room temperature to 900 °C at a rate of 10 °C min^{-1} under an air atmosphere.

5.4.3.4 Protein Content

The protein content was determined by ultraviolet (UV) light at 280 nm on a Cary 5000 UV–vis-NIR spectrophotometer (Agilent Technologies, Santa Clara, CA, USA). First, a calibration curve was done with bovine serum albumin (BSA) as standard protein at different concentrations (0.01, 0.05, 0.10, 0.25 and 0.50 wt/v %). Then, the protein content was calculated by correlating the absorbance of each chitosan sample (dissolved in 1 *v*/*v* % HCl) with the corresponding concentration in the calibration curve.

5.4.3.5 Deproteinization and Identification of Proteins

The deproteinization step was performed using the enzyme proteinase K. In this case, a buffer solution consisting of 30 mM Tris-Cl, 30 mM EDTA, 5% Tween 20, 0.5% Triton X-100 and 800 mM GuHCl was prepared and pH was adjusted to 8.0. Chitosan in powder and flake form was added at a temperature of 50 °C, resulting in suspensions since chitosan is not soluble above its pK_a (6.2–6.5) [36,37]. Then, proteinase K was added at a concentration of 100 $\mu g \cdot mL^{-1}$ under shaking during 15 min and finally the temperature was increased to 60 °C to stop the enzyme effect. Deproteinized chitosan was washed, centrifuged and dried at 60 °C overnight.

The determination of proteins molecular weight was done using polyacrylamide gel electrophoresis (PAGE) in the presence of sodium lauryl sulfate (SDS) at a concentration of 15% Tris-HCl. In this case, 40 µL of filtrate from a 4 wt/v % chitosan (before and after deproteinization) suspension in water at pH 7.0 was injected into the gel. Silver staining was used for the recognition of the protein bond.

5.4.3.6 Scanning Electron Microscopy (SEM)

Particle Size. SEM images of chitosan powder and flakes were obtained using a JSM-7600 TFE field emission gun (JEOL, Calgary, AB, Canada) operated at 2 kV. The particle size and thickness were determined using Image-Pro® Plus software (version 5.1 from Media Cybernetics, Rockville, MD, USA) and taking the average value of 1000 particles.

Elemental Analysis. The qualitative determination of chitosan powder and flakes composition was done via Energy Dispersive X-ray spectroscopy (EDS) using a JEOL JSM-840A scanning electron microscope (Oxford Instruments, Abingdon-on-Thames, United Kingdom) operating at 20 kV.

5.4.3.7 Attenuated Total Reflectance Spectroscopy (ATR)

The potential solubility of chitosan powder and flakes during the AB tests was evaluated via ATR. Chitosan suspensions were prepared in the same conditions as for the AB tests, filtrated at room temperature by using Grade 1 Qualitative filter paper (Whatman^{TM} porous size of 11 μm), and then analyzed by placing one droplet of the filtrate directly on the surface of the ATR crystal and left overnight until complete drying before acquiring the spectra. These were recorded on a Perkin-Elmer Spectrum 65 FT-IR spectrometer (Perkin-Elmer, Woodbridge, ON, Canada) with a resolution of 4 cm^{-1} and 32 accumulations in the wavenumber range of 600 to 4000 cm^{-1}.

5.4.3.8 Transmission Electron Microscopy (TEM)

TEM analyses on fresh bacteria were performed according to the method of Arkoun et al. [63]. Briefly, overnight cultures containing 10^6 colony forming units per milliliter (CFU/mL) of the selected bacteria were centrifuged (8000 rpm/3 min) and the resulting pellets were resuspended in a 2 *v*/*v* % glutaraldehyde solution (phosphate buffer saline, PBS at pH 7.4) to fix the cells at 4 °C overnight. Then, 10 μL of each sample was deposited on Formvar carbon-coated grids containing one drop of 1% Alcian Blue. Cells were then subjected to 5 min post-fixation with paraformaldehyde (2 *v*/*v* %, PBS) and grids were stained using a drop of filtered 2 *v*/*v* % phosphotungstic acid (PTA, pH 7.0) for 30 s. A series of filtration and/or washing treatment were performed after each step in order to remove excess liquid, fixative or staining. Finally, TEM observation was performed using a CM100 transmission electron microscope (Philips Electron Optics, Eindhoven, The Netherlands) and digital micrographs were captured using an XR80 CCD digital camera (Advanced Microscopy Techniques, Woburn, MA USA).

5.4.3.9 Antibacterial (AB) Assays

In this study, one Gram-negative (*E. coli*) and two Gram-positive strains (*L. innocua* and *S. aureus*) were used (Figure 5.10). The microorganisms were grown in a nutritional rich medium (Brain Heart Infusion broth or BHI) under constant agitation for 24 h at 37 °C, in order to reach a density of 10^9 colony forming units per milliliter (CFU/mL). After 24 h, the bacteria culture were diluted in a

buffer, a non-permissive growth condition (phosphate buffered saline or PBS solution), in order to reach a density of approximately 10^6 CFU/mL. Preliminary AB tests showed that chitosan powder and flakes were not active at pH values higher than chitosan pK_a, and indicated the need of a solution state for the AB activity of chitosan. Therefore, the pH of the PBS solution was altered intentionally to 5.8 (with HCl 1 M). Chitosan powder and flakes were sterilized under UV light for 20 min prior to the preparation of the chitosan suspensions.

5.4.3.9.1 Effect of Chitosan Concentration

Chitosan suspensions at concentrations between 0.01 and 4 wt/v % were prepared in 5 mL of PBS containing approximately 10^6 CFU/mL of *E. coli*. Suspensions were incubated during 4 h at 37 ± 1 °C and 22% ± 1% relative humidity (RH) in a shaker. Serial dilutions of the inoculated suspensions were plated on BHI agar (unless otherwise specified) and incubated for 18 h at 37 ± 1 °C and 34% ± 1% RH for the counting of the surviving bacteria (CFU/mL). Plates were verified after 48 h to corroborate that the recovery of viable organisms from sub-lethal injury had not taken place. These dilution and enumeration methods were used for all the other antibacterial following tests described below:

5.4.3.9.2 Exposure of chitosan and filtrate from chitosan suspensions to E. coli

Chitosan suspensions at a concentration of 0.4 wt/v % were prepared in 5 mL of PBS and placed during 4 h at 37 ± 1 °C and 22% ± 1% RH in a shaker. Suspensions were filtrated at room temperature by using Grade 1 Qualitative filter paper (Whatman™ porous size of 11 μm). Then, chitosan suspensions and the filtrate from chitosan suspensions were inoculated with approximately 10^6 CFU/mL of *E. coli* and incubated during 4 h at 37 ± 1 °C and 22% ± 1% RH in the same shaker.

5.4.3.9.3 Exposure of $CaCO_3$ and chitosan solution to E. coli

Chitosan solution was prepared by dissolving 1 wt/v % chitosan flakes in 1 *v/v* % acetic acid aqueous solution, under magnetic stirring and at room temperature until complete dissolution of the solutes. Chitosan solution was diluted into 5 mL of PBS containing approximately 10^6 CFU/mL of *E. coli* until reach a concentration of 0.01 wt/v % chitosan. $CaCO_3$ suspensions at a concentration of 0.1 wt/v % were prepared in 5 mL PBS containing approximately 10^6 CFU/mL of *E. coli*. Samples were incubated during 4 h at 37 ± 1 °C and 22% ± 1% RH in a shaker.

5.4.3.9.4 Effect of Temperature

Chitosan suspensions at a concentration of 0.4 wt/v % were prepared in 5 mL of PBS containing approximately 10^6 CFU/mL of *E. coli*, and incubated during 4 h at two temperature conditions, 7 ± 1 °C and 37 ± 1 °C at 22% ± 1% RH in a shaker.

5.4.3.9.5 Effect of Salt Concentration and Ionic Strength

Chitosan suspensions at concentration of 0.4 wt/v % were prepared in 5 mL of PBS containing approximately 10^6 CFU/mL of *E. coli* and incubated during 4 h at 37 ± 1 °C and 22% ± 1% RH in a shaker. Two types of salt, NaCl and $MgCl_2$ at concentrations of 0.1 M and 1.0 M were added to the PBS medium before the inoculation of bacteria and the treatment with chitosan.

5.4.3.9.6 Effect of Bacterial Species

Chitosan suspensions at concentration of 0.4 wt/v % were prepared in 5 mL of PBS containing approximately 10^6 CFU/mL of *E. coli, L. innocua* or *S. aureus*, and incubated during 4 h at 37 °C and 22% ± 1% RH in a shaker.

5.4.3.9.7 Statistical Analysis

All AB tests were carried out in triplicate, and the average values with their standard deviation errors are reported. Results from the AB tests were analyzed statistically via Tukey pairwise comparisons with a confidence interval of 95% using the ANOVA-Minitab17® software (trial version, Minitab Inc., State College, PA, USA). Data were normalized by re-scaling in log form.

5.5 Conclusions

In this work we have shown that chitosan in a neat discontinuous solid state can exhibit high antibacterial activity under conditions close to those of contaminated food products. This activity can be altered by factors such as pH, temperature, ionic strength, chitosan concentration, purity and bacterial species, and shown to be favored by the removal of proteins in chitosan, acidic pH conditions, and lower salt content in the medium. In addition, the presence of a solid physical form in the medium enhanced significantly the AB activity of chitosan.

Our results show the potential direct use of chitosan powder and flakes in food protection at pH values lower than chitosan pK_a (6.2–6.7). Further research on chitosan AB activity should be

performed for a deeper understanding of the mechanisms and factors involved. In the scope of food protection, similar research could lead to the development of chitosan-based food packaging materials capable of inhibiting and eradicating bacteria growth.

5.6 Acknowledgements

The Fonds de Recherche du Québec-Nature et Technologies (FRQNT) is acknowledged for their funding of the present work. The authors also thank Vincent Darras and Michael Buschmann from the Biomaterials and Cartilage Laboratory (BCL) (Polytechnique Montréal) for their help with the GPC tests, Julian Zhu from the Chemistry Department (Université de Montréal) for the UV tests and Mounia Arkoun from the Chemical Engineering Department (Polytechnique Montréal) for the morphological characterization of bacterial cells via TEM. Finally, the authors acknowledge the reviewers of *Molecules* for their valuable comments to improve this manuscript.

Author Contributions

N.A. designed the study, collected test data, interpreted results and drafted the manuscript. F.D., M.-C.H. and A.A. designed the study, interpreted results and reviewed and edited the manuscript.

Conflicts of Interest

The authors declare no conflict of interest.

5.7 References

1. Goosen, M.F. *Applications of Chitin and Chitosan*; CRC Press LLC: Boca Raton, FL, USA, 1997.
2. Campos, M.; Cordi, L.; Duran, N.; Mei, L. Antibacterial Activity of Chitosan Solutions for Wound Dressing. *Macromol. Symp*. **2006**, *246–246*, 515–518.
3. Kumar, M.N.R. A review of chitin and chitosan applications. *React. Funct. Polym.* **2000**, *46*, 1–27.
4. Kong, M.; Chen, X.G.; Xing, K.; Park, H.J. Antimicrobial properties of chitosan and mode of action: A state of the art review. *Int. J. Food Microbiol*. **2010**, *144*, 51–63.

5. Chung, Y.C.; Chen, C.Y. Antibacterial characteristics and activity of acid-soluble chitosan. *Bioresour. Technol.* **2008**, *99*, 2806–2814.

6. Zheng, L.Y.; Zhu, J.F. Study on antimicrobial activity of chitosan with different molecular weights. *Carbohydr. Polym.* **2003**, *54*, 527–530.

7. Franklin, T.; Snow, G. *Biochemistry of Antimicrobial Action*; Chapman & Hall: London, UK, 1981.

8. Devlieghere, F.; Vermeulen, A.; Debevere, J. Chitosan: Antimicrobial activity, interactions with food components and applicability as a coating on fruit and vegetables. *J. Food Microbiol.* **2004**, *21*, 703–714.

9. Bhale, S.; No, H.K.; Prinyawiwatkul, W.; Farr, A.; Nadarajah, K.; Meyers, S.P. Chitosan coating improves shelf life of eggs. *J. Food Sci.* **2003**, *68*, 2378–2383.

10. Ouattara, B.; Simard, R.E.; Piette, G.; Bégin, A.; Holley, R.A. Inhibition of surface spoilage bacteria in processed meats by application of antimicrobial films prepared with chitosan. *Int. J. Food Microbiol.* **2000**, *62*, 139–148.

11. Yingyuad, S.; Ruamsin, S.; Reekprkhon, D.; Douglas, S.; Pongamphai, S.; Siripatrawan, U. Effect of chitosan coating and vacuum packaging on the quality of refrigerated grilled pork. *Packag. Technol. Sci.* **2006**, *19*, 149–157.

12. No, H.K.; Meyers, S.P.; Prinyawiwatkul, W.; Xu, Z. Applications of chitosan for improvement of quality and shelf life of foods: A review. *J. Food Sci.* **2007**, *72*, R87–R100.

13. Liu, N.; Chen, X.G.; Park, H.J.; Liu, C.G.; Liu, C.S.; Meng, X.H.; Yu, L.J. Effect of MW and concentration of chitosan on antibacterial activity of *Escherichia coli*. *Carbohydr. Polym.* **2006**, *64*, 60–65.

14. No, H.K.; Park, N.Y.; Lee, S.H.; Meyers, S.P. Antibacterial activity of chitosans and chitosan oligomers with different molecular weights. *Int. J. Food Microbiol.* **2002**, *74*, 65–72.

15. No, H.K.; Kim, S.H.; Lee, S.H.; Park, N.Y.; Prinyawiwatkul, W. Stability and antibacterial activity of chitosan solutions affected by storage temperature and time. *Carbohydr. Polym.* **2006**, *65*, 174–178.

16. Helander, I.; Nurmiaho-Lassila, E.L.; Ahvenainen, R.; Rhoades, J.; Roller, S. Chitosan disrupts the barrier properties of the outer membrane of Gram-negative bacteria. *Int. J. Food Microbiol.* **2001**, *71*, 235–244.

17. Chen, Y.M.; Chung, Y.C.; Woan Wang, L.; Chen, K.T.; Li, S.Y. Antibacterial properties of chitosan in waterborne pathogen. *J. Environ. Sci. Health A* **2002**, *37*, 1379–1390.

18. Dutta, P.; Tripathi, S.; Mehrotra, G.; Dutta, J. Perspectives for chitosan based antimicrobial films in food applications. *J. Food Chem.* **2009**, *114*, 1173–1182.

19. Beverlya, R.L.; Janes, M.E.; Prinyawiwatkula, W.; No, H.K. Edible chitosan films on ready-to-eat roast beef for the control of *listeria monocytogenes*. *Food Microbiol.* **2008**, *25*, 534–537.

20. Sánchez-González, L.; Cháfer, M.; Hernández, M.; Chiralt, A.; González-Martínez, C. Antimicrobial activity of polysaccharide films containing essential oils. *Food Control* **2011**, *22*, 1302–1310.

21. Martínez-Camacho, A.P.; Cortez-Rocha, M.O.; Castillo-Ortega, M.M.; Burgos-Hernández, A.; Ezquerra-Brauer, J.M.; Plascencia-Jatomea, M. Antimicrobial activity of chitosan nanofibers obtained by electrospinning. *Polym. Int.* **2011**, *60*, 1663–1669.

22. Torres-Giner, S.; Ocio, M.; Lagaron, J. Development of active antimicrobial fiber-based chitosan polysaccharide nanostructures using electrospinning. *J. Eng. Life Sci.* **2008**, *8*, 303–314.

23. Ignatova, M.; Starbova, K.; Markova, N.; Manolova, N.; Rashkov, I. Electrospun nano-fibre mats with antibacterial properties from quaternised chitosan and poly (vinyl alcohol). *Carbohydr. Res.* **2006**, *341*, 2098–2107.

24. Ardila, N.; Medina, N.; Arkoun, M.; Heuzey, M.-C.; Ajji, A.; Panchal, C.J. Chitosan–bacterial nanocellulose nanofibrous structures for potential wound dressing applications. *Cellulose* **2016**, *23*, 3089–3104.

25. Ardila, N.; Daigle, F.; Heuzey, M.C.; Ajji, A. Effect of chitosan physical form on its antibacterial activity against pathogenic bacteria. *J. Food Sci.* **2017**, Article accepted for publication.

26. Qi, L.; Xu, Z.; Jiang, X.; Hu, C.; Zou, X. Preparation and antibacterial activity of chitosan nanoparticles. *Carbohydr. Res.* **2004**, *339*, 2693–2700.

27. Kong, M.; Chen, X.G.; Liu, C.S.; Liu, C.G.; Meng, X.H.; Yu, L.J. Antibacterial mechanism of chitosan microspheres in a solid dispersing system against *E. coli*. *Colloids Surf. B* **2008**, *65*, 197–202.

28. Kong, M.; Chen, X.-G.; Xue, Y.-P.; Liu, C-S.; Yu, L.-J.; Ji, Q.-X.; Cha, D.S.; Park, H.J. Preparation and antibacterial activity of chitosan microshperes in a solid dispersing system. *Front. Mater. Sci. China* **2008**, *2*, 214–220.

29. Yien, L.; Zin, N.M.; Sarwar, A.; Katas, H. Antifungal activity of chitosan nanoparticles and correlation with their physical properties. *Int. J. Biomater*. **2012**, *2012*, 632698.

30. Lertsutthiwong, P.; How, N.C.; Chandrkrachang, S.; Stevens, W.F. Effect of chemical treatment on the characteristics of shrimp chitosan. *J. Met. Mater. Miner.* **2002**, *12*, 11–18.

31. Sini, T.K.; Santhosh, S.; Mathew, P.T. Study on the production of chitin and chitosan from shrimp shell by using bacillus subtilis fermentation. *Carbohydr. Res*. **2007**, *342*, 2423–2429.

32. Muzzarelli, R.A.A.; Raith, G.; Tubertini, O. Separation of trace elements from see water, brine and sodium and magnesium salt solutions by chromatography on chitosan. *J. Chromatogr.* **1970**, *47*, 414-420.

33. Cho, Y.I.; No, H.K.; Meyers, S.P. Physicochemical characteristics and functional properties of various commercial chitin and chitosan products. *J. Agric. Food Chem.* **1998**, *46*, 3839–3843.

34. Kumirska, J.; Czerwicka, M.; Kaczyński, Z.; Bychowska, A.; Brzozowski, K.; Thöming, J.; Stepnowski, P. Application of spectroscopic methods for structural analysis of chitin and chitosan. *Mar. Drugs* **2010**, *8*, 1567–1636.

35. Paulino, A.T.; Simionato, J.I.; Garcia, J.C.; Nozaki, J. Characterization of chitosan and chitin produced from silkworm crysalides. *Carbohydr. Polym.* **2006**, *64*, 98–103.

36. Pillai, C.; Paul, W.; Sharma, C.P. Chitin and chitosan polymers: Chemistry, solubility and fiber formation. *Prog. Polym. Sci.* **2009**, *34*, 641–678.

37. Yao, K.; Li, J.; Yao, F.; Yin, Y. *Chitosan-Based Hydrogels: Functions and Applications*; CRC Press: Boca Raton, FL, USA, 2011.

38. Jia, Z.; Xu, W. Synthesis and antibacterial activities of quaternary ammonium salt of chitosan. *Carbohydr. Res.* **2001**, *333*, 1–6.

39. Synowiecki, J.; Al-Khateeb, N.A. Production, properties, and some new applications of chitin and its derivatives. *Crit. Rev. Food Sci. Nutr.* **2003**, *43*, 145–171.

40. Tsai, G.J.; Su, W.H. Antibacterial activity of shrimp chitosan against *Escherichia coli*. *J. Food Prot.* **1999**, *62*, 239–243.

41. Chen, Y.-L.; Chou, C.-C. Factors affecting the susceptibility of S*taphylococcus aureus* CCRC 12657 to water soluble lactose chitosan derivative. *Food Microbiol.* **2005**, *22*, 29–35.

42. Cho, J.; Heuzey, M.-C.; Bégin, A.; Carreau, P.J. Physical gelation of chitosan in the presence of β-glycerophosphate: The effect of temperature. *Biomacromolecules* **2005**, *6*, 3267–3275.

43. Wang, Q.Z.; Chen, X.G.; Liu, N.; Wang, S.X.; Liu, C.S.; Meng, X.H.; Liu, C.G. Protonation constants of chitosan with different molecular weight and degree of deacetylation. *Carbohydr. Polym.* **2006**, *65*, 194–201.

44. Jeon, Y.-J.; Park, P.-J.; Kim, S.-K. Antimicrobial effect of chitooligosaccharides produced by bioreactor. *Carbohydr. Polym.* **2001**, *44*, 71–76.

45. Chung, Y.C.; Wang, H.L.; Chen, Y.M.; Li, S.L. Effect of abiotic factors on the antibacterial activity of chitosan against waterborne pathogens. *Bioresour. Technol*. **2003**, *88*, 179–184.

46. Raafat, D.; Sahl, H.G. Chitosan and its antimicrobial potential–a critical literature survey. *Microb. Biotechnol.* **2009**, *2*, 186–201.

47. Crow, D.R. *Principles and Applications of Electrochemistry*; CRC Press: Boca Raton, FL, USA, 1994.

48. Guibal, E. Interactions of metal ions with chitosan-based sorbents: A review. *Sep. Purif. Technol.* **2004**, *38*, 43–74.

49. Tadmor, R.; Hernandez-Zapata, E.; Chen, N.; Pincus, P.; Israelachvili, J.N. Debye length and double-layer forces in polyelectrolyte solutions. *Macromol.* **2002**, *35*, 2380–2388.

50. Smith, A.M.; Lee, A.A.; Perkin, S. The electrostatic screening length in concentrated electrolytes increases with concentration. *J. Phys. Chem. Lett.* **2016**, *7*, 2157–2163.

51. Lefrou, C.; Fabry, P.; Poignet, J.-C. *Electrochemistry: The Basics, with Examples*; Springer Science & Business Media: New York, NY, USA, 2012; Chapter 3, p. 132.

52. Hajmeer, M.; Ceylan, E.; Marsden, J.L.; Fung, D.Y. Impact of sodium chloride on *Escherichia coli* O157:H7 and *Staphylococcus aureus* analysed using transmission electron microscopy. *Food Microbiol.* **2006**, *23*, 446–452.

53. Eaton, P.; Fernandes, J.C.; Pereira, E.; Pintado, M.E.; Malcata, F.X. Atomic force microscopy study of the antibacterial effects of chitosans on *Escherichia coli* and *Staphylococcus aureus*. *Ultramicroscopy* **2008**, *108*, 1128–1134.

54. Manni, L.; Ghorbel-Bellaaj, O.; Jellouli, K.; Younes, I.; Nasri, M. Extraction and characterization of chitin, chitosan, and protein hydrolysates prepared from shrimp waste by treatment with crude protease from *bacillus cereus* SV1. *Appl. Biochem. Biotechnol.* **2010**, *162*, 345–357.

55. Chen, L.-C.; Kung, S.-K.; Chen, H.-H.; Lin, S.-B. Evaluation of zeta potential difference as an indicator for antibacterial strength of low molecular weight chitosan. *Carbohydr. Polym.* **2010**, *82*, 913–919.

56. Chung, Y.C.; Su, Y.P.; Chen, C.C.; Jia, G.; Wang, H.L.; Wu, J.G.; Lin, J.G. Relationship between antibacterial activity of chitosan and surface characteristics of cell wall. *Acta Pharmacol. Sin.* **2004**, *25*, 932–936.

57. Dickson, J.S.; Koohmaraie, M. Cell surface charge characteristics and their relationship to bacterial attachment to meat surfaces. *Appl. Environ. Microbiol.* **1989**, *55*, 832–836.

58. Goy, R.C.; Morais, S.T.; Assis, O.B. Evaluation of the antimicrobial activity of chitosan and its quaternized derivative on *E. coli* and *S. aureus* growth. *Rev. Bras. Farmacogn.* **2015**, *26*, doi:10.1016/j.bjp.2015.09.010.

59. Tsai, G.J.; Su, W.H.; Chen, H.C.; Pan, C.L. Antimicrobial activity of shrimp chitin and chitosan from different treatments and applications of fish preservation. *Fish. Sci.* **2002**, *68*, 170–177.

60. Ahmad, A.; Sumathi, S.; Hameed, B. Adsorption of residue oil from palm oil mill effluent using powder and flake chitosan: Equilibrium and kinetic studies. *Water Res.* **2005**, *39*, 2483–2494.

61. Qi, L.; Xu, Z. Lead sorption from aqueous solutions on chitosan nanoparticles. *Colloids Surf. A* **2004**, *251*, 183–190.

62. Qi, L.; Xu, Z.; Jiang, X.; Li, Y.; Wang, M. Cytotoxic activities of chitosan nanoparticles and copper-loaded nanoparticles. *Bioorg. Med. Chem. Lett.* **2005**, *15*, 1397–1399.

63. Arkoun, M.; Daigle, F.; Heuzey, M.-C; Ajji, A. Antibacterial electrospun chitosan-based nanofibers: a bacterial membrane perforator. *Food Sci. Nutr.* **2017**, doi:10.1002/fsn3.468.

64. Huang, M.; Khor, E.; Lim, L.-Y. Uptake and cytotoxicity of chitosan molecules and nanoparticles: Effects of molecular weight and degree of deacetylation. *Pharm. Res.* **2004**, *21*, 344–353.

65. Tsaih, M.L.; Chen, R.H. Molecular weight determination of 83% degree of decetylation chitosan with non-gaussian and wide range distribution by high-performance size exclusion chromatography and capillary viscometry. *J. Appl. Polym. Sci.* **1999**, *71*, 1905–1913.

66. Lavertu, M.; Darras, V.; Buschmann, M.D. Kinetics and efficiency of chitosan reacetylation. *Carbohydr. Polym.* **2012**, *87*, 1192–1198.

67. Association of Official Analytic Chemist (AOAC). *Official Methods of Analysis*, 16th ed.; Association of Official Analytic Chemist: Washington, DC, USA, 1995.

Sample Availability

Some samples of the compounds could be available from the authors upon request.

CHAPTER 6: ARTICLE 2: CHITOSAN ELECTROSPRAYING: MAPPING OF PROCESS STABILITY AND DROPLET FORMATION

Nury Ardila, Zineb Ajji, Marie-Claude Heuzey and Abdellah Ajji

Research Center for High Performance Polymer and Composite Systems (CREPEC), Department of Chemical Engineering, Polytechnique Montréal, P.O. Box 6079, Station Centre-Ville, Montréal, QC H3C 3A7, Canada

(This work was submitted to *Journal of Aerosol Science* on April 3rd, 2017)

6.1 Abstract

Chitosan micro and nanospheres were produced by a one-step electrospraying process. The influence of several solution and process parameters on droplet morphology, collection yield and process stability was investigated. In addition, the mapping of the process stability was established according to various dimensionless numbers: Reynolds (*Re*), electric Peclet *(Pe*), Weber (*We*) and Froude (*Fr*) numbers and an electrostatic force parameter (Ω). Chitosan (medium molecular weight)/acetic acid (CS/AcOH) solutions at 1 and 2 wt/v % CS, and at 70 and 90 v/v % AcOH content, allowed the production of micro and nanoparticles. A solution surface tension below 36 mN/m, a relatively low conductivity between 0.015 to 0.089 S/m and a shear viscosity between 0.08 to 1.65 Pa s, were required for process stability, micro and nanoparticle formation and collection. The optimal process conditions included pumping of CS/AcOH solutions through a 22G needle, at flow rate of 0.2 mL/h, a voltage of 33 kV and a distance of 11 cm from the needle tip to collector plate. In general, the stability in the electrospraying of CS/AcOH solutions required relatively low values for *Re*, *Fr* and Ω, but relatively high values for *Pe* and *We* numbers.

6.2 Introduction

Chitosan is a linear polysaccharide with molecular structure consisting of glucosamine and *N*-acetyl glucosamine units. Chitosan is obtained by the *N*-deacetylation of chitin, the second most abundant polysaccharide in nature, after cellulose. However, the *N*-deacetylation is almost never

complete (Kumar, 2000). When the DDA is higher than 50 %, chitin is named chitosan (Rinaudo, 2006). The degree of deacetylation (DDA) usually ranges from 66-95 %, depending on the method used for its production, whilst the molecular weight (MW) of most commercial chitosan grades ranges from 4 to 2000 kDa (Agnihotri, Mallikarjuna, & Aminabhavi, 2004; Sinha et al., 2004). DDA and MW are the two main parameters influencing the physicochemical properties of chitosan such as solubility, crystallinity, viscosity, reactivity and processability (Kumirska, Weinhold, Thöming, & Stepnowski, 2011; Rinaudo, 2006). The unique properties of chitosan including its natural origin, availability, biodegradability, biocompatibility, mucoadhesivity, hemostatic properties, non-toxicity and antibacterial activity make it of great interest in a wide range of applications such as biomedical, pharmaceutical, water and waste treatment, cosmetology, agriculture and food industries (Agnihotri et al., 2004; Kumar, 2000; Rinaudo, 2006; Sinha et al., 2004).

Recently, the fabrication of chitosan micro and nanoparticles have been widely investigated in the biomedical field for drug- and gene-delivery applications due to their small size and large surface area to weight ratio (Agnihotri et al., 2004; Sinha et al., 2004). Several methods have been employed for their production (Agnihotri et al., 2004; Arya, Chakraborty, Dube, & Katti, 2009; Sinha et al., 2004). The most often used are emulsion cross-linking reaction, coacervation/precipitation, spray-drying, emulsion droplet coalescence and ionic gelation. Others such as reverse micellar and sieving methods are less common. The selection of any method depends of several factors such as particle size requirement, process, chemical and thermal stability and residual toxicity associated with the final product (Agnihotri et al., 2004; Mitra & Dey, 2011). Lately, the electrospraying process has been used as a relatively simple and low-cost technique for the fabrication of micro and nanoparticles. In addition of being a one-step process technique, it does not require subsequent purification steps and the process allows to control particle size, particle size distribution and form (Arya et al., 2009; Bock, Dargaville, & Woodruff, 2012; Kuo, Niu, Chang, Kuo, & Bair, 2004).

The principle of electrospraying was established based on the theory of deformation of charged droplets developed by Rayleigh (1882), Zeleny (1914) and Taylor (1964), which states that an electric field applied to a liquid droplet exiting a capillary is capable of deforming the interface of the droplet. Figure 6.1 shows a schematic of the electrospraying process, which consists in the application of a high electric field to a polymeric solution being pumped through a syringe.

Typically, the process involves three stages. The first one implies pumping of the solution through the needle, where simple shear flow occurs. However, at the exit of the needle, a complex flow develops with extensional and shear components (Haward, Sharma, Butts, McKinley, & Rahatekar, 2012). In the second stage, the charged liquid flowing out of the nozzle deforms in a meniscus with a characteristic shape known as Taylor cone (Rutledge & Fridrikh, 2007), from the apex of which a jet is ejected and elongated by an external electric field (Hohman, Shin, Rutledge, & Brenner, 2001). A balance among the electrostatic, gravity, inertia, viscoelastic and surface tension forces determines the deformation of the fluid (Feng, 2002, 2003; Jaworek & Sobczyk, 2008). Uniaxial elongational flow caused by the electrical forces acting on the jet occurs (Hohman et al., 2001). Finally, in the last stage, the jet is disintegrated into charged droplets when the electrostatic forces in the fluid are able to overcome those due to viscosity and surface tension (Sultan, Ashgriz, Guildenbecher, & Sojka, 2011). In electrospraying, different modes for droplet formation have been identified (Jaworek & Krupa, 1999), but only the cone-jet mode is known to produce a stable process (Bock et al., 2012). Once formed, the charged droplets travel to a collector plate while the solvent is evaporated. Many different parameters including process (flow rate, needle size, voltage, distance from needle tip to plate collector and temperature), environmental (humidity, pressure and temperature), and the intrinsic properties of the solution (conductivity, surface tension and viscosity, which depend mainly on the polymer concentration and molecular weight, as well as the solvent type) are important factors in determining process stability, droplet formation and morphology. However, solution parameters are considered to be the most critical (Park et al., 2007).

Several fundamental studies on electrospinning - a process in which fibers are formed instead of particles - have allowed the determination of a set of governing equations for the second stage, which is considered a steady-stretching process (Carroll & Joo, 2006; Feng, 2002; Pantano, Gañán-Calvo, & Barrero, 1994) and is common for both electrospinning and electrospraying (Hohman et al., 2001). Modeling of development of this stage has been performed by Reneker, Yarin, Fong, and Koombhongse (2000), Hohman et al. (2001), Feng (2002), among others, following the earlier works of Pantano et al. (1994), Gañán-Calvo (1997a,b) and Spivak and Dzenis (1998). The governing and dimensionless equations representing the mass, electric charge and momentum balances as well as the Coulomb's law for electric field for the steady jet can be found elsewhere (Feng, 2002; Hohman et al., 2001). Table 6.1 reports the dimensionless numbers identified as the

most representative for describing the process. They were obtained from the dimensionless form of the governing equations and include the Reynolds (*Re*), electric Peclet (*Pe*), Weber (*We*) and Froude (*Fr*) numbers and the electrostatic force parameter (Ω), among others (Feng, 2002; Hohman et al., 2001). These numbers allow the identification of the multiple process and solution parameters implied in the electrospraying process (aforementioned), as well as their interaction.

Several and extensive investigations have been published on the electrospinning of chitosan for fiber formation (Ardila et al., 2016; Geng, Kwon, & Jang, 2005; Homayoni, Ravandi, & Valizadeh, 2009; Ohkawa, Cha, Kim, Nishida, & Yamamoto, 2004; Ohkawa, Minato, Kumagai, Hayashi, & Yamamoto, 2006; Schiffman & Schauer, 2007). However, relatively few studies have addressed the electrospraying ability of chitosan to produce dry solid micro and nanoparticles. For instance, Kuo et al. (2004), Arya et al. (2009) and Zhang and Kawakami (2010) evaluated the effect of different process or solution parameters to control the obtained morphology in terms of particle size and size distribution. Chitosan particles with sizes in the range of 124 to 940 nm in diameter were reported. However, their studies comprised the analysis of only one chitosan grade characterized by a given MW and DDA. Recently, Gómez-Mascaraque, Sanchez, and López-Rubio (2016) reported the effect of chitosan molecular weight on the electrospraying of chitosan microspheres, and its correlation with electrical conductivity, viscosity and surface tension of the solutions. Although this work shows similarity with our study, process parameters were not addressed and only one DDA grade was considered. In addition, the viscosity of the solutions was studied at a shear rate of 200 s^{-1} which is far from the one calculated given the flow rate and needle size in real electrospraying conditions (would be around 0.6 s^{-1} when considering their process conditions).

Therefore, there is room for further analysis of this process in the case of chitosan. The present research work aims at studying both process and solution parameters to produce chitosan micro and nanospheres by electrospraying from five chitosan grades differing in MW and DDA. Process parameters such as flow rate, needle size, voltage, distance from needle tip to collector plate and electric field strength are analyzed first. Then, solution parameters including chitosan and acetic acid concentration, chitosan molecular weight and deacetylation degree, solvent type, which mainly determines the viscosity, surface tension and conductivity of the solutions are considered thereafter. Finally, the electrospraying ability of chitosan is mapped and established for the first time using dimensionless numbers governing the process, particularly *Re*, *Fr*, *Pe*, *We* and Ω, which

allow to correlate the most important variables involved with the obtained particle morphological characteristics.

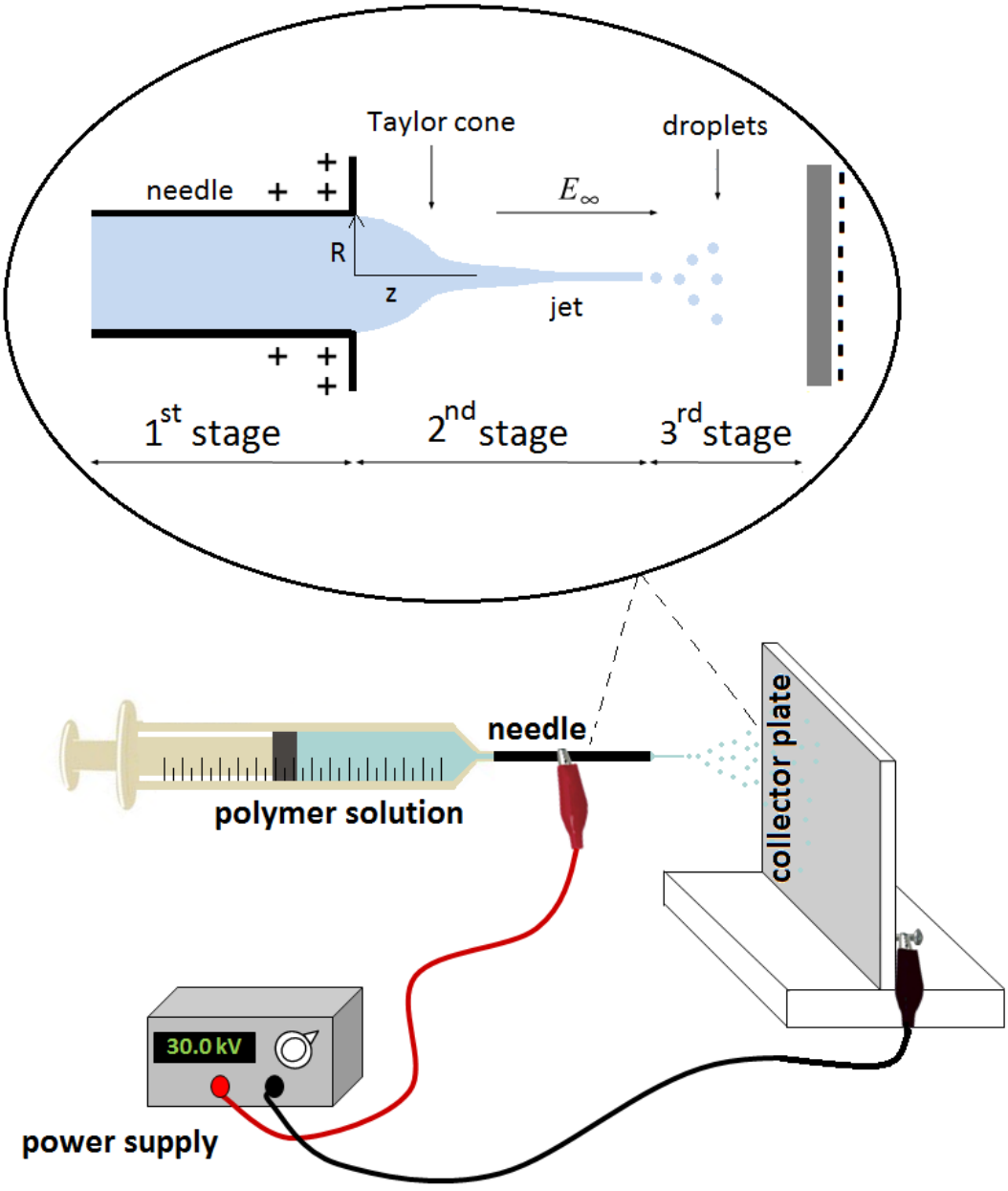

Figure 6.1: Schematic of the electrospraying process.

Table 6.1: Dimensionless numbers ruling the electrospraying process

Dimensionless number			
Electric Peclet number	$Pe = \frac{2\bar{\varepsilon} v_0}{R_0 K}$	Dielectric constant ratio	$\beta = \frac{\varepsilon}{\bar{\varepsilon}} - 1$
Reynolds number	$Re = \frac{\rho v_0 R_0}{\eta_0}$	Aspect ratio	$\chi = \frac{L}{R_0}$
Weber number	$We = \frac{\rho v_0^2 R_0}{\gamma}$	Deborah number	$De = \lambda \frac{v_0}{R_0} = \frac{\lambda}{t_0}$
Froude number	$Fr = \frac{v_0^2}{g R_0}$	Viscosity ratio	$r_\eta = \frac{\eta_p}{\eta_0}$
Electrostatic force parameter	$\Omega = \frac{\bar{\varepsilon} E_0^2}{\rho v_0^2}$	Electric field strength	$E_{\inf} = \frac{E_\infty}{E_0} = \frac{\Delta V / d}{E_0}$

In order of appearance per columns, $\bar{\varepsilon}$: dielectric constant of the air, v_0: velocity of the jet, R_0: Initial radius of the jet (needle), K: conductivity of the solution, ρ: density of the solution, η_0: viscosity of the solution, γ: surface tension, g: gravitational constant, E_0: initial external electric field, ε: dielectric constant of the jet, L: length of the jet, λ: relaxation time, t_0: time, η_p: polymer viscosity, η_0: solvent viscosity, E_∞: uniform spatially external electric field, ΔV: voltage and d: electrospraying distance.

6.3 Materials and Methods

6.3.1 Materials

Chitosan (CS) grades with different weight average molecular weight (M_W) and degree of deacetylation (DDA) were obtained from BioLog GmbH (Germany) and Primex (Iceland), and are presented in Table 6.2, along with nomenclature. Acetic acid (AcOH), trifluoroacetic acid (TFA), hydrochloric acid (HCl), citric acid (CA) and lactic acid (LA) aqueous solutions (≥ 85% in volume) were purchased from Sigma Aldrich (Canada). All chemicals used in this study were of analytical grade and used without further purification.

Table 6.2: Chitosan grades

Nomenclature	DDA (%)	M_W (kDa)	PDI	Company
B1*	90	183	-	Biolog GmbH
B2	90	207	1.67	Biolog GmbH
B3	90	344	1.72	Biolog GmbH
P1	95	57	2.24	Primex
P2	95	134	2.25	Primex

* Main chitosan grade used in this study.

6.3.2 Methods

6.3.2.1 Solution preparation and characterization

Chitosan at different concentrations (1, 2 and 3 wt/v %) was dissolved in different aqueous acetic acid concentrations (10, 30, 50, 70 and 90 v/v %). Other acids were also considered: hydrochloric acid (1 v/v %), citric acid (10, 30, 50 v/v %), lactic acid (1, 10, 50, 90, 100 v/v %), and pure TFA. Chitosan concentration was selected to be higher than the critical overlap concentration (C^*) for chitosan, which is reported to be in the range of 0.1-0.12 wt/v % (Cho, Heuzey, Bégin, & Carreau, 2006; Pakravan, Heuzey, & Ajji, 2011). Dissolution was carried out under magnetic stirring at room temperature until complete dissolution of the solutes. Obtained solutions were characterized in terms of electric conductivity, surface tension and viscosity as follows: The electric conductivity of the solutions was measured with a conductimeter Inolab ® Cond 750 (WTH GMbH, Germany). Measurements were done in triplicate. Surface tension measurement was performed in a Dynamic Contact Angle Meter and Tensiometer (DCAT11) equipped with a Wilhelmy plate as a test piece (sensor). Tests were done in triplicate. The steady shear viscosity of the solutions was measured in a controlled stress rheometer (MCR-502, Anton Paar, Germany) equipped with a double Couette flow geometry. Steady state flow tests were performed from 0.1 to 500 s^{-1} at 25 ºC. Low viscosity silicon oil was used to cover the surface of the samples to avoid the evaporation of acetic acid during the test. Pakravan et al. (2011) showed that the incorporation of silicon oil did not affect the rheological properties of the chitosan solutions. Tests were done in duplicate.

Results for chitosan/acetic acid (CS/AcOH) solutions in terms of electric conductivity, surface tension and shear viscosity are presented in Supporting Information, Figures 6.10 to 6.12 respectively.

6.3.2.2 Electrospraying set-up

Electrospraying was performed on a homemade horizontal device containing a variable high DC voltage power supply (Gamma High Voltage Research, FL, USA) and a programmable microsyringe pump (Harvard Apparatus, PHD 2000, USA). Polymer solutions were pumped through a syringe fitted with a metallic needle (details provided below). Electrospinning of the different solutions was conducted at different flow rates, needle sizes and over a wide range of electric field strengths, by varying the voltage and distance between the needle tip and the grounded collector plate, as presented in Table 6.3. Solutions were electrosprayed from the same volume (0.25 mL) for the analysis of the process parameters. Once the conditions for process stability were established, the collection time was constant (30 min) for the study of the solution parameters. All experiments were conducted in a closed chamber at room temperature (22 ± 1 ºC), relative humidity of 20-30 % and under atmospheric pressure. Chitosan micro and nano spheres were collected on aluminium foil attached to a stationary collector plate located at a certain distance from the tip of the needle. Collected particles were dried overnight under a chemical fume hood for the evaporation of any remaining solvent.

Table 6.3: Process parameters of electrospraying and range of analysis

Parameter	Value	Units
Electrospraying distance	5-25	cm
Diameter of needle	18 (0.84), 22 (0.41), 26 (0.26)	Gauge (mm)[a]
Flow rate	0.2-0.8	mL/h
Voltage	9-35	kV

[a] Internal diameter

6.3.2.3 Scanning electron microscopy (SEM)

The surface morphology of chitosan micro and nano spheres was observed by Scanning Electron Microscope, (SEM, JEOL JSM-7600TFE field emission gamma) operated at 2 kV. Particle size and distributions were analyzed using the Image-Pro Plus® software, taking the average of at least 100 or 300 particles depending on the particles collected (electrospraying of chitosan solutions containing 10-50 % and 70-90 v/v % AcOH content, respectively).

6.4 Results and Discussion

6.4.1 Effect of process parameters in electrospraying

Parameters including flow rate, needle size, voltage, needle tip to collector plate distance and electric field strength were investigated in this part of the study. Only one CS/AcOH solution was analyzed to keep solution properties such as viscosity, surface tension and conductivity constant. The CS/AcOH solution used was prepared at a concentration of 1 wt/v % (sample B1) in 50 v/v % AcOH. This chitosan grade was chosen since it has a moderate molecular weight (183 kDa), while the concentration was selected to avoid the formation of entanglements which can lead to fiber formation. Critical entanglement concentration for chitosan has been reported to be around 1.3-1.4 wt/v % for a chitosan with an average MW of 85 kDa (Pakravan et al., 2011). The high AcOH content was considered to have a relatively high conductivity and low surface tension (Figures 6.10 and 6.11 in Supporting Information), conditions that are required for solution deformation and driving of the jet, which favor process by electrospraying.

6.4.1.1 Effect of flow rate and needle size

Figure 6.2 presents SEM images showing the effects of flow rate and needle size, in terms of shear rate, in the electrospraying of a solution consisting of 1 wt/v % (sample B1) in 50 v/v % AcOH at 25 kV/10 cm. In general, the nanoparticle size increases when the flow rate increases. In addition, flow rates of 0.2 and 0.5 mL/h and lower needle gauges (higher size), such as 22G and 18G, favor nanoparticles collection on the aluminum foil. By contrast, when the flow rate was increased to 0.8 mL/h the yield (collected amount of particles) decreased mainly due to occasional dripping of the solution, given the relatively high flow rate. The yield also decreased when the solution is processed using a needle size of 26G. This effect is most probably due to other spraying modes

that could have developed (oscillating-jet, precession, or multi jet-mode spraying) rather than the cone and jet mode, given the low needle size and the high flow rate at such electric field, as presented by Jaworek and Krupa (1999), and Jaworek and Sobczyk (2008). In addition, the higher speed at which the solution is ejected from the tip of the needle could contribute to a low yield. For instance, for a flow rate of 0.2 mL/h, the ejection speed increased about 10 times (from 0.1 to 1.0 mm/s) by decreasing the needle diameter (from 18 to 26G). In addition, the ejection speed increases with flow rate, and a solution processed at 0.8 mL/h in a 26G needle solution is ejected at a rate of 4.2 mm/s. The increase in the ejection speed yields less material collected per unit area, since the spot area (area sprayed on the collector plate) increases, for example from 10 to 14 cm (in diameter) when the spraying is at 0.1 and 1.0 mm/s, respectively (needle of 18 and 26G, and at a flow rate of 0.2 mL/h). Therefore, a higher nanoparticle collection is observed at 0.2 mL/h for needles with higher diameter (18 and 22G). For these conditions, particles display an average diameter of 187 and 141 nm, respectively. In addition, the process was more stable and particle sizes were the smallest when using the 22G needle. Hence, this needle was used throughout the following tests. Finally, an increase in the shear rate of the solution causes the appearance of nanoparticles with an elongated form (Figure 6.2e to 6.2h) mainly due to a higher deformation of the solution due to shear (Figure 6.12 of the supporting information).

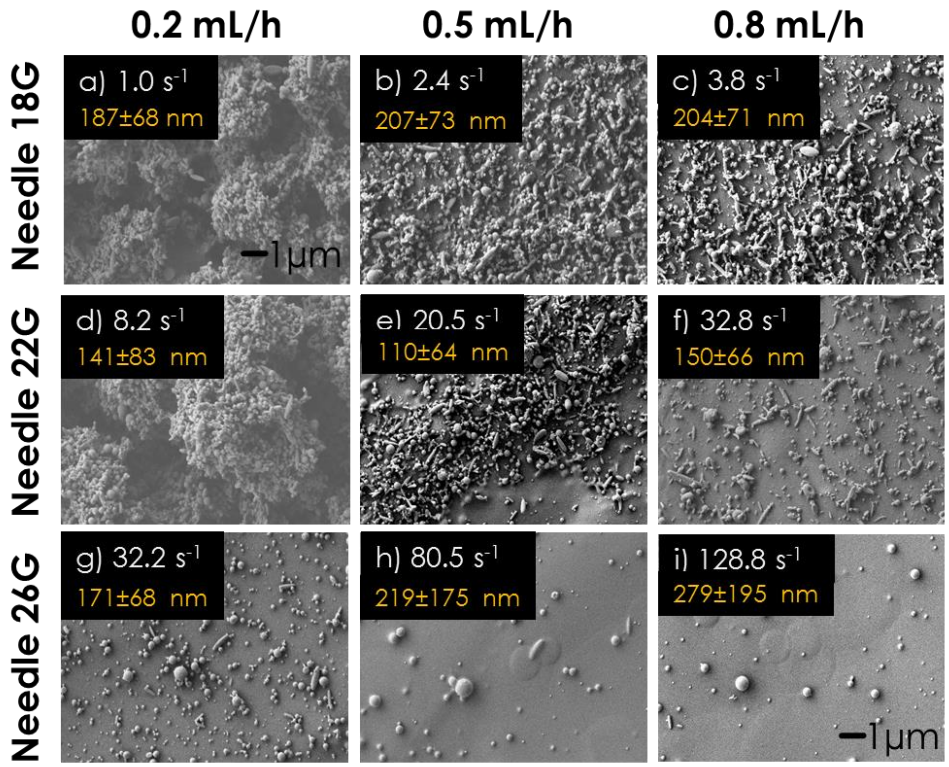

Figure 6.2: SEM images showing the effect of flow rate and needle size, in terms of shear rate, on the electrospraying of 1 wt/v % (sample B1) solution in 50 v/v % AcOH, at 25 kV/10 cm.

6.4.1.2 Voltage, distance and electric field strength

Arc discharges occurred in the electrospraying of CS/AcOH solutions when the distance from the needle tip to the collector plate was 5 cm or lower, and at voltages greater than 40 kV. In addition, a minimum electrostatic force of 1.2-1.5 kV/cm was required to allow the deformation of the droplet and attraction to the collector plate. Lower values than 1 kV/cm produced dripping and/or sputtering of the solution.

Figure 6.3 presents SEM images showing the effect of electrospraying voltage and distance, in terms of the electric field strength, on the morphology and particle collection yield for a solution consisting of 1 wt/v % (sample B1) in 50 v/v % AcOH, electrosprayed at 0.2 mL/h and with a 22G needle. Regarding the morphology, nanoparticles are formed independently of the electric field strength, from 1.7 to 7 kV/cm. However, at electric field strengths between 3.5 and 7.0 kV/cm (Figure 6.3a-7.3c and 6.3f), an incomplete evaporation of the solvent can be noticed (which is mainly attributed to the short electrospraying distance and consequently to an improper contraction

and solidification of droplets); whilst at electric field strengths between 1.7 to 2.3 kV/cm (Figure 6.3g-6.3i), the presence of elongated forms can be observed. This latter is most probably due to the relatively low electric field strength, which may cause solution deformation but without sufficient strength to allow droplet formation. Nevertheless, nanoparticles with lower sizes are formed at these low electric field strengths. Kuo et al. (2004) demonstrated a linear relationship and an increase in chitosan microsphere size for electric field strengths between 5.5 and 6.5 kV/cm. Here, two independent linear relationships can be established for nanoparticle size (not presented here for the sake of brevity): one, for electric field strengths between 2.3 to 3.5 kV/cm and another for 5.0 to 7.0 kV/cm, in which size increases when increasing the electric field.

Results also show that the electric field strength notably influences the particle collection yield. Low electric field strengths between 1.7 to 3.0 kV/cm allow obtaining large yield, whilst higher field strengths reduce it significantly. Similar results were observed when the solution was processed at the same flow rate (0.2 mL/h) and with a larger needle size (18G). Therefore, results suggest that there is a maximum electric field strength (or potential force) to apply to the solution, which prevent the burst of the droplet (allowing the occurrence of a continuous jet) and spraying outside the target. For instance, the spot diameter (sprayed area) when spraying the solution at 1.7, 5.0 and 7.0 kV/cm is 10, 12 and 12.5 cm, respectively. Hence, there is less material per unit area at high electric field. Notwithstanding that low electric field strength seems to represent ideal conditions for process, a closer look at different areas of the collected material allow to identify different regions between 1.7 and 2.5 kV/cm. Figure 6.13 of the Supporting Information presents a further analysis of the morphology of the nanoparticles formed at electric field strengths between 1.7 and 2.5 kV/cm. Different regions can be clearly identified, which indicate the occurrence of some instabilities in the process, mainly related to a sudden breakup of the jet given the relatively low electric field strength. Therefore, a large droplet may be deposited over the electrosprayed particles and erase their form. Consequently, results indicate that the best condition for the solution electrospraying is 3 kV/cm.

The effect of distance and voltage by keeping constant the electric field at 3 kV/cm was also investigated. Figure 6.4 shows the morphology of a solution consisting of 2 wt/v % (sample B1) in 70 v/v % AcOH processed at 0.2 mL/h and with a 22G needle. Different distances and voltages were considered, but the electric field was fixed at 3 kV/cm. A higher yield and lower particle sizes were obtained when a voltage of 33 kV at 11 cm was applied (Figure 6.4d). Similar tendencies

were observed for solutions consisting of 1 wt/v % in 70 v/v % AcOH and 2 % in 90 v/v % AcOH for the same sample (results not shown). Therefore, voltage, distance and electric field strength are significant parameters defining both particle size and collection yield.

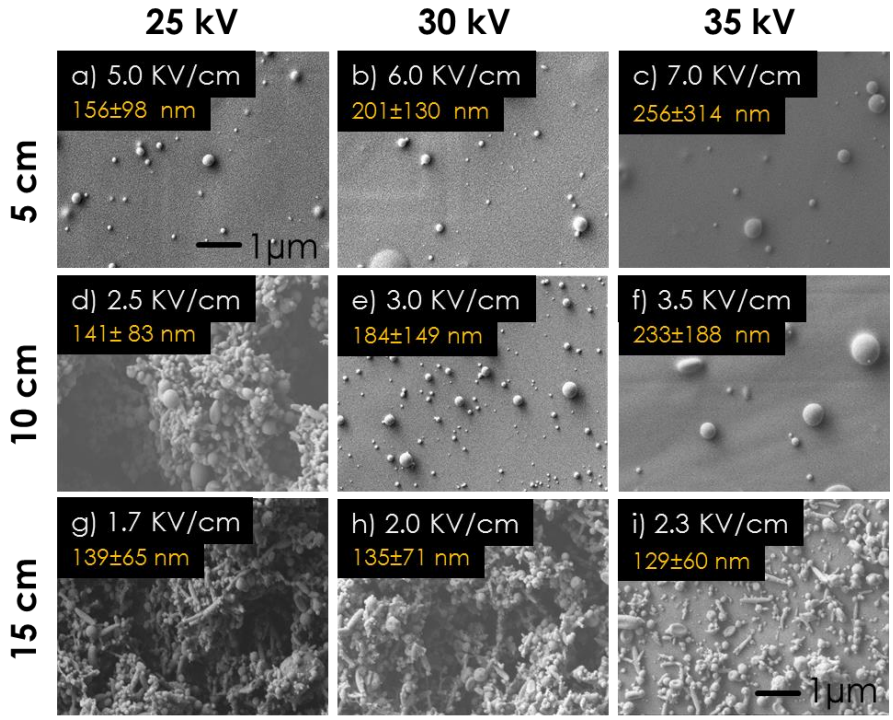

Figure 6.3: SEM images showing the effect of distance and voltage, in terms of electric field on the electrospraying of 1 wt/v % (sample B1) in 50 v/v % AcOH, at 0.2 mL/h and a 22G needle.

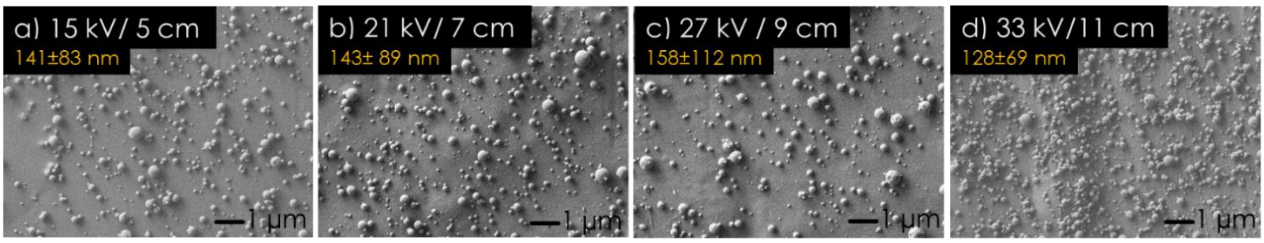

Figure 6.4: SEM images showing the effect of distance and voltage, in terms of electric field on the electrospraying of 2 wt/v % (sample B1) in 70 v/v % AcOH, at 0.2 mL/h and a 22G size.

6.4.2 Effect of solution parameters in electrospraying

In electrospraying, both process and solution parameters are important for defining process and morphology. According to the results above, process parameters determine the yield (collected

amount), morphology, particle size and process stability. In this section, solutions parameters are discussed to analyze their effect on process and morphology. The influence of solution parameters is explained in terms of solution properties: namely conductivity, surface tension and viscosity, which are in turn mainly dependent on chitosan concentration, MW and DDA, as well as solvent type and content.

6.4.2.1 Chitosan and acetic acid concentration

Figure 6.5 shows the effect of CS and AcOH concentration on the morphology of CS/AcOH solutions processed by electrospraying in a 22G needle, at 0.2 mL/h and 3 kV/cm. CS/AcOH solutions with polymer concentrations less than 1 wt/v % were insufficient to electrospray and dripping resulted, regardless of AcOH content or process conditions. The evaporation of excess solvent may not be rapid enough to form solid nanospheres with solutions that contain low concentrations of chitosan and excessive solvent (Park et al., 2007). By contrast, solutions with polymer concentrations above 3 wt/v % were too viscous to electrospray. This is because the high viscosity impedes the continuous flow of the polymer solution through the needle and the electric field strength, even if high, was not sufficient to deform the solution until obtaining a stable jet and subsequent particle formation. Consequently, only solutions between 1 and 3 wt/v % of chitosan were tested. According to Figure 6.12 in the Supporting Information, solution viscosity is affected by both chitosan and AcOH content, but the effect is more pronounced when changing the polymer concentration. Regarding electrospraying, in general as AcOH content increases, the particle collection yield increases, regardless of the CS concentration. Low particle collection is observed for solutions containing between 10 and 50 v/v % AcOH presumably due to the high conductivity and high surface tension of the solutions (Figures 6.10 and 6.11 of Supporting Information), which both decrease the stability of the process (Chen, Pui, & Kaufman, 1995; Zhang & Kawakami, 2010). At 10 and 30 v/v % AcOH, occasional sputtering of the solution occurs. Consequently, the formation of large droplets with a wide particle size distribution is observed. The low yield was observed for other chitosan solutions at 50 v/v % AcOH content or less, independently of chitosan MW or concentration.

By increasing AcOH content up to 70 v/v %, homogeneous particles with a narrow particle size distribution were formed, particularly for 1 and 2 wt/v % (sample B1). A further increase in AcOH content up to 90 v/v % results in an increase in the diameter and distribution of particle size. This

is most probably due to the increase in viscosity and decrease in conductivity of the solutions, which may hinder deformation and spraying of the solution and cause solution jet resistance to separate into droplets (Hartman, Brunner, Camelot, Marijnissen, & Scarlett, 2000; Zhang & Kawakami, 2010). The dimensionless number π_η introduced by Rosell-Llompart and de La Mora (1994) allows determining the effect of viscosity on the process of droplet formation:

$$\pi_\eta = \frac{\left(\gamma^2 \rho \left(\frac{\varepsilon \varepsilon_0}{K}\right)\right)^{1/3}}{\eta} \quad (1)$$

where γ, ρ, ε, K and η are the surface tension, solution density, dielectric constant, conductivity and viscosity, respectively.

The effect of viscosity on droplet size can be neglected when $\pi_\eta >> 1$. Otherwise, an increase in solution viscosity would increase droplet size (Wang et al., 2015; Zhang & Kawakami, 2010). Since π_η values for all solutions in this study are $\pi_\eta << 1$, it is concluded that viscosity increases particle size, as observed experimentally (in the range of 70 to 90 v/v % AcOH). Besides, the decrease in conductivity when increasing the AcOH from 70 to 90 v/v % may increase particle diameter due to a decrease in Coulomb repulsion (Zhang & Kawakami, 2010).

For 3 wt/v % (sample B1) in 70 and 90 v/v % AcOH content, the collection of particles decreases mainly due to the high viscosity of the solution. Experimentally, it was observed that the electric field is not able to completely deform the droplet until obtaining a stable jet. In addition, the relatively high viscosity of the solution prevents a complete breakup and only few particles are deposited on the collector plate. This would explain the low sizes observed in Figure 6.5n. Nonetheless, at 3 wt/v % B1 in 90 v/v % AcOH, fibers start forming because the polymer concentration is higher than the concentration at which entanglements are produced. This will be explained below.

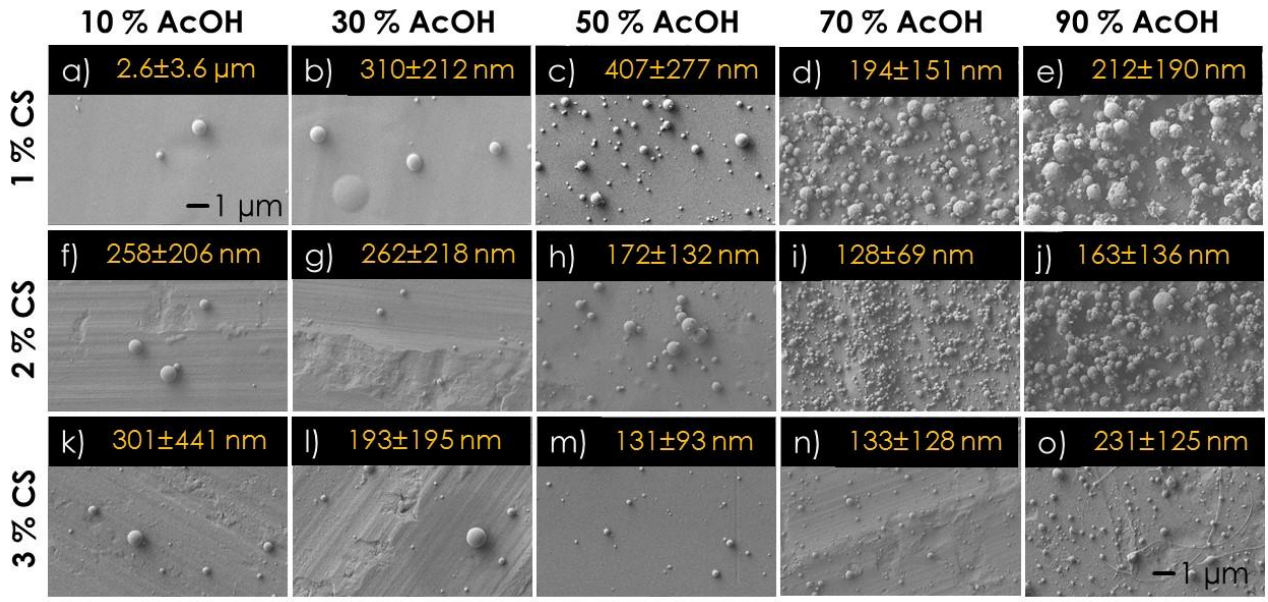

Figure 6.5: SEM images showing the effect of chitosan (wt/v %) and acetic acid concentration (v/v %) on the electrospraying of chitosan (sample B1), at 3 kV/cm, 0.2 mL/h and needle size 22.

6.4.2.2 Chitosan MW and DDA

Figure 6.6 shows the droplet morphology for several chitosan grades (differing in MW and DDA, Table 6.2), after electrospraying at different CS and AcOH concentrations. All these solutions vary slightly with conductivity but display similar surface tension values (Figure 6.10 and 6.11 of Supporting Information), which were not affected significantly by MW or DDA. Low MW CS (P1, 57 kDa) requires higher chitosan concentrations to obtain a reasonable particle collection, compared to other samples with higher MW. This is most probably due to a higher critical concentration, as will be discussed below. However, high concentrations (7 wt/v % CS) cause sputtering of the solution (results not shown). Since at a given CS and AcOH concentration, conductivity and surface tension are practically the same, the low yield for this chitosan grade is explained by its lower viscosity, which causes dripping of the solution (Figure 6.6a, 6.6f, 6.6k and 6.6s). For instance, at 1 wt/v % CS and 90 v/v % AcOH, the shear viscosity increases from 0.02 to 0.15 Pa.s when increasing the MW from 57 to 134 kDa (chitosan grades P1 and P2, respectively), at the same DDA (95 %). Low particle collection yield is also observed when increasing the CS from 2 to 3 wt/v % in medium MW CS (134 and 183 kDa, which corresponds to samples P2 and B1, respectively) (Figure 6.6t, 6.6u, 6.6w, and 6.6x). In this case, the decrease in the yield is mainly due to a significant increase in viscosity while the conductivity of the solution is low. For example,

for sample P2 (134 kDa), the shear viscosity increases from 0.93 to 2.77 Pa.s when increasing CS content from 2 to 3 wt/v %, respectively, at 70 v/v % AcOH. Consequently, even though surface tension is low at 70 v/v % AcOH, the electric field can deform but is unable to completely break the droplet at the needle tip. Thus, the stretched solution arrives entirely to the lower part of the collector. The same tendency was observed for sample B1 (183 kDa) at 3 wt/v %.

Regarding morphology, results from Figure 6.6 indicate that nanoparticles with good yield are obtained from solutions having shear viscosities between 0.08 to 1.65 Pa.s, if we exclude the high MW CS (B3). The shear viscosity of the respective solutions was evaluated at the maximum apparent shear rate encountered at the needle wall (8.2 s^{-1}), based on the dimensions of the needle geometry and the process flow rate, as explained by Pakravan et al. (2011). The more uniform nanoparticles are obtained from medium MW CS (samples B1 and B2) at relatively low CS concentrations (1 and 2 wt/v %). Nanoparticles with the lower size of 128 nm are produced from a solution containing 2 wt/v % B1 in 70 v/v % AcOH (Figure 6.6m).

Fiber formation is observed for high MW B3 (344 kDa) at 1 wt/v % CS, 70 and 90 v/v % AcOH (Figure 6.6e and 6.6j) and for medium MW B2 (207 kDa) at 2 wt/v % CS and 90 v/v % AcOH (Figure 6.6r). However, as shown in Figure 6.6, all previous solutions (Figure 6.6e, 6.6j and 6.6r) have viscosity values close to other solutions for which fiber formation is not observed (Figure 6.6q, 6.6m and 6.6n). Hence, the electrospraying ability of chitosan needs to be explained by other criteria than shear viscosity, surface tension and conductivity. The latter two do not change significantly for all solutions, as can be seen in Figure 6.6, and could be considered as constant. Some studies (McKee, Wilkes, Colby, & Long, 2004; Pakravan et al., 2011; Shenoy, Bates, Frisch, & Wnek, 2005) have reported the solution characteristic critical chain overlap and entanglement concentrations (C^* and C_e, respectively) as important parameters explaining the electrospinnability of several polymers. For neutral polymers, Shenoy et al. (2005) reported stable fiber formation at polymer concentrations $C>>C^*$. McKee et al. (2004) and McKee, Hunley, Layman and Long (2006) showed that beaded and bead-free fibers were formed at C_e and 2-2.5 C_e, respectively, for neutral polymers while this concentration increased up to 8-10 C_e for fiber formation in the case of polyelectrolytes. For chitosan of 85 kDa and 97.5% DDA, Pakravan et al. (2011) reported C^* of 0.1-0.12 wt % and C_e of 1.3-1.4 wt %. In the work of Pakravan et al. (2011), and in the present work, the critical overlap concentration, C^* is calculated at the point at which the viscosity of the solution is twice the viscosity of the solvent (Dobrynin, Colby, & Rubinstein, 1995; Rubinstein,

Colby, & Dobrynin, 1994), while the critical entanglement concentration C_e is calculated by the method proposed by Colby, Fetters, Funk and Graessley (1991), as will be presented below.

Table 6.4 displays C^* and C_e for chitosan solutions at 70 and 90 v/v % AcOH. They vary between 0.03-0.12 % and 1.0-2.6 %, respectively. For C_e, a value of 1.0 wt/v % is obtained for the higher MW (sample B3) and would explain the fiber formation observed in Figure 6.6e and 6.6j, since C=C_e. However, according to McKee et al. (2006), polymer concentration is too low and consequently beaded fibers are formed. C_e may also explain fiber formation for solutions at 2 wt/v % (sample B2) in 90 v/v % AcOH. However, the differences observed in morphology in Figure 6.6n and Figure 6.6r suggest that AcOH content may also play an important role, since the values for C_e do not vary for these solutions, but they differ in AcOH content (70 and 90 v/v %, respectively). Hence, at 70 v/v % AcOH, the lower solvent content would result in a higher level of interactions between chitosan chains due to strong inter and intra chain hydrogen bonding. Consequently, bead formation may be favored. By contrast, higher AcOH content would favor chitosan chains stretching and fiber formation. This can be explained based on rheological behaviour of the solutions. Figure 6.14 of the Supporting Information shows the variation of viscosity with shear rate of the solutions. At a shear rate of 8.2 s^{-1}, a 2 % B2 solution exhibits more shear thinning at 90 than at 70 v/v % AcOH content. A shear thinning behaviour of the chitosan solution can be interpreted as due to a reduction in entanglement density due to shear. Hence, rheological behaviour of the solution with 90 v/v % AcOH suggests that this solution would display higher fiber formation. On the other hand, the relative higher conductivity of the 2 % B2 solution at 70 v/v % AcOH may facilitate the breakup of the jet, allowing bead formation.

Regarding DDA content, results show that DDA may play an important role in electrospraying, even though it does not affect conductivity nor surface tension of the solutions, but shear viscosity. Figure 6.6 shows that at the same chitosan and AcOH contents, P2 solutions present higher viscosity than B1 solutions, despite the fact that the MW of the latter is higher. This may be explained by the DDA which is higher for sample P1, and consequently, the electrostatic repulsions between chitosan chains are stronger, which may increase the viscosity of the solutions and complicate their process. Hence, DDA is considered as having a relative importance in the electrospraying ability of chitosan. However, future tests should be conducted on chitosan grades with same MW but differing in DDA content to validate this argument.

Based on the findings for C^* and C_e, the results suggest that the concentration required for electrospraying depends mostly on CS MW as follows: for low MW CS (57 kDa): $25\ C^* \leq C \leq 1.6\ C_e$ and for medium MW CS (134-207 kDa): $14\ C^* \leq C \leq 1.5\ C_e$. In these conditions, adequate particle formation and collection is expected. High MW CS (344 kDa) produce beaded fibers at $C=C_e$.

Table 6.4: Chain overlap (C^*) and critical entanglement concentration (C_e) for chitosan at 70 and 90 v/v % AcOH content

Chitosan		P1	P2	B1	B2	B3
C^* (%)	70 v/v % AcOH	0.12	0.04	0.07	0.07	0.06
	90 v/v % AcOH	0.06	0.04	0.03	0.03	0.03
C_e (%)	70 v/v % AcOH	2.5	1.2	1.3	1.1	1.0
	90 v/v % AcOH	2.6	1.4	1.2	1.2	1.0

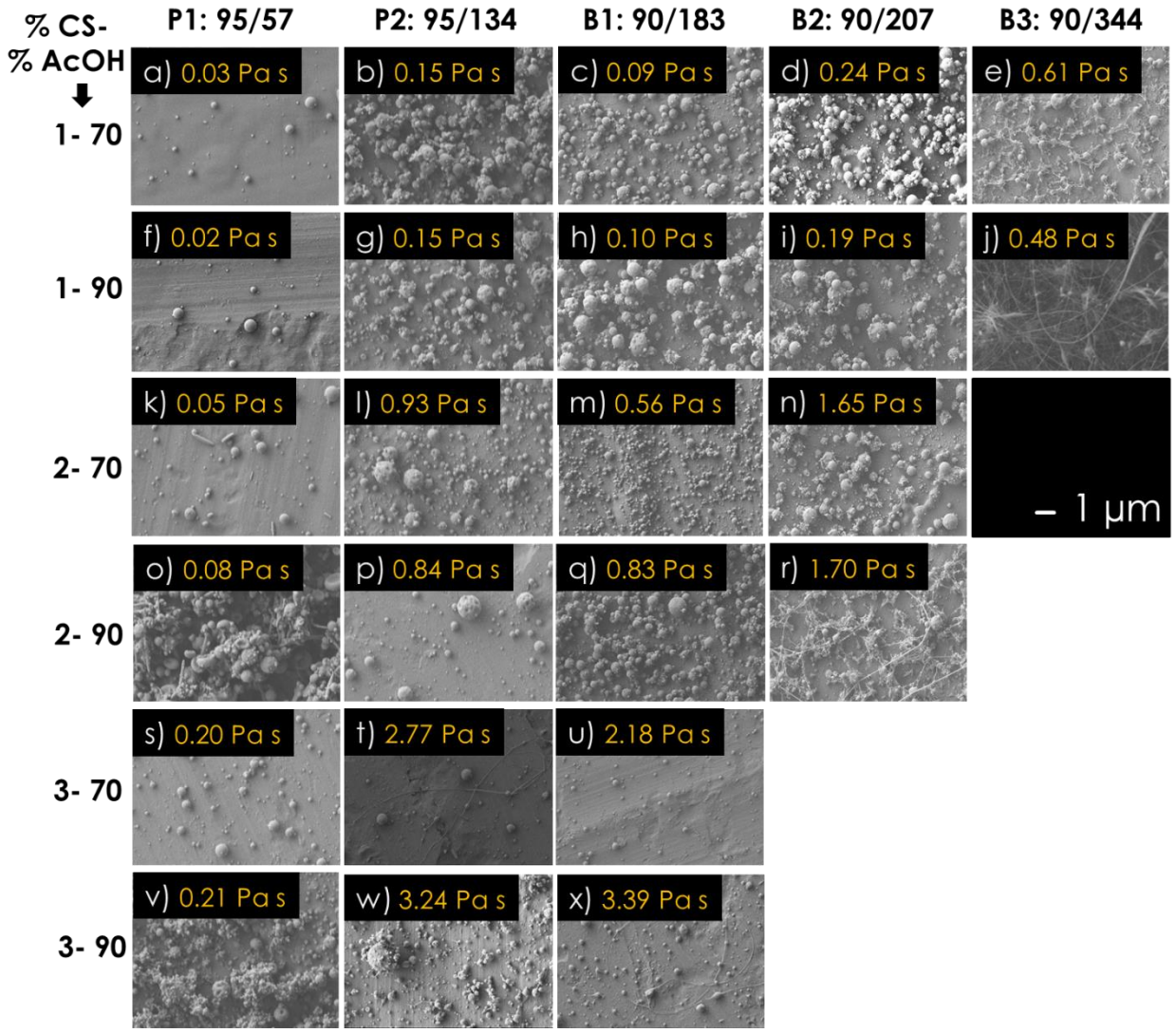

Figure 6.6: SEM images showing the effect of chitosan MW and DDA on the electrospraying of chitosan, at 3 kV/cm, 0.2 mL/h and needle size 22G. The shear viscosity of the respective solutions was evaluated at the maximum apparent shear rate encountered at the needle wall (8.2 s^{-1}) and is indicated in each case. The scale bar is the same (1 µm) for all the SEM images.

6.4.2.3 Solvent type

Several solvents including hydrochloric acid (HCl), citric acid (CA), trifluoroacetic acid (TFA), lactic acid (LA) and acetic acid (AcOH) were used to solubilize chitosan and tested in electrospraying. Figure 6.7 illustrates the effect of AcOH, TFA and LA. Chitosan nanoparticles are obtained in AcOH as discussed so far (Figure 6.7a). At the same chitosan content and process conditions, hollow particles with a larger size are observed when TFA is used (Figure 6.7b).

Differences in morphology are mainly due to the lower boiling point of TFA with respect to AcOH (72.4 ºC vs. 118 ºC). Consequently, TFA with its higher vapor pressure than AcOH, results in a higher solvent volatility. This result suggests that CS solutions in TFA should be processed at higher flow rates than in AcOH. However, other process and solution parameters should also be taken into consideration. On the other hand, no particle formation is observed when the solvent is LA, HCl or CA, independently of the chitosan content (from 1 to 3 wt/v %). In all those cases, a sputtering of the solution is obtained on the collector, as observed in Figure 6.7c for LA. This result is mainly due to the high surface tension of these solvents (and hence CS solutions), making it difficult to process the solution (Zhang & Kawakami, 2010). For instance, CS in HCl was soluble only at low concentration of the acid (1 v/v %) and a surface tension of about 74 mN/m was measured. By contrast, CS was soluble in citric acid at high concentrations of the acid in water (10, 30 and 50 wt/v). However, the solutions also had a high surface tension (62-72 mN/m), which prevented their process by electrospraying. Finally, CS was soluble in LA at low and high concentrations of the acid (1, 10, 30 and 50 v/v %, and in pure acid). The lower surface tension was obtained when CS was in pure LA, with a value of 44 mN/m. However, this value was still too high for jet and particle formation via electrospraying. Therefore, in addition to a low surface tension such as those measured in AcOH and TFA (36.2 and 15.6 mN/m, respectively), a relatively low volatility of the solvent is also required.

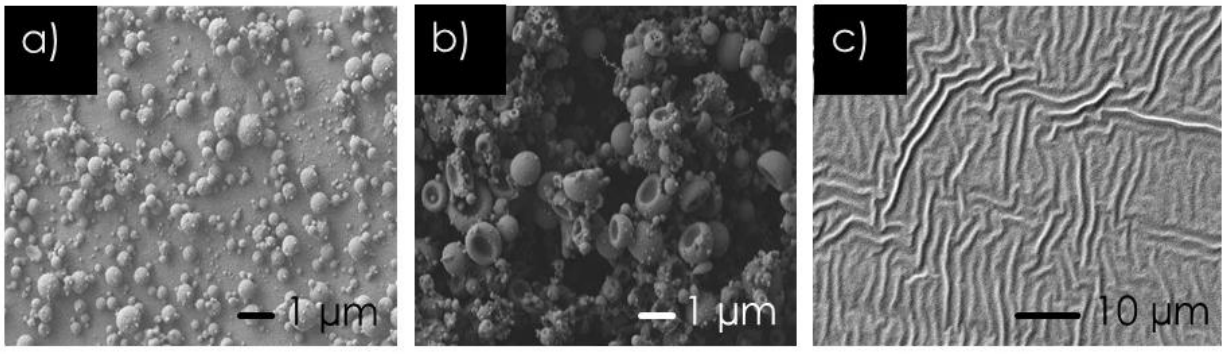

Figure 6.7: SEM images showing the effect of solvent type on the electrospraying of chitosan (sample B1): a) 1 wt/v % CS in 70 v/v % AcOH; b) 1 wt/v % CS in TFA; c) 1 wt/v % CS in LA. Process conditions: needle 22G, 3 kV/cm and 0.2 mL/h.

6.4.3 Mapping of the electrospraying ability of chitosan as function of dimensionless numbers

Up to now, it was shown that both process and solution parameters influence chitosan electrospraying. Production of chitosan micro and nanospheres with a good yield were successfully achieved when process CS/AcOH solutions having a surface tension lower than 36 mN/m, a conductivity between 0.015 to 0.089 S/m and a viscosity between 0.08 to 1.65 Pa.s (at the maximum shear rate at the needle, 8.2 s^{-1}) in a 22G needle pumped at 0.2 mL/h at 3 kV/cm. Table 6.5 shows the optimum values for the process and production of chitosan nanospheres with an average size of 128 ± 69 nm via electrospraying. All the experimental conditions tested and discussed so far allow the calculation of the dimensional numbers governing the electrospraying process of CS/AcOH solutions. Froude number and the electrostatic force parameter define the optimal process conditions, while Reynolds, Peclet and Weber numbers establish the range relating the solution parameters, as shown in Figure 6.8 and 6.9, respectively.

Figure 6.8a shows the dimensionless number *Fr* as function of flow rate and needle size. *Fr* number indicates the ratio of inertial to gravitational forces. Results suggest that relatively low *Fr* numbers ($Fr < 5 \times 10^{-3}$) favor process stability and particle collection yield. That is, a given needle size, relatively low velocities and for instance, a low flow rate will assure the stability in the cone-jet mode. Unstable jet can be obtained at a high needle size and very low velocities, or when $Fr < 0.01 \times 10^{-3}$.

Figure 6.8b shows the dimensionless number Ω as function of the electric field strength and the flow rate, when considering a 22G needle size. Ω indicates the magnitude of the electrostatic forces relative to inertia, and variables including the electric field strength, the density and velocity of the jet, and therefore the flow rate, are related. Results indicate that relatively low Ω number in the range between 1.0×10^3 and 5.0×10^3 favor process stability and particle collection yield. That is, a relatively low electric field strength at a low flow rate, will favor the electrospraying. An increase in the flow rate will require an increase in the electric field strength to maintain the stability of the process. Ω lower than 1.0×10^3 may cause the dripping of the solution while higher values than 5.0×10^3 may allow too few particle deposition and the sputtering of the solution in addition to the possibility of multiple jet formation.

Figure 6.9 shows the interrelation between the dimensionless numbers *Re*, *Pe* and *We*, containing the solution parameters of viscosity, conductivity and surface tension, respectively. Both *Re* and *Pe* depend on chitosan and AcOH contents. However, *Re* is more affected by chitosan than by AcOH concentration. At concentrations of 2 and 3 wt/v % CS, *Re* is almost independent of AcOH content. On the contrary, *We* number is only affected by AcOH, since the surface tension of the solutions are barely affected by chitosan concentration, as shown in Figure 6.11 of the Supporting Information. The region between these curves indicates the favourability of electrospraying for chitosan, which is the required conditions for achieving the cone jet mode. The results indicate that process stability and particle collection yield is governed by these dimensionless numbers and are achieved at relatively high *Pe* and *We* ($Pe > 3.78x10^{-10}$, $We > 0.96x10^{-6}$), while maintaining *Re* relatively low ($0.1\text{-}1.0x10^{-3}$).

Table 6.5: Optimum parameters to produce chitosan nanospheres with an average size of 128 ± 69 nm via electrospraying

Process		**Solution**	
Parameter	**Value**	**Parameter (units)**	**Value**
Needle size	22G	Surface tension*	0.036 N m
Flow rate, Q	0.2 mL/h	Viscosity*	0.56 Pa s
Distance, d	11 cm	Conductivity*	0.089 S/m
Voltage, V	33 kV	CS MW	183 kDa
Electric field strength, E	3 kV/cm	CS content	2 %
		AcOH content	70 v/v %

*These parameters are directly related to CS MW as well as CS and AcOH contents.

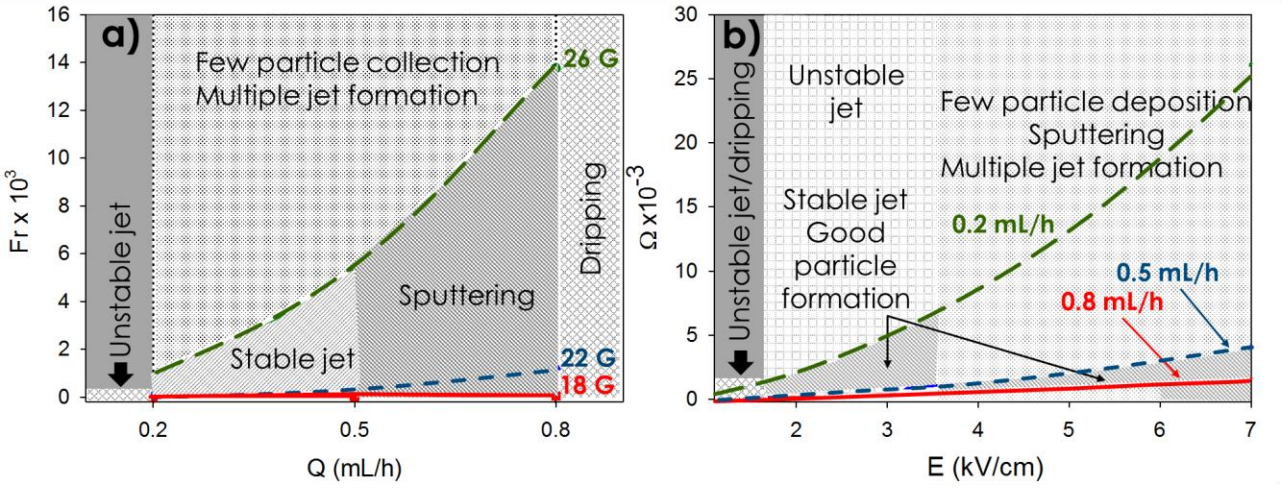

Figure 6.8: Dimensionless numbers establishing the process conditions in the electrospraying of CS/AcOH solutions: a) Froud number (*Fr*) as function of flow rate (*Q*), and b) Electrostatic force parameter (Ω) as function of electric field strength (E). Ω was calculated when considering R_0 from needle size 22G.

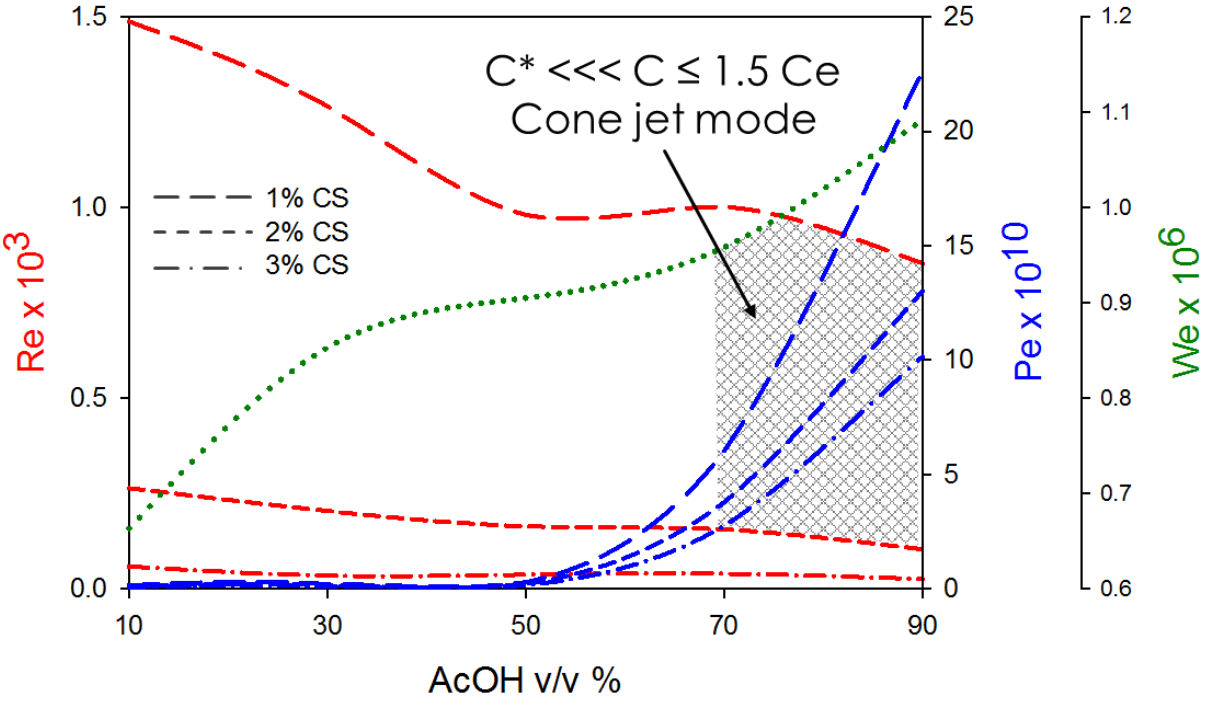

Figure 6.9: Dimensionless numbers representing the solution parameters in the electrospraying of CS/AcOH solutions: *Re*, *Pe* and *We* as function of CS and AcOH content. Dotted lines (in green color) indicate that *We* is independent of CS concentration.

6.5 Conclusions

Dry chitosan micro and nanospheres were produced by a one-step electrospraying process. A systematic study of the process determined that both solution and process parameters are critical for process stability, particle formation and collection yield. Nanospheres with a size of 128 nm in average were produced from CS/AcOH solutions from medium molecular weight CS (183 kDa) at 2 wt/v % CS, and at 70 v/v % AcOH content. The optimal process conditions included pumping the solution through a 22G needle, at flow rate of 0.2 mL/h, using a voltage of 33 kV over a distance of 11 cm from the needle tip to collector plate. In general, the stability of CS/AcOH solutions electrospraying required relatively low values for *Re*, *Fr* and Ω numbers, but relatively high values for *Pe* and *We*. Mapping of the electrospraying process for chitosan solutions was achieved using dimensionless numbers, and it indicates the regions and conditions that favor both process stability and particle formation.

6.6 Acknowledgments

The Fonds de Recherche du Québec - Nature et Technologies (FRQNT) is acknowledged for funding of the present work.

Author contributions

N.A. designed the study, collected test data, interpreted results and drafted the manuscript. Z.A. collected test data, M.-C.H. and A.A. designed the study, interpreted results and reviewed and edited the manuscript. All authors have approved the final version of the article.

6.7 Supporting information

Characterization of Chitosan/acetic acid (CS/AcOH) solutions

Chitosan/ acetic acid (CS/AcOH) solutions were characterized in terms of conductivity, pH, surface tension and viscosity. Figure 6.10 presents the differences in conductivity for the solutions at different polymer and AcOH concentrations. The conductivity of the solvent (AcOH in water) initially increases with concentration up to 20 %, and then decreases gradually down to 0 at 100 % AcOH. When CS is added, the conductivity increases notably up to a maximum value at 10 % and

then decreases with a quasi-linear pattern. This decrease is due to the low degree of disassociation of the acid (Zhang & Kawakami, 2010). In addition, by increasing CS concentration, and at low AcOH content (1-20 v/v %), the conductivity increases by about 2 and 2.5 fold from 1 to 2 and to 3 wt/v % CS. However, the effect of CS concentration on the conductivity of the samples decreases as the AcOH increases, and at 90% v/v % AcOH the conductivity is almost independent of CS content. Regarding MW and DDA, conductivity increases slightly as MW and DDA increase. However, the CS and AcOH concentration are the parameters that affect notably the conductivity of the different CS/AcOH solutions. According to the values obtained, all analyzed solutions are considered as highly conductive since their value is greater than 100 µS/cm (Zhang & Kawakami, 2010).

Figure 6.11 shows the surface tension of the different CS/AcOH solutions. The surface tension decreases continually with AcOH content from 74.7 mN/m, which corresponds to the value of the surface tension of water, to 28.4 mN/m, which corresponds to the surface tension of 100 % AcOH. From 10 to 50 % AcOH content, addition of CS decreases surface tension of the solution; and from 70 to 90 % AcOH, surface tension is not affected by CS but by AcOH content. In addition, as with conductivity, surface tension does not change significantly with MW as reported in another study (Gómez-Mascaraque, Sanchez, & López-Rubio, 2016) nor with DDA.

Figure 6.12 presents the viscosity of CS/AcOH solutions as a function of the shear rate, at different CS and AcOH concentrations for the CS grade B1. At 1 wt/v % CS, solutions present a Newtonian behavior along the range of shear rates tested, independently of the AcOH content. At a concentration of 2 and 3 wt/v % and from 1 to 70 v/v % AcOH, solutions present a slight shear thinning behavior that become more accentuated when the concentration of AcOH reaches 90 v/v %. A higher shear thinning behavior of the polymer solution can be interpreted as a result of a reduction in entanglement density due to shear. The shear viscosity is an important solution property to consider in solutions electrospraying since simple shear flow occurs inside the needle right before the solution is deformed by the electric field strength. According to Figure 6.12, the viscosity of the solutions depends on the shear rate encountered at the needle wall (maximum shear rate) in electrospraying. The latter was calculated based on the dimensions of the needle geometry and flow rate, as explained by Pakravan *et al.* [23]. The calculated shear rates are in the range of 1.0 to 3.8 s^{-1}, 8.2 to 32.8 s^{-1} and 32.2 to 128 s^{-1} for needle gauges of 18, 22 and 26G, respectively, in the range of flow rates analyzed (0.2 to 0.8 mL/h). These appear as dotted lines in Figure 6.12.

Therefore, needle size and flow rate determine shear rate at the needle wall, which will in turn define a characteristic value of the solution viscosity during process.

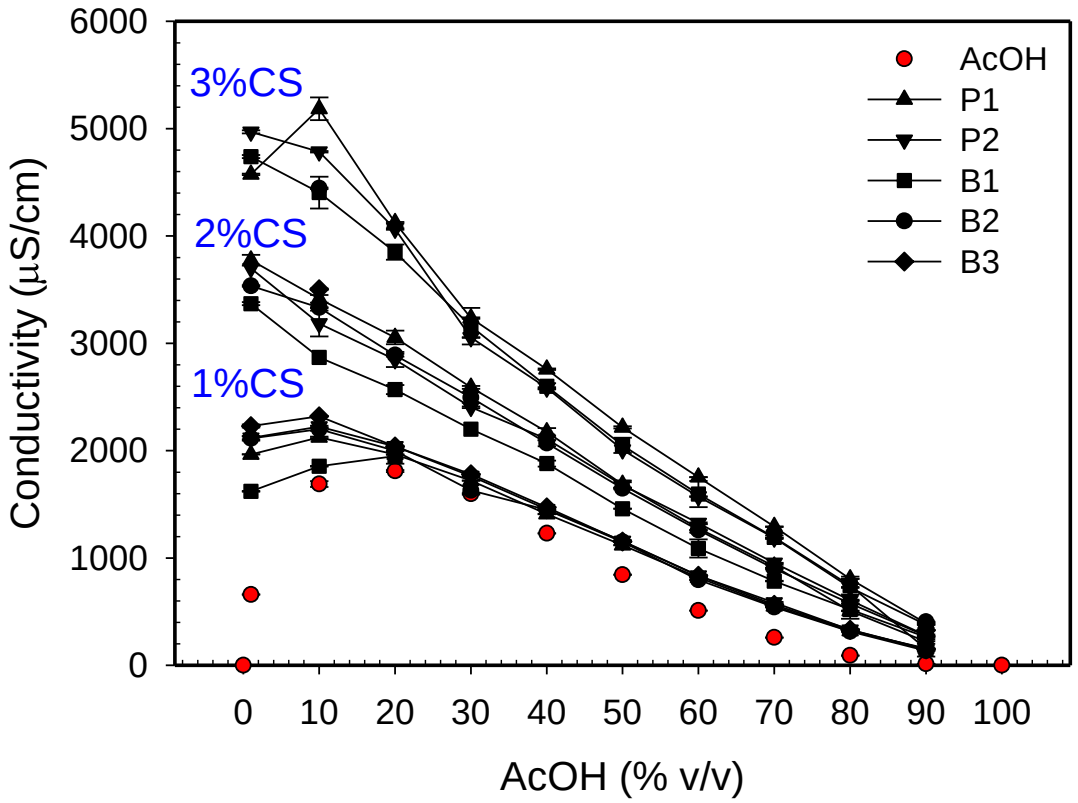

Figure 6.10: Conductivity of CS/AcOH solutions with different AcOH contents for various chitosan grades.

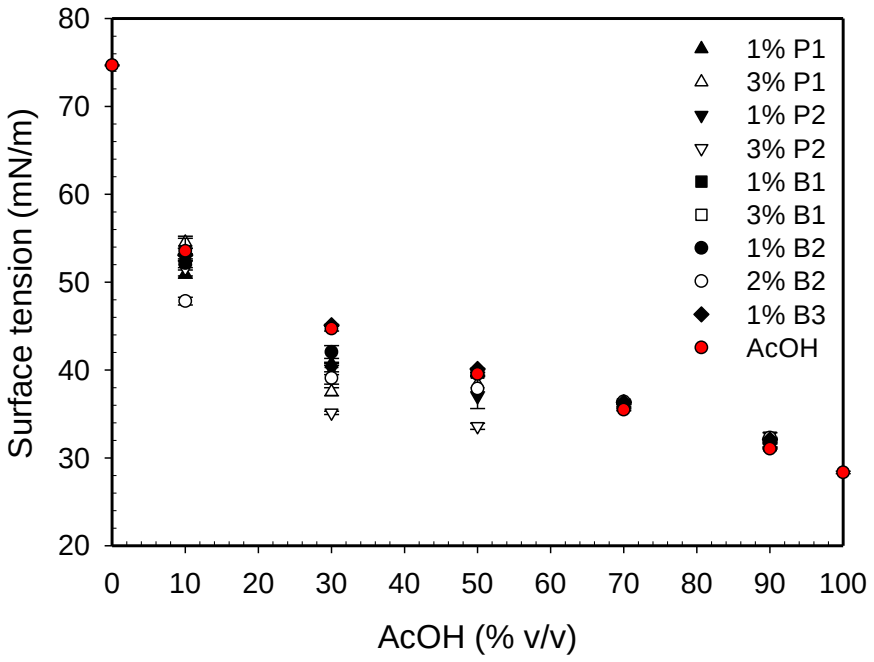

Figure 6.11: Surface tension of CS/AcOH solutions with different AcOH contents for various chitosan grades.

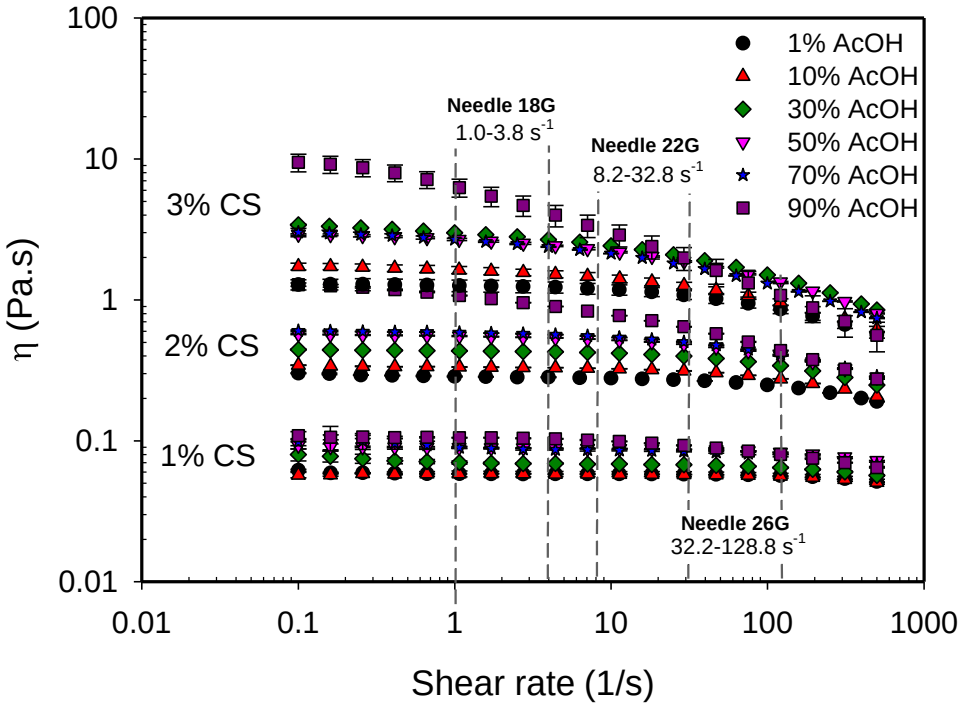

Figure 6.12: Viscosity of CS/AcOH solutions as a function of shear rate for chitosan grade B1. The doted lines represent the maximum shear rate at the needle wall calculated from the needle size and flow rate.

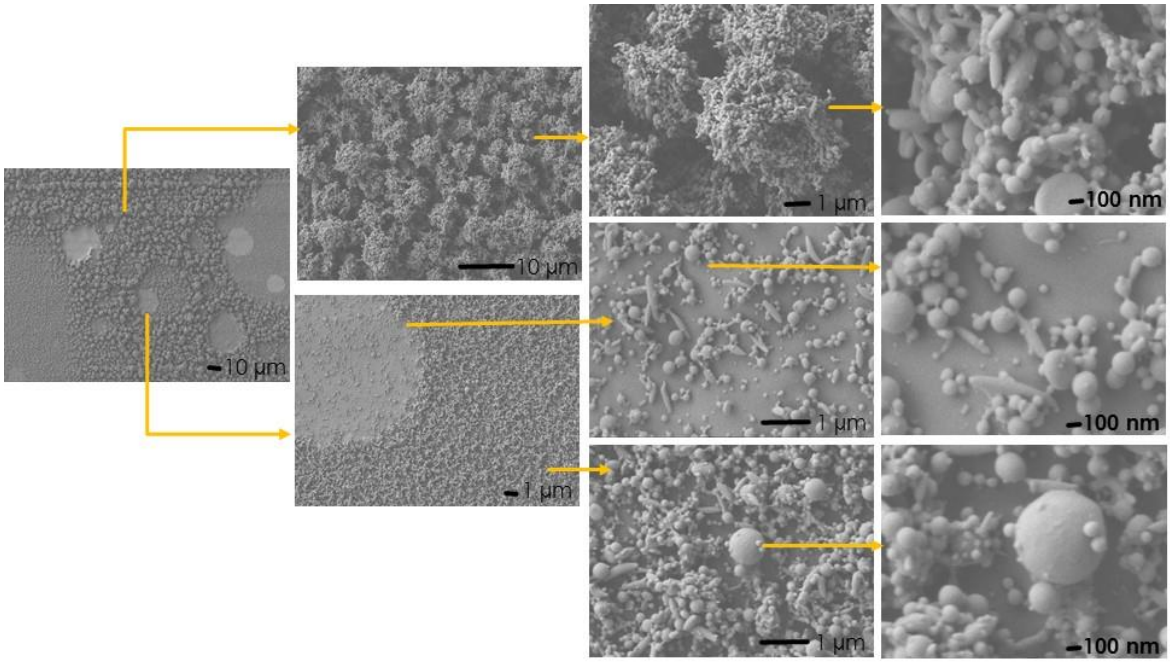

Figure 6.13: SEM images of different regions in the collected area after electrospraying 1 % CS_{B1} in 50 %AcOH at 0.2 mL/h and a 22G needle.

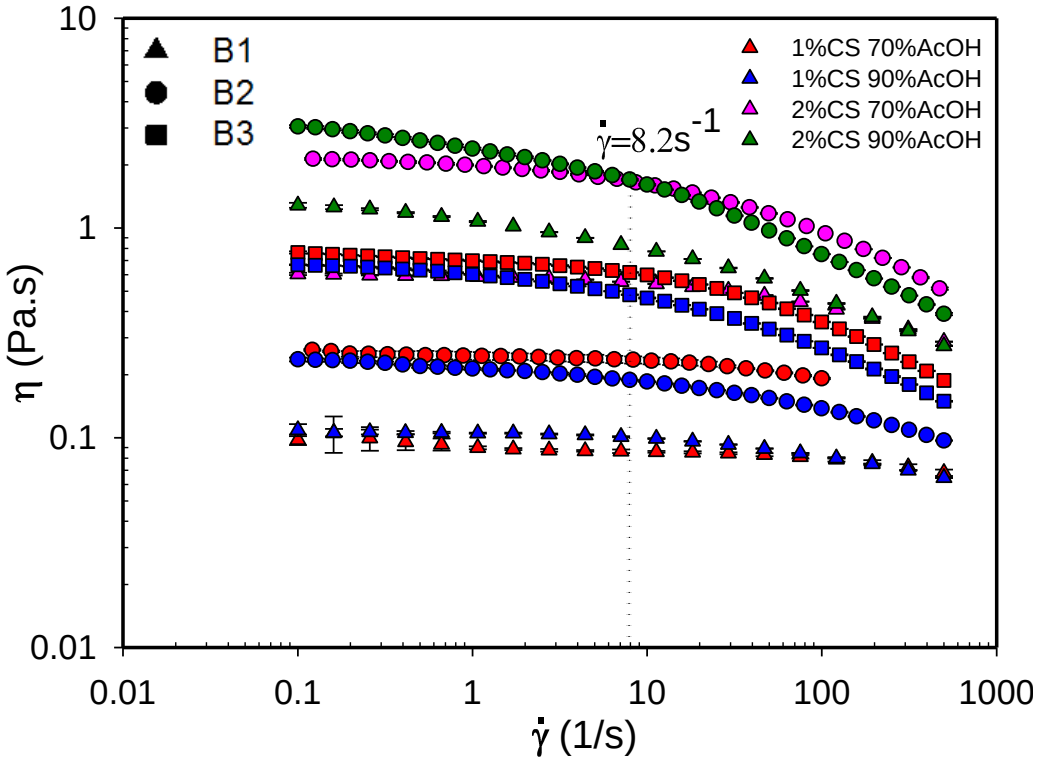

Figure 6.14: Viscosity as a function of shear rate for solutions containing chitosan with a 90 % DDA: B1 (183 kDa), B2 (207 kDa) and B3 (344 kDa).

6.8 References

Agnihotri, S. A., Mallikarjuna, N. N., & Aminabhavi, T. M. (2004). Recent advances on chitosan-based micro-and nanoparticles in drug delivery. *Journal of Controlled Release, 100*(1), 5-28.

Ardila, N., Medina, N., Arkoun, M., Heuzey, M. C., Ajji, A., & Panchal, C. J. (2016). Chitosan–bacterial nanocellulose nanofibrous structures for potential wound dressing applications. *Cellulose*, *23*(5), 3089-3104.

Arya, N., Chakraborty, S., Dube, N., & Katti, D. S. (2009). Electrospraying: A facile technique for synthesis of chitosan‐based micro/nanospheres for drug delivery applications. *Journal of Biomedical Materials Research Part B: Applied Biomaterials, 88*(1), 17-31.

Bock, N., Dargaville, T., & Woodruff, M. (2012). Electrospraying of polymers with therapeutic molecules: State of the art. *Progress in Polymer Science*, *37*(11), 1510-1551.

Carroll, C. P., & Joo, Y. L. (2006). Electrospinning of viscoelastic Boger fluids: Modeling and experiments. *Physics of fluids, 18* (5), 053102.

Chen, D.-R., Pui, D. Y., & Kaufman, S. L. (1995). Electrospraying of conducting liquids for monodisperse aerosol generation in the 4 nm to 1.8 μm diameter range. *Journal of Aerosol Science*, *26*(6), 963-977.

Cho, J., Heuzey, M.-C., Bégin, A., & Carreau, P. J. (2006). Viscoelastic properties of chitosan solutions: Effect of concentration and ionic strength. *Journal of Food Engineering, 74*(4), 500-515.

Colby, R. H., Fetters, L. J., Funk, W. G., & Graessley, W. W. (1991). Effects of concentration and thermodynamic interaction on the viscoelastic properties of polymer solutions. *Macromolecules, 24*(13), 3873-3882.

Dobrynin, A. V., Colby, R. H., & Rubinstein, M. (1995). Scaling theory of polyelectrolyte solutions. *Macromolecules, 28*(6), 1859-1871.

Feng, J. (2002). The stretching of an electrified non-Newtonian jet: A model for electrospinning. *Physics of fluids, 14*(11), 3912-3926.

Feng, J. (2003). Stretching of a straight electrically charged viscoelastic jet. *Journal of Non-Newtonian Fluid Mechanics, 116*(1), 55-70.

Ganan-Calvo, A. M. (1997a). On the theory of electrohydrodynamically driven capillary jets. Journal of Fluid Mechanics, 335, 165-188.

Ganan-Calvo, A., Davila, J., & Barrero, A. (1997b). Current and droplet size in the electrospraying of liquids. Scaling laws. *Journal of Aerosol Science, 28*(2), 249-275.

Geng, X., Kwon, O.-H., & Jang, J. (2005). Electrospinning of chitosan dissolved in concentrated acetic acid solution. *Biomaterials, 26*(27), 5427-5432.

Gómez-Mascaraque, L. G., Sanchez, G., & López-Rubio, A. (2016). Impact of molecular weight on the formation of electrosprayed chitosan microcapsules as delivery vehicles for bioactive compounds. *Carbohydrate Polymers, 150*, 121-130.

Hartman, R., Brunner, D., Camelot, D., Marijnissen, J., & Scarlett, B. (2000). Jet break-up in electrohydrodynamic atomization in the cone-jet mode. *Journal of Aerosol Science, 31*(1), 65-95.

Haward, S. J., Sharma, V., Butts, C. P., McKinley, G. H., & Rahatekar, S. S. (2012). Shear and extensional rheology of cellulose/ionic liquid solutions. *Biomacromolecules, 13*(5), 1688-1699.

Hohman, M. M., Shin, M., Rutledge, G., & Brenner, M. P. (2001). Electrospinning and electrically forced jets. I. Stability theory. *Physics of fluids, 13*(8), 2201-2220.

Homayoni, H., Ravandi, S. A. H., & Valizadeh, M. (2009). Electrospinning of chitosan nanofibers: Processing optimization. *Carbohydrate Polymers, 77*(3), 656-661.

Jaworek, A., & Krupa, A. (1999). Classification of the modes of EHD spraying. *Journal of Aerosol Science, 30*(7), 873-893.

Jaworek, A., & Sobczyk, A. (2008). Electrospraying route to nanotechnology: An overview. *Journal of Electrostatics, 66*(3), 197-219.

Kumar, M. N. R. (2000). A review of chitin and chitosan applications. *Reactive and functional polymers, 46*(1), 1-27.

Kumirska, J., Weinhold, M. X., Thöming, J., & Stepnowski, P. (2011). Biomedical Activity of Chitin/Chitosan Based Materials—Influence of Physicochemical Properties Apart from Molecular Weight and Degree of N-Acetylation. *Polymers, 3*(4), 1875-1901.

Kuo, S. M., Niu, G. C. C., Chang, S. J., Kuo, C. H., & Bair, M. S. (2004). A one‐step method for fabricating chitosan microspheres. *Journal of Applied Polymer Science, 94*(5), 2150-2157.

McKee, M. G., Wilkes, G. L., Colby, R. H., & Long, T. E. (2004). Correlations of solution rheology with electrospun fiber formation of linear and branched polyesters. *Macromolecules, 37*(5), 1760-1767.

McKee, M. G., Hunley, M. T., Layman, J. M., & Long, T. E. (2006). Solution rheological behavior and electrospinning of cationic polyelectrolytes. *Macromolecules, 39*(2), 575-583.

Mitra, A., & Dey, B. (2011). Chitosan microspheres in novel drug delivery systems. *Indian journal of pharmaceutical sciences, 73*(4), 355.

Ohkawa, K., Cha, D., Kim, H., Nishida, A., & Yamamoto, H. (2004). Electrospinning of chitosan. *Macromolecular Rapid Communications, 25*(18), 1600-1605.

Ohkawa, K., Minato, K.-I., Kumagai, G., Hayashi, S., & Yamamoto, H. (2006). Chitosan nanofiber. *Biomacromolecules, 7*(11), 3291-3294.

Pakravan, M., Heuzey, M.-C., & Ajji, A. (2011). A fundamental study of chitosan/PEO electrospinning. *Polymer, 52*(21), 4813-4824.

Pantano, C., Ganan-Calvo, A., & Barrero, A. (1994). Zeroth-order, electrohydrostatic solution for electrospraying in cone-jet mode. *Journal of Aerosol Science, 25*(6), 1065-1077.

Park, C. H., Kim, M. Y., Yoo, J. Y., Kim, K. H., Lee, J. C., & Lee, J. (2007). *Preparation of Polymer/Drug Nano‐and Micro‐Particles by Electrospraying.* Paper presented at the Macromolecular Symposia WILEY‐VCH Verlag, *249*(1), 116-119.

Rayleigh, L. (1882). XX. On the equilibrium of liquid conducting masses charged with electricity. *The London, Edinburgh, and Dublin Philosophical Magazine and Journal of Science, 14*(87), 184-186.

Reneker, D. H., Yarin, A. L., Fong, H., & Koombhongse, S. (2000). Bending instability of electrically charged liquid jets of polymer solutions in electrospinning. *Journal of Applied physics, 87*(9), 4531-4547.

Rinaudo, M. (2006). Chitin and chitosan: properties and applications. *Progress in Polymer Science, 31*(7), 603-632.

Rosell-Llompart, J., & de La Mora, J. F. (1994). Generation of monodisperse droplets 0.3 to 4 μm in diameter from electrified cone-jets of highly conducting and viscous liquids. *Journal of Aerosol Science, 25*(6), 1093-1119.

Rubinstein, M., Colby, R. H., & Dobrynin, A. V. (1994). Dynamics of semidilute polyelectrolyte solutions. *Physical Review Letters, 73*(20), 2776.

Rutledge, G. C., & Fridrikh, S. V. (2007). Formation of fibers by electrospinning. *Advanced drug delivery reviews, 59*(14), 1384-1391.

Schiffman, J. D., & Schauer, C. L. (2007). Cross-linking chitosan nanofibers. *Biomacromolecules, 8*(2), 594-601.

Shenoy, S. L., Bates, W. D., Frisch, H. L., & Wnek, G. E. (2005). Role of chain entanglements on fiber formation during electrospinning of polymer solutions: good solvent, non-specific polymer–polymer interaction limit. *Polymer, 46*(10), 3372-3384.

Sinha, V., Singla, A., Wadhawan, S., Kaushik, R., Kumria, R., Bansal, K., & Dhawan, S. (2004). Chitosan microspheres as a potential carrier for drugs. *International Journal of Pharmaceutics, 274*(1), 1-33.

Spivak, A., & Dzenis, Y. (1998). Asymptotic decay of radius of a weakly conductive viscous jet in an external electric field. *Applied Physics Letters, 73*(21), 3067-3069.

Sultan, F., Ashgriz, N., Guildenbecher, D., & Sojka, P. (2011). Electrosprays *Handbook of Atomization and Sprays*: Springer, 727-753.

Taylor, G. (1964). Disintegration of water drops in an electric field. *Proceedings of the Royal Society of London. Series A. Mathematical and Physical Sciences, 280*(1382), 383-397.

Wang, X.-X., Ju, X.-J., Sun, S.-X., Xie, R., Wang, W., Liu, Z., & Chu, L.-Y. (2015). Monodisperse erythrocyte-sized and acid-soluble chitosan microspheres prepared via electrospraying. *RSC Advances, 5*(43), 34243-34250.

Zeleny, J. (1914). The electrical discharge from liquid points, and a hydrostatic method of measuring the electric intensity at their surfaces. *Physical Review, 3*(2), 69.

Zhang, S., & Kawakami, K. (2010). One-step preparation of chitosan solid nanoparticles by electrospray deposition. *International Journal of Pharmaceutics, 397*(1), 211-217.

CHAPTER 7: ARTICLE 3: EFFECT OF CHITOSAN PHYSICAL FORM ON ITS ANTIBACTERIAL ACTIVITY AGAINST PATHOGENIC BACTERIA

Nury Ardila[1], France Daigle[2], Marie-Claude Heuzey[1] and Abdellah Ajji[1]

[1] Research Center for High Performance Polymer and Composite Systems (CREPEC), Department of Chemical Engineering, Polytechnique Montréal, P.O. Box 6079, Station Centre-Ville, Montréal, QC H3C 3A7, Canada

[2] Department of Microbiology, Infectiology and Immunology, Pavillon Roger-Gaudry, Université de Montréal, P.O. Box 6128, Station Centre-ville, Montréal, QC H3C 3J7, Canada

(This work was published online in *Journal of Food Science* on January 31st, 2017)

7.1 Abstract

The antibacterial activity of chitosan (CS) nanospheres, in comparison with other physical forms, was investigated against *Salmonella enterica* serovar Typhimurium and *Staphylococcus aureus*, which are 2 foodborne harmful pathogens. Results showed that the antibacterial efficacy of CS nanospheres: (1) was superior to that displayed by CS in powder and solution form; (2) was higher against *S. aureus* than against *Salmonella* Typhimurium; and (3) was dependent on the temperature and pH of the medium depending on the strain. For *S.* Typhimurium, a higher activity was displayed at 37 °C, in which 99.9 % of the population was eradicated independently of the pH, followed by 20 °C and 7 °C, in which acidic pH conditions favored a higher susceptibility of bacteria to the effect of CS. On the contrary, *S. aureus* was less susceptible to the pH and temperature conditions of the medium, and no statistical difference in the antibacterial effect was observed for pH 5.8 and 8.0 at 20 and 37 °C. However, at 7 °C a slightly higher activity was displayed at pH 5.8 than at 8.0.

7.2 Introduction

Chitosan (CS) is a natural nontoxic polysaccharide obtained by the alkaline deacetylation of chitin and typically contains between 0% and 30% of *N*-acetyl glucosamine and 70% to 100% of glucosamine units (Muzzarelli 1973, Goosen 1997). The free amino groups in CS are known to be responsible for its physicochemical and biological properties, including its intrinsic antibacterial activity (Kumar 2000), which can be influenced by environmental and microbial factors and the intrinsic properties of CS itself (No and others 2002, Dutta and others 2009, Kong and others 2010).

CS can be obtained or prepared in different physical forms such as powder and flakes (neat forms), solutions, films, fibers, micro and nanoparticles, which allow a wide range of applications in biomedicine, water treatment, food industry, agriculture and cosmetology, and so on. (Goosen 1997, Kumar 2000, El-hefian and others 2011). Up to now, several studies have examined the antimicrobial activity of CS solutions (Chen and others 2002, Tsai and others 2002, Chung and others 2003, Zheng and Zhu 2003, Campos and others 2006, Chung and Chen 2008), gel (Goy and others 2015) and films (Ouattara and others 2000a, b, Zivanovic and others 2005, Beverlya and others 2008, Dutta and others 2009) on different microbial species. More recently, micro and nanosize morphologies have been fabricated to increase CS bioactivity and performance, and to enhance CS/cell interactions (Qi and others 2004, Kong and others 2008a, b, Xing and others 2008, 2009a, b, Yien and others 2012). CS nanofibers have been mainly produced using the electrospinning process from neat CS aqueous acetic acid solutions (Geng and others 2005, Homayoni and others 2009) and CS solubilized in trifluoroacetic acid (TFA) (Ohkawa and others 2004, 2006, Schiffman and Schauer 2007), and/or by blending with co-spinnable materials such as poly(ethylene oxide), poly(lactic acid) and poly(vinyl alcohol) (Ignatova and others 2006, 2009, Pakravan and others 2011, Ardila and others 2016). All these CS-based fibrous structures showed promising results regarding antibacterial activity (Ignatova and others 2006, 2009, Ardila and others 2016). On the other hand, the use of CS micro and nanoparticles have been widely investigated in the biomedical field for drug delivery applications due to their small size and large surface to weight ratio. Several methods have been employed for their production, including emulsion cross-linking reaction, coacervation / precipitation, spray-drying, emulsion droplet coalescence, ionic gelation and electrospraying (Agnihotri and others 2004, Sinha and others 2004, Bock and others 2011). The latter is particularly known for being a simple one-step processing

method that produces highly charged particles and which do not require extra purification steps (Jaworek 2007). Regarding the antibacterial activity, some studies have evaluated the efficacy of CS micro and nanoparticles on account of the minimum inhibitory concentration (MIC) and minimum bactericidal concentration (MBC) values determined by turbidimetric methods. For instance, Qi and others (2004) reported an MBC for CS solution of 64 µg/mL, compared with 1 and 2 µg/mL for CS nanoparticles against *Escherichia coli* K88 and ATCC 25922, respectively; for *Staphylococcus aureus* ATCC 25923, an MBC value of 32 and 4 µg/mL was reported for CS in solution and nanoparticle form, respectively; whilst that for *Salmonella enterica* serovar Typhimurium, the MBC values reported were 64 and 4 µg/mL for CS in solution and nanoparticle form. Yien and others (2012) also reported a higher activity of low and high molecular weight (MW) CS nanoparticles with respect to CS in solution against different fungal species. The MIC_{90} for low and high MW weight CS nanoparticles against *Candida albicans* was 0.25-0.86 and 0.6-1.0 mg/mL, respectively. Against *Fusarium solani* it was 0.86 to 1.2 and 0.5 to 1.2 mg/mL for low and high MW, respectively, whilst the MIC_{90} for CS in solution was 3 mg/mL for both levels of MW. On the other hand, Kong and others (2008a) reported a similar antibacterial activity for CS microspheres and solution. A total inhibition of *S. aureus* by a CS concentration of 1 mg/mL was observed.

Even though the antibacterial activity of CS has been widely studied, no report has compared the effect of particle size, nor has analyzed the effect of pH and temperature on antibacterial activity of CS nanospheres. The study of these effects is of great importance on accounting the many possible applications, such as in food packaging and in the biomedical field. More specifically, the present research work investigates the effect of physical form and particle size, namely solution, powder and nanospheres, on CS antibacterial activity, under the same experimental conditions. In addition, the effect of pH, temperature and bacterium species on the effectiveness of CS nanospheres against *Salmonella enterica* serovar Typhimurium and *Staphylococcus aureus* is explored, which are pathogenic strains commonly associated with foodborne infection. This study aims at shedding light on the superior antibacterial activity of CS nanospheres in various conditions, and propose a mechanism behind it.

7.3 Materials and Methods

7.3.1 Materials

(CS) in powder form with 95 % degree of deacetylation (DDA), 57 kDa average MW, 25 kDa number-average MW and a polydispersity (PDI) of 2.24 was obtained from Primex (Iceland). Glacial acetic acid was purchased from Sigma Aldrich.

Cultures of pathogens *S. aureus* (54-73) and *S.* Typhimurium (SL1344) were obtained from the Laboratory of Microbiology (Université de Montréal, Québec, Canada).

7.3.2 Methods

7.3.2.1 CS physical forms

CS in powder form was used as received. CS solution was prepared by dissolving 1 wt/v % CS in 1 v/v % acetic acid aqueous solution. Dissolution was carried out under magnetic stirring at room temperature until complete dissolution of the solutes. CS nanospheres were prepared using the electrospraying process. First, a solution of 3 wt/v % of CS in 70 v/v % aqueous acetic acid was prepared. Our study on CS electrospraying has determined that 70 v/v % of acetic acid is required for nanosphere formation and collection. The electrospraying process was performed using a homemade horizontal setup containing a programmable microsyringe pump (Harvard Apparatus, PHD 2000, USA) and a variable high DC voltage power supply (Gamma High Voltage Research, FL, USA). Polymer solution was pumped through a syringe fitted with a metallic 22-gauge needle (i.d. 0.41 mm, o.d. 0.72 mm) at a flow rate of 0.2 mL/h, using a voltage of 33 kV at a distance of 11 cm between the needle tip and the grounded plate collector. Electrospraying was conducted in a chamber at room temperature, a relative humidity of 30 to 40 % and under atmospheric pressure. CS nanospheres were collected on aluminum foil attached to a stationary collector plate and then were dried overnight under a chemical fume hood for the evaporation of any remaining solvent.

7.3.2.2 Morphology

The morphology of CS powder and nanospheres was observed by scanning electron microscopy, (SEM, JEOL JSM-7600TFE field emission gun) operated at 2 kV. The particle diameter and size

distribution were analyzed using the Image-Pro Plus® software by taking an average of about 1000 particles.

7.3.2.3 Antibacterial tests

The antibacterial activity of CS under different physical forms (powder, solution and nanospheres) was evaluated against 2 pathogenic bacteria: *S.* Typhimurium (Gram-negative) and *S. aureus* (Gram-positive). Bacteria were grown in a rich medium (Luria Bertani or LB broth) under constant agitation for 24 h at 37 ºC, until reaching a density of approximately 10^9 colony forming units (CFU)/mL. Then, the bacterial culture was diluted in de-ionized distilled water medium (pH 5.8 and 8.0 altered by using HCl or NaOH 0.1 M), in order to have a density of approximately 10^6 CFU/mL. CS in powder, solution, and nanosphere forms were immersed (after sterilization under UV light for 20 min) at a concentration of 0.01 wt/v % CS, into 5 mL of the culture medium containing *S.* Typhimurium or *S. aureus*. Subsequently, tubes were incubated at 7, 20 and 37 °C for 4 h in an incubator shaker (New Brunswick). Dilutions of the inoculated suspensions were prepared and deposited on LB agar plates and incubated for 18 h at 37 °C for the counting of the surviving bacteria (CFU/mL). Plates were verified after 48 h to corroborate that the recovery of viable organisms from sub-lethal injury had not taken place. Experiments were carried out in triplicate.

Preliminary tests showed that zeta potential values differ greatly depending on the medium of testing, which may influence the antibacterial activity of CS nanospheres. For instance, at a pH of 5.8, CS nanospheres displayed an overall positive surface charge of + 53.3 mV when measured in deionized distilled water, but a value of + 18.4 mV when measured in a buffered solution (PBS). These differences may be explained as a consequence of diffuse layer (charge screening) when in PBS, given the relative high salt content of this medium (11.16 wt/v % of NaCl, KCl, $Na_2HPO_4.7H_2O$ and KH_2PO_4). Therefore, antibacterial tests were performed in water, to promote the antibacterial effect.

Preliminary tests suggested the use of 0.01 wt/v % CS for the comparison of the antibacterial activity under different physical forms. Given the relative low CS concentration, the pH of the CS suspensions was not affected after the 4 h of incubation. Lower concentrations were not possible due to limitations to precisely weight CS in powder form.

7.3.2.4 Zeta potential and particle size

CS nanospheres were suspended in 5 ml of de-ionized distilled water (pH 5.8 and 8.0 altered by using HCl or NaOH 0.1 M), and stirred for 10 min at 100 rpm. The CS solution was diluted in 5 ml of de-ionized distilled water at pH 5.8, and stirred in the same conditions than CS nanospheres. The zeta potential of the CS solution was measured only at pH 5.8. When adjusting the pH solution to 8.0, a precipitate was observed, given the poor solubility of CS in solution at pH above its pKa (6.2-6.5) (Pillai and others 2009, Yao and others 2011). Zeta potential was determined by laser Doppler velocimetry and phase analysis light scattering (M3-PALS) using a Malvern Zetasizer Nano ZSP instrument (Malvern Instruments Ltd., Malvern, Worcestershire, UK). The zeta potential was determined from the direction and velocity of the molecules in the applied electric field. The Smoluchowski model was used to convert the electrophoretic mobility measurements into zeta potential values. The temperature of the cell was maintained at 25 °C. The data presented are the average values of 3 individual measurements.

The potential solubility of CS nanospheres during the antibacterial tests at pH 5.8 (given the pH of the medium is lower than chitosan's pKa, chitosan amino groups undergo protonation and therefore may display certain solubility in the medium) was tested via dynamic light scattering (DLS) by analyzing particle size. The mean particle size measurement (Z-average) was performed at a fixed angle of 173° using a Zetasizer Nano ZSP instrument (Malvern Instruments, Worcestershire, UK) equipped with a 4 mW He–Ne laser (633 nm wavelength) at 25 °C. Droplet sizing was performed at 10-s intervals in a particle-sizing cell using backscattering technology. Z-average diameter (mean) of particles was calculated based on the Stokes–Einstein equation, assuming particles to be spherical. This assumption is considered reasonable given the physical form and size of CS nanospheres. Given the physical dimensions of CS in powder form, it was not possible to measure its zeta potential (pH 5.8 and 8.0) nor determine its size by DLS for the evaluation of its potential solubility. Each data points are the mean of triplicate measurements on 3 independent samples.

7.3.2.5 Statistical analysis

Antibacterial and zeta potential measurements were carried out in triplicate, and the average values with their standard deviations are reported. Zeta potential results were analyzed statistically using the Student's *t*-test to determine differences. Level of significance is denoted as $P<0.05$. Statistical analysis for the antibacterial results were performed in two ways. The effect of CS physical form

was analyzed by using Tukey pairwise comparisons with a confidence interval of 95 %. The effect of temperature and pH for each strain was analyzed by adjusting the data to a Generalized linear model and then using Dunnet pairwise comparisons. These analyses were performed in ANOVA-Minitab17® software and all data were normalized by re-scaling in log form.

7.4 Results and Discussion

7.4.1 Morphology

Figure 7.1 presents the SEM micrographs of CS powder and nanospheres, and their particle size distribution. CS in powder form (Figure 7.1a) has an irregular shape and a size of 55 µm, on average, whilst CS nanospheres (Figure 7.1b) exhibit a regular spherical shape and present a diameter of 178 nm, in average. Both CS forms exhibit a wide particle size distribution, and about 30% of CS nanospheres are in the order of 100 nm in size.

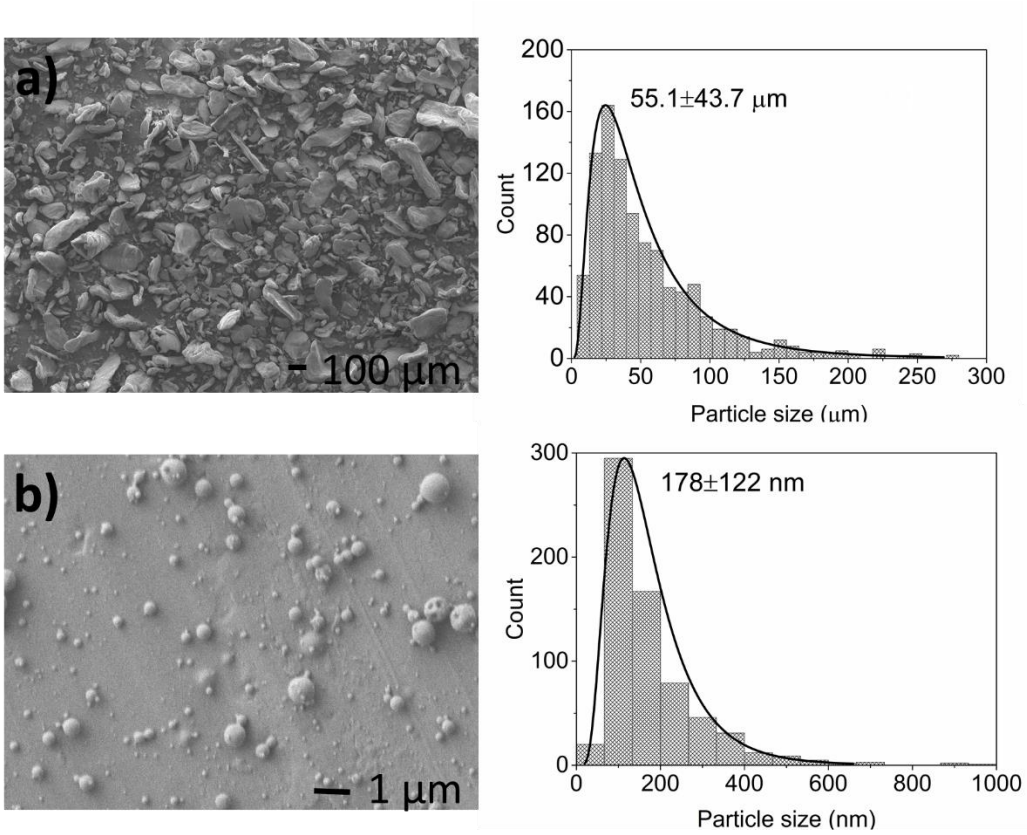

Figure 7.1: Morphology and particle size distribution (log-normal) of chitosan a) in powder form and b) nanospheres. This figure has been modified with respect to the original article.

7.4.2 Zeta potential and solubility of CS nanospheres

Zeta potential illustrates the surface charge and the electrostatic interactions between particles. Table 7.1 reports the zeta potential of CS solution and CS nanospheres in de-ionized distilled water at pH 5.8 and 8.0. Given the size of CS in powder form, it was not possible to measure the zeta potential and the measurements were out of the range.

In the case of CS nanospheres, zeta potential decreases with pH. For instance, they display an overall positive surface charge of +53.3 and +14.8 mV when measured at pH 5.8 and 8.0, respectively. This decrease may be interpreted as a consequence of de-protonation of CS amino groups. Therefore, as the pH increases, charged amino groups promoting the stability of CS nanospheres fade. However, results indicate that at pH 8.0, CS nanospheres still display a positive surface charge, probably as a result of their interaction with the few ions in the medium (Na^+), given that the pH of de-ionized distilled water was altered with NaOH intentionally. This result is consistent with the findings of Gan and others (2005) who reported a pH of 9.0 as the isoelectric point for CS nanoparticles prepared by ionic gelation.

Table 7.1: Zeta potential (mV) and mean particle size (Z-average) of 0.01% chitosan

Chitosan form	Zeta potential (mV)		Size (nm)	
	pH 5.8	pH 8.0	pH 5.8	pH 8.0
Solution	34.4 ± 6.0a	-	-	-
Nanospheres	53.3 ± 0.7b	14.8 ± 0.7c	459.1 ± 91.9a	797.3 ± 213.2a

Means that do not share a letter in each group are significantly different ($p<0.05$) according to Student's t-test.

On the other hand, results show a significantly higher zeta potential value for CS nanospheres in comparison to CS solution at pH 5.8 (+53.3 vs. +34.4 mV, respectively) and consequently, display a higher stability. The lower zeta potential in CS solution is the result of the presence of more ions in solution (from acetic acid). Similar zeta potential values of between +51 kV (Qi and others 2004) and +35 to +55 kV (Yien and others 2012) were reported for CS nanoparticles prepared by ionic gelation. Differences with our results may be due to the preparation process and the CS concentration, MW and DDA. It was reported that zeta potential increases when increasing CS

MW (for example, when increasing the MW from 70 to 310 kDa, the zeta potential increases from +35 to +38, +43 to +50, and +47 to +55 mV, for a chitosan concentration 1, 2 and 3 mg/mL, respectively) (Chen and others 2010, Yien and others 2012). Results regarding the effect on CS concentration are contradictory. For example, Yien and others (2012) showed an increase in zeta potential values (for example from +35 to +47 mV, when increasing the chitosan concentration of 1 to 3 mg/mL for low MW chitosan of 70 kDa. Similar tendency was observed for high MW chitosan of 310 kDa at the same chitosan concentrations) whilst Gan and others (2005) reported a decrease, when increasing CS concentration (for example from +43 to +34 mV, when increasing the chitosan concentration from 0.5 to 3 mg/mL, respectively, for chitosan of low MW-value not specified. Similar tendency was observed for medium and high MW chitosan).

Nanoparticles with low surface charge (+20 mV or lower) encounter weaker electrostatic repulsion, which can promote particle aggregation due to van der Walls inter-particle attraction (Gan and others 2005, Yien and others 2012). This statement is in accordance with the differences in particle size observed via SEM and DLS (at pH 5.8 and 8.0). Table 7.1 presents the particle size (Z-average) obtained by DLS for CS nanospheres. Before contact with the medium, CS nanospheres have an average diameter of 178 nm (Figure 7.1b, by SEM), but once in the medium, their average diameter increases up to 459 nm and 797 nm (Table 7.1, by DLS) at pH 5.8 and 8.0, respectively. In addition to a likely swelling once in the medium, possible agglomeration of particles may occur at pH 8.0, given their low stability reflected in their low zeta potential value (+14.8 mV). This is reflected in the high particle size observed (797 nm, Table 7.1). In addition, nanospheres suspended at pH 5.8 may undergo partial solubilisation. Indeed, after 4 h at pH 5.8, particle size decreases to 315 nm, and the reduction continues after 13 d until 256 nm. This reduction on the particle size should be considered when analyzing the antibacterial activity of CS nanospheres and for future applications as well.

On the other hand, for dilute solutions such as 0.01 % CS (overlap concentration, C*=0.1-0.12 wt%; Pakravan and others 2011), the intrinsic viscosity [η] can be used to get an approximate value of the radius of gyration ($\langle R_G \rangle$) of a polymeric molecule in a solvent by the following relation (Carreau and others 1997, Cho and others 2006): $\langle R_G \rangle^3 = \frac{[\eta]\,\bar{M}_n}{\phi}$ where $\bar{M}_n$ is the number-average MW and ϕ is a universal constant (2.1×10^{23} mol^{-1}). Given that [η] is 280.4 mL g^{-1} and $\bar{M}_n$ is 25 kDa, the radius of gyration is 32.1 nm. Hence in solution, CS chains will display a size of about

64.2 nm. This approximation is consistent with the equation proposed by Berth and Dautzenberg (2002) to calculate the radius of gyration given $\bar{M}_w$: $\langle R_G \rangle\ (nm) = 0.075 M_w^{0.55} = 31\ nm$.

7.4.3 Effect of physical form on the antibacterial activity of CS

Figure 7.2 shows the antibacterial activity of CS under different physical forms at the same CS concentration (0.01%) and pH (5.8), against *S.* Typhimurium and *S. aureus*. Preliminary tests suggested the use of 0.01 wt/v % CS for the comparison of the antibacterial activity. Lower concentrations were limited due to weight CS in powder form.

Given that the pH of the medium is lower than CS pKa (6.2-6.5; Pillai and others 2009, Yao and others 2011), CS amino groups in all physical forms are considered protonated and therefore capable of interacting with the negatively charged bacteria surface. This can be corroborated when looking at the zeta potential values for CS in solution and nanosphere form (Table 7.1). Although it was not possible to determine the zeta potential value of CS in powder (due to large particle size), their amino groups are assumed protonated just as for CS nanospheres.

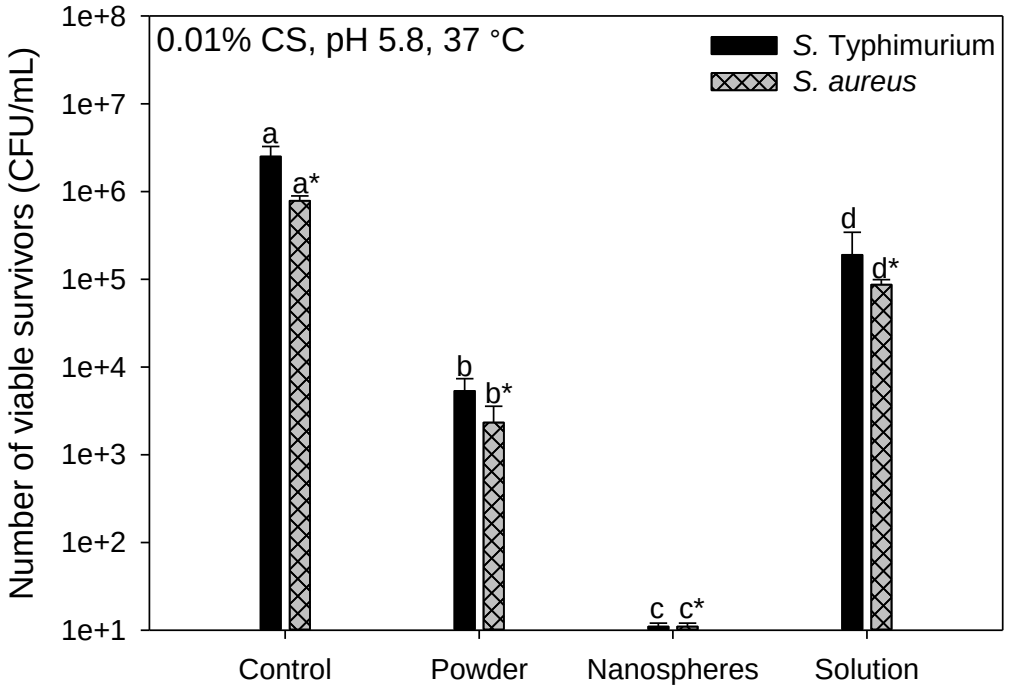

Figure 7.2: Antibacterial activity of chitosan under different physical forms. The number of viable organisms was the same after 18 and 48 h incubation on the agar plates, suggesting that recovery from sub-lethal injury had not taken place. For each strain, means that do not share a letter are

significantly different with a confidence level of 95% by Tukey Pairwise Comparisons. Statistical analysis was done separately for *S.* Typhimurium and *S. aureus* (samples with and without *).

CS nanospheres displayed the highest activity, followed by CS in powder and solution form. Therefore, CS physical form and size influence its antibacterial activity. Furthermore, as particle size decreases, the antibacterial effect of CS is enhanced since CS nanospheres display a significant higher activity than CS in powder form (6.4 compared with 2.9 log reduction in bacterial density). This result may be explained by the larger specific surface area (SSA) of contact of CS nanospheres (SSA=112 m^2/g) with bacteria cell wall than in CS powder (SSA=0.36 m^2/g). The specific surface area was calculated based on the dimensions of the CS powder and nanoparticles, considering them as spheres having a bulk density of 0.3 g/cm^3 (Cho and others 1998). Hence, there are more protonated amino groups at the nanosphere surface available to interact with the negatively charged bacteria cell wall, which results in a higher antibacterial activity. In addition, CS nanospheres can interact more effectively with the cell wall given their small size. Different studies have demonstrated that the surface area plays a major role in the antimicrobial activity. For instance, Yamamoto (2001) reported that the antibacterial activity of zinc oxide powders against *E. coli* increased considerably when decreasing the particle size from 0.8 to 0.1 μm. A similar trend, but with a lower impact, was observed when powders were tested against *S. aureus*. In another study, Martinez-Gutierrez and others (2010) also reported a significantly increase in the antimicrobial activity of silver and titanium nanoparticles when their particle size decreased from 250-300 to 20-25 nm, against different Gram-positive and Gram-negative strains, including *E. coli* and *S. aureus*.

CS nanospheres are also more effective than CS in solution. The lower activity of the solution may be explained due the lower zeta potential value. Similar findings were reported in which CS nanoparticles were more active than CS in solution against different bacterial (*E. coli, S. choleraesuis*, *S.* Typhimurium and *S. aureus*; Qi and others 2004) and fungal species (*Candida albicans* and *Fusarium solani*; Yien and others 2012). It has been suggested that the higher activity of CS nanoparticles was the result of a higher affinity and a better interaction with bacteria cell surface due to the higher surface charge and compact and small character, compared to CS in solution (Qi and others 2004, Yien and others 2012). As a matter of fact, our results show that CS nanospheres display a higher surface charge (zeta potential value +53.3 compared with +34.4 mV), which may have contributed to a higher interaction with the negatively charged cell surface. In addition, the distribution in particle size of CS nanospheres (Figure 7.1b) reveals that about 30%

of nanospheres are in the order of 100 nm or less in size, which may also contribute to a higher efficacy and adsorption when in contact with the bacterial cell surface. On the contrary, it is believed that even though CS in solution interacts with the cell wall, it will remain as a free form in the medium rather than adhering permanently into cells. A study carried out by Ma and Lim (2003) demonstrated that the cellular uptake of CS in solution was lower than that of CS nanoparticles since the CS molecules in solution were located extracellularly. This suggested that CS nanoparticles might be able to diffuse into cells, affecting their cellular membrane, and would explain the higher antibacterial activity obtained in this work for CS nanoparticles with respect to CS in solution.

Finally, the higher activity of CS powder compared to that of CS in solution is explained as follows. At pH 5.8, CS in solution may have lost part of its physical form and be partially present as agglomerates, whilst CS in powder may still conserve its physical form, while with reduced size, as it happens for CS nanospheres at the same pH (partial solubilisation). In addition, CS powder can serve as a physical support that may maximize the attachment of bacteria. For instance, the size of CS powder is 37 to 81 times higher than the size of *S.* Typhimurium cells (rod shape with 1.5 ± 0.4 μm in length and 0.7 ± 0.1 μm in width; Ardila and others 2017). Thereafter, the interaction of protonated CS amino groups with the negatively charged groups at bacteria cell surface may cause the disruption and the permeability of the cell membrane, the leakage of cellular components and therefore cell death (Chung and Chen 2008, Kong and others 2010).

Similar results and trends were obtained when evaluating the antibacterial activity of the different CS forms against *S. aureus* (Figure 7.2).

7.4.4 Effect of pH, temperature and bacterium species

The antibacterial efficacy of CS nanospheres against *S.* Typhimurium and *S. aureus* was evaluated at different pH and temperature conditions, as reported in Figure 7.3. The evaluation of these factors is of great importance with respect to food packaging and biomedical applications.

7.4.4.1 Bacterium species

Figure 7.3 shows that the antibacterial activity of CS nanospheres is stronger against *S. aureus* than against *S.* Typhimurium, regardless of the pH of the medium and the incubation temperature. The

same trend against these strains was observed by other authors in the case of CS and CS oligomer solutions in acidic pH conditions (No and others 2002, Tsai and others 2002, Qi and others 2004).

CS nanospheres were more effective against the Gram-positive, *S. aureus* than the Gram-negative, *S.* Typhimurium, presumably due to the presence of outer membrane lipid barrier in the latter (Zhong and others 2008, Kong and others 2010).

On the other hand, results suggest that the antibacterial activity of CS nanospheres is independent of the form and size of the cells. For instance, *S.* Typhimurium cells have a rod-shape of 1.5 µm in length and 0.7 µm in width, whilst *S. aureus* cells have a spherical shape of 0.8 µm in diameter (Ardila and others 2017). Hence, CS nanospheres might have had larger contact with the surface of *S.* Typhimurium cells than with the ones of *S. aureus*. However, a higher activity was found against S. aureus, which have the smaller size and therefore the lower surface area to the adsorption of CS nanospheres.

7.4.4.2 Temperature

Figure 7.3 shows that the temperature of incubation may limit or favor the antibacterial action of CS. CS nanospheres display a higher antibacterial activity at 37 ºC than at 20 and 7 ºC for *S.* Typhimurium. In the case of *S. aureus,* the antibacterial efficacy is also lower at 7 ºC, but, no difference was observed at 20 and 37 ºC, in which the total concentration of bacteria was eradicated. It has been suggested that low temperature conditions may affect the bacteria surface electronegativity (Tsai and Su 1999). Consequently, the interaction of CS nanospheres with the cell surface may be limited. On the other hand, high temperature conditions may favor the solubility of CS, specially in acidic pH values, lowering the size of CS nanospheres. The decrease in particle size would improve the interaction of nanoparticles with cell walls and therefore would have a positive impact on the antibacterial action of nanospheres. Temperature can also affect the adsorption/adhesion of nanoparticles onto the cell wall surface. As temperature affects the Brownian motion, high temperature conditions favor the stability and distribution of the suspended nanospheres in the cell wall, avoiding particle aggregation. Besides, temperature enhances membrane fluidity, favoring the interaction of the cell surface with chitosan nanospheres. Notwithstanding the more limited antibacterial activity at 7 ºC in *S.* Typhimurium, the results show that bacterial density is reduced by about 1.8 and 1.6 log CFU/ml (at pH 5.8 and 8.0, respectively),

which represent a decrease in more than 97 % of bacteria. This result shows its potential use for different applications, including low temperature conditions such as in food packaging.

7.4.4.3 pH

The effect of pH on the antibacterial activity of CS nanospheres can be observed at the temperatures of incubation of 7 and 20 ºC in the case of *S.* Typhimurium and at 7 ºC in the case of *S. aureus*. As seen in Figure 7.3, CS nanospheres display slightly higher antibacterial activity in acidic pH conditions (5.8) than at slightly basic pH (8.0). This can be explained as a consequence of the greater surface charge and the lower particle size at pH 5.8 in comparison with pH 8.0 for CS nanospheres, as shown in Table 7.1. In addition, lower particle sizes could be expected at pH 5.8 after 4 h of incubation, given the potential solubility of CS in acidic conditions, as previously discussed. Nevertheless, results also show that CS nanospheres display similar antibacterial activity, independently of the pH, against *S.* Typhimurium incubated at 37 ºC and against *S. aureus* incubated at 20 and 37 ºC. It suggests that CS nanospheres display a unique antibacterial effect in slightly basic conditions, such as pH 8.0. Contrary to these results, CS in powder form did not display any antibacterial activity at this pH for any of the bacterial species at 7 ºC nor 37 ºC (results not shown). Other studies on CS solutions, films and nanofibers (Kong and others 2010) also reported that acidic conditions were required for the antibacterial activity of CS. In addition to the results of the current study, Kong and others (2008b) reported a similar trend at a pH of 7.5 for the case of CS microspheres having 62.6 % DDA at concentrations of 500 and 1000 ppm. In their study, it was suggested that the inhibitory effect might be related to the hydrophobic interactions of the *N*-acetyl groups of CS microspheres with bacteria cells. In the present work, if existing, this influence should be minor given the high DDA of CS (95 %). On the other hand, neutral pH conditions may favor the chelating capacity of CS towards cations from the cell walls (Guibal 2004). Hence, based on the different experimental conditions that were evaluated and the obtained results in the current study, the zeta potential measurements nor the particle size alone cannot explain the similar antibacterial activity obtained at pH 5.8 and 8.0 at high temperature conditions.

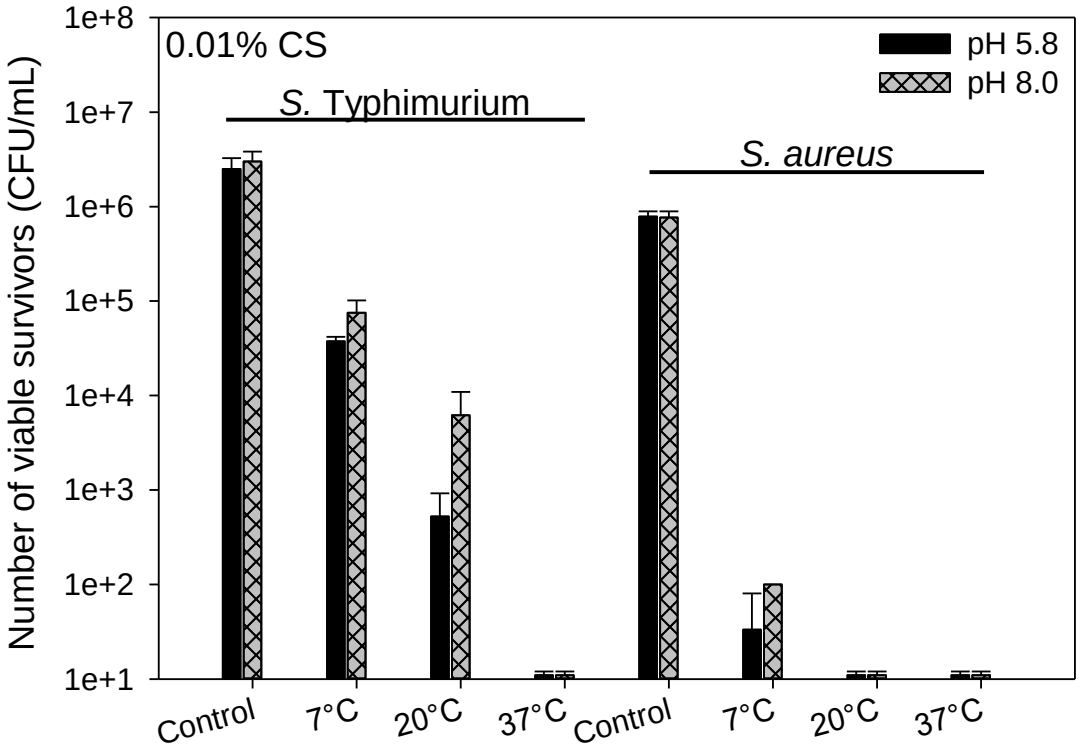

Figure 7.3: Influence of pH, temperature and bacterium species on the antibacterial activity of chitosan nanospheres. The number of viable organisms was the same after 18 and 48 h incubation on the agar plates, suggesting that recovery from sub-lethal injury had not taken place. For *S.* Typhimurium: pH and temperature significatively affects the antibacterial activity (p=0.001 and 0.001, respectively) at a confidence level of 95%. For *S. aureus*: pH and temperature significatively affects the antibacterial activity (p=0.001) at a 95% confidence level.

Our findings suggest that CS nanospheres may display a different mode of antibacterial action than CS in solution and powder form, in which acidic conditions are required for the protonation of CS amino groups, the subsequent interaction with bacteria cell wall and the exertion of the antibacterial effect. First, surface effects may be considered: as discussed previously, zeta potential values show that CS nanospheres display a positive surface charge at pH 5.8 and 8.0. Hence, it is hypothesized that CS nanospheres may adsorb on the bacteria cell wall independently of the pH conditions, given their small size and positive charge. The higher surface charge and the lower particle size at pH 5.8 would explain the higher antibacterial effect in low temperature conditions. The interaction of CS nanoparticles with the negatively charged phospholipid components (anionic groups such as phosphate and carboxyl) may cause cell damage and rupture, affecting the cell permeability and producing the leakage of cellular components leading to cell death (Xing and others 2009a, Kong

and others 2010). Nanospheres may, in addition, form an impermeable layer on the cell surface, inhibiting the adsorption of essential nutrients and disturbing the normal metabolism of the cells. Since cellular uptake of CS nanoparticles has been reported to be higher than CS in solution (Ma and Lim 2003), a higher adsorption of CS nanoparticles into the cells would explain the higher antibacterial activity observed for nanospheres at pH 8.0 when compared with CS in solution at pH 5.8. This mechanism would also explain the higher activity of CS nanospheres at pH 5.8 with respect to pH 8.0 in low temperature conditions. The lower particle size and the higher surface charge would facilitate the larger adsorption/interaction of CS into/with the cell. It is noteworthy to mention that about 30 % of CS nanospheres are smaller than 100 nm and acidic pH conditions may increase this percentage, favoring the antibacterial effect.

Second, chelating effects may be involved. While in acidic pH conditions protonated CS amino groups can trigger electrostatic interactions with anionic compounds, at neutral and basic pH values, CS may act as a chelating agent by binding to trace elements and metal cations, either from the cell wall or from the medium (Guibal 2004). For instance, adhesion of chitosan with Mg^{2+} and Ca^{2+} ions (by forming metal complexes via chelation reaction), from the cell wall may cause the destabilization and disintegration of the cell membrane (Chung and Chen 2008), whilst the latter may reduce availability of the essential nutrients for the normal bioactivity of the cells (Rabea and others 2003, Kong and others 2008b, 2010). Kong and others (2008b) verified via SEM that *E. coli* cells adhered to the surface of CS microparticles and provided evidence for the disruption of the cells. The antibacterial activity was reported to be due to the chelating capacity of CS towards Mg^{2+} ions of the *E. coli* membrane, with subsequent changes in the outer membrane structure and cell permeability. In the current study CS has a high DDA, which means that it owns many amino groups to chelate with divalent cations. Hence, it is suggested that chelating effects become more important for CS nanospheres at neutral or slightly above pH conditions, given the antibacterial activity reported at pH 8.0. Hence, chelating effects can explain the activity observed in neutral conditions, and suggest that they are comparable to the electrostatic interactions triggered at acidic pH, given the similar antibacterial effect observed at high temperature (37 ºC) for both pH 5.8 and 8.0.

Lastly, besides the surface and chelating effects, it is hypothesized that permeation might also play an important role. Our morphological results showed a wide particle size distribution of CS nanospheres (Figure 7.1) with about 30 % of CS nanospheres smaller than 100 nm. It is speculated

that smaller CS nanospheres of few nanometers might enter the cell through pervasion, consequently altering the DNA and mRNA functions, and other physiological activities of cells (Rabea and others 2003, Kong and others 2010). As acidic conditions may further reduce the particle size, this mechanism would also explain the higher activity at pH 5.8. However, up to now, no evidence that CS can penetrate the cell wall has been shown.

Based on the antibacterial results, it is speculated that more than one mechanism could be responsible for the antibacterial activity of CS nanospheres. Further research and characterization should be conducted to elucidate the exact mechanism(s) of the antibacterial action.

The findings of this study may differ from other previous studies due to differences in the experimental conditions. Further investigation should be addressed in order to elucidate the mechanism of inhibition of CS nanospheres, their incorporation into existing food packaging, their interaction with real food systems as well as their possible effect on the body in case of ingestion.

7.5 Conclusions

CS physical form highly influences its antibacterial activity. CS nanospheres displayed higher antibacterial activity than CS in powder and solution form against foodborne pathogens such as *S.* Typhimurium and *S. aureus*. Besides, a larger antibacterial effect was found against *S. aureus*. On the other hand, pH and temperature conditions did not limit the antibacterial efficacy of CS nanospheres, contrary to other physical forms, which are not completely active at low temperature and at neutral/slightly basic pH conditions. These results show the high inhibitory effect of CS nanospheres and their potential incorporation into conventional food packaging (film, cardboard, aluminum) for providing them with antibacterial activity and therefore to better guarantee food safety.

Practical Application

Chitosan (CS) nanospheres are highly effective against pathogen bacteria including *Salmonella* Typhimurium and *Staphylococcus aureus*, which are commonly found in food spoilage. Contrary to other CS forms, CS nanospheres are potential candidates for incorporation into food packaging and food safety given their high antibacterial activity at pH and temperature conditions of food preservation.

7.6 Acknowledgments

The Fonds de Recherche du Québec-Nature et Technologies (FRQNT) is acknowledged for funding of the present work. The authors also thank Chansheng Wang from the Chemical Engineering Department (Polytechnique Montréal) for his help with the zeta potential and dynamic light scattering measurements. Finally, the authors thank the reviewers of *Journal of Food Science* for their valuable comments to improve this manuscript.

Author Contributions

N. Ardila designed the study, collected test data, interpreted results and drafted the manuscript. F. Daigle, M-C Heuzey and A. Ajji designed the study, interpreted results and reviewed and edited the manuscript.

7.7 References

Agnihotri SA, Mallikarjuna NN, Aminabhavi TM. 2004. Recent advances on chitosan-based micro-and nanoparticles in drug delivery. J Control Release 100:5-28.

Ardila N, Medina N, Arkoun M, Heuzey MC, Ajji A, Panchal CJ. 2016. Chitosan–bacterial nanocellulose nanofibrous structures for potential wound dressing applications. Cellulose 23:3089-3104.

Ardila N, Daigle F, Heuzey MC, Ajji A. 2017. Antibacterial Activity of Neat Chitosan Powder and Flakes. Molecules 22:100.

Berth G, Dautzenberg H. 2002. The degree of acetylation of chitosans and its effect on the chain conformation in aqueous solution. Carbohydr Polym 47:39-51.

Beverlya RL, Janes ME, Prinyawiwatkula W, No HK. 2008. Edible chitosan films on ready-to-eat roast beef for the control of *Listeria monocytogenes*. Food Microbiol 25:534-537.

Bock N, Woodruff MA, Hutmacher DW, Dargaville TR. 2011. Electrospraying, a reproducible method for production of polymeric microspheres for biomedical applications. Polymers 3:131-149.

Campos M, Cordi L, Duran N, Mei L. 2006. Antibacterial activity of chitosan solutions for wound dressing. Macromol Symp. Wiley Online Library.

Carreau PJ, De Kee DC, Chhabra RP. 1997. Rheology of Polymeric Systems: Principles and Applications. Cincinnati, OH: Hanser-Garner Publications.

Chen LC, Kung SK, Chen HH, Lin SB. 2010. Evaluation of zeta potential difference as an indicator for antibacterial strength of low molecular weight chitosan. Carbohydr Polym 82:913-919.

Chen YM, Chung YC, Woan-Wang L, Chen KT, Li SY. 2002. Antibacterial properties of chitosan in waterborne pathogen. J Environ Sci Health A 37:1379-1390.

Cho J, Heuzey M-C, Bégin A, Carreau PJ. 2006. Viscoelastic properties of chitosan solutions: Effect of concentration and ionic strength. J Food Eng 74:500-515.

Cho YI, No HK, Meyers SP. 1998. Physicochemical characteristics and functional properties of various commercial chitin and chitosan products. J Agric Food Chem 46:3839-3843.

Chung YC, Chen CY. 2008. Antibacterial characteristics and activity of acid-soluble chitosan. Bioresource Technol 99:2806-2814.

Chung YC, Wang HL, Chen YM, Li SL. 2003. Effect of abiotic factors on the antibacterial activity of chitosan against waterborne pathogens. Bioresource Technol 88:179-184.

Dutta P, Tripathi S, Mehrotra G, Dutta J. 2009. Perspectives for chitosan based antimicrobial films in food applications. Food Chem 114:1173-1182.

El-hefian EA, Nasef MM, Yahaya AH. 2011. Chitosan Physical Forms: A short review. Aust J Basic Appl Sci 5:670-677.

Gan Q, Wang T, Cochrane C, McCarron P. 2005. Modulation of surface charge, particle size and morphological properties of chitosan–TPP nanoparticles intended for gene delivery. Colloids Surf B Biointerfaces 44:65-73.

Geng X, Kwon O-H, Jang J. 2005. Electrospinning of chitosan dissolved in concentrated acetic acid solution. Biomaterials 26:5427-5432.

Goosen MF. 1997. Applications of chitin and chitosan. Florida: CRC Press Llc

Goy RC, Morais ST, Assis OB. 2015. Evaluation of the antimicrobial activity of chitosan and its quaternized derivative on *E. coli* and *S. aureus* growth. Rev Bras Farmacogn 26 :122-127.

Guibal E. 2004. Interactions of metal ions with chitosan-based sorbents: a review. Sep Purif Technol 38:43-74.

Homayoni H, Ravandi SAH, Valizadeh M. 2009. Electrospinning of chitosan nanofibers: Processing optimization. Carbohydr Polym 77:656-661.

Ignatova M, Manolova N, Markova N, Rashkov I. 2009. Electrospun Non-Woven Nanofibrous Hybrid Mats Based on Chitosan and PLA for Wound-Dressing Applications. Macromol Biosci 9:102-111.

Ignatova M, Starbova K, Markova N, Manolova N, Rashkov I. 2006. Electrospun nano-fiber mats with antibacterial properties from quaternised chitosan and poly (vinyl alcohol). Carbohydr Res 341:2098-2107.

Jaworek A. 2007. Micro-and nanoparticle production by electrospraying. Powder technol 176:18-35.

Kong M, Chen X-g, Xue Y-p, Liu C-s, Yu L-j, Ji Q-x, Cha DS, Park HJ. 2008a. Preparation and antibacterial activity of chitosan microspheres in a solid dispersing system. Front Mater Sci 2:214-220.

Kong M, Chen XG, Liu CS, Liu CG, Meng XH, Yu LJ. 2008b. Antibacterial mechanism of chitosan microspheres in a solid dispersing system against *E. coli*. Colloids Surf B Biointerfaces 65:197-202.

Kong M, Chen XG, Xing K, Park HJ. 2010. Antimicrobial properties of chitosan and mode of action: a state of the art review. Int J Food Microbiol 144:51-63.

Kumar MNR. 2000. A review of chitin and chitosan applications. React Funct Polym 46:1-27.

Martinez-Gutierrez F, Olive PL, Banuelos A, Orrantia E, Nino N, Sanchez EM, Ruiz F, Bach H, Av-Gay Y. 2010. Synthesis, characterization, and evaluation of antimicrobial and cytotoxic effect of silver and titanium nanoparticles. Nanomedicine: Nanotechnology, Biology and Medicine 6:681-688.

Ma Z, Lim LY. 2003. Uptake of chitosan and associated insulin in Caco-2 cell monolayers: a comparison between chitosan molecules and chitosan nanoparticles. Pharm Res 20:1812-1819.

Muzzarelli RA. 1973. Natural chelating polymers; alginic acid, chitin and chitosan. Oxford: Pergamon Press.

No HK, Park NY, Lee SH, Meyers SP. 2002. Antibacterial activity of chitosans and chitosan oligomers with different molecular weights. Int J Food Microbiol 74:65-72.

Ohkawa K, Cha D, Kim H, Nishida A, Yamamoto H. 2004. Electrospinning of chitosan. Macromolr Rapid Commun 25:1600-1605.

Ohkawa K, Minato K-I, Kumagai G, Hayashi S, Yamamoto H. 2006. Chitosan nanofiber. Biomacromolecules 7:3291-3294.

Ouattara B, Simard R, Piette G, Begin A, Holley R. 2000a. Diffusion of Acetic and Propionic Acids from Chitosan-based Antimicrobial Packaging Films. J Food Sci 65:768-773.

Ouattara B, Simard RE, Piette G, Bégin A, Holley RA. 2000b. Inhibition of surface spoilage bacteria in processed meats by application of antimicrobial films prepared with chitosan. Int J Food Microbiol 62:139-148.

Pakravan M, Heuzey M-C, Ajji A. 2011. A fundamental study of chitosan/PEO electrospinning. Polymer 52:4813-4824.

Pillai C, Paul W, Sharma CP. 2009. Chitin and chitosan polymers: Chemistry, solubility and fiber formation. Prog Polym Sci 34:641-678.

Qi L, Xu Z, Jiang X, Hu C, Zou X. 2004. Preparation and antibacterial activity of chitosan nanoparticles. Carbohydr Res 339:2693-2700.

Rabea EI, Badawy ME-T, Stevens CV, Smagghe G, Steurbaut W. 2003. Chitosan as antimicrobial agent: applications and mode of action. Biomacromolecules 4:1457-1465.

Schiffman JD, Schauer CL. 2007. Cross-linking chitosan nanofibers. Biomacromolecules 8:594-601.

Sinha V, Singla A, Wadhawan S, Kaushik R, Kumria R, Bansal K, Dhawan S. 2004. Chitosan microspheres as a potential carrier for drugs. Int J Pharm 274:1-33.

Tsai GJ, Su WH. 1999. Antibacterial activity of shrimp chitosan against *Escherichia coli*. J Food Prot 62:239-243.

Tsai GJ, Su WH, Chen HC, Pan CL. 2002. Antimicrobial activity of shrimp chitin and chitosan from different treatments and applications of fish preservation. Fisheries Sci 68:170-177.

Xing K, Chen XG, Kong M, Liu CS, Cha DS, Park HJ. 2009a. Effect of oleoyl-chitosan nanoparticles as a novel antibacterial dispersion system on viability, membrane permeability and cell morphology of *Escherichia coli* and *Staphylococcus aureus*. Carbohydr Polym 76:17-22.

Xing K, Chen XG, Li YY, Liu CS, Liu CG, Cha DS, Park HJ. 2008. Antibacterial activity of oleoyl-chitosan nanoparticles: A novel antibacterial dispersion system. Carbohydr polym 74:114-120.

Xing K, Chen XG, Liu CS, Cha DS, Park HJ. 2009b. Oleoyl-chitosan nanoparticles inhibits *Escherichia coli* and *Staphylococcus aureus* by damaging the cell membrane and putative binding to extracellular or intracellular targets. Int J Food Microbiol 132:127-133.

Yao K, Li J, Yao F, Yin Y. 2011. Chitosan-based hydrogels: functions and applications. London, New York: CRC Press.

Yamamoto O. 2001. Influence of particle size on the antibacterial activity of zinc oxide. Int J Inorg Mater 3:643-646.

Yien L, Zin NM, Sarwar A, Katas H. 2012. Antifungal activity of chitosan nanoparticles and correlation with their physical properties. Int J Biomater:1-10.

Zheng LY, Zhu JF. 2003. Study on antimicrobial activity of chitosan with different molecular weights. Carbohydr Polym 54:527-530.

Zhong Z, Xing R, Liu S, Wang L, Cai S, Li P. 2008. Synthesis of acyl thiourea derivatives of chitosan and their antimicrobial activities *in vitro*. Carbohydr Res 343:566-570.

Zivanovic S, Chi S, Draughon AF. 2005. Antimicrobial activity of chitosan films enriched with essential oils. J Food Sci 70:M45-M51.

CHAPTER 8: GENERAL DISCUSSION

The insolubility of chitosan in neutral and basic pH conditions may limit the applications of most chitosan-based systems. For instance, in this PhD thesis it was demonstrated that acidic pH conditions (pH< chitosan's pKa) favoring the protonation and solubility of chitosan powder and flakes were required for the exertion of any antibacterial effect, contrary to chitosan nanospheres, in which particle size favoring chitosan-cell interactions play a major role in the antibacterial activity, as will be discussed below. Both chitosan powder and flakes were inactive in a neutral medium, independently of the chitosan concentration and bacterial density. Regarding chitosan solutions and films, several studies have demonstrated that, as the pH increases, the antibacterial activity decreases considerably because of a lower degree of protonation in chitosan amino groups [67, 122, 161, 162]. Although this drawback has been overcome with the use of chitosan derivatives, including quaternized chitosan (which may provide more protonated amino groups-NH_3^+- available for interaction with negatively charged cell surface), their production methods are still under study and far from being considered for industrial applications.

In general, food has an acid or slightly neutral pH, which would favor that chitosan solutions, films or powder and flakes may act as antimicrobial agents. However, coating of food by chitosan solutions may be inadequate for most kind of food, including meat, fruits and vegetables. Besides, dipping without a polymer matrix may result in a rapid diffusion of the solution within the bulk of food, alter the food pH and affect its organoleptic and nutritional properties [14]. Similarly, chitosan powder and flakes may be inadequate for some type of food, despite their potential direct use as antibacterial agents. On the other hand, the weak mechanical and barrier properties of chitosan films may limit their use as active films for food packaging applications [111, 112].

On the contrary, chitosan nanoparticles may offer several advantages, as opposed to the other systems discussed. For instance, in this PhD thesis, we could demonstrate the enhanced antibacterial activity of chitosan nanospheres with respect to chitosan powder and solution form, and when reducing chitosan particle size, inferring that particle size has a major effect. Besides, the antibacterial activity of nanospheres was found to be independent of the medium pH, which is the major difference with respect to other chitosan forms (powder, flakes, solution and films). It was suggested that different mechanism could happen for chitosan nanospheres, as presented in Chapter 7. Briefly, given their small size, nanospheres may adsorb on bacterial surface

independently of the medium pH. At acidic pH, it is believed that the adsorption is due to electrostatic attraction of the positively charged amino groups and negatively charged cell wall. At neutral or slightly basic pH conditions, the mechanism is most probably due to chelating effects and chitosan amino groups may bind to metal cations and trace elements (such as Ca^{2+} and Mg^{2+}) from the cell wall or the medium. Once adsorbed, nanospheres may interfere with the biological activities of the cells, by either forming an impermeable layer and blocking the release of enzymes that are necessary for the absorption of nutrients and/or hindering the leakage of toxic components, or by binding with essential elements for the metabolism from the medium. Lastly, it was suggested that given their small size, nanospheres may diffuse into the cells and alter the mRNA and DNA activities, independently of the medium pH. Therefore, for all the above, nanospheres are considered promising for food related applications.

Recently, the electrospraying process has emerged as a relatively new technique for the fabrication of micro and nanoparticles for drug delivery applications. Electrospraying offer several advantages in comparison with other technologies for nanoparticle formation, including emulsion cross-linking, coacervation/precipitation, spray drying, ionic gelation, as discussed in Chapter 2.2. The main advantage of using electrospraying resides in the control over particle size, morphology and the production of nanoparticles in one single step process. Besides, nanoparticles do not require extra purification steps, including the removal of remaining solvent, because it evaporates during processing. In addition, electrospraying allows transforming a chitosan solution into pure chitosan nanoparticles, by employing a non-toxic solvent such as acetic acid. Furthermore, the processing can be carried out without the need of any co-spinning agent, contrary to the production of chitosan nanofibers, via electrospinning. The direct incorporation of chitosan micro and nanoparticles into conventional food packaging materials (such as polyethylene, polypropylene, aluminium, etc.) through electrospraying could be an alternative of industrial interest for providing of antibacterial properties. This alternative may lead to the formulation of new antibacterial food packaging materials.

However, despite the advantages of the electrospraying process, different aspects should be taken into consideration. First, the scale up for industrial production should be considered. Although the electrospraying technique is well recognized at lab scale, there is still a challenge for implementing it at an industrial level [149]. Nevertheless, drug industry is focusing in exploring this technology for biomedical and pharmaceutical applications. Second, the adhesion of chitosan nanoparticles

onto different surfaces (rugosity, type of matrix) as well as the need of a treatment (such as corona or plasma surface modification) should be considered. The direct electrospraying of a chitosan solution onto an aluminum foil resulted in nanoparticles that were easily removable from the film. Third, the stability of nanoparticles onto the surface matrix (conventional packaging, for example) should be looked at. Four, the effect of chitosan nanoparticles on the thermal, mechanical, optical ad barrier properties of the matrix should be considered. For instance, chitosan nanoparticles displayed a typical white spot once they were in the aluminum foil, suggesting that their use could be limited for packaging where transparency is required. Five, the migration of nanoparticles into food should be looked at. Contaminated food need to be in direct contact with chitosan nanoparticles to exploit their antibacterial effect. However, nanoparticles can migrate into food, and consequently not only affect its organoleptic properties but also be ingested. Hence, the study of cytotoxicity and biocompatibility of these nanoparticles toward human cells should be addressed in a future work. Chitosan is a non-toxic material with a lethal dose value (LD_{50}), similar to the one reported for sugar (16 vs. 30 g/kg body weight) [117]. However, Health Canada [163] reported that in long term, a prolonged exposure to chitosan can cause a decrease in the absorption of essential minerals for the body. For this reason, capsules containing chitosan for slimming and reducing cholesterol should be taken with meals. Regarding the cytotoxic activity, Qi *et al.* [164] reported a high cytotoxicity of chitosan nanoparticles toward tumor cells but a low toxicity toward human liver cells. Finally, the antibacterial activity of chitosan nanospheres should be tested in real food conditions, such as refrigeration temperature (2-4 ºC), presence of nutrients that can limit the antibacterial effect of chitosan (including salts, lipids, proteins), competition with other intrinsic bacteria (natural and contamination flora). In this case, humidity, which is one of the major factors contributing to the deterioration of food, should also be taking into consideration. Moreover, chitosan nanospheres were tested as in a liquid medium which favored their interaction with bacteria. Therefore, tests should be addressed in solid state to mimic real conditions for food. On the other hand, when chitosan nanofibers were part of multilayer food packaging they exhibited promising results in the reduction of bacteria growth and the extension of the shelf life of meat [52].

During the accomplishment of the current research work, we encounter several problems. The first was to condense and understand all the information regarding the antibacterial activity of chitosan. The lack of a standardized method for the evaluation of the antibacterial activity made it difficult

to compare the results from different authors. Second, given the extensive number of factors which may influence the antibacterial action of chitosan, and the duration of the experiments (including the repeatability), we had to prioritize and select only the most relevant factors for food related applications (pH, temperature, ionic strength, cell strains). However, other factors such as chitosan source should be considered. This point is of particular relevance, given the allergies that can be provoked when using a chitosan from marine sources, whose protein content is still over a certain limit. Besides, in the first part of the present research work, it was found that remaining proteins can also limit the antibacterial effect. Therefore, other sources of chitosan, such as from mushrooms and insects, and having different protein content, should be considered for future work.

One of the biggest challenges in the second part of the study was to prepare reproducible chitosan nanospheres for the evaluation of the antibacterial effect against pathogenic bacteria. The extensive number of parameters influencing the electrospraying process hindered the straight production and demanded for a complete study of their interaction. Hence, the third part of the study was focused on the stability of the process to produce chitosan nanospheres. In this case, it was necessary to establish proper relations in terms of dimensionless number that characterized the process and that regrouped the most important variables during processing. Once the influence of the main parameters was established, the mapping of the process was defined. It is noteworthy to mention that the study was conducted in a short period to have less variation in the environmental conditions such as humidity of the chamber. Preliminary results demonstrated that differences in the relative humidity produced different outcomes in both processing and morphology. At relatively high concentrations of chitosan, and for high molecular weight chitosan, it was found that low humidity values (between 2 and 20%) allowed fiber formation, while higher humidity (between 30 to 45%) facilitated the spraying of the solutions and nanospheres formation. Hence, all electrospraying tests were conducted at humidity values between 30 and 40%. The mapping correlating the most important variables allow to predict the stability regions of the process when the environmental conditions remained constant. On the other hand, the study of the process was carried out mostly on chitosan solutions with acetic acid as solvent. This is of great convenience given the intended potential food related applications. Although other solvents, such as TFA are also promising for processing and nanoparticle formation, its toxicity during evaporation step and/or residual traces in nanospheres can be of great concern.

Finally, one main concerns that may limit the processing and applicability of chitosan nanospheres in the food packaging sector is the cost of the raw material, chitosan. Despite its high availability from marine sources, its price is still high (up to 10 times higher) in comparison with conventional polymers such as poly(lactic acid) and poly(ethylene), depending on the purity degree. Therefore, other chitosan sources should be explored as previously discussed.

CHAPTER 9: CONCLUSIONS AND RECOMMENDATIONS

9.1 Conclusions

This research focused on the production of chitosan micro and nanospheres for their potential incorporation into conventional food packaging materials. To do so, the evaluation of the antibacterial action of chitosan was evaluated first on a discontinuous solid form, such as neat chitosan powder and flakes. The first part of this research evaluated the influence of the main factors involved in food related applications such as pH, temperature, ionic strength, bacterial species on the antibacterial activity of chitosan. In addition, the effect of chitosan concentration and purity was analyzed. The following conclusions can be drawn from the results:

1. Particulate solid chitosan displayed antibacterial activity only when the pH of the medium is lower than chitosan pKa, suggesting that a partial solubility of these forms is required for the exertion of the antibacterial effect.
2. Chitosan antibacterial activity is favored at low pH and low salt concentrations, and at high temperature conditions.
3. Chitosan concentration may limit or favor the antibacterial effect, depending on the purity (protein content). The antibacterial activity increases with chitosan concentration in high purity chitosan samples. However, the presence of impurities such as proteins may be detrimental for the antibacterial action and can favor the proliferation of bacteria into the medium.
4. *E. coli* strains were found more sensitive to the action of chitosan than *S. aureus* and *L. innocua* strains.
5. Chitosan powder and flakes may serve as physical support enhancing the antibacterial effect.

The second part of this research focused on the mapping of the processability of chitosan/acetic acid solutions for stability and nanospheres formation via electrospraying. The following conclusions can be drawn from the results:

1. Chitosan (medium molecular weight)/acetic acid solutions at 1 and 2 wt/v % chitosan, and at 70 and 90 v/v % acetic acid content, allowed the production of micro and nanoparticles.

2. A surface tension below 36 mN/m, a relative low conductivity between 0.015 to 0.089 S/m and a shear viscosity between 0.08 to 1.65 Pa s, were required for process stability, micro and nanoparticle formation and collection.
3. Optimal processing conditions included pumping of chitosan solutions through a 22G needle, at a flow rate of 0.2 mL/h, a voltage of 33 kV and a distance of 11 cm from the needle tip to collector plate.
4. The stability in the electrospraying of chitosan solutions required relatively low values for *Re*, *Fr* and Ω but relatively high values for *Pe* and *We* numbers.

The third part of this research focused on the evaluation of several environmental and microbial factors on the antibacterial action of chitosan nanospheres. Besides, the effect of chitosan physical form and shape was considered. The following conclusions can be drawn from the results:

1. Chitosan physical form highly influences its antibacterial activity. Chitosan nanospheres displayed higher antibacterial activity than chitosan in powder and solution form against foodborne pathogens such as *S.* Typhimurium and *S. aureus*.
2. *S. aureus* strains were found more sensitive to the antibacterial action of chitosan nanospheres than *S.* Typhimurium strains.
3. pH and temperature conditions did not limit the antibacterial efficacy of chitosan nanospheres, contrary to other physical forms, which are not completely active at low temperature and at neutral/slightly basic pH conditions.

The electrospraying process may provide a novel way for incorporating chitosan nanospheres into conventional food packaging material to confer antimicrobial properties and help to extend the shelf-life of food products.

9.2 Recommendations

The following aspects are recommended to be explored in future works:

1. Study the mechanism of action of chitosan nanospheres via TEM observation of the cells and evaluating the leakage of components.

2. Investigate the effect of chitosan source (marine vs. mushrooms and insects) on the antibacterial action of chitosan.
3. Evaluation of the solubility limits required for the antibacterial effect of chitosan powder and flakes.
4. Study of the influence of environmental conditions including temperature, humidity and drying conditions on processing and morphology for nanoparticle formation via electrospraying.
5. Study the effect of DDA in the electrospray ability of chitosan.
6. Evaluate the optimal nanoparticle size for maximum efficiency in the antibacterial effect.
7. Investigate the direct incorporation and adhesion of chitosan micro and nanoparticles into conventional food packaging materials such as polyethylene, polypropylene, aluminium foil, etc. through electrospraying. Different surface roughness, matrices and treatments should be considered.
8. Study the effect of chitosan on the thermal, mechanical, optical and barrier properties of the polymer matrix containing chitosan nanoparticles.
9. Evaluate the antibacterial activity of chitosan nanoparticles electrosprayed on the surface of different polymer matrix. Perform *in situ* and *in vitro* tests.
10. Perform antibacterial tests at static conditions instead of inoculated liquid medium at different pH and temperature conditions.
11. Evaluate the migration of chitosan nanoparticles into food, their effect on the organoleptic properties as well as the study of cytotoxicity and biocompatibility of these nanoparticles towards human cells, in case they are ingested.
12. Evaluate the encapsulation of chitosan micro and nanospheres with essential oils, such as eugenol and thymol to further increase the antibacterial effect and its processing via electrospraying.

BIBLIOGRAPHY

[1] F. Käferstein, Y. Motarjemi, and D. W. Bettcher, "Foodborne disease control: a transnational challenge", *Emerging infectious diseases,* vol. 3, p. 503, 1997.

[2] M. Egan, M. Raats, S. Grubb, A. Eves, M. Lumbers, M. Dean, and M. Adams, "A review of food safety and food hygiene training studies in the commercial sector", *Food Control,* vol. 18, pp. 1180-1190, 2007.

[3] C. Weeks, "More Canadians suffer food poisoning", http:// classifieds.canada.com/ remembering/story.html?id=ee66451e-aa59-4bf1-90d7-7ecd7985f582, *Postmedia network Inc*., 2005-2010.

[4] P. H. A. C, "Food Safety", www.publichealth.gc.ca, *Public Health Agency of Canada*, 2013.

[5] I. Simard Tremblay, "Comment réduire le gaspillage alimentaire dans l'industrie agroalimentaire au Québec?", Université de Sherbrooke, 2015.

[6] M. Campos, L. Cordi, N. Duran, and L. Mei, "Antibacterial activity of chitosan solutions for wound dressing", in *Macromolecular Symposia*, pp. 515-518, 2006.

[7] Y. C. Chung and C. Y. Chen, "Antibacterial characteristics and activity of acid-soluble chitosan", *Bioresource Technology,* vol. 99, pp. 2806-2814, 2008.

[8] Y. C. Chung, H. L. Wang, Y. M. Chen, and S. L. Li, "Effect of abiotic factors on the antibacterial activity of chitosan against waterborne pathogens", *Bioresource Technology,* vol. 88, pp. 179-184, 2003.

[9] B. Li, X. Wang, R. Chen, W. Huangfu, and G. Xie, "Antibacterial activity of chitosan solution against *Xanthomonas* pathogenic bacteria isolated from Euphorbia pulcherrima", *Carbohydrate Polymers,* vol. 72, pp. 287-292, 2008.

[10] L. Y. Zheng and J. F. Zhu, "Study on antimicrobial activity of chitosan with different molecular weights", *Carbohydrate Polymers,* vol. 54, pp. 527-530, 2003.

[11] R. L. Beverlya, M. E. Janes, W. Prinyawiwatkula, and H. K. No, "Edible chitosan films on ready-to-eat roast beef for the control of *Listeria monocytogenes*", *Food Microbiology,* vol. 25, pp. 534-537, 2008.

[12] S. Chi, S. Zivanovic, and M. Penfield, "Application of chitosan films enriched with oregano essential oil on bologna–active compounds and sensory attributes", *Food Science and Technology International,* vol. 12, pp. 111-117, 2006.

[13] P. Dutta, S. Tripathi, G. Mehrotra, and J. Dutta, "Perspectives for chitosan based antimicrobial films in food applications", *Food Chemistry,* vol. 114, pp. 1173-1182, 2009.

[14] B. Ouattara, R. E. Simard, G. Piette, A. Bégin, and R. A. Holley, "Inhibition of surface spoilage bacteria in processed meats by application of antimicrobial films prepared with chitosan", *International journal of food microbiology,* vol. 62, pp. 139-148, 2000.

[15] Y. M. Chen, Y. C. Chung, L. Woan Wang, K. T. Chen, and S. Y. Li, "Antibacterial properties of chitosan in waterborne pathogen", *Journal of Environmental Science and Health, Part A,* vol. 37, pp. 1379-1390, 2002.

[16] G. J. Tsai, W. H. Su, H. C. Chen, and C. L. Pan, "Antimicrobial activity of shrimp chitin and chitosan from different treatments and applications of fish preservation", *Fisheries Science,* vol. 68, pp. 170-177, 2002.

[17] B. Ouattara, R. Simard, G. Piette, A. Begin, and R. Holley, "Diffusion of Acetic and Propionic Acids from Chitosan-based Antimicrobial Packaging Films", *Journal of food science,* vol. 65, pp. 768-773, 2000.

[18] S. Zivanovic, S. Chi, and A. F. Draughon, "Antimicrobial activity of chitosan films enriched with essential oils", *Journal of food science,* vol. 70, pp. M45-M51, 2005.

[19] M. Kong, X. G. Chen, C. S. Liu, C. G. Liu, X. H. Meng, and L. J. Yu, "Antibacterial mechanism of chitosan microspheres in a solid dispersing system against *E. coli*", *Colloids and Surfaces B: Biointerfaces,* vol. 65, pp. 197-202, 2008.

[20] L. Qi, Z. Xu, X. Jiang, C. Hu, and X. Zou, "Preparation and antibacterial activity of chitosan nanoparticles", *Carbohydrate Research,* vol. 339, pp. 2693-2700, 2004.

[21] L. Yien, N. M. Zin, A. Sarwar, and H. Katas, "Antifungal activity of chitosan nanoparticles and correlation with their physical properties", *International journal of biomaterials,* 2012.

[22] R. A. Muzzarelli, "Natural chelating polymers; alginic acid, chitin and chitosan", 1973.

[23] M. Rinaudo, "Chitin and chitosan: properties and applications", *Progress in Polymer Science,* vol. 31, pp. 603-632, 2006.

[24] K. Kurita, "Chitin and chitosan: functional biopolymers from marine crustaceans", *Marine Biotechnology,* vol. 8, p. 203, 2006.

[25] M. N. R. Kumar, "A review of chitin and chitosan applications", *Reactive and functional polymers,* vol. 46, pp. 1-27, 2000.

[26] M. F. Goosen, *Applications of chitin and chitosan*. Florida: CRC PressI Llc, 1997.

[27] P. Lertsutthiwong, N. C. How, S. Chandrkrachang, and W. F. Stevens, "Effect of Chemical Treatment on the Characteristics of Shrimp Chitosan", *Journal of Metals, Materials and Minerals,* vol. 12, pp. 11-18, 2002.

[28] M. Rao, J. Munoz, and W. Stevens, "Critical factors in chitin production by fermentation of shrimp biowaste", *Applied Microbiology and Biotechnology,* vol. 54, pp. 808-813, 2000.

[29] J. Brugnerotto, J. Desbrieres, L. Heux, K. Mazeau, and M. Rinaudo, "Overview on structural characterization of chitosan molecules in relation with their behavior in solution", in *Macromolecular Symposia,* pp. 1-20, 2001.

[30] V. Sinha, A. Singla, S. Wadhawan, R. Kaushik, R. Kumria, K. Bansal, and S. Dhawan, "Chitosan microspheres as a potential carrier for drugs", *International Journal of Pharmaceutics,* vol. 274, pp. 1-33, 2004.

[31] S. A. Agnihotri, N. N. Mallikarjuna, and T. M. Aminabhavi, "Recent advances on chitosan-based micro-and nanoparticles in drug delivery", *Journal of Controlled Release,* vol. 100, pp. 5-28, 2004.

[32] K. Harish Prashanth and R. Tharanathan, "Chitin/chitosan: modifications and their unlimited application potential—an overview", *Trends in Food Science & Technology,* vol. 18, pp. 117-131, 2007.

[33] M. N. Ravi Kumar, "A review of chitin and chitosan applications", *Reactive and functional polymers,* vol. 46, pp. 1-27, 2000.

[34] R. A. A. Muzzarelli, A. Ferrero, M. Pizzali, *Talanta,* vol. 19, p. 1222, 1972.

[35] R. A. A. Muzzarelli, *J. Chromatogr.*, vol. 47, p. 414, 1970.

[36] C. Pillai, W. Paul, and C. P. Sharma, "Chitin and chitosan polymers: Chemistry, solubility and fiber formation", *Progress in Polymer Science,* vol. 34, pp. 641-678, 2009.

[37] K. Yao, J. Li, F. Yao, and Y. Yin, *Chitosan-based hydrogels: functions and applications*: CRC Press, 2011.

[38] M. Hamdine, M.-C. Heuzey, and A. Bégin, "Effect of organic and inorganic acids on concentrated chitosan solutions and gels", *International journal of biological macromolecules,* vol. 37, pp. 134-142, 2005.

[39] M. Rinaudo, G. Pavlov, and J. Desbrieres, "Influence of acetic acid concentration on the solubilization of chitosan", *Polymer,* vol. 40, pp. 7029-7032, 1999.

[40] M. Rinaudo, G. Pavlov, and J. Desbrieres, "Solubilization of chitosan in strong acid medium", *International Journal of Polymer Analysis and Characterization,* vol. 5, pp. 267-276, 1999.

[41] T. Sannan, K. Kurita, and Y. Iwakura, "Studies on chitin, 2. Effect of deacetylation on solubility", *Die Makromolekulare Chemie,* vol. 177, pp. 3589-3600, 1976.

[42] J. Desbrieres, "Viscosity of semiflexible chitosan solutions: influence of concentration, temperature, and role of intermolecular interactions", *Biomacromolecules,* vol. 3, pp. 342-349, 2002.

[43] J. Cho, M.-C. Heuzey, A. Bégin, and P. J. Carreau, "Viscoelastic properties of chitosan solutions: Effect of concentration and ionic strength", *Journal of Food Engineering,* vol. 74, pp. 500-515, 2006.

[44] E. A. El-Hefian, E. S. Elgannoudi, A. Mainal, and A. H. Yahaya, "Characterization of chitosan in acetic acid: Rheological and thermal studies", *Turk. J. Chem,* vol. 34, pp. 47-56, 2010.

[45] C. Kienzle-Sterzer, D. Rodriguez-Sanchez, and C. Rha, "Flow behavior of a cationic biopolymer: Chitosan", *Polymer Bulletin,* vol. 13, pp. 1-6, 1985.

[46] R. Chen, W. Lin, and J. Lin, "Effects of pH, ionic strength, and type of anion on the rheological properties of chitosan solutions", *Acta polymerica,* vol. 45, pp. 41-46, 1994.

[47] J. Kumirska, M. X. Weinhold, J. Thöming, and P. Stepnowski, "Biomedical Activity of Chitin/Chitosan Based Materials—Influence of Physicochemical Properties Apart from Molecular Weight and Degree of N-Acetylation", *Polymers,* vol. 3, pp. 1875-1901, 2011.

[48] R. C. Goy, S. T. Morais, and O. B. Assis, "Evaluation of the antimicrobial activity of chitosan and its quaternized derivative on *E. coli* and *S. aureus* growth," *Revista Brasileira de Farmacognosia,* 2015.

[49] M. Ignatova, N. Manolova, N. Markova, and I. Rashkov, "Electrospun Non-Woven Nanofibrous Hybrid Mats Based on Chitosan and PLA for Wound-Dressing Applications", *Macromolecular Bioscience,* vol. 9, pp. 102-111, 2009.

[50] M. Ignatova, K. Starbova, N. Markova, N. Manolova, and I. Rashkov, "Electrospun nano-fibre mats with antibacterial properties from quaternised chitosan and poly (vinyl alcohol)", *Carbohydrate Research,* vol. 341, pp. 2098-2107, 2006.

[51] M. Arkoun, F. Daigle, M. C. Heuzey, and A. Ajji, "Antibacterial electrospun chitosan-based nanofibers: A bacterial membrane perforator", *Journal of Food Science and nutrition,* doi:10.1002/fsn3.468, 2017.

[52] M. Arkoun, F. Daigle, M. C. Heuzey, and A. Ajji, "Mechanism of Action of Electrospun Chitosan-Based Nanofibers against Meat Spoilage and Pathogenic Bacteria", *Molecules,* vol. 22, pp. 585, 2017.

[53] M. Kong, X. G. Chen, Y. P. Xue, C. S. Liu, L. J. Yu, Q. X. Ji, D. S. Cha, and H. J. Park, "Preparation and antibacterial activity of chitosan microshperes in a solid dispersing system", *Frontiers of Materials Science in China,* vol. 2, pp. 214-220, 2008.

[54] K. Xing, X. G. Chen, M. Kong, C. S. Liu, D. S. Cha, and H. J. Park, "Effect of oleoyl-chitosan nanoparticles as a novel antibacterial dispersion system on viability, membrane permeability and cell morphology of *Escherichia coli* and *Staphylococcus aureus*", *Carbohydrate Polymers,* vol. 76, pp. 17-22, 2009.

[55] K. Xing, X. G. Chen, Y. Y. Li, C. S. Liu, C. G. Liu, D. S. Cha, and H. J. Park, "Antibacterial activity of oleoyl-chitosan nanoparticles: A novel antibacterial dispersion system", *Carbohydrate polymers,* vol. 74, pp. 114-120, 2008.

[56] K. Xing, X. G. Chen, C. S. Liu, D. S. Cha, and H. J. Park, "Oleoyl-chitosan nanoparticles inhibits *Escherichia coli* and *Staphylococcus aureus* by damaging the cell membrane and putative binding to extracellular or intracellular targets", *International journal of food microbiology,* vol. 132, pp. 127-133, 2009.

[57] J. Gómez-Estaca, A. López de Lacey, M. López-Caballero, M. Gómez-Guillén, and P. Montero, "Biodegradable gelatin–chitosan films incorporated with essential oils as antimicrobial agents for fish preservation", *Food Microbiology,* vol. 27, pp. 889-896, 2010.

[58] L. Sánchez-González, M. Cháfer, M. Hernández, A. Chiralt, and C. González-Martínez, "Antimicrobial activity of polysaccharide films containing essential oils", *Food Control,* vol. 22, pp. 1302-1310, 2011.

[59] R. Muzzarelli, R. Tarsi, O. Filippini, E. Giovanetti, G. Biagini, and P. Varaldo, "Antimicrobial properties of *N*-carboxybutyl chitosan", *Antimicrobial agents and chemotherapy,* vol. 34, pp. 2019-2023, 1990.

[60] S. Yingyuad, S. Ruamsin, D. Reekprkhon, S. Douglas, S. Pongamphai, and U. Siripatrawan, "Effect of chitosan coating and vacuum packaging on the quality of refrigerated grilled pork", *Packaging technology and science,* vol. 19, pp. 149-157, 2006.

[61] V. K. Juneja, H. Thippareddi, L. Bari, Y. Inatsu, S. Kawamoto, and M. Friedman, "Chitosan protects cooked ground beef and turkey against *Clostridium perfringens* spores during chilling", *Journal of food science,* vol. 71, pp. M236-M240, 2006.

[62] S. R. Kanatt, R. Chander, and A. Sharma, "Chitosan and mint mixture: A new preservative for meat and meat products", *Food Chemistry,* vol. 107, pp. 845-852, 2008.

[63] I. Helander, E. L. Nurmiaho-Lassila, R. Ahvenainen, J. Rhoades, and S. Roller, "Chitosan disrupts the barrier properties of the outer membrane of Gram-negative bacteria", *International journal of food microbiology,* vol. 71, pp. 235-244, 2001.

[64] M. Kong, X. G. Chen, K. Xing, and H. J. Park, "Antimicrobial properties of chitosan and mode of action: a state of the art review", *International journal of food microbiology,* vol. 144, pp. 51-63, 2010.

[65] S. Bhale, H. K. No, W. Prinyawiwatkul, A. Farr, K. Nadarajah, and S. P. Meyers, "Chitosan coating improves shelf life of eggs", *Journal of food science,* vol. 68, pp. 2378-2383, 2003.

[66] Y. J. Jeon, P. J. Park, and S. K. Kim, "Antimicrobial effect of chitooligosaccharides produced by bioreactor", *Carbohydrate Polymers,* vol. 44, pp. 71-76, 2001.

[67] H. K. No, N. Y. Park, S. H. Lee, and S. P. Meyers, "Antibacterial activity of chitosans and chitosan oligomers with different molecular weights", *International journal of food microbiology,* vol. 74, pp. 65-72, 2002.

[68] S. Bautista-Baños, A. Hernández-Lauzardo, M. Velázquez-del Valle, M. Hernández-López, E. Ait Barka, E. Bosquez-Molina, and C. Wilson, "Chitosan as a potential natural compound to control pre and postharvest diseases of horticultural commodities", *Crop Protection,* vol. 25, pp. 108-118, 2006.

[69] N. Ardila, F. Daigle, M. C. Heuzey, and A. Ajji, "Effect of chitosan physical form on its antibacterial activity against pathogenic bacteria", *Journal of Food Science,* vol. 82, pp. 679-686, 2017.

[70] P. Darmadji and M. Izumimoto, "Effect of chitosan in meat preservation", *Meat Science,* vol. 38, pp. 243-254, 1994.

[71] I. Sebti, A. Martial ‐ Gros, A. Carnet ‐ Pantiez, S. Grelier, and V. Coma, "Chitosan polymer as bioactive coating and film against *Aspergillus niger* contamination", *Journal of food science,* vol. 70, pp. M100-M104, 2005.

[72] Y. Okawa, M. Kobayashi, S. Suzuki, and M. Suzuki, "Comparative study of protective effects of chitin, chitosan, and *N*-acetyl chitohexaose against *Pseudomonas aeruginosa* and *Listeria monocytogenes* infections in mice", *Biological and Pharmaceutical Bulletin,* vol. 26, pp. 902-904, 2003.

[73] S. Roller and N. Covill, "The antifungal properties of chitosan in laboratory media and apple juice", *International Journal of Food Microbiology,* vol. 47, pp. 67-77, 1999.

[74] A. Ghaouth, J. Arul, R. Ponnampalam, and M. Boulet, "Chitosan coating effect on storability and quality of fresh strawberries", *Journal of food science,* vol. 56, pp. 1618-1620, 1991.

[75] E. I. Rabea, M. E. T. Badawy, C. V. Stevens, G. Smagghe, and W. Steurbaut, "Chitosan as antimicrobial agent: applications and mode of action", *Biomacromolecules,* vol. 4, pp. 1457-1465, 2003.

[76] K. Kurita, "Chemistry and application of chitin and chitosan", *Polymer Degradation and Stability,* vol. 59, pp. 117-120, 1998.

[77] N. Liu, X. G. Chen, H. J. Park, C. G. Liu, C. S. Liu, X. H. Meng, and L. J. Yu, "Effect of MW and concentration of chitosan on antibacterial activity of *Escherichia coli*", *Carbohydrate Polymers,* vol. 64, pp. 60-65, 2006.

[78] A. Martínez-Camacho, M. Cortez-Rocha, J. Ezquerra-Brauer, A. Graciano-Verdugo, F. Rodriguez-Félix, M. Castillo-Ortega, M. Yépiz-Gómez, and M. Plascencia-Jatomea, "Chitosan composite films: Thermal, structural, mechanical and antifungal properties", *Carbohydrate Polymers,* vol. 82, pp. 305-315, 2010.

[79] A. Muñoz-Bonilla and M. Fernández-García, "Polymeric materials with antimicrobial activity", *Progress in Polymer Science,* vol. 37, pp. 281-339, 2012.

[80] S. Park, K. Marsh, and J. Rhim, "Characteristics of different molecular weight chitosan films affected by the type of organic solvents", *Journal of food science,* vol. 67, pp. 194-197, 2002.

[81] F. J. Pavinatto, L. Caseli, and O. N. Oliveira Jr, "Chitosan in nanostructured thin films", *Biomacromolecules,* vol. 11, pp. 1897-1908, 2010.

[82] P. Srinivasa, M. Ramesh, K. Kumar, and R. Tharanathan, "Properties of chitosan films prepared under different drying conditions", *Journal of Food Engineering,* vol. 63, pp. 79-85, 2004.

[83] M. Liu, Y. Zhou, Y. Zhang, C. Yu, and S. Cao, "Preparation and structural analysis of chitosan films with and without sorbitol", *Food Hydrocolloids,* 2013.

[84] M. Z. Elsabee, H. F. Naguib, and R. E. Morsi, "Chitosan based nanofibers, review", *Materials Science and Engineering: C,* 2012.

[85] S. Torres-Giner, M. Ocio, and J. Lagaron, "Development of Active Antimicrobial Fiber-Based Chitosan Polysaccharide Nanostructures using Electrospinning", *Engineering in Life Sciences,* vol. 8, pp. 303-314, 2008.

[86] X. Geng, O. H. Kwon, and J. Jang, "Electrospinning of chitosan dissolved in concentrated acetic acid solution", *Biomaterials,* vol. 26, pp. 5427-5432, 2005.

[87] C. Kriegel, K. Kit, D. McClements, and J. Weiss, "Electrospinning of chitosan–poly (ethylene oxide) blend nanofibers in the presence of micellar surfactant solutions", *Polymer,* vol. 50, pp. 189-200, 2009.

[88] B. Narayan, "Nanofibrous Structure of Chitosan for Biomedical Applications", *Journal of Nanomedicine & Biotherapeutic Discovery*, 2012.

[89] N. Ardila, N. Medina, M. Arkoun, M. C. Heuzey, A. Ajji, and C. J. Panchal, "Chitosan-bacterial nanocellulose nanofibrous structures for potential wound dressing applications", *Cellulose,* vol. 23, pp. 3089-3104, 2016.

[90] Y. Ai, S. Guo, Q. Zhang, J. Qiao, X. Gao, J. Nie, and D. Yang, "Preparation of chitosan/alginate microcapsules by high-voltage electrostatic method", *Frontiers of Chemistry in China,* vol. 6, pp. 48-53, 2011.

[91] R. Bhattarai, N. Dhandapani, and A. Shrestha, "Drug delivery using alginate and chitosan beads: An Overview", *Chronicles of Young Scientists,* vol. 2, p. 192, 2011.

[92] N. Bock, M. A. Woodruff, D. W. Hutmacher, and T. R. Dargaville, "Electrospraying, a reproducible method for production of polymeric microspheres for biomedical applications", *Polymers,* vol. 3, pp. 131-149, 2011.

[93] L. Brannon-Peppas, "Recent advances on the use of biodegradable microparticles and nanoparticles in controlled drug delivery", *International Journal of Pharmaceutics,* vol. 116, pp. 1-9, 1995.

[94] G. Coppi, V. Iannuccelli, E. Leo, M. T. Bernabei, and R. Cameroni, "Chitosan-alginate microparticles as a protein carrier", *Drug development and industrial pharmacy,* vol. 27, pp. 393-400, 2001.

[95] S. Freiberg and X. Zhu, "Polymer microspheres for controlled drug release", *International Journal of Pharmaceutics,* vol. 282, pp. 1-18, 2004.

[96] V. Guarino, W. A. K. WK, and L. Ambrosio, "Biodegradable microparticles and nanoparticles by electrospraying techniques", *Journal of applied biomaterials & functional materials,* vol. 10, pp. 191-196, 2012.

[97] P. He, S. S. Davis, and L. Illum, "Chitosan microspheres prepared by spray drying", *International Journal of Pharmaceutics,* vol. 187, pp. 53-65, 1999.

[98] P. He, S. S. Davis, and L. Illum, "*In vitro* evaluation of the mucoadhesive properties of chitosan microspheres", *International Journal of Pharmaceutics,* vol. 166, pp. 75-88, 1998.

[99] Y. Huang, M. Yeh, and C. Chiang, "Formulation factors in preparing BTM–chitosan microspheres by spray drying method", *International Journal of Pharmaceutics,* vol. 242, pp. 239-242, 2002.

[100] J. Ko, H. Park, S. Hwang, J. Park, and J. Lee, "Preparation and characterization of chitosan microparticles intended for controlled drug delivery", *International Journal of Pharmaceutics,* vol. 249, pp. 165-174, 2002.

[101] W. Pasanphan, P. Rimdusit, S. Choofong, T. Piroonpan, and S. Nilsuwankosit, "Systematic fabrication of chitosan nanoparticle by gamma irradiation", *Radiation Physics and Chemistry,* vol. 79, pp. 1095-1102, 2010.

[102] G. Sun, X. Z. Zhang, and C. C. Chu, "Formulation and characterization of chitosan-based hydrogel films having both temperature and pH sensitivity", *Journal of Materials Science: Materials in Medicine,* vol. 18, pp. 1563-1577, 2007.

[103] N. Boucard, C. Viton, and A. Domard, "New aspects of the formation of physical hydrogels of chitosan in a hydroalcoholic medium", *Biomacromolecules,* vol. 6, pp. 3227-3237, 2005.

[104] N. Bhattarai, J. Gunn, and M. Zhang, "Chitosan-based hydrogels for controlled, localized drug delivery", *Advanced drug delivery reviews,* vol. 62, pp. 83-99, 2010.

[105] Y. Wan, X. Lu, S. Dalai, and J. Zhang, "Thermophysical properties of polycaprolactone/chitosan blend membranes", *Thermochimica Acta,* vol. 487, pp. 33-38, 2009.

[106] Y. J. Seol, J. Y. Lee, Y. J. Park, Y. M. Lee, I. C. Rhyu, S. J. Lee, S. B. Han, and C. P. Chung, "Chitosan sponges as tissue engineering scaffolds for bone formation", *Biotechnology letters,* vol. 26, pp. 1037-1041, 2004.

[107] C. Chen, L. Dong, and M. K. Cheung, "Preparation and characterization of biodegradable poly (L-lactide)/chitosan blends", *European polymer journal,* vol. 41, pp. 958-966, 2005.

[108] L. Liu, Y. Li, H. Liu, and Y. E. Fang, "Synthesis and characterization of chitosan-graft-polycaprolactone copolymers", *European polymer journal,* vol. 40, pp. 2739-2744, 2004.

[109] A. Dufresne, J. Y. Cavaillé, D. Dupeyre, M. Garcia-Ramirez, and J. Romero, "Morphology, phase continuity and mechanical behaviour of polyamide 6/chitosan blends", *Polymer,* vol. 40, pp. 1657-1666, 1999.

[110] E. A. El-hefian, M. M. Nasef, and A. H. Yahaya, "Chitosan Physical Forms: A short review", *Australian Journal of Basic and Applied Sciences,* vol. 5, pp. 670-677, 2011.

[111] V. Alexeev, E. Kelberg, G. Evmenenko, and S. Bronnikov, "Improvement of the mechanical properties of chitosan films by the addition of poly (ethylene oxide)", *Polymer Engineering & Science,* vol. 40, pp. 1211-1215, 2000.

[112] C. Caner, P. Vergano, and J. Wiles, "Chitosan film mechanical and permeation properties as affected by acid, plasticizer, and storage", *Journal of food science,* vol. 63, pp. 1049-1053, 1998.

[113] V. Coma, A. Martial-Gros, S. Garreau, A. Copinet, F. Salin, and A. Deschamps, "Edible antimicrobial films based on chitosan matrix", *Journal of food science,* vol. 67, pp. 1162-1169, 2002.

[114] M. Matet, M. C. Heuzey, and A. Ajji, "Morphology and antibacterial properties of plasticized chitosan/metallocene polyethylene blends", *Journal of Materials Science,* vol. 49, pp. 5427-5440, 2014.

[115] M. Matet, M. C. Heuzey, A. Ajji, and P. Sarazin, "Plasticized chitosan/polyolefin films produced by extrusion", *Carbohydrate polymers,* vol. 117, pp. 177-184, 2015.

[116] M. Matet, M. C. Heuzey, E. Pollet, A. Ajji, and L. Avérous, "Innovative thermoplastic chitosan obtained by thermo-mechanical mixing with polyol plasticizers", *Carbohydrate polymers,* vol. 95, pp. 241-251, 2013.

[117] E2456-06, "ASTM E2456-06 Standard Terminology Relating to Nanotechnology", *American Society for Testing Materials,* 2012.

[118] S. Mitra, U. Gaur, P. Ghosh, and A. Maitra, "Tumour targeted delivery of encapsulated dextran–doxorubicin conjugate using chitosan nanoparticles as carrier", *Journal of Controlled Release,* vol. 74, pp. 317-323, 2001.

[119] K. Arai, T. Kinumaki, and T. Fujita, "Toxicity of chitosan", *Bull. Tokai. Region. Fish. Res. Lab.,* pp. 89-94, 1968.

[120] A. Anitha, V. Divya Rani, R. Krishna, V. Sreeja, N. Selvamurugan, S. Nair, H. Tamura, and R. Jayakumar, "Synthesis, characterization, cytotoxicity and antibacterial studies of chitosan, *O*-carboxymethyl and *N,O*-carboxymethyl chitosan nanoparticles", *Carbohydrate Polymers,* vol. 78, pp. 672-677, 2009.

[121] A. Bégin and M.-R. Van Calsteren, "Antimicrobial films produced from chitosan", *International journal of biological macromolecules,* vol. 26, pp. 63-67, 1999.

[122] F. Devlieghere, A. Vermeulen, and J. Debevere, "Chitosan: antimicrobial activity, interactions with food components and applicability as a coating on fruit and vegetables", *Food Microbiology,* vol. 21, pp. 703-714, 2004.

[123] L. Ilium, "Chitosan and its use as a pharmaceutical excipient", *Pharmaceutical research,* vol. 15, pp. 1326-1331, 1998.

[124] U. S, FDA, "GRAS notice-Shrimp derived chitosan," vol. GRAS notice No 443, 2013.

[125] N. Ardila, F. daigle, M. C. Heuzey, and A. Ajji, "Antibacterial Activity of Neat Chitosan Powder and Flakes," *Molecules,* vol. 22, pp. 1-19, 2017.

[126] T. Sun, D. Zhou, J. Xie, and F. Mao, "Preparation of chitosan oligomers and their antioxidant activity", *European Food Research and Technology,* vol. 225, pp. 451-456, 2007.

[127] K. Roy, H. Q. Mao, S. K. Huang, and K. W. Leong, "Oral gene delivery with chitosan–DNA nanoparticles generates immunologic protection in a murine model of peanut allergy", *Nature medicine,* vol. 5, pp. 387-391, 1999.

[128] A. Frenot and I. S. Chronakis, "Polymer nanofibers assembled by electrospinning", *Current opinion in colloid & interface science,* vol. 8, pp. 64-75, 2003.

[129] H. Jiang, D. Fang, B. Hsiao, B. Chu, and W. Chen, "Preparation and characterization of ibuprofen-loaded poly (lactide-co-glycolide)/poly (ethylene glycol)-g-chitosan electrospun membranes", *Journal of Biomaterials Science, Polymer Edition,* vol. 15, pp. 279-296, 2004.

[130] R. Jayakumar, M. Prabaharan, S. Nair, and H. Tamura, "Novel chitin and chitosan nanofibers in biomedical applications", *Biotechnology advances,* vol. 28, pp. 142-150, 2010.

[131] G. Crini, P.-M. Badot, and E. Guibal, *Chitine et chitosane: du biopolymère à l'application*, Presses Univ. Franche-Comté, 2009.

[132] S. Hirano, "Chitin biotechnology applications", *Biotechnology annual review,* vol. 2, pp. 237-258, 1996.

[133] S. Haider and S. Y. Park, "Preparation of the electrospun chitosan nanofibers and their applications to the adsorption of Cu (II) and Pb (II) ions from an aqueous solution", *Journal of Membrane Science,* vol. 328, pp. 90-96, 2009.

[134] K. Desai, K. Kit, J. Li, and S. Zivanovic, "Morphological and surface properties of electrospun chitosan nanofibers", *Biomacromolecules,* vol. 9, pp. 1000-1006, 2008.

[135] J. Zeleny, "The electrical discharge from liquid points, and a hydrostatic method of measuring the electric intensity at their surfaces", *Physical Review,* vol. 3, p. 69, 1914.

[136] G. Taylor, "Disintegration of water drops in an electric field", *Proceedings of the Royal Society of London. Series A. Mathematical and Physical Sciences,* vol. 280, pp. 383-397, 1964.

[137] N. Arya, S. Chakraborty, N. Dube, and D. S. Katti, "Electrospraying: A facile technique for synthesis of chitosan-based micro/nanospheres for drug delivery applications", *Journal of Biomedical Materials Research Part B: Applied Biomaterials,* vol. 88, pp. 17-31, 2009.

[138] N. Bock, T. Dargaville, and M. Woodruff, "Electrospraying of polymers with therapeutic molecules: State of the art", *Progress in Polymer Science,* 2012.

[139] S. Zhang, K. Kawakami, M. Yamamoto, Y. Masaoka, M. Kataoka, S. Yamashita, and S. Sakuma, "Coaxial electrospray formulations for improving oral absorption of a poorly water-soluble drug", *Molecular Pharmaceutics,* vol. 8, pp. 807-813, 2011.

[140] S. G. Kumbar, S. Bhattacharyya, S. Sethuraman, and C. T. Laurencin, "A preliminary report on a novel electrospray technique for nanoparticle based biomedical implants coating: precision electrospraying", *Journal of Biomedical Materials Research Part B: Applied Biomaterials,* vol. 81, pp. 91-103, 2007.

[141] B. Amsden and M. Goosen, "An examination of factors affecting the size, distribution and release characteristics of polymer microbeads made using electrostatics", *Journal of Controlled Release,* vol. 43, pp. 183-196, 1997.

[142] S. Zhang and K. Kawakami, "One-step preparation of chitosan solid nanoparticles by electrospray deposition", *International Journal of Pharmaceutics,* vol. 397, pp. 211-217, 2010.

[143] M. Pakravan, M. C. Heuzey, and A. Ajji, "A fundamental study of chitosan/PEO electrospinning", *Polymer,* vol. 52, pp. 4813-4824, 2011.

[144] C. H. Park, M. Y. Kim, J. Y. Yoo, K. H. Kim, J. C. Lee, and J. Lee, "Preparation of Polymer/Drug Nano- and Micro- Particles by Electrospraying", in *Macromolecular Symposia*, pp. 116-119, 2007.

[145] A. Greiner and J. H. Wendorff, "Electrospinning: a fascinating method for the preparation of ultrathin fibers", *Angewandte Chemie International Edition,* vol. 46, pp. 5670-5703, 2007.

[146] A. Jaworek, "Micro-and nanoparticle production by electrospraying", *Powder technology,* vol. 176, pp. 18-35, 2007.

[147] G. Z. Yang, H. P. Li, J. H. Yang, J. Wan, and D. G. Yu, "Influence of Working Temperature on The Formation of Electrospun Polymer Nanofibers", *Nanoscale Research Letters,* vol. 12, p. 55, 2017.

[148] S. L. Shenoy, W. D. Bates, H. L. Frisch, and G. E. Wnek, "Role of chain entanglements on fiber formation during electrospinning of polymer solutions: good solvent, non-specific polymer–polymer interaction limit", *Polymer,* vol. 46, pp. 3372-3384, 2005.

[149] L. Peltonen, H. Valo, R. Kolakovic, T. Laaksonen, and J. Hirvonen, "Electrospraying, spray drying and related techniques for production and formulation of drug nanoparticles", *Expert Opinion on Drug Delivery,* vol. 7, pp. 705-719, 2010.

[150] F. Meng, Y. Jiang, Z. Sun, Y. Yin, and Y. Li, "Electrohydrodynamic liquid atomization of biodegradable polymer microparticles: effect of electrohydrodynamic liquid atomization variables on microparticles", *Journal of Applied Polymer Science,* vol. 113, pp. 526-534, 2009.

[151] Y. Xu and M. A. Hanna, "Electrospray encapsulation of water-soluble protein with polylactide: Effects of formulations on morphology, encapsulation efficiency and release profile of particles", *International journal of pharmaceutics,* vol. 320, pp. 30-36, 2006.

[152] Y. Wu, S. J. Kennedy, and R. L. Clark, "Polymeric particle formation through electrospraying at low atmospheric pressure", *Journal of Biomedical Materials Research Part B: Applied Biomaterials,* vol. 90, pp. 381-387, 2009.

[153] J. Feng, "The stretching of an electrified non-Newtonian jet: A model for electrospinning" *Physics of fluids,* vol. 14, p. 3912, 2002.

[154] M. M. Hohman, M. Shin, G. Rutledge, and M. P. Brenner, "Electrospinning and electrically forced jets. I. Stability theory" *Physics of fluids,* vol. 13, p. 2201, 2001.

[155] S. M. Kuo, G. C. C. Niu, S. J. Chang, C. H. Kuo, and M. S. Bair, "A one-step method for fabricating chitosan microspheres", *Journal of Applied Polymer Science,* vol. 94, pp. 2150-2157, 2004.

[156] H. Homayoni, S. A. H. Ravandi, and M. Valizadeh, "Electrospinning of chitosan nanofibers: Processing optimization", *Carbohydrate Polymers,* vol. 77, pp. 656-661, 2009.

[157] K. Ohkawa, D. Cha, H. Kim, A. Nishida, and H. Yamamoto, "Electrospinning of chitosan", *Macromolecular Rapid Communications,* vol. 25, pp. 1600-1605, 2004.

[158] K. Ohkawa, K. I. Minato, G. Kumagai, S. Hayashi, and H. Yamamoto, "Chitosan nanofiber", *Biomacromolecules,* vol. 7, pp. 3291-3294, 2006.

[159] J. D. Schiffman and C. L. Schauer, "Cross-linking chitosan nanofibers", *Biomacromolecules,* vol. 8, pp. 594-601, 2007.

[160] L. G. Gómez-Mascaraque, G. Sanchez, and A. López-Rubio, "Impact of molecular weight on the formation of electrosprayed chitosan microcapsules as delivery vehicles for bioactive compounds", *Carbohydrate Polymers,* vol. 150, pp. 121-130, 2016.

[161] X. Fei Liu, Y. Lin Guan, D. Zhi Yang, Z. Li, and K. De Yao, "Antibacterial action of chitosan and carboxymethylated chitosan", *Journal of Applied Polymer Science,* vol. 79, pp. 1324-1335, 2001.

[162] G. J. Tsai and W. H. Su, "Antibacterial activity of shrimp chitosan against *Escherichia coli*", *Journal of Food Protection*, vol. 62, pp. 239-243, 1999.

[163] H. C., "Chitosan", http://webprod.hc-sc.gc.ca/nhpid-bdipsn/atReq.do?atid=chitosan&lang=eng, *Health Canada*, Accessed: 30-05-2017.

[164] L. Qi, Z. Xu, X. Jiang, Y. Li, and M. Wang, "Cytotoxic activities of chitosan nanoparticles and copper-loaded nanoparticles", Bioorganic & medicinal chemistry letters, vol. 15, pp. 1397-1399, 2005.

APPENDICES

APPENDIX A - ARTICLE 4: CHITOSAN-BACTERIAL NANOCELLULOSE NANOFIBROUS STRUCTURES FOR POTENTIAL WOUND DRESSING APPLICATIONS

Nury Ardila[a], Nelson Medina[a], Mounia Arkoun[a], Marie-Claude Heuzey[a], Abdellah Ajji[a], Chandra J. Panchal[b]

[a]CREPEC, Department of Chemical Engineering, Polytechnique Montréal, P.O. Box 6079, Station Centre-Ville, Montréal, Québec, Canada H3C 3A7

[b]Axcelon Biopolymers Corporation, #216-700 Richmond Street London, Ontario, Canada N6A 5C7

(This work was published online in *Cellulose* on August 1st, 2016)

A.1 Abstract

The fabrication of nonwoven mats containing chitosan and bacterial nanocellulose by electrospinning were considered using two different approaches: (i) simultaneous spinning of chitosan and bacterial nanocellulose solutions using two separate syringes towards the same target and (ii) coaxial electrospinning, where chitosan and bacterial nanocellulose were simultaneously electrospun through a spinneret composed of two concentric needles to produce core-shell structures. Co-spinning agents were required in both approaches. A direct blend of chitosan and bacterial nanocellulose and subsequent electrospinning was not feasible due to the incompatibility of their respective solvents. The first approach led to the production of mats containing both chitosan and bacterial nanocellulose nanofibers. However, few bacterial nanocellulose fibers were deposited on the collector. Addition of polylactide as a co-spinning agent and an increase in solution temperature (from 22 to 60 ºC) during electrospinning was required to improve both fiber formation and collection. On the other hand, coaxial electrospinning showed the best results for the production of nanofibers containing both chitosan and bacterial nanocellulose. Nanofibers with a good yield were obtained by using a chitosan/poly(ethylene oxide) (2.4/0.6 wt/v %) aqueous solution as the inner layer, and a bacterial nanocellulose solution (0.6 wt/v %) as the outer layer.

Co-electrospun nanofibers had a diameter of 85 nm in average, and a narrow size distribution. The core/shell nanostructure was validated by transmission electron microscopy whilst energy-dispersive X-ray spectroscopy analysis showed that the nanofibers contained both chitosan and bacterial nanocellulose along their structure. Finally, the mats obtained by the coaxial approach exhibited strong antimicrobial activity with a decrease of 99.9 % of an *Escherichia coli* population.

A.2 Introduction

Cellulose and chitosan are both linear polysaccharides with molecular structures consisting of D-glucose units linked by β-1,4-glucosidic bonds, and differ by the pendant groups at the C-2 position, i.e., hydroxyl for cellulose and acetyl amine units for chitosan (Sekwon 2010). Chitosan is obtained from chitin after deacetylation and purification processes. Chitin is the second most abundant polysaccharide on Earth, after cellulose (Muzzarelli 1973). Chitin is extracted mainly from the exoskeleton of marine crustaceans such as crabs, shrimps, crawfish and lobsters (Goosen 1997). Cellulose can be produced naturally by plant photosynthesis, or via microbial synthesis through various microorganism species including Acetobacter xylinum, Acetobacter hansenii and Acetobacter pasteurianus (Siró and Plackett 2010; Mohite and Patil 2014). Compared to cellulose from plants, bacterial cellulose has higher purity, higher crystallinity, higher degree of polymerization and interesting characteristics, such as higher surface area per unit mass and higher water holding capacity (Siró and Plackett 2010; Mohite and Patil 2014). In addition, a better in vivo compatibility with tissues has been reported for bacterial cellulose (Gama et al. 2012).

Besides their abundance and renewability, intrinsic properties such as biocompatibility, biodegradability and non-toxicity make chitosan and cellulose attractive for different applications. In particular, chitosan is widely recognized as having antimicrobial and hemostatic properties (Goosen 1997; Sekwon 2010), whilst bacterial nanocellulose is of interest in the biomedical area owing to its regenerative ability in wound healing and moisture retaining properties (Gama et al. 2012; Mohite and Patil 2014). Moreover, bacterial cellulose is ideal for cell immobilization and support due to its nanostructure and morphological similarity with collagen (Costa et al. 2012; Basmaji et al. 2015). The combination of the aforementioned properties can be of significant interest for the biomedical industry in the scope of new materials designed for wound dressing applications.

However, despite their good properties, processing of either bacterial cellulose or chitosan alone is a difficult task since they are not thermoplastic materials, nor soluble in most common solvents. In addition, their common processing becomes even more challenging if both materials are intended to be used together to take advantage of their individual properties. The limited solubility of chitosan and bacterial cellulose is mainly attributed to the length of their chains, the high crystallinity, the rigidity of their structure and the strong inter and intramolecular hydrogen bonding (McCormick et al. 1985; Swatloski et al. 2002). Chitosan is commonly dissolved in dilute acids such as acetic and formic acids. Cellulose (and bacterial cellulose) requires the use of more complex systems such as *N*,*N*-dimethyl acetamide/lithium chloride (DMAc/LiCl) (El-Kafrawy 1982; McCormick et al. 1985; Matsumoto et al. 2001; Röder et al. 2001). Other solvents such as N-methyl-2-pyrrolidinone/LiCl (NMP/LiCl), N-methylmorpholine N-oxide (NMMO) (El-Kafrawy 1982; Kulpinski 2005; Greiner and Wendorff 2007) and ionic liquids have also been reported (Schlufter et al. 2006; Okushita et al. 2012). However, the latter may lead to degradation (Schlufter et al. 2006) or induce structural modifications to cellulose (Okushita et al. 2012). On other hand, the DMAc/LiCl solvent system has been widely used for the dissolution of different types of cellulose over a wide range of concentrations, and without side reactions such as derivatization nor degradation (Matsumoto et al. 2001; Röder et al. 2001). DMAc causes inter crystalline swelling, increases accessibility of the solvent to the cellulose chains and weakens the hydrogen bonds between the cellulose molecules (Röder et al. 2001). The addition of LiCl and no other salt is required to bond cellulose and DMAc via electrostatic interactions (El-Kafrawy 1982; McCormick et al. 1985). Nevertheless, differences in molecular structure and crystallinity between cellulose from different biological sources may vary its solubility regarding the solvent systems employed (Matsumoto et al. 2001). Lastly, regardless of the solvent, cellulose is commonly subjected to "activation procedures" such as freeze drying, swelling in water or solvent exchange, treatment with liquid ammonia and heating, in order to break hydrogen bonds and favor dissolution (McCormick et al. 1985; Röder et al. 2001; Potthast et al. 2002; Kim et al. 2006). In the latter case, temperature should be maintained below 85 ºC to avoid degradation of cellulose in DMAc and DMAc/LiCl solution (Potthast et al. 2002; Kim et al. 2006).

Recently, a lot of attention has been paid to the production of submicron size fibers by electrospinning. Resulting nonwoven mats exhibit distinctly high specific surface area, typically

ranging from 10 to 500 m^2/g, small pore size and high porosity (Greiner and Wendorff 2007; Pakravan et al. 2012).

The electrospinning of neat chitosan solutions has been widely investigated (Ohkawa et al. 2004, 2006; Geng et al. 2005; Schiffman and Schauer 2007; Homayoni et al. 2009). Blending chitosan with materials with high spinnability such as poly(ethylene oxide) (PEO) (Subramanian et al. 2005; Desai et al. 2008; Pakravan et al. 2011), poly(lactide) (PLA) (Ignatova et al. 2009) and poly(vinyl alcohol) (PVA) (Ohkawa et al. 2004; Li and Hsieh 2006) have been reported to facilitate its processing and fiber formation, as well as to improve fibrous mats characteristics. In particular, a chitosan/PEO blend ratio of 80/20 has displayed good processability and high yield and chitosan content (Bhattarai et al. 2005; Desai et al. 2008; Pakravan et al. 2011). It has been suggested that in the electrospinning process PEO may act as a carrier of chitosan via hydrogen bonding (Pakravan et al. 2011). For applications that require antimicrobial properties, a lower amount of the carrier polymer is preferable.

Conversely, a limited number of publications can be found on the electrospinning of cellulose and bacterial cellulose. Cellulose has been electrospun from NMMO/water (Kulpinski 2005; Kim et al. 2006; Greiner and Wendorff 2007), DMAc/LiCl (Kim et al. 2005, 2006; Frenot et al. 2007) and ionic liquids (Ahn et al. 2012) into fibers with diameters in the sub and micrometer range, whilst one study has performed the electrospinning of chemically modified bacterial cellulose in chloroform/acetone (Costa et al. 2012). Nevertheless, in most cases, the processing was challenging with low yield (collection) and poor quality of fibers, and in some studies it involved several steps. In particular, in NMMO/water, the composition for spinning cellulose was very narrow and solution temperatures between 70 and 110 ºC were required, which can degrade cellulose (Kim et al. 2006).

In order to improve fiber formation, yield and decrease fiber size, different approaches have been considered in the case of vegetal-derived cellulose. Some studies performed the electrospinning of cellulose derivatives such as cellulose acetate (Liu and Hsieh 2002; Liu and Tang 2007), with a subsequent conversion to cellulose fibers by a deacetylation process in the presence of NaOH. However, this process can lead to side reactions including incomplete conversion and degradation, may require extra purifications steps, as well as cause changes in the fibers surface and organization (Röder et al. 2001; Liu and Hsieh 2002; Kim et al. 2006). Other authors electrospun cellulose

derivatives mixed with co-spinning agents such as PEO (Frenot et al. 2007) while other studies focused on the effect of different processing parameters in the morphology and final characteristics (Liu and Hsieh 2002; Kulpinski 2005; Kim et al. 2005, 2006; Xu et al. 2008).

As with cellulose and bacterial cellulose, little attention has been paid to the processing of chitosan-cellulose and chitosan-bacterial cellulose blends. Recently, Lin et al. (2013) and Cao et al. (2016) reported the preparation of chitosan-bacterial cellulose and chitosan-cellulose composite membranes, by dipping neat bacterial cellulose and cellulose casting film membranes into chitosan solutions. Ostadhossein et al. (2015) reported the fabrication of chitosan/bacterial cellulose films by solvent casting. In all these studies, cytocompatibility and antibacterial activity against *Escherichia coli* and *Staphylococcus aureus* was reported.

Regarding the electrospinning of these blends, Park et al. (2011) investigated the electrospinning of chitosan-cellulose fibers by using an ionic liquid (1-ethyl-e-methylimidazolium acetate) as solvent. Despite the authors successfully produced fibers of micrometer size, these were not uniform and a low yield was obtained. In addition, electrospinning was difficult to control due to the high viscosity, high ionic strength and low volatility of the solvent, and a collecting bath was required to remove the solvent. To our knowledge, no other study has been reported on the electrospinning of chitosan-cellulose nor chitosan-bacterial cellulose blends. Processing of these materials via electrospinning could allow to control fiber size and porosity, which are important for wound dressing applications. In addition, the antibacterial properties can benefit from the nanostructure character of the nanofibers. On the other hand, bacterial cellulose has a higher purity and does not contain hemicellulose, lignin, pectin and other materials compared with cellulose from plants (Phisalaphong and Jatupaiboon 2008; Lin et al. 2013; Mohite and Patil 2014). Also, bacterial cellulose exhibit higher biocompatibility with tissues (Gama et al. 2012; Mohite and Patil 2014). These properties are in favor of the use of bacterial cellulose rather than cellulose from plants for biomedical applications, including wound healing.

The main objective of the present study is to develop antimicrobial chitosan/bacterial nanocellulose structures for potential wound dressing applications. To the best of our knowledge, this is the first time that the electrospinning of these blends is considered. This study is conducted through two different one step-electrospinning approaches: (i) simultaneous electrospinning of chitosan and bacterial nanocellulose through two separate solutions and syringes and (ii) concentric coaxial

electrospinning. In addition, the direct electrospinning of the basic materials is analyzed. The morphological details of the produced nanostructures, such as fiber diameter and distribution, porosity and content, are characterized by scanning electron microscopy (SEM), transmission electron microscopy (TEM) and energy-dispersive X-ray spectroscopy (EDS). Finally, the antimicrobial properties of the electrospun mats are investigated against a non-pathogen strain of *Escherichia coli*.

A.3 Experimental

A.3.1 Materials

Chitosan (CS) in powder form (95 % degree of deacetylation (DDA) and 57 kDa weight average molecular weight) was obtained from Primex (Iceland). Bacterial nanocellulose (BNC) in film form (16.6 ± 1.2 µm thickness) was provided by Axcelon Biopolymers Corporation (London, ON, Canada). Dimethylacetamide (DMAc) 99.5 % and lithium chloride (LiCl) were purchased from Anachemia Science and Fisher Scientific Company, respectively. Poly(ethylene oxide) (PEO) (powder form and viscosity average molecular weight of 600 kDa), glacial acetic acid, lactic acid (LA) solution (≥ 85% in volume) and glycerol were purchased from Sigma-Aldrich. Poly(lactide) (PLA, 4060D) was purchased from Nature Works LLC. All chemicals used in this study were of analytical grade and used without further purification.

Cultures of *Escherichia coli* (*E. coli* strain DH5α, non-pathogen) were obtained from the Laboratory of Microbiology, Infectiology and Immunology (Université de Montréal, Québec, Canada).

A.3.2 Methods

A.3.2.1 Solution preparation

CS at a concentration of 3 wt/v % was dissolved in 50 v/v % acetic acid under stirring during 24 h at room temperature. PEO - a co-spinning agent for CS - at a concentration of 3 wt/v % was dissolved in 50 v/v % acetic acid under stirring at room temperature overnight. The CS/PEO blend was obtained by mixing the respective CS and PEO solutions at an 80/20 (wt/wt) ratio. The resulting solution was homogenized during 2 h under stirring. For the dissolution of BNC, the

DMAc/LiCl system was used. BNC films were first cut manually -until obtaining pieces of few centimeters in size, approximately, and immersed with liquid nitrogen until complete evaporation of nitrogen (approximately 30 s). They were then cryogenically grinded in an IKA mill crushing A10 operated at 20 000 rpm. These steps were repeated approximately 5 times until obtaining flakes of millimeter size to facilitate dissolution. Then, a BNC solution was prepared by dissolving 0.6 wt/v % grinded BNC in a DMAc solution containing 3 wt/v % LiCl, under constant stirring during 2 h at 80 ºC to facilitate dissolution. The BNC solution was further mixed overnight at room temperature. The 0.6 wt/v % concentration was the maximum content of BNC that could be dissolved in this solvent system. PLA - a co-spinning agent for BNC - at a concentration of 10 (wt/v) % was dissolved in DMAc in the presence of 3 wt/v % LiCl under stirring for 2 days at room temperature. Then, BNC/PLA blends were prepared by mixing BNC and PLA solutions at different ratios (1:1 and 1:3 (v/v)). These solutions were homogenized during 2 h under stirring.

A.3.2.2 Electrospinning

Figure A.1 presents the direct electrospinning of the basic materials and the two approaches that were considered here for the production of chitosan/bacterial nano cellulose (CS/BNC) nanofibrous structures: parallel and coaxial electrospinning. Electrospinning was performed on a homemade horizontal setup containing a programmable micro-syringe pump (Harvard Apparatus, PHD 2000, USA) and a variable high DC voltage power supply (Gamma High Voltage Research, FL, USA). Polymer solutions were pumped through a syringe fitted with a metallic needle (details provided in respective sections below). Electrospinning of the different solutions was conducted over a wide range of electric field strengths (1-5 kV/cm), by varying the voltage (15-35 kV) and the distance between the needle tip and the grounded collector plate (5 to 15 cm), at different flow rates (0.1 to 1.5 mL/h), and solutions temperatures (22 and 60 ºC). All experiments were conducted in a chamber at a relative humidity of 20-30 % and under atmospheric pressure. Fibers were collected on aluminum foil attached to a stationary collector plate. Collected electrospun fibers were dried overnight under a chemical fume hood for the evaporation of any remaining solvent.

A.3.2.2.1 Electrospinning of basic materials (direct electrospinning)

First, the separate electrospinnability of BNC and CS/PEO blend was investigated. Then, the feasibility of electrospinning a blend containing both CS and BNC along with co-spinning agents was considered. BNC solution and BNC/PLA blends were directly electrospun through a 22-gauge

(i.d. 0.41 mm, o.d. 0.72 mm) at 0.3 mL/h and 3.0, and 2.3 kV/cm, respectively. Electrospinning of the CS/PEO blend was done using an 18-gauge needle size (i.d. 0.84 mm, o.d.1.27 mm) at 0.5 mL/h and 2.0 kV/cm.

A.3.2.2.2 Parallel electrospinning

This approach was considered to produce mats containing both chitosan and bacterial nanocellulose intertwined respective fibers. CS/PEO and BNC solutions, and CS/PEO and BNC/PLA (1:3) solutions were electrospun simultaneously towards the same target from two different needles to produce random mixing of converging jets of the two separate solutions. The needle size and the flow rate in electrospinning were the same as those employed in the direct electrospinning of each individual solution. Two different microsyringe pumps were required in this approach and an electric field of 3.0 kV/cm was applied for both solutions.

A.3.2.2.3 Coaxial electrospinning

This method was considered to produce chitosan/bacterial nanocellulose mats containing both components in each individual fiber, but in separate layers instead than in a blend. CS/PEO blend and BNC solution were electrospun through a coaxial spinneret comprised of an inner 21-gauge needle (i.d. 0.51 mm, o.d. 0.83 mm) concentrically mounted on an outer 15-gauge needle (i.d. 1.37 mm, o.d. 1.83 mm) to produce core-shell structures. Core and shell solutions were electrospun at 0.5 mL/h and 0.3 mL/h, respectively and at 2.3 kV/cm. The core solution had to be electrospun at a higher flow rate than the shell one in order to get a stable process of fiber formation. CS/PEO and BNC solutions were alternated between core and shell to evaluate their processability and resulting morphology.

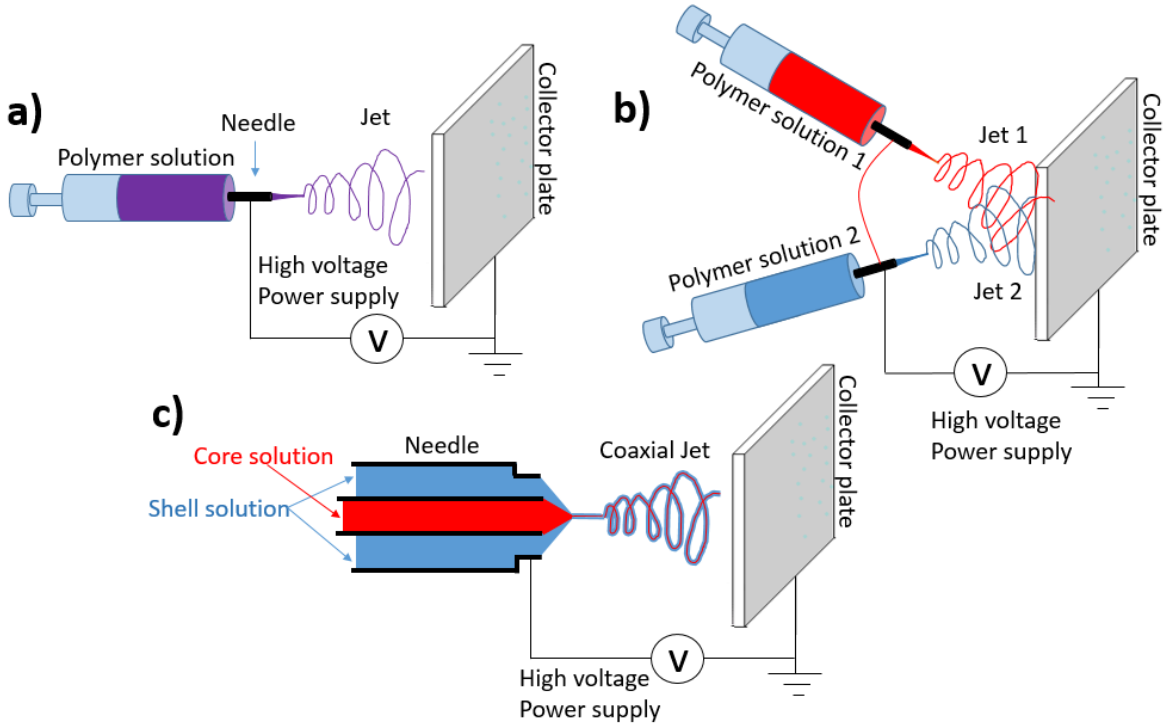

Figure A.1: Different approaches used in this work for the production of nanofibrous structures: a) direct spinning of the basic materials, b) parallel and c) coaxial electrospinning set up.

A.3.2.3 Characterization

The surface morphology of the electrospun fibers was observed by scanning electron microscopy, (SEM, JEOL JSM-7600TFE field emission gamma) operated at 2 kV. Electrospun fiber diameters and their distribution were analyzed using the Image-Pro Plus software ® by taking an average of 300 fibers. The analysis of mat composition was performed in the same SEM equipment under energy-dispersive X-ray spectroscopy (EDS) mode operated at 10 kV. The morphological and compositional characterization of the core-shell structure was performed on a transmission electron microscope (TEM, JEOL JEM-2100F) operated at 200 kV. In this case, fibers were directly collected onto a standard TEM copper grid coated with an amorphous carbon film.

Prepared electrospun CS/PEO/BNC mats were submerged in an aqueous solution of 50 % (v/v) acetic acid for 10 minutes in order to remove the PEO and chitosan and quantify the BNC content. The extracted mats were then dried at room temperature overnight to remove the remaining solvent and then characterized by SEM.

The rheological properties of the CS/PEO and BNC solutions were measured in a controlled stress rheometer (MCR-502, Anton Paar, Germany) equipped with a double Couette flow geometry. Strain, frequency sweep and simple shear flow tests were conducted. Strain sweep tests were carried out from 0.0001 to 1 at frequencies of 0.628 and 62.8 rad/s at 25 ºC for the determination of the linear viscoelastic (LVE) region. A strain of 0.05 was determined to be in the LVE regime for both polymeric solutions. Frequency sweep tests were carried out from 0.5 to 500 rad/s at 0.05 strain amplitude and 25 ºC. Steady state flow tests were performed from 0.1 to 500 s^{-1} at 25 ºC. Tests were done in duplicate. Surface tension measurements of CS/PEO and BNC solutions were performed in a dynamic contact angle meter and tensiometer (DCAT11, Future Digital Scientific Co, Long Island High-Tech, USA) equipped with a Wilhelmy plate as a test piece (sensor). Tests were done in triplicate. The conductivity of the solutions was measured with a conductimeter Inolab ® Cond 750 (WTH GMbH, Germany). Measurements were done in triplicate.

The antibacterial properties of the nanofibers were evaluated by using a non-pathogen *E. coli* (DH5α) strain as a model bacterium. Bacteria were grown in a nutritional-rich medium (Luria Bertani or LB broth) under constant agitation for 24 h at 37 ºC, in order to reach a density of 10^9 Colony Forming Units (CFU)/mL. After 24 h, the bacteria culture was diluted in a phosphate buffered saline (PBS, pH 5.8) solution, in order to reach a density of 10^6 CFU/mL. Mats of 25 x 25 mm^2 area were prepared and immersed (after sterilization under UV light for 20 min) into culture tubes containing 5 mL of the PBS inoculated with *E. coli*. Subsequently, tubes were incubated at 37 °C for 4 h in an orbital incubator shaker (New Brunswick). Dilutions of the inoculated suspensions were prepared and deposited on LB agar plates and incubated overnight at 37 °C for the counting of the surviving bacteria (CFU/mL). CS/PEO fiber mats and bacterial nanocellulose in film form, with the same surface area, were used as positive and negative controls, respectively. Experiments were carried out in triplicate.

A.4 Results and discussion

A.4.1 Electrospinning of basic materials

Figure A.2a presents the SEM micrograph for the native BNC film and Figure A.2b-f, the SEM images from direct electrospinning of different solutions containing either CS or BNC. Figure A.3 presents their fiber size distribution. The best conditions for the continuous processing of the fibers

were a range of voltage between 25 to 35 kV, a distance between the needle tip and the collector plate of 7 to 15 cm and a flow rate of 0.3 and 0.5 mL/h for the solutions containing BNC and CS, respectively. Such low flow rates were required to allow the complete evaporation of the solvent, have a stable processing and avoid the agglomeration of fibers after arriving on the collector plate. The specific electrospinning parameters for each solution are given in the label of Figure A.2.

Figures A.2b and A.3a show that beaded-free nanofibers with an average diameter of 44 nm were obtained from the CS/PEO 80/20 solution. According to Pakravan et al. (Pakravan et al. 2011), blending chitosan with a co-spinning agent such as PEO is necessary to facilitate its processing and make it electrospinnable.

Figure A.2c shows that at first sight BNC is electrospinnable. Nonetheless, a very small yield, large fiber size (3.0 µm) and some instabilities in the processing were observed. The electrospun fibers were formed at the tip of the needle but remained straight in the electric field without arriving to the collector plate. This phenomenon was previously reported by Frenot et al. (2007) for solutions containing enzymatically treated cellulose in the same solvent system. They suggested that this behavior is related to salt, mainly the Li^+ and Cl^- ions present in the formed fibers, in which the high charge density may cause an overall positive charge on the fibers that forces them to remain straight in the negative field. The processing of the BNC solution at 60 ºC did not improve fiber formation nor their collection. Hence, in order to improve processing and yield, BNC was blended with an electrospinnable material which could be dissolved in the same solvent system (DMAc/LiCl), in this case PLA.

Figure A.2d reveals that at a BNC/PLA blend ratio of 1:1, fibers merged into forming a film-like structure that resembles the native BNC film, as previously observed in Figure A.2a. By increasing the blend ratio to 1:3 (Figure A.2e), fiber formation and collection was notably improved and nanofibers of 220 nm in average diameter were obtained, as shown in Figure A.3b. Furthermore, better structure and yield were observed by increasing the blend ratio to 1:5 and the electrospinning temperature to 60 ºC, as presented in Figure A.2f. In this case, nanofibers with an average diameter of 42 nm were obtained, as shown in Figure A.3c. However, despite the improvement in fiber collection and processability, the blending with PLA yielded an overall low BNC content.

On the other hand, the direct electrospinning of blends containing BNC and CS/PEO solution was not possible mostly because of the incompatibility of the solvents. A phase separation was notably

observed as soon as the two solutions were put in contact. The addition of other components was also examined but without promising results regarding processing, yield and morphology. Hence, the other two approaches, parallel and coaxial electrospinning were considered for the production of mats containing both chitosan and bacterial nanocellulose.

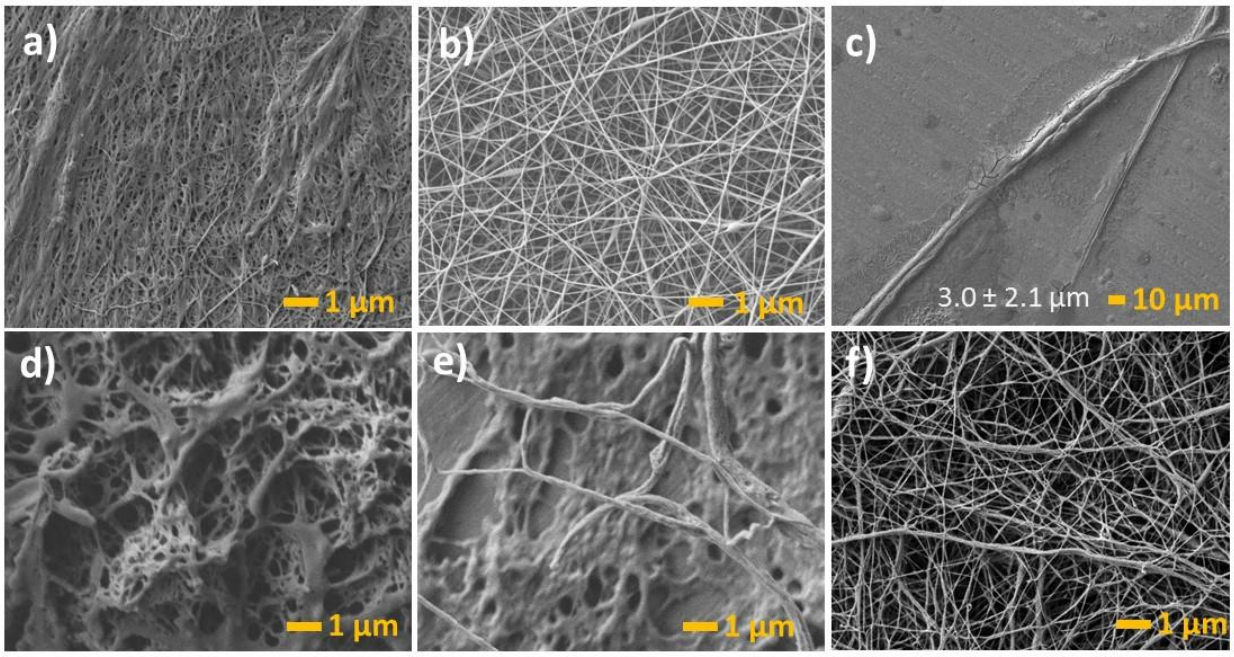

Figure A.2: SEM micrographs and their size distribution: a) BNC in film form; and mats obtained from direct electrospinning of: b) CS/PEO @ 0.5 mL/h and 2.0 kV/cm; c) BNC @ 0.3 mL/h and 3.0 kV/cm; d) BNC/PLA (1:1) @ 0.3 mL/h and 2.3 kV/cm; e) BNC/PLA (1:3) @ 0.3 mL/h and 2.3 kV/cm and f) BNC/PLA (1:5) @ 0.3 mL/h, 2.3 kV/cm and 60 ºC.

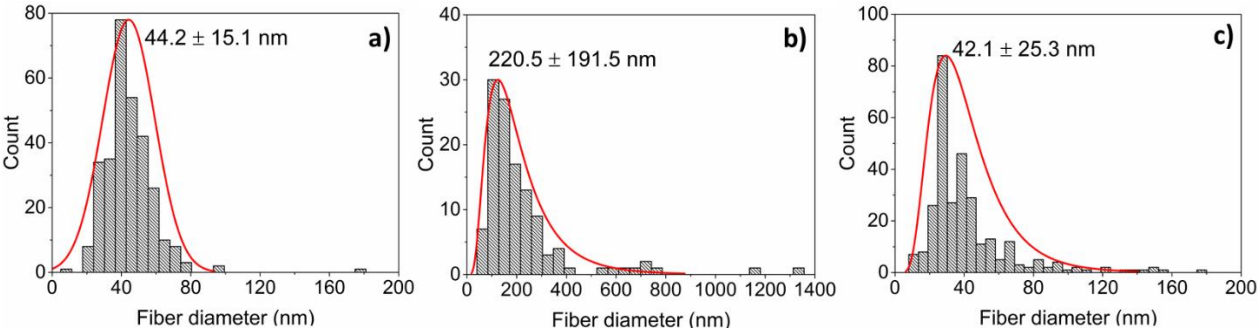

Figure A.3: Fiber size distribution of the mats from Figure A.2: a) CS/PEO @ 0.5 mL/h and 2.0 kV/cm; b) BNC/PLA (1:3) @ 0.3 mL/h and 2.3 kV/cm; and c) BNC/PLA (1:5) @ 0.3 mL/h, 2.3 kV/cm and 60 ºC.

A.4.2 Parallel electrospinning

In order to obtain mats containing both CS and BNC, and considering that the electrospinning of a blend containing both CS and BNC was not successful, the electrospinning of separate solutions converging towards the same target was considered. The goal was to produce randomly mixed individual fibers of chitosan and bacterial nanocellulose.

Figure A.4 shows the CS/BNC mats obtained from the simultaneous electrospinning of CS/PEO with BNC or with BNC/PLA (1:3) solutions, at 22 and 60 ºC. EDS analysis of the mats is presented in Figure A.5.

Regarding the mats containing CS/PEO and BNC fibers, Figure A.4a reveals that CS/PEO fibers were certainly present, as known from the good spinnability of this system, whilst BNC fibers could not be clearly identified, as they were in Figure A.2c. As shown, nanofibers had a diameter of 41 nm in average, which is close to the one of CS/PEO fibers alone (Figure A.3a). This indicates that the higher yield and flow rate at which the CS/PEO solution was electrospun might have hidden the few fibers from BNC (Figure A.2c).

By contrast, two types of fibers could be clearly identified in the SEM image of Figure A.4b, which correspond to CS/PEO and BNC/PLA fibers. The thicker fibers are most probably from the latter blend. In average, the nanofibers had a diameter of 63 nm, which lies between the one of CS/PEO fibers (44 nm, Figure A.3a) and BNC/PLA fibers (220 nm, Figure A.3b), when electrospun individually. This result tended to indicate the presence of the two types of fibers.

Not surprisingly, when the temperature of the BNC/PLA solution was increased to 60 ºC as shown in Figure A.4c, fibers looked more homogeneous and the average nanofibers diameter was reduced to 46 nm.

In order to verify the presence of BNC in the mats of Figure A.4, chlorine (Cl) was subjected to detection by EDS analysis, since it was in salt form in the BNC solution. It was assumed that the presence of Cl (salt) implied the presence of BNC in the mats, as reported by other authors for vegetal cellulose in the same solvent system (Kim et al. 2005, 2006). EDS spectrum in Figure A.5a indicates that in the case of CS/PEO fibers, elements such as carbon and oxygen were detected, which belong to chitosan, PEO and cellulose. In addition, fluoride and silicon were detected. They may originate from the dry film lube (Fluorocarbon) aerosol that was applied on the aluminum foil

for this particular sample, to easily detach the CS/PEO mats. Besides these, aluminum was also detected, which was mainly due to the foil used to collect the mats. No Cl whatsoever was detected. By contrast, Figure A.5b, c show that, in addition to C and O, Cl was detected in the mats containing BNC, even in small quantities, which further suggest that both CS and BNC were present in the mats. The low chlorine content detection was in accordance to the low flow rate at which the solutions containing BNC were electrospun, with respect to the one containing CS. Experimentally, the stability in the processing of BNC solution was only achieved at a flow rate of 0.3 mL/h, whilst that solution containing CS could be processed at a higher flow rate of 0.5 mL/h. In addition, a low ratio of BNC in the BNC/PLA blend, could also contribute to the low amount of Cl detection.

However, even though mats containing both CS and BNC were successfully obtained, the BNC content in the mats was low (less than 0.6 wt/v % in the case of BNC and 0.2 wt/v % in the BNC/PLA blend) when compared with CS (2.4 wt/v %). This corresponds to 6 to 20 times higher content of CS with respect to BNC, when taking into account the flow rates at which the solutions were processed. This was clearly considered insufficient to take advantage of the BNC properties, and therefore a second approach – coaxial electrospinning – was considered to increase yield and BNC content.

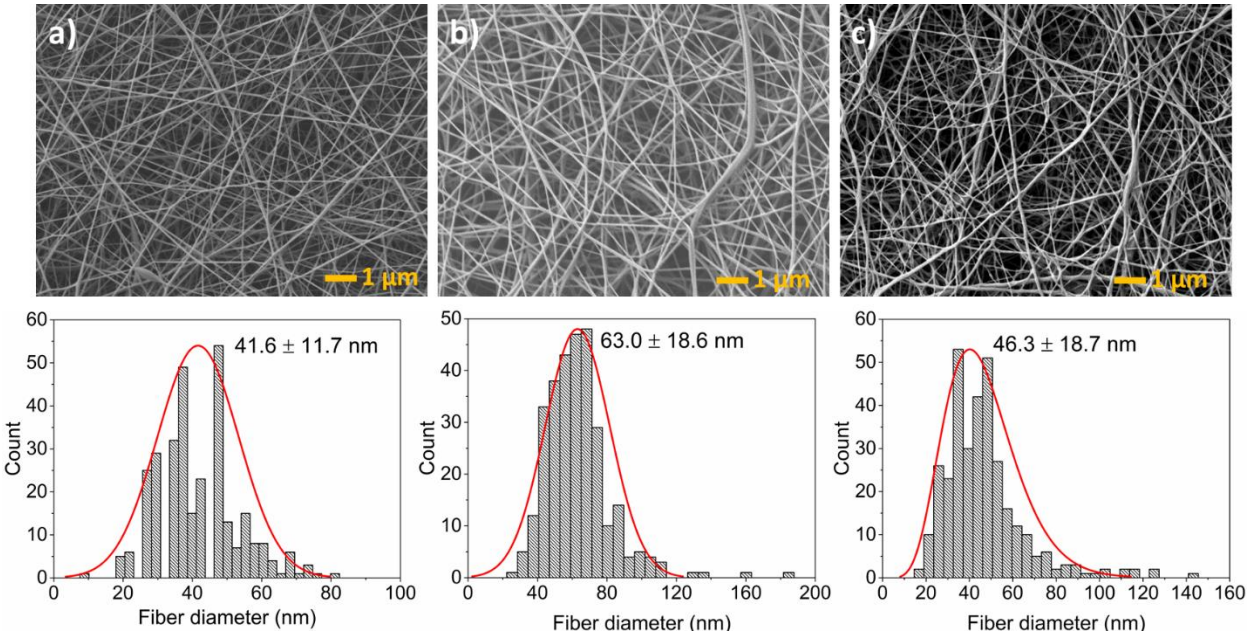

Figure A.4: CS/BNC structures from parallel electrospinning and their fiber size distribution. Randomly mixed fibers of: a) CS/PEO and BNC (22 °C); b) CS/PEO and BNC/PLA (22 °C); c)

CS/PEO and BNC/PLA (60 ºC). CS/PEO was electrospun@ 0.5 mL/h and 3.0 kV/cm whilst BNC and BNC/PLA blends @ 0.3 mL/h and 3.0 kV/cm.

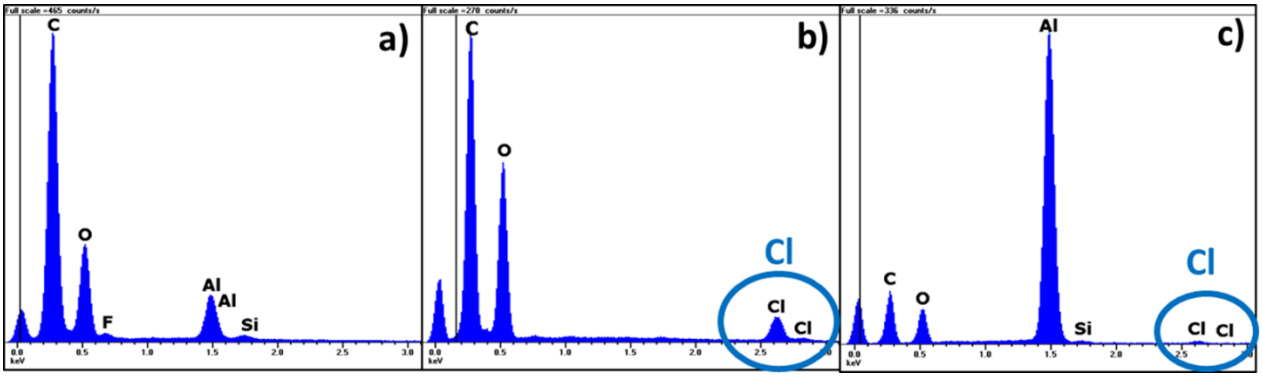

Figure A.5: EDS analysis of the electrospun mats: a) CS/PEO; b) CS/PEO and BNC; c) CS/PEO and BNC/PLA. Sample a) was electrospun directly whilst samples b) and c) represent the randomly mixed fibers from the parallel electrospinning.

A.4.3 Coaxial electrospinning

Figure A.6 presents the SEM micrographs and the size distribution when CS/PEO and BNC solutions were electrospun coaxially. According to the results, nonwoven mats containing CS, PEO and BNC with different structures were obtained, depending on the position of the core and shell solutions. CS/BNC beaded-fibers were obtained when the BNC solution was in the core and the CS/PEO was in the shell, as shown in Figure A.6a. Fibers and beads presented a diameter of 31 and 187 nm in average, respectively. In addition to beads, some agglomerates were also observed. Similar results were obtained when varying the flow rates of the solutions (0.8 mL/h in the core and 0.5 mL/h in the shell; and 0.3 mL in the core and 0.5 mL/h in the shell). By contrast, uniform bead-free fibers were observed when the core and shell solutions were interchanged (CS/PEO in the core and BNC in the shell), as observed in Figure A.6b. In this case, fibers presented a larger diameter of 85 nm in average. Structural and dimensional differences in the obtained mats indicated that the position of the inner and outer solutions affected significantly the morphology.

In order to elucidate the importance of using a spinnable solution as a carrier and to explain the differences in the morphology obtained, the properties of the solutions (namely viscosity, surface tension and conductivity) were examined.

First, when CS/PEO is in the core, a single jet might be elongated and maintained, given the own electrospinnability of this solution as discussed before. Hence, CS/PEO can serve as a carrier for the processing of BNC, which is hardly spinnable by itself. On the contrary, when CS/PEO is in the shell, BNC solution by itself might not maintain the jet, leading to instabilities in the processing, reflected by beaded-fibers and some agglomerates. Consequently, it is inferred that a carrier solution must be used in the core (CS/PEO) to drive the jet for an efficient pull out of the solution, and consequently lead to fiber formation.

Second, the rheological properties, surface tension and conductivity of the CS/PEO and BNC solutions may explain furthermore the differences in the morphology obtained. Figure A.7 presents the viscosity of the solutions as a function of shear rate. CS/PEO behaves as a Newtonian fluid whilst BNC solution exhibits a markedly shear thinning behavior along the range of shear rates tested. A shear thinning behavior of the polymer solution can be interpreted as a result of a reduction in entanglement density, or de-structuration due to shear. Hence, the CS/PEO solution could maintain the entanglements under shear, unlike BNC, which could have allowed a better stability in the electrospun jet when the former solution was in the core. Figure A.8 presents the complex viscosity and the damping factor (tan delta) of the solutions as a function of the angular frequency. The damping factor is a solution property that can be taken as a measurement of the viscoelastic properties of the solutions, which are important for explaining fiber formation. According to the results for complex viscosity, CS/PEO and BNC solutions behave as Newtonian and shear thinning fluids, respectively, in the angular frequency range tested, as already observed in simple shear. On the other hand, Figure A.8 also shows that CS/PEO solution behaves as a viscoelastic fluid whilst BNC presents a gel-like behavior. Hence, when CS/PEO was in the core, the viscoelastic properties could have led to a higher stability of the jet since this solution could be stretched more easily, whilst maintaining entanglements. According to Dror et al. (2007), viscoelastic polymer solutions should be used in the core for a stable coaxial process. On the contrary, when BNC was in the core, it is assumed that the significant reduction in entanglement density with shear could have promoted instabilities in the co-electrospun jet. Further on, the gel-like behavior could have contributed to more instabilities as the hydrogen bonding present in the gel can be easily broken.

Table A.1 presents the viscosity, conductivity and surface tension of CS/PEO and BNC solutions. The viscosity values were evaluated at the shear rate encountered at the needle wall (maximum

shear rate) in coaxial electrospinning. The latter was calculated based on the dimensions of the coaxial geometry and the processing flow rate, as explained by Pakravan et al. (2012). The calculated shear rates were 0.3, 1.5 and 10.7 s^{-1}, on the wall of the outer needle, annulus and inner needle, respectively. These values are illustrated by dotted lines in Figure A.7. The obtained viscosities for the CS/PEO and BNC solutions allowed to infer that a higher viscosity in the shell was required for the process stability and coaxial fiber formation. Therefore, when CS/PEO was in the core and BNC in the shell, the higher viscosity of the BNC allowed to hold the CS/PEO and to form a sheath around the core fluid by containing the latter and forming the core-shell structure. According to Yarin (2011), viscous tractions are responsible for the formation of coaxial jets and allow the entrainment of the core solution. This happens when the outer solution has a higher viscosity than the inner. Conversely, the higher viscosity of BNC when it was in the core may have caused the breakup of the jet, as demonstrated by the presence of beaded-fibers. To sum up, it is believed that in the coaxial setup, the CS/PEO solution serves as a carrier to successfully buildup the nanofibers, and the higher viscosity of the BNC solution promotes the stability and formation of the core/shell fibers.

Finally, it is hypothesized that a lower surface tension of the core solution (CS/PEO) with respect to the shell (BNC) enables the formation of a stable Taylor cone, and favors the entrainment of the core into the shell. On the contrary, a higher surface tension of the core solution would allow instabilities, as the ones observed in the present study. Regarding the conductivity, Yu et al. (2004) speculated that higher conductivity of the core solution, and therefore a higher charge density, could lead to a higher pulling of the core solution by the electric field at a higher rate than the supply of the feed line, leading to instabilities in the co-electrospinning process. Consequently, beaded fibers will be obtained, as the ones observed when the BNC was in the core, as a result of the high conductivity and surface tension with respect to the CS/PEO solution.

In order to corroborate the formation of the core-shell structure, TEM, EDS analysis and a treatment with acetic acid (in order to remove chitosan and PEO), were performed on the CS/PEO-BNC mats.

Figure A.9 shows the TEM and the EDS analysis of the CS/PEO-BNC mats. TEM imaging allowed to identify two regions: the inner one from the CS/PEO solution and the outer one corresponding to BNC. EDS analysis by SEM observation showed that peaks of C, N, O, Cu, Zn, Si and Cl were

detected in both core and shell. In particular, Cu detection was linked to the TEM grid, whilst the detection of N and Cl suggested the presence of CS and BNC, respectively, in the coaxial structure. The EDS analysis by TEM (not shown) also revealed the presence of Cl in both core and shell, and both in fibers and beads. Hence, results suggested that CS and BNC had no preferable location in the core or shell, even though they were deposited in respective positions.

Figure A.10 presents the CS/PEO/BNC mats after treatment with 50 % (v/v) acetic acid solution. The acid treatment was done to remove both CS and PEO, and to analyze the remaining structure. As a result of the extraction, the nonwoven mat structure collapsed and fibers were completely disintegrated, regardless if CS/PEO was in the core (Figure A.10a) or in the shell (Figure A.10b). Nonetheless, when in the shell, two different kind of remaining structures were observed. A nano porous film-like co-continuous structure (Figure A.10b-1) with pore size of the same order of magnitude than the beads observed previously in Figure A.6a; and a structure with larger pore sizes (Figure A.10b-2), maybe as a result of the removal of possible agglomerates. Accordingly, results from acid treatment confirmed that both CS and BNC were present in both core and shell, as previously stated from the EDS analysis.

To sum up, nanofibers with high yield and good fiber structure containing both CS and BNC were obtained when CS/PEO and BNC solutions were electrospun in the core and shell, respectively. Given the fact that PEO is an easily electrospinnable polymer, it is believed that the CS/PEO solution serves as a spinning carrier during the process. Oppositely to the parallel electrospinning approach, coaxial electrospinning allowed to a higher yield, a more homogeneous fiber structure and a higher BNC content (0.6 wt/v % in comparison with 0.2 wt/v% when blended with PLA) in the final mats, since this solution could be processed without addition of PLA. Furthermore, removal of PEO by water treatment would result in a neat CS/BNC porous mat.

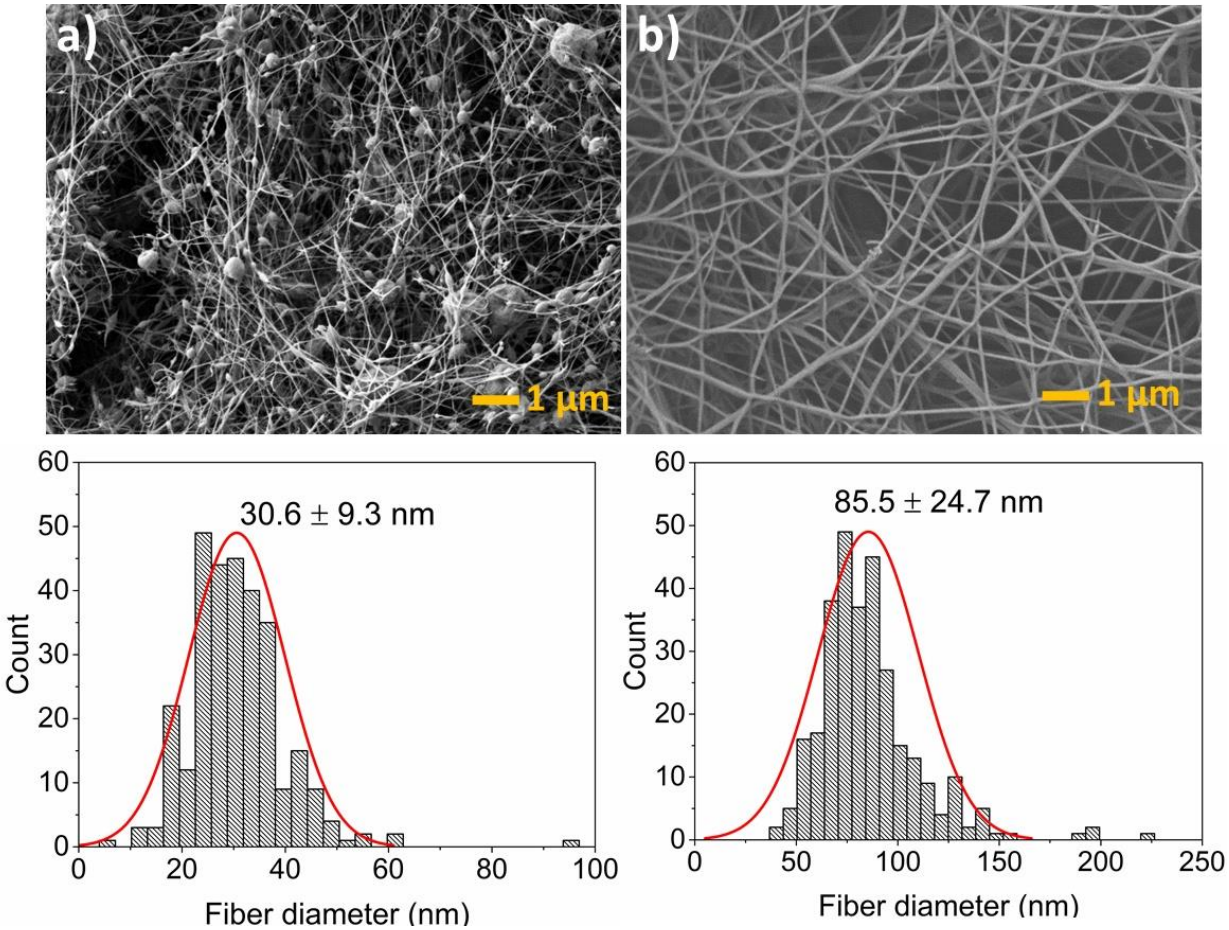

Figure A.6: CS/PEO-BNC core-shell structures: a) CS/PEO in the shell and BNC in the core; b) CS/PEO in the core and BNC in the shell. Core @ 0.5 mL/h, shell @ 0.3 mL/h and 2.3 kV/cm.

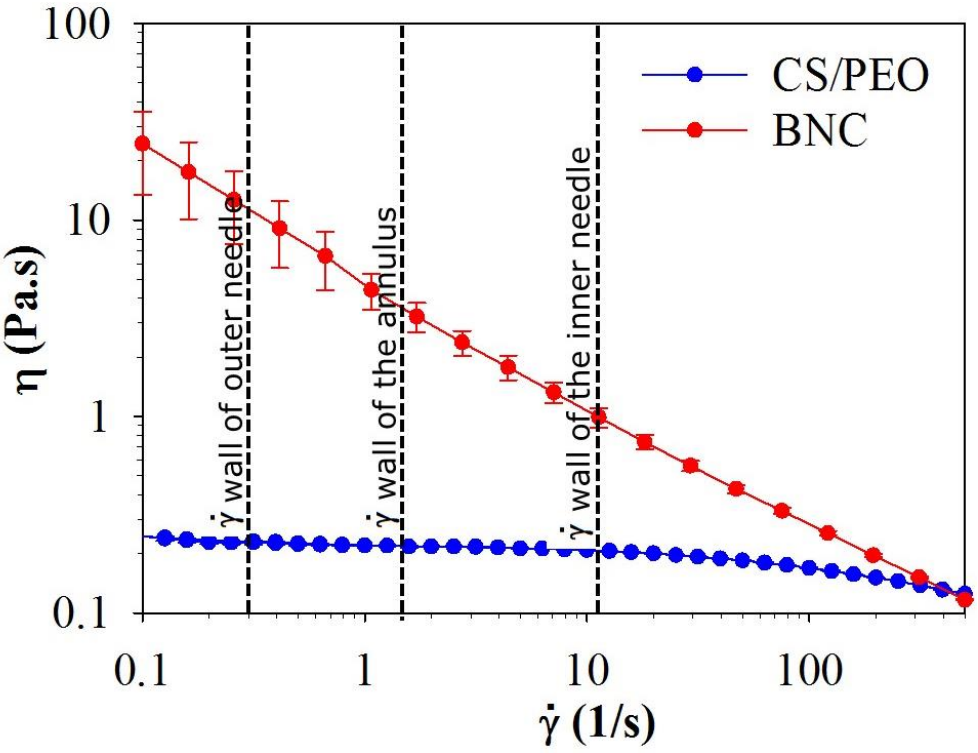

Figure A.7: Viscosity vs. shear rate for CS/PEO and BNC solutions.

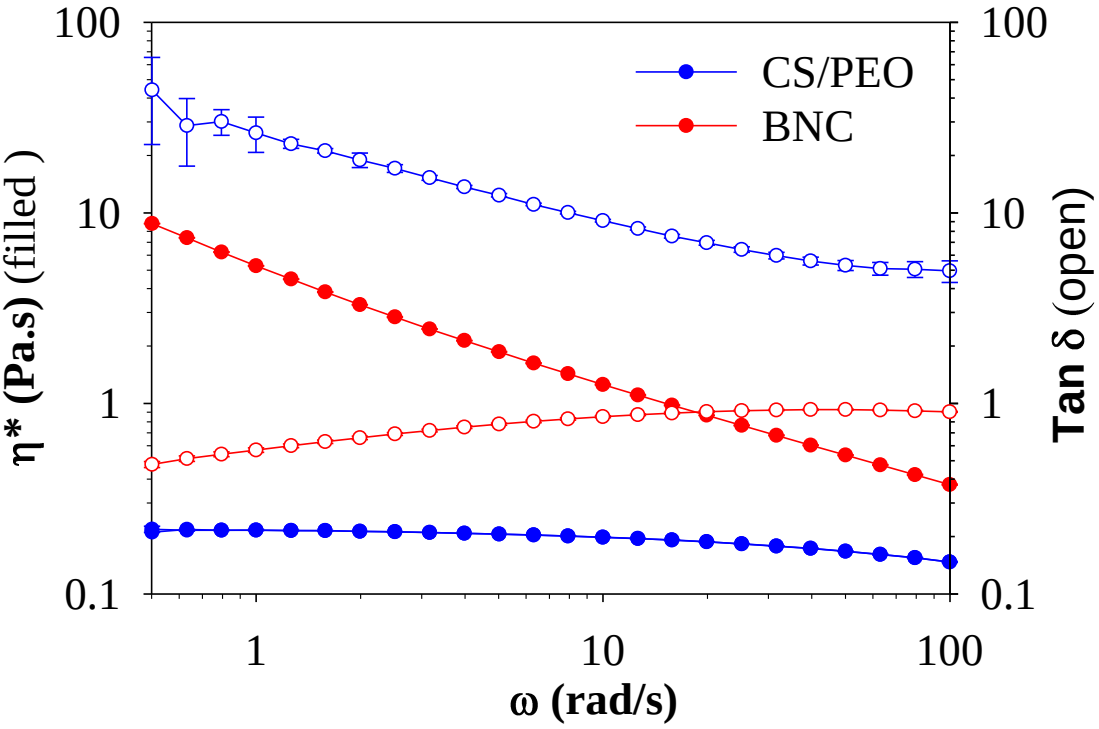

Figure A.8: Viscoelastic properties of the CS/PEO and BNC solutions: Complex viscosity vs. frequency and tan delta vs. frequency.

Table A.1: Properties of the electrospun solutions

Solution	**Shear viscosity** [Pa s]		**Conductivity** [µS cm^{-1}]	**Surface tension** [mN m^{-1}]
	core	shell		
CS/PEO	0.2	0.2	1605 ± 10	35.9 ± 0.4
BNC	1.3	3.4-13	5027± 41	43.2 ± 0.1

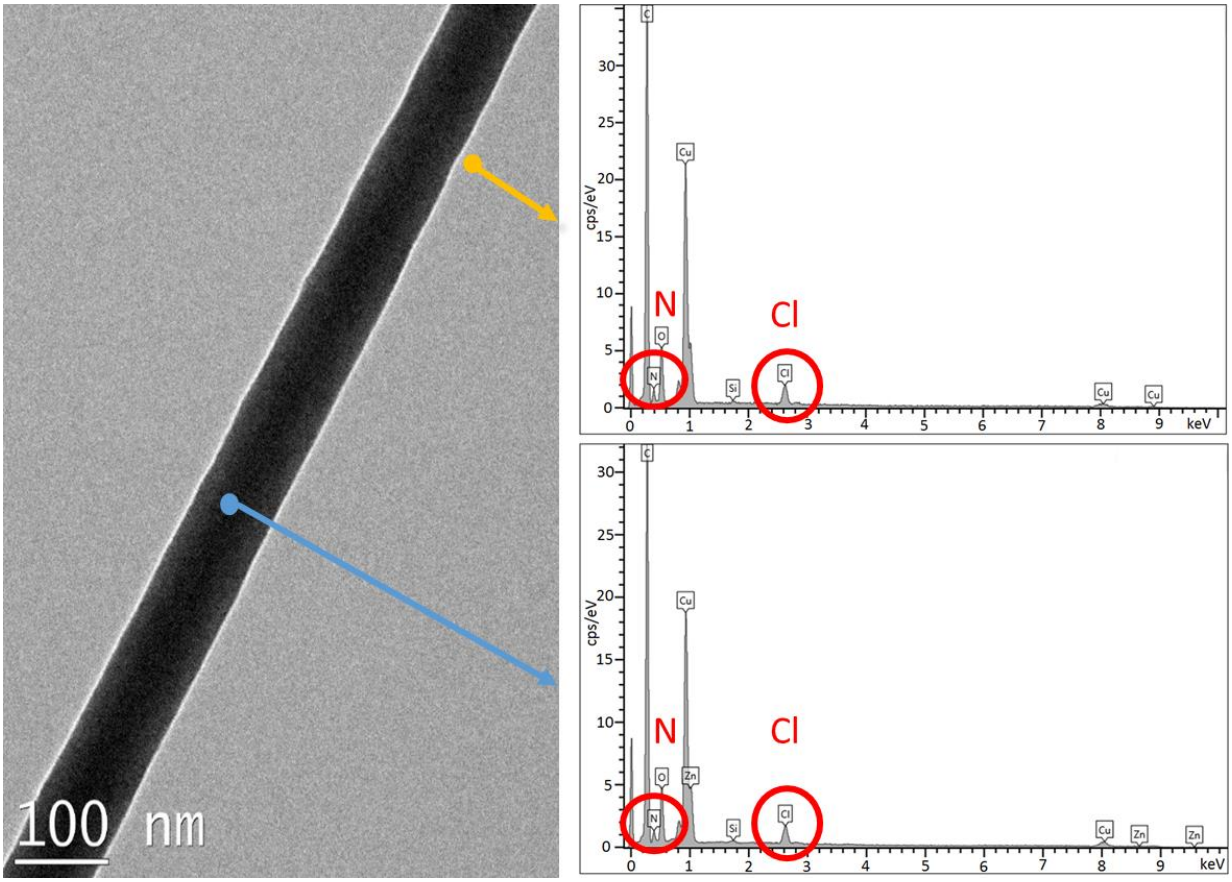

Figure A.9: TEM and EDS analysis (by SEM) of the CS/PEO-BNC core-shell structure. Sample was analyzed from a TEM copper grid support.

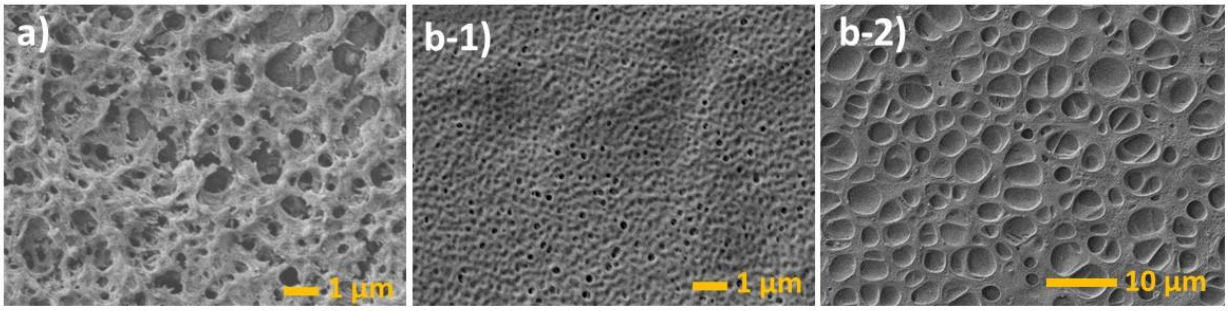

Figure A.10: SEM image of CS/PEO-BNC mats after treatment with 50% acetic acid solution: a) CS/PEO in the core, BNC in the shell; and b) CS/PEO in the shell, BNC in the core (different magnifications).

A.4.4 Antibacterial properties

Figure A.11 reports the antibacterial properties of the BNC film (as received) in comparison with CS/PEO nanofibers and CS/PEO/BNC structures obtained from the parallel and coaxial electrospinning approaches. According to the results, the BNC film did not exhibit antibacterial properties by itself and instead, an increase in bacterial population was observed with respect to the control. This may be the result of a nutrient effect since for obtaining BNC, bacteria require glucose, fructose, mannitol, among other sources of carbon as substrate (Horii 2000; Mohite and Patil 2014). On the contrary, CS/PEO nanofibers displayed a high antibacterial activity and a decrease of 100% bacterial density was achieved.

The antibacterial properties of the BNC were notably increased when CS was incorporated: the randomly-mixed CS/PEO and BNC fibers obtained by the parallel processing reduced bacterial density by about 2 log (CFU/mL) whilst the CS/PEO/BNC fibers obtained by the coaxial processing reduced it by 4 log (CFU/mL), regardless if chitosan was added in the core or in the shell. This reduction indicated that the core/shell structures were more effective than the mixed fibers from the parallel process, even if chitosan was initially in the core solution. Contrary to our finding, a higher activity was expected from the mixed fibers, and at least of the same order of magnitude than when chitosan was in the shell in the coaxial fibers, given the fact that more amino groups can be exposed to contact with bacterial surface. The lower activity observed in the mats from the parallel process may be explained by a lower chitosan content in the selected mats for the antibacterial tests (about half of the chitosan concentration with respect to the one in the coaxial

approach, even when the same volume was electrospun). This most probably results from the difficulty in converging the CS/PEO and BNC fibers to the same area on the collector plate, besides a possible repulsion between charged jets (Greiner and Wendorff 2007).

On the other hand, the similar and high antibacterial activity displayed in the coaxial fibers indicated that chitosan was equally effective either if it was initially in the core or in the shell. This confirms that the coaxial fibers containing chitosan in the core may be discontinuous and form an intermittent core/shell structure, with intermixed layers.

The antibacterial activity of chitosan is the result of the ionic interactions between the positively charged amino groups and the negatively charged bacteria surface, leading to loss of membrane permeability, cell leakage and death (Kong et al. 2010). Simple visual inspection of the CS/PEO and CS/PEO-BNC nanofiber mats, before and after the antibacterial tests, suggests that fibers are stable at pH 5.8. However, as nanofibers contain PEO, which is soluble in water, certain solubility of PEO is expected. In addition, chitosan may solubilize partially, given that the pH of the medium (5.8) is lower than chitosan pKa (6.2-6.5). Consequently, both released chitosan in the medium and the one remaining in the nanofiber mats may contribute to the antibacterial effect.

Regarding the mechanism of antibacterial action of the CS/PEO-BNC nanofibers, it is suggested that the protonation of chitosan amino groups at the nanofiber surface are the ones conferring the antibacterial activity. The nanofiber structure allows for a greater interaction with bacterial cell wall. In addition, it is believed that nanofiber mats may serve as physical support favoring the interaction and adsorption of bacteria.

In this work, we have demonstrated the antibacterial activity of chitosan/bacterial cellulose fiber mats produced by parallel and coaxial electrospinning. Further research should be addressed in terms of biocompatibility, regenerative properties, water holding capacity and mechanical properties of the fiber mats. Regenerated cellulose in BNC/PLA and CS/PEO-BNC nanofibers can exhibit different properties than native BNC, including crystallinity. For instance, native cellulose from plants and bacterial cellulose present generally a crystalline structure Type-I, but, solubilization and processing conditions may cause recrystallization, and transform into Type-II (Kim et al. 2005, 2006; Shanshan et al. 2012; Ostadhossein, 2015). Crystallinity can also significantly decrease after processing. Kim et al. (2005, 2006) found that cellulose fibers obtained from DMAc/LiCl were mostly amorphous, while Shanshan et al. (2012) reported a decrease in the

crystallinity (from 79 to 38%) of regenerated bacterial cellulose films using NMMO as solvent, with respect to neat bacterial cellulose. Therefore, possible differences between native BNC and regenerated one prepared by electrospinning, as well as their impact in the aforementioned properties (biocompatibility, regenerative properties, water holding capacity and mechanical properties), which are critical for wound dressing applications, should be considered in the future.

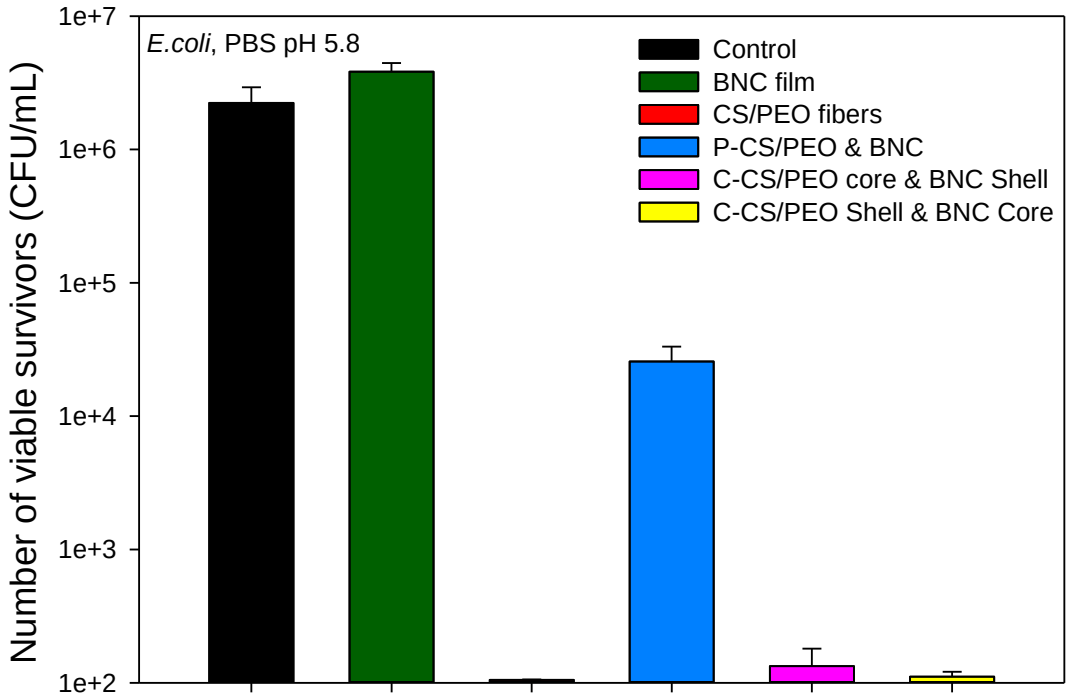

Figure A.11: Inhibitory effects of different CS/PEO/BNC structures toward *E. coli*. P-parallel and C-coaxial electrospinning. The pH of the PBS solution was adjusted to 5.8 in order to protonate chitosan and activate its antibacterial activity

A.5 Conclusions

In this work we demonstrated that nanometer sized nonwoven mats containing CS and BNC could be successfully obtained in a one-step electrospinning process, either through parallel or coaxial approaches. The direct electrospinning of blends containing both BNC and CS was not possible, most probably because of the incompatibility of their respective solvents.

Although the parallel electrospinning approach showed that mats containing both CS and BNC were successfully obtained, the BNC content was low (less than 0.6 wt/v % in the case of BNC and 0.2 wt/v % in the BNC/PLA blend, in comparison with 2.4 wt/v % CS). This corresponds to 6 to

20 times higher content of CS with respect to BNC, when taking into account the flow rates at which the solutions were processed.

The coaxial electrospinning approach showed the best results for the production of fibers containing CS and BNC. A good yield and fiber formation was obtained by using the CS/PEO blend in the core as a carrier. BNC content was also improved since this solution could be processed without blending with PLA, as was required in the parallel approach.

The addition of CS to BNC provided good antibacterial properties. The CS/BNC mats reduced *E. coli* bacterial density by more than 99 %. These novel nanofibers have interesting potential applications in the biomedical field for wound healing dressing.

A.6 Acknowledgements

The authors thank the Fonds de Recherche du Québec-Nature et Technologies (FRQNT) and the Natural Sciences and Engineering Research Council of Canada (NSERC) for their financial support of this work. The authors would like also to acknowledge Prof. France Daigle from the Department of Microbiology, Infectiology and Immunology, Université de Montréal for her training and support in the antibacterial tests. Finally, the authors thank the reviewers of Cellulose for their valuable comments to improve this manuscript.

A.7 References

Ahn Y, Lee SH, Kim HJ, Yang YH, Hong JH, Kim YH, Kim H (2012) Electrospinning of lignocellulosic biomass using ionic liquid. Carbohydr Polym 88:395-398

Basmaji P, de Olyveira G, Manzine Costa L, Francozo G, da Costa Oliveira J (2015) Nanoderm Extracellular Matrix for Reconstructive Surgery Applications. Peertechz J Biomed Eng 1:021-024

Bhattarai N, Edmondson D, Veiseh O, Matsen FA, Zhang M (2005) Electrospun chitosan-based nanofibers and their cellular compatibility. Biomaterials 26:6176-6184

Cao Z, Xiaogang L, Hao Z, Zhen F, Zhi S, Ning C, Yanan X, Faquan Y (2016) A facile and green strategy for the preparation of porous chitosan-coated cellulose composite membranes for potential applications as wound dressing. Cellulose 23:1349-1361

Costa LMM, de Olyveira GM, Basmaji P, Xavier Filho L (2012) Nanopores structure in electrospun bacterial cellulose. J Biomater Nanobiotechnol 3:92

Desai K, Kit K, Li J, Zivanovic S (2008) Morphological and surface properties of electrospun chitosan nanofibers. Biomacromolecules 9:1000-1006

Dror Y et al. (2007) One-Step Production of Polymeric Microtubes by Co-electrospinning. Small 3:1064-1073

El-Kafrawy A (1982) Investigation of the cellulose/LiCl/Dimethylacetamide and cellulose/LiCl/N-methyl-2-pyrrolidinone solutions by 13C NMR spectroscopy. J Appl Polym Sci 27:2435-2443

Frenot A, Henriksson MW, Walkenström P (2007) Electrospinning of cellulose-based nanofibers. J Appl Polym Sci 103:1473-1482

Gama M, Gatenholm P, Klemm D (2012) Bacterial nanocellulose: a sophisticated multifunctional material. CRC Press, London New York

Geng X, Kwon O-H, Jang J (2005) Electrospinning of chitosan dissolved in concentrated acetic acid solution. Biomaterials 26:5427-5432

Goosen MF (1997) Applications of chitin and chitosan. CRC Press Llc, Florida

Greiner A, Wendorff JH (2007) Electrospinning: a fascinating method for the preparation of ultrathin fibers. Angew Chem Int Ed 46:5670-5703

Homayoni H, Ravandi SAH, Valizadeh M (2009) Electrospinning of chitosan nanofibers: Processing optimization. Carbohydr Polym 77:656-661

Horii F (2000) Structure of cellulose: Recent developments in its characterization. Wood and Cellulosic Chemistry, Second edition Taylor & Francis Inc:83-108

Ignatova M, Manolova N, Markova N, Rashkov I (2009) Electrospun Non-Woven Nanofibrous Hybrid Mats Based on Chitosan and PLA for Wound-Dressing Applications. Macromol Biosci 9:102-111

Kim CW, Frey MW, Marquez M, Joo YL (2005) Preparation of submicron-scale, electrospun cellulose fibers via direct dissolution. J Polym Sci Part B Polym Phys 43:1673-1683

Kim C-W, Kim D-S, Kang S-Y, Marquez M, Joo YL (2006) Structural studies of electrospun cellulose nanofibers. Polymer 47:5097-5107

Kong M, Chen XG, Xing K, Park HJ (2010) Antimicrobial properties of chitosan and mode of action: a state of the art review. Int J Food Microbiol 144:51-63

Kulpinski P (2005) Cellulose nanofibers prepared by the N-methylmorpholine-N-oxide method. J Appl Polym Sci 98:1855-1859

Li L, Hsieh Y-L (2006) Chitosan bicomponent nanofibers and nanoporous fibers. Carbohydr Res 341:374-381

Lin W-C, Lien C-C, Yeh H-J, Yu C-M, Hsu S-h (2013) Bacterial cellulose and bacterial cellulose–chitosan membranes for wound dressing applications. Carbohydr Polym 94:603-611

Liu H, Hsieh YL (2002) Ultrafine fibrous cellulose membranes from electrospinning of cellulose acetate. J Polym Sci Part B Polym Phys 40:2119-2129

Liu H, Tang C (2007) Electrospinning of cellulose acetate in solvent mixture *N*, *N*-dimethylacetamide (DMAc)/acetone. Polym J 39:65-72

Matsumoto T, Tatsumi D, Tamai N, Takaki T (2001) Solution properties of celluloses from different biological origins in LiCl·DMAc. Cellulose 8:275-282

McCormick CL, Callais PA, Hutchinson Jr BH (1985) Solution studies of cellulose in lithium chloride and *N*, *N*-dimethylacetamide. Macromolecules 18:2394-2401

Mohite BV, Patil SV (2014) A novel biomaterial: bacterial cellulose and its new era applications. Biotechnol Appl Biochem 61:101-110

Muzzarelli RA (1973) Natural chelating polymers; alginic acid, chitin and chitosan. Pergamon Press, Oxford

Ohkawa K, Cha D, Kim H, Nishida A, Yamamoto H (2004) Electrospinning of chitosan. Macromol Rapid Commun 25:1600-1605

Ohkawa K, Minato K-I, Kumagai G, Hayashi S, Yamamoto H (2006) Chitosan nanofiber. Biomacromolecules 7:3291-3294

Okushita K, Chikayama E, Kikuchi J (2012) Solubilization mechanism and characterization of the structural change of bacterial cellulose in regenerated states through ionic liquid treatment. Biomacromolecules 13:1323-1330

Ostadhossein F, Mahmoudi N, Morales-Cid G, Tamjid E, Navas-Martos FJ, Soriano-Cuadrado B, López JM, Simchi A (2015) Development of Chitosan/Bacterial Cellulose Composite Films Containing Nanodiamonds as a Potential Flexible Platform for Wound Dressing. Materials 8:6401-6418

Pakravan M, Heuzey M-C, Ajji A (2011) A fundamental study of chitosan/PEO electrospinning. Polymer 52:4813-4824

Pakravan M, Heuzey M-C, Ajji A (2012) Core–shell structured PEO-chitosan nanofibers by coaxial electrospinning. Biomacromolecules 13:412-421

Park TJ, Yeon JJ, Sung-Wook C, Hongkwan P, Hyungsup K, Eunkyoung K, Sang HL, Jung HK (2011) Native chitosan/cellulose composite fibers from an ionic liquid via electrospinning. Macromol Research 19:213-215

Phisalaphong M, Jatupaiboon N (2008) Biosynthesis and characterization of bacteria cellulose–chitosan film. Carbohydr Polym 74: 482-488

Potthast A, Rosenau T, Sixta H, Kosma P (2002) Degradation of cellulosic materials by heating in DMAc/LiCl. Tetrahedron Lett 43:7757-7759

Röder T, Morgenstern B, Schelosky N, Glatter O (2001) Solutions of cellulose in *N*, *N*-dimethylacetamide/lithium chloride studied by light scattering methods. Polymer 42:6765-6773

Schiffman JD, Schauer CL (2007) Cross-linking chitosan nanofibers. Biomacromolecules 8:594-601

Schlufter K, Schmauder HP, Dorn S, Heinze T (2006) Efficient Homogeneous Chemical Modification of Bacterial Cellulose in the Ionic Liquid 1-*N*-Butyl-3-methylimidazolium Chloride. Macromol Rapid Commun 27:1670-1676

Sekwon K (2010) Chitin, chitosan, oligosaccharides and their derivatives: biological activities and applications. CRC Press Inc., London New York

Shanshan G, Jianqing W, Zhengwei J (2012) Preparation of cellulose films from solution of bacterial cellulose in NMMO. Carbohydr Polym 87:1020-1025

Siró I, Plackett D (2010) Microfibrillated cellulose and new nanocomposite materials: a review. Cellulose 17:459-494

Subramanian A, Vu D, Larsen GF, Lin H-Y (2005) Preparation and evaluation of the electrospun chitosan/PEO fibers for potential applications in cartilage tissue engineering. J Biomater Sci Polymer Ed 16:861-873

Swatloski RP, Spear SK, Holbrey JD, Rogers RD (2002) Dissolution of cellose with ionic liquids. J Am Chem Soc 124:4974-4975

Xu S, Zhang J, He A, Li J, Zhang H, Han CC (2008) Electrospinning of native cellulose from nonvolatile solvent system. Polymer 49:2911-2917

Yarin A (2011) Coaxial electrospinning and emulsion electrospinning of core–shell fibers. Polymer Adv Tech 22:310-317

Yu JH, Fridrikh SV, Rutledge GC (2004) Production of submicrometer diameter fibers by two-fluid electrospinning. Adv. Mater 16:1562-1566

APPENDIX B - GOVERNING EQUATIONS IN THE ELECTROSPRAYING PROCESS

The electrospraying process typically involves three stages (Figure B.1). The first one implies the pumping of the solution through the needle, where simple shear flow occurs. However, at the exit of the needle, a complex flow develops with extensional and shearing components [1]. In the second stage, the charged liquid flowing out from the nozzle gets deformed in a meniscus with a characteristic shape known as Taylor cone [2], from the apex of which a jet is ejected and elongated by an external electric field [3]. A balance among the electrostatic forces, gravity, inertia, viscoelastic forces and surface tension determines the deformation of the fluid [4-6]. Uniaxial elongational flow caused by the electrical forces acting on the jet occurs [3]. Finally, in the last stage, the jet is disintegrated into charged droplets when the electrostatic forces in the fluid are able to overcome the viscosity and surface tension [7]. In electrospraying, different modes for droplet formation have been identified [8], but only the cone-jet mode is known to produce a stable process [9]. Once formed, the charged droplets travel to a collector plate while the solvent is evaporated. Different parameters including processing (flow rate, needle size, voltage, distance from needle tip to plate collector and temperature), environmental (humidity, pressure and temperature), and the intrinsic properties of the solution (conductivity, surface tension and viscosity, which depend mainly on the polymer concentration and molecular weight, as well as the solvent type) are important factors in determining processing stability, droplet formation and morphology. However, solution parameters are considered to be the most critical [10].

The governing equations for the electrospraying process are reported in the literature and developed here for the second stage, which is considered a steady-stretching process [4, 11, 12]. This stage is common for both electrospraying and electrospinning processes [3]. Modeling of the development of this stage have been proposed by Hohman *et al.* [3], Feng [4] and Reneker *et al.* [13], among others, following the earlier works of Gañán-Calvo [12, 14, 15] and Spivak and Dzenis [16].

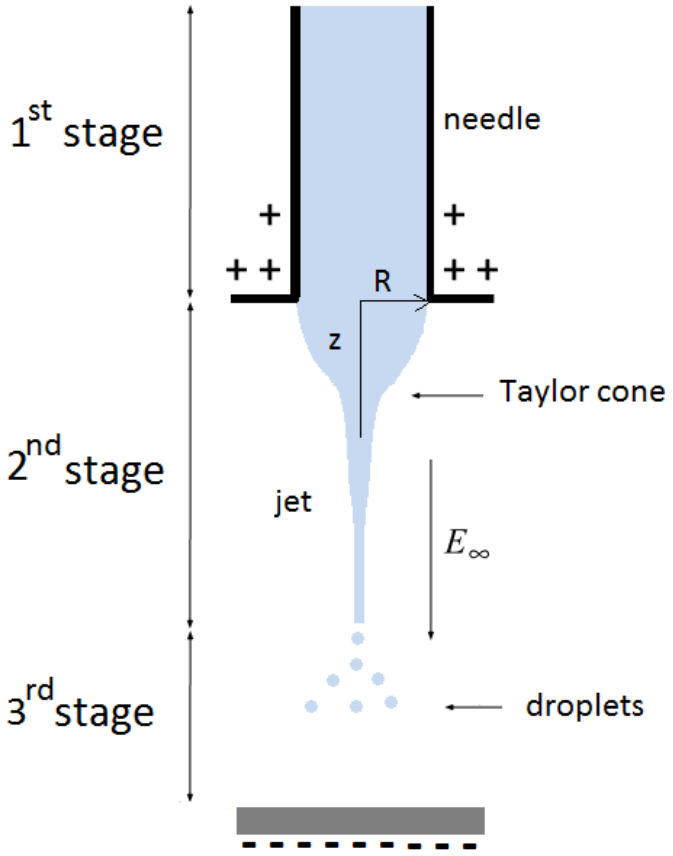

Figure B.12: Different stages in the electrospraying process.

B.1 Nomenclature

t: Time

ρ: Fluid density

R: Radius of the jet (variable)

R_0: Initial radius of the jet (radius of the needle)

v: Axial velocity of the jet ($v = v_z$)

v_0: Initial velocity of the jet

v_θ: Θ-component of the velocity of the jet

v_r: Radial component of the velocity of the jet

$\dot{m}_0$: Mass flow rate at “plane 0”

$\dot{m}_1$: Mass flow rate at “plane 1”

Q_0: Volumetric flow rate at “plane 0”

Q_1: Volumetric flow rate at “plane 1”

Q: Constant volumetric flow rate

I: Constant total current carried by the jet

J: Magnitude of current density

K: Conductivity of the liquid

$\boldsymbol{E}$: Electric field

E: Axial component of the electric field inside the jet evaluated at the surface

$\tilde{E}$: Axial component of the electric field at the interface

E_n: Normal component of the electric field at the surface

$\bar{E}_n$: Normal component of the electric field outside the jet

E_t: Tangential component of the electric field at the surface

$\bar{E}_t$: Tangential component of the electric field outside the jet

E_r: Radial component of the electric field inside the jet evaluated at the surface

$\bar{E}_r$: Radial component of the electric field outside the jet

E_∞: Uniform spatially external electric field $\left(E_\infty = {}^{\Delta V}/_{d}\right)$

E_0: Initial external electric field

d: Electrospraying distance (gap)

ΔV: Applied potential difference

σ: Surface charge density

σ_0: Initial surface charge density

$\underline{\underline{\Pi}}$: Total stress tensor

p: Pressure

$\underline{\underline{I}}$: Identity tensor

g: Gravity

$\underline{\underline{\tau}}$: Extra stress tensor

τ_{rr}: Viscous radial normal stress

τ_{zz}: Viscous axial normal stress

t_n^e: Normal force exerted on the jet by the electric field

t_t^e: Tangential force exerted on the jet by the electric field

ε: Dielectric constant (permittivity) of the jet

$\bar{\varepsilon}$: Dielectric constant (permittivity) of the air

ε_0: Dielectric constant (permittivity) of the vacuum

$\|*\|$: Indicates the jump of a quantity across the surface of the jet

γ: Surface tension

T: Tensile force in the jet

$\lambda(z)$: Linear charge density along the jet

$\bar{\Phi}$: Electrostatic potential outside the jet

$\bar{\Phi}_\infty$: Electrostatic potential due to the external field in the absence of jet

v': $v' = {dv}/{dz}$

T': $T' = {dT}/{dz}$

σ': $\sigma' = {d\sigma}/{dz}$

E': $E' = {dE}/{dz}$

R': $R' = {dR}/{dz}$

$\eta(\dot{\gamma})$: Scalar function representing the non-Newtonian viscosity

η: Shear viscosity

$\bar{\eta}$: Elongational viscosity

η_0: Zero-shear rate viscosity

$\underline{\underline{\dot{\gamma}}}$: Rate of strain tensor

$\dot{\gamma}$: Shear rate or rate of strain, $\dot{\gamma} = \left|\underline{\underline{\dot{\gamma}}}\right|$

$\dot{\varepsilon}(t)$: Elongation rate

$\dot{\varepsilon}_0$: Constant elongation rate

$\nabla\underline{v}$: Gradient of the velocity field

L: Length of the jet

$\overset{\nabla}{\underline{\underline{\tau_p}}}$: Upper convected derivative for the extra stress tensor

α: Mobility factor

λ: Relaxation time

η_s: Solvent viscosity

η_p: Polymer viscosity

B.2 Hypotheses

1. The jet is considered as a liquid continuum [17].
2. Steady state $(\partial/\partial t = 0)$ [4, 11, 12].
3. Isothermal flow (constant temperature).
4. Unidirectional elongational flow.
5. Axisymmetric flow $(\partial/\partial\theta = 0)$.
6. Incompressible fluid $(\rho = \text{constant})$.
7. The fluid is dielectric with charges only on its surface [18].
8. Standard assumptions for slender jets [3, 4, 15]:
   - The jet radius R decreases slowly with respect to the axial direction z: $|dR(z)/dz| \lll 1$
   - The axial velocity $(v_z = v)$ is uniform in the cross section of the jet.
9. $v_\theta = 0$
10. $v_r = v_R = v_R(R, z)$
11. $v_z = v = v(z)$
12. $v_R \lll v_z$
13. As the jet thins, the surface charge density σ varies, which in turn affects the electric field E, and the tensile force T. Therefore, for simplicity σ, E and T besides R and v are assumed to be uniform on the cross-section of the jet and to vary only along z, whose origin is at the nozzle.
14. There is not significant evaporation of the solvent in the jet (mass transfer effects are neglected) [19].
15. Air drag force is negligible on the jet [3, 13]. This force becomes important once the jet breakup into droplets [20].
16. Ambient conditions (humidity, pressure, temperature) are considered constant during the process.

B.3 Governing equations for stable jet

The jet is governed by four steady state equations representing the conservation of mass and electric charges, the linear momentum balance and the Coulomb's law for the electric field [3, 4]. The balances are done for the second stage showed in Figure B.12, from the tip of the needle to the end of the jet.

B.3.1 Mass conservation

In steady state, the mass flow rate entering the jet is equal to the mass flow rate exiting.

$$\dot{m}_0 = \dot{m}_1 \tag{B.1}$$

$$\rho Q_0 = \rho Q_1 \tag{B.2}$$

$$v_0 \pi R_0^2 = v_1 \pi R_1^2 = Q = \text{constant} \tag{B.3}$$

$$\boxed{v\pi R^2 = Q} \tag{B.4}$$

where v, R and Q are the velocity, radius and volumetric flow rate of the jet, respectively.

B.3.2 Electric charge conservation

The current carried by the jet has two components: the current that flows through the jet due to its bulk conductivity and the presence of the electric field inside the jet; and the current produced by the charge convected on the surface of the jet [21].

Current conducted within the jet [22]:

$$I_{bulk} = \pi R^2 J = \pi R^2 KE \tag{B.5}$$

Current conducted by the surface charge [22]:

$$I_{surf.charge} = 2\pi RJ = 2\pi R\sigma v \tag{B.6}$$

where J is the magnitude of the current density, K is the solution conductivity, E is the axial component of the electric field and σ is the surface charge density.

In steady state these expressions transform into:

$$\boxed{\pi R^2 KE + 2\pi Rv\sigma = I_{total}} \tag{B.7}$$

B.3.3 Momentum conservation

Momentum balance is formulated by considering the forces on a short section of the jet (Figure B.13) [4].

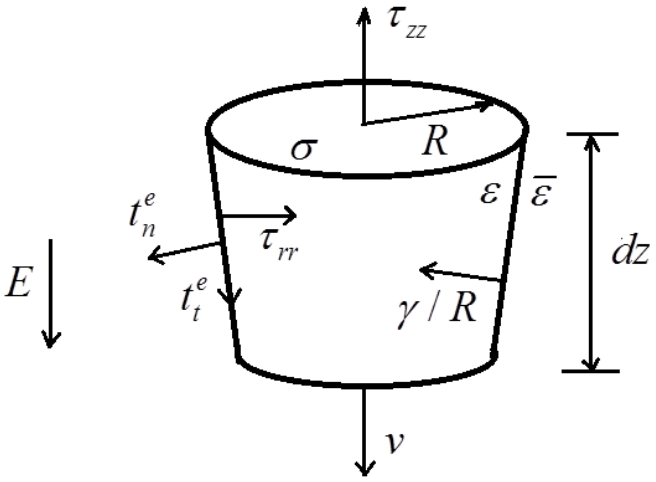

Figure B.13: Momentum balance on a short section of the jet [4]

Starting from the equation of motion which expresses the conservation of linear momentum in a flowing fluid [23, 24]:

$$\frac{\partial(\rho \underline{v})}{\partial t} = -\nabla \cdot \left(\rho \underline{v}\, \underline{v}\right) - \nabla \underline{\underline{\Pi}} + \rho \underline{g} + \text{other forces} \tag{B.8}$$

The total stress tensor $\underline{\underline{\Pi}}$ can be written as:

$$\underline{\underline{\Pi}} = p \underline{\underline{I}} + \underline{\underline{\tau}} \tag{B.9}$$

Then, in steady state (see section B.2) the equation of motion becomes:

$$\underline{0} = -\nabla \cdot \left(\rho \underline{v}\, \underline{v}\right) - \nabla \mathrm{p} - \nabla \cdot \underline{\underline{\tau}} + \rho g + \text{other forces} \tag{B.10}$$

The first term on the right-end side represent the inertial forces; the second one, the surface force due to pressure; the third one, the surface force due to viscous shear and normal stresses; the fourth one, the body force due to gravity; and the last one includes the forces due to the surface tension and the electric field.

Developing each term and assuming constant density (see section B.2):

$$\nabla \cdot \left(\rho \underline{v}\, \underline{v}\right) = \rho \begin{pmatrix} \frac{1}{r}\frac{\partial}{\partial r}(r v_r^2) + \frac{1}{r}\frac{\partial}{\partial \theta}(v_\theta v_r) + \frac{\partial}{\partial z}(v_z v_r) - \frac{v_\theta^2}{r} \\ \frac{1}{r^2}\frac{\partial}{\partial r}(r^2 v_r v_\theta) + \frac{1}{r}\frac{\partial}{\partial \theta}\left(v_\theta^2\right) + \frac{\partial}{\partial z}(v_z v_\theta) + \frac{v_\theta v_r - v_r v_\theta}{r} \\ \frac{1}{r}\frac{\partial}{\partial r}(r v_r v_z) + \frac{1}{r}\frac{\partial}{\partial \theta}(v_\theta v_z) + \frac{\partial}{\partial z}(v_z^2) \end{pmatrix}_{r\theta z}$$

$$\nabla p = \begin{pmatrix} \frac{\partial p}{\partial r} \\ \frac{1}{r}\frac{\partial p}{\partial \theta} \\ \frac{\partial p}{\partial z} \end{pmatrix}_{r\theta z}$$

$$\nabla \cdot \underline{\underline{\tau}} = \begin{pmatrix} \frac{1}{r}\frac{\partial}{\partial r}(r\tau_{rr}) + \frac{1}{r}\frac{\partial \tau_{\theta r}}{\partial \theta} + \frac{\partial \tau_{zr}}{\partial z} - \frac{\tau_{\theta\theta}}{r} \\ \frac{1}{r^2}\frac{\partial}{\partial r}(r^2\tau_{r\theta}) + \frac{1}{r}\frac{\partial \tau_{\theta\theta}}{\partial \theta} + \frac{\partial \tau_{z\theta}}{\partial z} + \frac{\tau_{\theta r} - \tau_{r\theta}}{r} \\ \frac{1}{r}\frac{\partial}{\partial r}(r\tau_{rz}) + \frac{1}{r}\frac{\partial \tau_{\theta z}}{\partial \theta} + \frac{\partial \tau_{zz}}{\partial z} \end{pmatrix}_{r\theta z}$$

$$\rho \underline{\mathrm{g}} = \rho \begin{pmatrix} \mathrm{g}_r \\ \mathrm{g}_\theta \\ \mathrm{g}_z \end{pmatrix}_{r\theta z}$$

Simplifying by using the hypotheses (4, 5, 8-12) mentioned in section B.2, and neglecting shear terms, since the flow is mainly elongational, we obtain:

$$\begin{pmatrix} 0 \\ 0 \\ 0 \end{pmatrix} = -\rho \begin{pmatrix} 0 \\ 0 \\ \frac{\partial v_z^2}{\partial z} \end{pmatrix} - \begin{pmatrix} \frac{\partial p}{\partial r} \\ \frac{1}{r}\frac{\partial p}{\partial \theta} \\ \frac{\partial p}{\partial z} \end{pmatrix} - \begin{pmatrix} \frac{1}{r}\frac{\partial}{\partial r}(r\tau_{rr}) \\ 0 \\ \frac{\partial \tau_{zz}}{\partial z} \end{pmatrix} + \rho \begin{pmatrix} 0 \\ 0 \\ \mathrm{g} \end{pmatrix} + \text{other forces} \qquad \text{(B.11)}$$

Surface tension. Surface tension γ acts normally to the jet surface. Its contribution must appear not only in the radial but also in the axial component of the momentum balance due to the shape of the jet (Figure B.13).

Electrostatic forces. t_n^e and t_t^e are the normal and tangential forces exerted on the jet by the electric field. Those forces are related to the surface charge density (σ), the electric field (E) and the

dielectric constants of the jet (ε) and air ($\bar{\varepsilon}$), and can be determined with help of the leaky dielectric model [4, 18]:

$$t_n^e = \left\| \frac{\varepsilon}{2}(E_n^2 - E_t^2) \right\| \approx \frac{\sigma^2}{2\bar{\varepsilon}} - \frac{\bar{\varepsilon}-\varepsilon}{2} E^2 \tag{B.12}$$

$$t_t^e = \sigma E_t \approx \sigma E \tag{B.13}$$

Now, by considering Eq. B.11 and the contributions of the electrostatic and surface tension forces, it is possible to have the radial and axial equations for the momentum balance:

Momentum balance in the radial direction:

At the jet surface:

$$-p + \tau_{rr} = t_n^e - \frac{\gamma}{R} \tag{B.14}$$

From this equation it is possible to obtain and expression for the pressure, p:

$$\boxed{p = \tau_{rr} - t_n^e + \frac{\gamma}{R} = \tau_{rr} - \frac{\sigma^2}{2\bar{\varepsilon}} + \frac{\bar{\varepsilon}-\varepsilon}{2} E^2 + \frac{\gamma}{R}} \tag{B.15}$$

Momentum balance in the axial direction:

$$\rho \frac{d}{dz}(v_z^2) = \frac{d}{dz}(-p + \tau_{zz} + \rho g + \text{surface tension} + \text{electrostatic force} \tag{B.16}$$

Considering the component of the electrostatic force in the axial direction as well as their contribution of the normal because of the jet form, and adding the respective contribution of the surface tension force, Eq. B.16 becomes:

$$\boxed{\rho \frac{d}{dz}(\pi R^2 v_z^2) = \frac{d}{dz}[\pi R^2(-p + \tau_{zz})] + \pi R^2 \rho g + \frac{\gamma}{R} 2\pi R \frac{dR}{dz} + 2\pi R \left(t_t^e - t_n^e \frac{dR}{dz} \right)} \tag{B.17}$$

where dR/dz represents the slope of the jet.

Final equation for the momentum balance:

Inserting Eq. B.12, B.13 and B.15 into Eq. B.17 and using the hypotheses 8 and 13 from section B.2 it is obtained:

$$\rho v v' = \frac{T'}{\pi R^2} + \frac{\sigma\sigma'}{\bar{\varepsilon}} + (\varepsilon - \bar{\varepsilon})EE' + \frac{\gamma}{R^2}R' + \rho g + 2\frac{\sigma E}{R} \tag{B.18}$$

where v represents the velocity of the jet in the z direction, the prime components the derivative with respect to z and the term $T = \pi R^2(\tau_{zz} - \tau_{rr})$ represents the tensile force in the jet and the stress components τ_{zz} and τ_{rr} depend on the fluid constitutive model.

Tensile force in the jet:

In theoretical work to date, the rheology of the polymer jet has been represented by a Newtonian viscosity [3, 25], a power-law viscosity [16] the linear Maxwell equation [13, 26], the Oldroyd-B [27], the FENE-P [11] and the Giesekus [5] constitutive equation. Feng has found this latter as a model that strikes a good balance between simplicity and satisfactory prediction for elongational rheology in addition of capturing elastic effects of viscoelastic fluids [5]. Here, to calculate the tensile force of the jet a generalized Newtonian constitutive relation is used in terms of simplicity.

The generalized Newtonian fluid model [23]:

$$\underline{\underline{\tau}} = \eta(\dot{\gamma})\underline{\underline{\dot{\gamma}}} \tag{B.19}$$

As considered in section B.2, the flow of the jet is mainly elongational. The kinematics for this type of flow are the following [23]:

$$\underline{v} = \begin{pmatrix} -\frac{1}{2}\dot{\varepsilon}(t)x_1 \\ -\frac{1}{2}\dot{\varepsilon}(t)x_2 \\ \dot{\varepsilon}(t)x_3 \end{pmatrix}_{123} , \dot{\varepsilon}(t) > 0 \tag{B.20}$$

For steady elongational flow, $\dot{\varepsilon}(t) = \dot{\varepsilon}_0 = \text{constant}$. Hence, the rate of strain tensor is:

$$\underline{\underline{\dot{\gamma}}} = \nabla\underline{v} + (\nabla\underline{v})^T = \begin{pmatrix} -\dot{\varepsilon}_0 & 0 & 0 \\ 0 & -\dot{\varepsilon}_0 & 0 \\ 0 & 0 & 2\dot{\varepsilon}_0 \end{pmatrix}_{123} \text{ and } |\dot{\gamma}| = \sqrt{3\dot{\varepsilon}_0} \tag{B.21}$$

Finally, the stress tensor is:

$$\underline{\underline{\tau}} = \eta(\dot{\gamma})\underline{\underline{\dot{\gamma}}} = \begin{pmatrix} -\eta(\dot{\gamma})\dot{\varepsilon}_0 & 0 & 0 \\ 0 & -\eta(\dot{\gamma})\dot{\varepsilon}_0 & 0 \\ 0 & 0 & 2\eta(\dot{\gamma})\dot{\varepsilon}_0 \end{pmatrix}_{123} \tag{B.22}$$

From this equation it is possible to obtain:

$$\tau_{33} - \tau_{11} = 3\eta(\dot{\gamma})\dot{\varepsilon}_0 = 3\eta v' = \bar{\eta} v' \tag{B.23}$$

Where $\eta(\dot{\gamma}) = \eta$ is the shear viscosity and $\bar{\eta}$ is the elongational viscosity; hence, the tensile force of the jet is:

$$T = \pi R^2 3\eta v' \tag{B.24}$$

B.3.4 Coulomb's law for electric field

According to Hohman *et al.* [3] it is possible to write the electric field outside the slender jet as if it was due to an effective linear charge density (considering both free and induced charges on the jet surface) of charge $\lambda(z)$ along the z-axis.

To determine the linear charge density, Gauss' law is applied over two cylindrical surfaces having the same length and which are coaxial with the jet as shown in: the surface S_1 which lies just inside the interface and contains no charge (and no effective charge), and the surface S_2 which lies just outside the interface and contains the effective charge $\lambda(z)dz$.

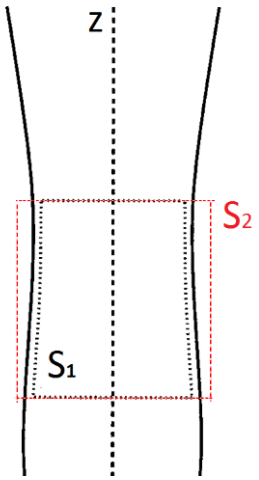

Figure B.14: Gaussian surfaces: S_1 lies just inside the interface and S_2 lies just outside the interface and thus contains charge [3]

a. Gauss' law over S_1:

$$0 = \oint_{S_1} \underline{E} \cdot \hat{n} dA = \left[2\pi R E_r + \frac{d}{dz}(\pi R^2 E)\right] dz \tag{B.25}$$

where E_r and E are the radial and axial components of the electric field inside the jet evaluated at the jet surface. From Eq. B.25 it is obtained:

$$E_r = -\frac{1}{2\pi R}\frac{d}{dz}(\pi R^2 E) \tag{B.26}$$

b. Gauss' law over S_2 [3]:

$$4\pi\lambda(z)dz = \oint_{S_2} \underline{E}\cdot\hat{n}dA = \left[2\pi R\overline{E}_r + \frac{d}{dz}(\pi R^2 E)\right]dz \tag{B.27}$$

where $\bar{E}_r$ denotes the radial component of the electric field outside the jet. From Eq. B.27, it is possible to find the charge per unit length, $\lambda(z)$:

$$\lambda(z) = \frac{1}{2}R\bar{E}_r + \frac{1}{4}\frac{d}{dz}(R^2 E) \tag{B.28}$$

For a slender jet it is known that [3]:

$$\bar{E}_r \approx \bar{E}_n = \frac{\varepsilon}{\bar{\varepsilon}}E_n + \frac{4\pi\sigma}{\bar{\varepsilon}} \tag{B.29}$$

Replacing Eq. B.26 and B.29 into Eq. B.28:

$$\lambda(z) = \frac{2\pi R\sigma}{\bar{\varepsilon}} - \frac{1}{4}\left(\frac{\varepsilon}{\bar{\varepsilon}} - 1\right)\frac{d}{dz}(R^2 E) \tag{B.30}$$

This effective linear charge is inserted into Coulomb's law for the electrostatic potential outside the jet. To find this electrostatic potential Hohman *et al.* [3] assumed that λ varies over a length scale, $L >>> R_0$:

$$\overline{\Phi}(z,R) = \overline{\Phi}_\infty + \int \frac{\lambda(z')dz'}{\sqrt{(z-z')^2 + R^2}}$$

$$\overline{\Phi}(z,R) \approx \overline{\Phi}_\infty + \lambda(z)\int \frac{dz'}{\sqrt{(z-z')^2 + R^2}}$$

$$\overline{\Phi}(z,R) \approx \overline{\Phi}_\infty - 2\ln\left(\frac{R_0}{L}\right)\lambda(z)$$

$$\overline{\Phi}(z,R) = \overline{\Phi}_\infty + \ln\left(\frac{L}{R_0}\right)\left[\frac{4\pi R\sigma}{\bar{\varepsilon}} - \frac{1}{2}\left(\frac{\varepsilon}{\bar{\varepsilon}} - 1\right)\frac{d}{dz}(R^2 E)\right] \tag{B.31}$$

where $\overline{\Phi}$ is the electrostatic potential outside the jet and $\overline{\Phi}_\infty$ is the electrostatic potential due to the external field in the absence of the jet, L is the entire length of the jet and R_0 is the initial jet radius.

Across the interface the tangential component of the electric field is continuous, so $\tilde{E} = \bar{E}_t = E_t \approx E$ and from Eq. B.31 is obtained the equation for the axial electric field inside the jet:

$$E = -\frac{d\Phi}{dz}$$

$$\boxed{E(z) = E_\infty - \ln\left(\frac{L}{R_0}\right)\left[\frac{4\pi}{\bar{\varepsilon}}\frac{d(\sigma R)}{dz} - \frac{1}{2}\left(\frac{\varepsilon}{\bar{\varepsilon}} - 1\right)\frac{d^2(ER^2)}{dz^2}\right]} \quad \text{(B.32)}$$

B.4 Dimensionless numbers of the process

The parameters used to make dimensionless the governing equations for the electrospraying are the following:

Length scale: R_0 characteristic radius of the jet

Velocity: $v_0 = \frac{Q}{\pi R_0^2}$

Electric field: $E_0 = \frac{I}{\pi R_0^2 K}$

Surface charge density: $\sigma_0 = \bar{\varepsilon} E_0$

The dimensionless variables are: $R^* = R/R_0$, $v^* = v/v_0$, $\sigma^* = \sigma/\sigma_0$ and $E^* = E/E_0$.

By using the dimensionless parameters, the dimensionless governing equations for the stable jet of the electrospraying process are derived:

B.4.1 Mass balance

$$v\pi R^2 = Q$$

Replacing the value for $Q = v_0 \pi R_0^2$ from section 0:

$$v\pi R^2 = v_0 \pi R_0^2$$

$$\left(\frac{v}{v_0}\right)\left(\frac{R}{R_0}\right)^2 = 1$$

$$\boxed{v^* R^{*2} = 1} \tag{B.33}$$

B.4.2 Electric charge balance

$$\pi R^2 KE + 2\pi R v\sigma = I$$

Replacing the dimensionless parameters defined in section 0: $K = \frac{I}{\pi R_0^2 E_0}$

$$\pi R^2 \left(\frac{I}{\pi R_0^2 E_0}\right) E + 2\pi R v\sigma = I$$

Diving all terms by $I = \frac{\pi R_0^2 K \sigma_0}{\bar{\varepsilon}}$ and regrouping:

$$\left(\frac{R}{R_0}\right)^2 \left(\frac{E}{E_0}\right) + 2\left(\frac{\bar{\varepsilon} v_0}{R_0 K}\right)\left(\frac{R}{R_0}\right)\left(\frac{v}{v_0}\right)\left(\frac{\sigma}{\sigma_0}\right) = 1$$

$$\boxed{R^{*2} E^* + 2Pe\, R^* v^* \sigma^* = 1} \tag{B.34}$$

B.4.3 Momentum balance

$$\rho v v' = \frac{T'}{\pi R^2} + \frac{\sigma\sigma'}{\bar{\varepsilon}} + (\varepsilon - \bar{\varepsilon}) E E' + \frac{\gamma}{R^2} R' + \rho g + 2\frac{\sigma E}{R}$$

Considered that:

$$z^* = \frac{z}{R_0} \rightarrow \frac{dz^*}{dz} = \frac{1}{R_0}$$

$$v^* = \frac{v}{v_0} \rightarrow v = v_0 v^* \rightarrow v' = \frac{dv}{dz} = \frac{d}{dz}(v_0 v^*) = v_0 \frac{dz^*}{dz}\frac{dv^*}{dz^*} = \left(\frac{v_0}{R_0}\right) v^{*\prime}$$

$$R^* = \frac{R}{R_0} \rightarrow R = R_0 R^* \rightarrow R' = \frac{dR}{dz} = \frac{d}{dz}(R_0 R^*) = R_0 \frac{dz^*}{dz}\frac{dR^*}{dz^*} = R^{*\prime}$$

$$\sigma^* = \frac{\sigma}{\sigma_0} \rightarrow \sigma = \sigma_0 \sigma^* \rightarrow \sigma' = \frac{d\sigma}{dz} = \frac{d}{dz}(\sigma_0 \sigma^*) = \sigma_0 \frac{dz^*}{dz}\frac{d\sigma^*}{dz^*} = \left(\frac{\sigma_0}{R_0}\right) \sigma^{*\prime}$$

$$E^* = \frac{E}{E_0} \rightarrow E = E_0 E^* \rightarrow E' = \frac{dE}{dz} = \frac{d}{dz}(E_0 E^*) = E_0 \frac{dz^*}{dz}\frac{dE^*}{dz^*} = \left(\frac{E_0}{R_0}\right) E^{*\prime}$$

$$\frac{d(R^2 \eta v')}{dz} = \frac{dz^*}{dz}\frac{d(R^2 \eta v')}{dz^*} = \frac{1}{R_0}\frac{d}{dz^*}\left[R^2 \eta \left(\frac{v_0}{R_0} v^{*\prime}\right)\right] = \frac{d}{dz^*}\left(\frac{R^2 \eta v_0}{R_0^2} v^{*\prime}\right)$$

Replacing the previous dimensionless variables and expressions in the momentum balance:

$$\rho(v_0 v^*)\left(\frac{v_0}{R_0} v^{*'}\right) = \frac{3\pi}{\pi R^2}\frac{d}{dz^*}\left(\frac{R^2 \eta v_0}{R_0^2} v^{*\prime}\right) + \frac{1}{\bar{\varepsilon}}(\sigma_0 \sigma^*)\left(\frac{\sigma_0}{R_0}\sigma^{*'}\right) +$$

$$+(\varepsilon - \bar{\varepsilon})(E_0 E^*)\left(\frac{E_0}{R_0} E^{*'}\right) + \frac{\gamma}{R^2} R^{*\prime} + \rho g + \frac{2}{R}(\sigma_0 \sigma^*)(E_0 E^*)$$

Multiplying all terms by $\frac{R_0}{\rho v_0^2}$, replacing $\sigma = \bar{\varepsilon} E_0$ and regrouping terms:

$$v^* v^{*\prime} = 3\left(\frac{\eta_0}{\rho v_0 R_0}\right)\left(\frac{R_0}{R}\right)^2 \frac{d}{dz^*}\left[\left(\frac{R}{R_0}\right)^2 \left(\frac{\eta}{\eta_0}\right) v^{*\prime}\right] + \left(\frac{\bar{\varepsilon} E_0^2}{\rho v_0^2}\right)\sigma^* \sigma^{*\prime} +$$

$$+\left(\frac{\bar{\varepsilon} E_0^2}{\rho v_0^2}\right)\left(\frac{\varepsilon - \bar{\varepsilon}}{\bar{\varepsilon}}\right) E^* E^{*\prime} + \left(\frac{\gamma}{\rho v_0^2 R_0}\right)\left(\frac{R_0}{R}\right)^2 R^{*\prime} + \left(\frac{g R_0}{v_0^2}\right) + 2\left(\frac{\bar{\varepsilon} E_0^2}{\rho v_0^2}\right)\left(\frac{R_0}{R}\right)\sigma^* E^*$$

$$v^* v^{*\prime} = \frac{3}{\mathrm{Re} R^{*2}}\frac{d(R^{*2} r_\eta v^{*\prime})}{dz^*} + \Omega \sigma^* \sigma^{*\prime} + \Omega \beta E^* E^{*\prime} + \frac{1}{\mathrm{We}}\frac{R^{*\prime}}{R^{*2}} + \frac{1}{\mathrm{Fr}} + 2\Omega \frac{\sigma^* E^*}{R^*}$$

$$\boxed{v^* v^{*\prime} = \frac{3}{\mathrm{Re} R^{*2}}\frac{d(R^{*2} r_\eta v^{*\prime})}{dz^*} + \frac{1}{\mathrm{We}}\frac{R^{*\prime}}{R^{*2}} + \frac{1}{\mathrm{Fr}} + \Omega\left(2\frac{\sigma^* E^*}{R^*} + \sigma^* \sigma^{*\prime} + \beta E^* E^{*\prime}\right)} \qquad \text{(B.35)}$$

In the case of using a viscoelastic constitutive equation such as the Giesekus model, as reported by Feng [5], instead of the Generalized Newtonian fluid model, Eq. B.35 changes by only the first term on the right side, and is the one related with the tensile force of the jet. The advantage of using this model is that it considers the nonlinear viscoelasticity that arises during the large-strain stretching of the polymer [5].

Giesekus model:

$$\underline{\tau} = \underline{\tau}_p + \underline{\tau}_s = \underline{\tau}_p + \eta_s\left(\nabla \underline{v} + \nabla \underline{v}^T\right) \qquad \text{(B.36)}$$

$$\underline{\underline{\tau}}_p + \lambda \overset{\nabla}{\underline{\underline{\tau}}}_p + \alpha \frac{\lambda}{\eta_p} \underline{\underline{\tau}}_p \cdot \underline{\underline{\tau}}_p = \eta_p \left(\nabla \underline{v} + \nabla \underline{v}^T \right) \tag{B.37}$$

where $\overset{\nabla}{\underline{\underline{\tau}}}_p$ indicates the upper convected derivative, α is the mobility factor, λ is the relaxation time and η_s and η_p are viscosities due to the solvent and polymer, respectively. Eq. B.37 can be reduced to two scalar equations for the polymer normal stress components [5]:

$$\tau_{prr} + \lambda\left(v\tau'_{prr} + v'\tau_{prr}\right) + \alpha \frac{\lambda}{\eta_p}\tau_{prr}^2 = -\eta_p v' \tag{B.38}$$

$$\tau_{pzz} + \lambda\left(v\tau'_{pzz} - 2v'\tau_{pzz}\right) + \alpha \frac{\lambda}{\eta_p}\tau_{pzz}^2 = 2\eta_p v' \tag{B.39}$$

According to Feng [5], the dimensionless momentum equation is:

$$v^* v^{*\prime} = \frac{3(1-r_\eta)}{\mathrm{Re}R^{*2}} \frac{d(R^{*2}v^{*\prime})}{dz^*} + \frac{1}{\mathrm{Re}} \frac{T_p^{*\prime}}{R^{*2}} + \frac{1}{\mathrm{We}} \frac{R^{*\prime}}{R^{*2}} + \frac{1}{\mathrm{Fr}} + \Omega\left(2\frac{\sigma^* E^*}{R^*} + \sigma^*\sigma^{*\prime} + \beta E^* E^{*\prime}\right) \tag{B.40}$$

where $T_p^* = R^{*2}N_1^* = R^{*2}\left(\tau_{pzz}^* - \tau_{prr}^*\right)$ is the dimensionless tensile force and N_1^* is the first normal stress difference of the polymer. In the same way than the conservation equations, the equations for the normal stress components (Eq. B.38 and B.39) are made dimensionless:

Eq. B.38:

$$\tau_{prr} + \lambda\left(v\tau'_{prr} + v'\tau_{prr}\right) + \alpha \frac{\lambda}{\eta_p}\tau_{prr}^2 = -\eta_p v'$$

In this case to make dimensionless the equation, a new dimensionless parameter $\tau_0 = \frac{\eta_0 v_0}{R_0}$ is needed where $\eta_0 = \eta_s + \eta_p$. Therefore:

$$\tau_{prr}^* = \frac{\tau_{prr}}{\tau_0} \rightarrow \tau_{prr} = \tau_0 \tau_{prr}^* \rightarrow \tau'_{prr} = \frac{d\tau_{prr}}{dz} = \tau_0 \frac{dz^*}{dz}\frac{d\tau_{prr}^*}{dz^*} = \frac{\tau_0}{R_0}\tau_{prr}^{*\prime}$$

Replacing into Eq.B.38:

$$\tau_0\tau_{prr}^* + \lambda\left(\frac{v_0\tau_0}{R_0}v^*\tau_{prr}^{*\prime} + \frac{v_0\tau_0}{R_0}v^{*\prime}\tau_{prr}^*\right) + \left(\frac{\alpha\lambda\tau_0^2}{\eta_p}\right)\tau_{prr}^{*2} = -\left(\frac{\eta_p v_0}{R_0}\right)v^{*\prime}$$

Dividing all terms by τ_0 and regrouping terms:

$$\tau_{prr}^{*} + \left(\frac{\lambda v_0}{R_0}\right) v^{*} \tau_{prr}^{*\prime} + \left(\frac{\lambda v_0}{R_0}\right) v^{*\prime} \tau_{prr}^{*} + \alpha \left(\frac{\lambda v_0}{R_0}\right)\left(\frac{\eta_0}{\eta_p}\right) \tau_{prr}^{*2} = -\left(\frac{\eta_p}{\eta_0}\right) v^{*\prime}$$

$$\tau_{prr}^{*} + De\left(v^{*} \tau_{prr}^{*\prime} + v^{*\prime} \tau_{prr}^{*}\right) + \alpha \frac{De}{r_\eta} \tau_{prr}^{*2} = -r_\eta v^{*\prime} \qquad \text{(B.41)}$$

Eq. B.39:

$$\tau_{pzz} + \lambda\left(v \tau_{pzz}' - 2v' \tau_{pzz}\right) + \alpha \frac{\lambda}{\eta_p} \tau_{pzz}^{2} = 2\eta_p v'$$

Introducing the same dimensionless number $\tau_0 = \frac{\eta_0 v_0}{R_0}$ and replacing into Eq. B.39:

$$\tau_{pzz}^{*} = \frac{\tau_{pzz}}{\tau_0} \rightarrow \tau_{pzz} = \tau_0 \tau_{pzz}^{*} \rightarrow \tau_{pzz}' = \frac{d\tau_{pzz}}{dz} = \tau_0 \frac{dz^{*}}{dz} \frac{d\tau_{pzz}^{*}}{dz^{*}} = \frac{\tau_0}{R_0} \tau_{pzz}^{*\prime}$$

$$\tau_0 \tau_{pzz}^{*} + \lambda\left(\frac{v_0 \tau_0}{R_0} v^{*} \tau_{pzz}^{*\prime} - 2\frac{v_0 \tau_0}{R_0} v^{*\prime} \tau_{pzz}^{*}\right) + \left(\frac{\alpha \lambda \tau_0^{2}}{\eta_p}\right) \tau_{pzz}^{*2} = 2\left(\frac{\eta_p v_0}{R_0}\right) v^{*\prime}$$

Dividing all terms by τ_0 and regrouping terms:

$$\tau_{pzz}^{*} + \left(\frac{\lambda v_0}{R_0}\right) v^{*} \tau_{pzz}^{*\prime} - 2\left(\frac{\lambda v_0}{R_0}\right) v^{*\prime} \tau_{pzz}^{*} + \alpha \left(\frac{\lambda v_0}{R_0}\right)\left(\frac{\eta_0}{\eta_p}\right) \tau_{pzz}^{*2} = 2\left(\frac{\eta_p}{\eta_0}\right) v^{*\prime}$$

$$\tau_{pzz}^{*} + De\left(v^{*} \tau_{pzz}^{*\prime} - 2v^{*\prime} \tau_{pzz}^{*}\right) + \alpha \frac{De}{r_\eta} \tau_{pzz}^{*2} = 2r_\eta v^{*\prime} \qquad \text{(B.42)}$$

As mentioned before, Eq. B.40 differs from Eq. B.35 by the term containing the tensile force of the jet. It was important to mention the model used by Feng since in the dimensionless form of the conservation equation another dimensionless number appears (the Deborah number, *De*) that considers the viscoelastic characteristics of the fluid and contribute to obtain a stable jet.

B.4.4 Coulomb's law for electric field

$$E = E_\infty - \ln\left(\frac{L}{R_0}\right)\left[\frac{4\pi}{\bar{\varepsilon}} \frac{d(\sigma R)}{dz} - \frac{1}{2}\left(\frac{\varepsilon}{\bar{\varepsilon}} - 1\right) \frac{d^2(ER^2)}{dz^2}\right]$$

Considering that:

$$E^* = \frac{E}{E_0} \rightarrow E = E_0 E^* \text{ and } \frac{dE}{dz} = \left(\frac{E_0}{R_0}\right)\frac{dE^*}{dz^*}$$

$$\frac{d(\sigma R)}{dz} = \frac{dz^*}{dz}\frac{d(\sigma R)}{dz^*} = \sigma_0 \frac{d(\sigma^* R^*)}{dz^*}$$

$$\frac{d(ER^2)}{dz} = \frac{dz^*}{dz}\frac{d(ER^2)}{dz^*} = E_0 R_0 \frac{d(E^* R^{*2})}{dz^*}$$

$$\frac{d^2(ER^2)}{dz^2} = \frac{d}{dz}\left[\frac{d(ER^2)}{dz}\right] = \frac{d}{dz}\left[E_0 R_0 \frac{d(E^* R^{*2})}{dz^*}\right] = E_0 R_0 \frac{dz^*}{dz}\frac{d}{dz^*}\left[\frac{d(E^* R^{*2})}{dz^*}\right]$$

$$= E_0 \frac{d^2(E^* R^{*2})}{dz^{*2}}$$

Replacing into the equation of Coulomb's law for electric field:

$$E_0 E^* = E_\infty - \ln\left(\frac{L}{R_0}\right)\left[\frac{4\pi\sigma_0}{\overline{\varepsilon}}\frac{d(\sigma^* R^*)}{dz^*} - \frac{1}{2}\left(\frac{\varepsilon}{\overline{\varepsilon}} - 1\right) E_0 \frac{d^2(E^* R^{*2})}{dz^{*2}}\right]$$

Dividing all terms by E_0 and simplifying:

$$E^* = \frac{E_\infty}{E_0} - \ln\left(\frac{L}{R_0}\right)\left[\frac{4\pi\sigma_0}{\sigma_0}\frac{d(\sigma^* R^*)}{dz^*} - \frac{1}{2}\left(\frac{\varepsilon}{\overline{\varepsilon}} - 1\right)\frac{E_0}{E_0}\frac{d^2(E^* R^{*2})}{dz^{*2}}\right]$$

$$\boxed{E^* = E_{\text{inf}} - \ln\chi\left(4\pi\frac{d(\sigma^* R^*)}{dz^*} - \frac{\beta}{2}\frac{d^2(E^* R^{*2})}{dz^{*2}}\right)} \quad \text{(B.43)}$$

The governing equations for the electrospraying process are now represented with the variables $R^*, E^*, \sigma^*, v^*, \tau^*_{pzz}$ and τ^*_{prr} that are dimensionless. In addition to allowing the identification of the dimensionless numbers describing the process, the dimensionless equations can be used for the modeling of the process to study its stability, to predict scaling laws with behavior of the jet and to produce operating diagrams where the process occurs as function of the experimental parameters.

From the dimensionless equations obtained in Eq. B.34, B.35 and B.43, the dimensionless numbers *Pe*, *Re*, *We*, *Fr*, Ω, β, χ, r_η and E_{inf} have been identified. The incorporation of a viscoelastic constitutive equation (such as Giesekus model) for obtaining the normal stresses difference in the tensile force T of the jet, allows the appearance of the additional dimensionless number *De* (in Eq.

B.41 and B.42), which considers the polymer viscoelastic effects. The obtained dimensionless numbers are summarized in Table B.2.

The dimensionless numbers help relating in a logical manner the different parameters affecting a process. In this way when many variables are implied, as in the case of electrospraying, the use of the dimensionless numbers is a good way to plan and to correlate experimental data, since in general, as the number of dimensionless groups is less than the number of variables, the number of experiments is reduced and the analysis is simplified.

Table B.2: Dimensionless numbers in the electrospraying process

Dimensionless number		Meaning
Electric Peclet number	$Pe = \frac{2\bar{\varepsilon}v_0}{R_0 K}$	Indicates the importance of charge convection relative to conduction
Reynolds number	$Re = \frac{\rho v_0 R_0}{\eta_0}$	Indicates the ratio of the inertial to viscous forces
Weber number	$We = \frac{\rho v_0^2 R_0}{\gamma}$	Indicates the ratio of inertial to surface tension forces
Froude number	$Fr = \frac{v_0^2}{\mathrm{g}R_0}$	Indicates the ratio of inertial to gravitational forces
Electrostatic force parameter	$\Omega = \frac{\bar{\varepsilon}E_0^2}{\rho v_0^2}$	Indicates the magnitude of the electrostatic forces relative to inertia
Dielectric constant ratio	$\beta = \frac{\varepsilon}{\bar{\varepsilon}} - 1$	Represents the magnitude of induced charges
Aspect ratio	$\chi = \frac{L}{R_0}$	Aspect ratio of the jet
Deborah number	$De = \lambda \frac{v_0}{R_0} = \frac{\lambda}{t_0}$	Ratio of the material relaxation time to the flow time scale
Viscosity ratio	$r_\eta = \frac{\eta_p}{\eta_0}$	Polymer solution viscosity to solvent viscosity
Electric field strength	$E_{\mathrm{inf}} = \frac{E_\infty}{E_0} = \frac{\Delta V/d}{E_0}$	Ratio of applied electric field to initial electric field

B.5 References

[1] S.J. Haward, V. Sharma, C.P. Butts, G.H. McKinley, S.S. Rahatekar, *Biomacromolecules*. **2012**, *13*, 5, p. 1688-1699.

[2] G.C. Rutledge, S.V. Fridrikh, *Advanced drug delivery reviews*. **2007**, *59*, 14, p. 1384-1391.

[3] M.M. Hohman, M. Shin, G. Rutledge, M.P. Brenner, *Physics of fluids*. **2001**, *13*, p. 2201.

[4] J. Feng, *Physics of fluids*. **2002**, *14*, p. 3912.

[5] J. Feng, *Journal of Non-Newtonian Fluid Mechanics*. **2003**, *116*, 1, p. 55-70.

[6] A. Jaworek, A. Sobczyk, *Journal of Electrostatics*. **2008**, *66*, 3, p. 197-219.

[7] F. Sultan, N. Ashgriz, D. Guildenbecher, P. Sojka, *Electrosprays*, in *Handbook of Atomization and Sprays*. **2011**, Springer. p. 727-753.

[8] A. Jaworek, A. Krupa, *Journal of Aerosol Science*. **1999**, *30*, 7, p. 873-893.

[9] N. Bock, T. Dargaville, M. Woodruff, *Progress in Polymer Science*. **2012**.

[10] C.H. Park, M.Y. Kim, J.Y. Yoo, K.H. Kim, J.C. Lee, J. Lee, Macromolecular Symposia, Wiley Online Library, **2007**.

[11] C.P. Carroll, Y.L. Joo, *Physics of fluids*. **2006**, *18*, p. 053102.

[12] C. Pantano, A. Ganan-Calvo, A. Barrero, *Journal of Aerosol Science*. **1994**, *25*, 6, p. 1065-1077.

[13] D.H. Reneker, A.L. Yarin, H. Fong, S. Koombhongse, *Journal of Applied physics*. **2000**, *87*, p. 4531.

[14] A. Ganan-Calvo, J. Davila, A. Barrero, *Journal of Aerosol Science*. **1997**, *28*, 2, p. 249-275.

[15] A.G. a n-Calvo, *J. Fluid Mech*. **1997**, *335*, p. 165.

[16] A. Spivak, Y. Dzenis, *Applied Physics Letters*. **1998**, *73*, 21, p. 3067-3069.

[17] S. Ramakrishna, *An introduction to electrospinning and nanofibers*, World Scientific, **2005**.

[18] D. Saville, *Annual review of fluid mechanics*. **1997**, *29*, 1, p. 27-64.

[19] J. Stephens, S. Frisk, S. Megelski, J. Rabolt, D.B. Chase, *Applied Spectroscopy*. **2001**, *55*, 10, p. 1287-1290.

[20] R. Hartman, D. Brunner, D. Camelot, J. Marijnissen, B. Scarlett, *Journal of Aerosol Science*. **2000**, *31*, 1, p. 65-95.

[21] R. Hartman, D. Brunner, D. Camelot, J. Marijnissen, B. Scarlett, *Journal of Aerosol Science*. **1999**, *30*, 7, p. 823-849.

[22] W. Benenson, H. Stöcker, *Handbook of physics*, Springer, **2002**.

[23] F.A. Morrison, *Understanding rheology*, Oxford University Press, USA, **2001**.

[24] R.B. Bird, W.E. Stewart, E.N. Lightfoot, *Transport phenomena*, Wiley. com, **2007**.

[25] M.M. Hohman, M. Shin, G. Rutledge, M.P. Brenner, *Physics of fluids*. **2001**, *13*, p. 2221.

[26] A. Yarin, S. Koombhongse, D. Reneker, *Journal of Applied physics*. **2001**, *89*, p. 3018.

[27] C.P. Carroll, Y.L. Joo, *Journal of Non-Newtonian Fluid Mechanics*. **2008**, *153*, 2, p. 130-148.